Towards the elucidation of pathophysiology of amyloid conversion of globular proteins

by

Guglielmo Verona

A thesis submitted in fulfilment of the requirements for the degree of Doctor of Philosophy

Centre for Amyloidosis and Acute Phase Proteins

Division of Medicine

University College London

2018

Declaration

I, Guglielmo Verona, confirm that the work presented in this thesis is my own and I have followed the analyses, which were not performed mainly by me. Where information has been derived from other sources, I confirm that this has been indicated in the thesis.

Signed

Abstract

Amyloidoses are a group of diseases caused by the conversion of soluble proteins into pathogenic ordered fibrillar aggregates. The mechanism driving *in vivo* the structural transformation of these proteins has not yet been clearly elucidated. My work has focused on two plasma proteins that make amyloid *in vivo* starting from precursors deeply different in terms of structure and function: transthyretin (TTR) and the apolipoprotein C-III variant, D25V (D25V apo C-III). Apo C-III is mostly synthesized by the liver and is a major component of HDL. We have described the first variant causing a genetic form of renal amyloidosis. In the work presented here, structural and functional characterization of the newly described D25V apo C-III variant was carried out together with the investigation of its aggregation mechanism, showing a modest loss of function and an increased tendency to aggregate in physiological buffer in the lipid-free state.

TTR is mainly synthesized by the liver and the choroid plexus in the CSF and is the main transporter of thyroxine in the CSF and the secondary transporter in plasma. The mechanism of TTR fibrillogenesis has been investigated for decades. Our group has recently proposed a new pathway for TTR amyloidogenis mediated by selective tryptic cleavage, in alternative to the commonly accepted low pH induced aggregation mechanism. Further characterization of the mechanism, including the identification of the culprit protease responsible for proteolytic cleavage *in vivo* was carried out showing a correlation between TTR stability and susceptibility to proteolysis. The inhibitory activity of stabilisers and their effect on protein structure and dynamics were also studied using a combination of spectroscopic techniques including NMR. The identification of the enzyme responsible for cleavage in vivo, opens up a completely new scenario for understanding the mechanism and the history of the disease *in vivo*.

Impact Statement

The data presented in this thesis offer an insight into the mechanism of aggregation of two distinct amyloidogenic proteins under physiological conditions.

D25V apo C-III was the first ever described amyloidogenic variant of human apo C-III. Considering the involvement of several apolipoproteins in the formation of amyloid deposits *in vivo*, the biochemical characterisation of the structure, function as well as the investigation of the aggregation mechanism of the D25V apo C-II variant could provide an insight into the mechanism driving the conversion of other proteins belonging to the same family from their functional state to insoluble amyloid fibrils.

The results obtained on TTR have an impact both within and outside academia. The results obtained by NMR spectroscopy represent the first clear demonstration of an allosteric effect exhibited by ligands upon binding, highlighting the role that this technique could have in the screening and development of new therapeutic drugs acting as TTR stabilisers. Furthermore, our group has proposed a new mechanism for TTR amyloidogenesis, defined ‘mechano-enzymatic mechanism’, which better resembles the *in vivo* scenario in comparison to the classic mechanism of low pH-induced dissociation and subsequent aggregation. The results presented in this thesis expand our understanding of the mechanism and identify a plausible protease responsible for proteolysis *in vivo*. Compounds able to stabilise TTR, such as tafamidis, have up to now been identified exclusively by their capacity to inhibit TTR dissociation and aggregation induced by low pH *in vitro*. However even with apparently complete pharmacological stabilisation of circulating TTR, the clinical benefit observed so far is limited to modest slowing of the progression of peripheral neuropathy. In the light of the discovery of the mechano-enzymatic mechanism, the evaluation of the ability of different TTR stabilisers to inhibit

proteolysis becomes crucial and opens up new possibilities in the field of drug discovery for both academia and pharmaceutical companies.

The benefit of having more effective compounds, able to completely stop the progression of the disease, would firstly give benefits to the patients affected by TTR amyloidosis around the world, who are the ultimate target of basic science research. The possibility to improve the quality of life of patients as well as the clinical outcome would translate in a reduction of the costs associated with the treatment of this relatively rare disease and could therefore be of extreme interest for the public health system.

Acknowledgements

First of all I would like to thank my supervisor, Professor Vittorio Bellotti who has guided me through the project and supported me when needed. He is a wonderful group leader and a great man. A big thank you goes to Dr Patrizia Mangione for all the precious suggestions that she has given me in the lab and for the exceptional support that she has offered me through the years.

I would then like to thank Dr Alessandra Corazza, who, despite joining the group recently, has truly become an essential part of it. Her help has been invaluable for the acquisition and analysis of the NMR data presented in chapter 5. I would also like to thank my colleagues, Dr Graham Taylor, Dr Nigel Rendell. A special thank you to Dr Stephan Ellmerich, who I played some incredible squash games with. My gratitude also goes to Prof Sir Mark Pepys for his support. I would also like to thank Professor John Christodoulou and Dr Christopher Waudby for both the scientific support and the possibility to access and use their facilities. A big thank you to Dr Lisa Cabrita for providing the reagents necessary for ^{2}H ^{13}C ^{15}N wild type TTR expression.

A special mention goes to Dr Diana Canetti, a great colleague to work with, but most importantly a very good friend. A big thank you to Paola, who has only recently joined the group, but has quickly become a key element and a good friend. I would also like to thank Lucia and all the other students who I have had the pleasure to work, chat and laugh with throughout all these years.

To Nicola, who has always been there next to me in bad and good times and whose belief in me has always pushed me forward. I would not have made it without you.

To my friends here and especially at home, who I have always been in touch and shared amazing moments with.

Finally, my warmest gratitude goes to my family, whose love, support and joy was never missed, despite the distance between us. I would not be who I am without you. To my dogs, Argo and Jago for being my hairy loyal friends.

Achievements

List of publications

- Mangione PP, **Verona G**, Corazza A, Marcoux J, Canetti D, Giorgetti S, Raimondi S, Stoppini M, Esposito M, Relini A, Canale C, Valli M, Marchese L, Faravelli G, Obici L, Hawkins PN, Taylor GW, Gillmore JD, Pepys MB, Bellotti V (2018). Plasminogen activation triggers transthyretin amyloidogenesis *in vitro*. J Biol Chem [Epub ahead of print] pii: jbc.RA118.003990
- Canetti D, Rendell NB, Di Vagno L, Gilbertson JA, Rowczenio D, Rezk T, Gillmore JD, Hawkins PN, **Verona G**, Mangione PP, Giorgetti S, Mauri P, Motta S, De Palma A, Bellotti V, Taylor GW (2017). Misidentification of transthyretin and immunoglobulin variants by proteomics due to methyl lysine formation in formalin-fixed paraffin-embedded amyloid tissue. Amyloid 24(4):233-241
- Raimondi S, Porcari R, Mangione PP, **Verona G**, Marcoux J, Giorgetti S, Taylor GW, Ellmerich S, Ballico M, Zanini S, Pardon E, Al-Shawi R, Simons JP, Corazza A, Fogolari F, Leri M, Stefani M, Bucciantini M, Gillmore JD, Hawkins PN, Valli M, Stoppini M, Robinson CV, Steyaert J, Esposito G, Bellotti V (2017). A specific nanobody prevents amyloidogenesis of D76N β_2-microglobulin in vitro and modifies its tissue distribution in vivo. Sci Rep 7:46711
- **Verona G**, Mangione PP, Raimondi S, Giorgetti S, Faravelli G, Porcari R, Corazza A, Gillmore JD, Hawkins PN, Pepys MB, Taylor GW, Bellotti V (2017). Inhibition of the mechano-enzymatic amyloidogenesis of transthyretin: role of ligand affinity, binding cooperativity and occupancy of the inner channel. Sci Rep 7(1):182
- Valleix S, **Verona G**, Jourde-Chiche N, Nédelec B, Mangione PP, Bridoux F, Mangé A, Dogan A, Goujon JM, Lhomme M, Dauteuille C, Chabert M, Porcari R, Waudby CA, Relini A, Talmud PJ, Kovrov O, Olivecrona G, Stoppini M, Christodoulou J, Hawkins PN, Grateau G, Delpech M, Kontush A, Gillmore JD, Kalopissis AD, Bellotti V (2016). D25V apolipoprotein C-III variant causes dominant hereditary systemic amyloidosis and confers cardiovascular protective lipoprotein profile. Nat Commun 7:10353
- Marcoux J, Mangione PP, Porcari R, Degiacomi MT, **Verona G**, Taylor GW, Giorgetti S, Raimondi S, Sanglier-Cianférani S, Benesch JL, Cecconi C, Naqvi MM, Gillmore JD, Hawkins PN, Stoppini M, Robinson CV, Pepys MB, Bellotti V (2015). A novel mechano-enzymatic cleavage mechanism underlies transthyretin amyloidogenesis. EMBO Mol Med 7(10):1337-49
- Porcari R, Proukakis C, Waudby CA, Bolognesi B, Mangione PP, Paton JF, Mullin S, Cabrita LD, Penco A, Relini A, **Verona G**, Vendruscolo M, Stoppini M, Tartaglia GG, Camilloni C, Christodoulou J, Schapira AH, Bellotti V (2015). The H50Q mutation induces a 10-fold decrease in the solubility of α-synuclein. J Biol Chem 290(4):2395-404

Posters and presentations

- UK-Israel Synergy Symposium London: Protein misfolding in ageing and neurodegeneration**,** London, UK (2018). Poster presentation
- IPR/RSC Joint Symposium, Osaka, Japan (2017). Poster presentation
- Rosetrees Trust 30th anniversary symposium (2017). Poster presentation
- EMPIR NeuroMet meeting (2017), Goteborg, Sweden. Oral presentation
- APAM annual meeting (2017). Poster presentation
- 1st Joint Annual Symposium of the Departments of Biology and Biotechnology, Molecular Medicine, CNR Institute of Molecular Genetic Pavia, Italy. Oral presentation
- UK/Japan Workshop on Amyloidosis, London, UK (2016). Oral presentation
- Rosetrees Trust PhD symposium (2016). Poster presentation
- UCL, Division of Medicine Research Student Day 2016. Oral presentation
- ISA 2016 XV Symposium on Amyloidosis, Uppsala, Sweden. Poster presentation
- UK/Japan/Italy Workshop on Amyloidosis, London, UK (2015). Oral presentation

Table of contents

List of figures

List of tables

Chapter 1. General introduction

1.1 Amyloidoses

The German physician Rudolf Virchow introduced the term *amyloid* in 1854 to describe the corpora amylacea found in the brain, which he erroneously thought were made of cellulose due to their capacity to stain with iodine. Five years later, in 1859, Friederich and Kekule identified the presence of protein material in the deposits, thus shifting the attention initially on “amyloid as a single protein and later as a class of proteins, with a propensity to undergo changes in conformation which resulted in fibril formation” (Sipe JD and Cohen AS, 2000). The advance in both medical and biochemical knowledge over the last 150 years has led to the contemporary definition of “amyloidoses as a generic term used to describe a wide range of human diseases characterized by the misfolding and extracellular accumulation, in the form of highly organised fibrillary aggregates, of various proteins” (Gillmore JD & Hawkins PN, 2013). Such aggregates “arise from the failure of a specific peptide or protein to adopt, or remain in, its native functional conformational state with subsequent reduction in the quantity of protein that is available to play its physiological role” (Chiti F & Dobson CM, 2007). Within the protein conformational diseases, amyloidoses represent the largest group of misfolding diseases where specific peptides or proteins convert from their soluble functional states into toxic and highly insoluble amyloid fibrils which can deposit in human tissues (Sipe JD, 1992; fig. 1).

These diseases, although known for more than 150 years, have only recently been increasingly recognized in the pathogenesis of many human diseases with enormous social and medical impact and which are indeed associated with the formation of extracellular plaques or intracellular inclusions of protein aggregates with amyloid-like features.

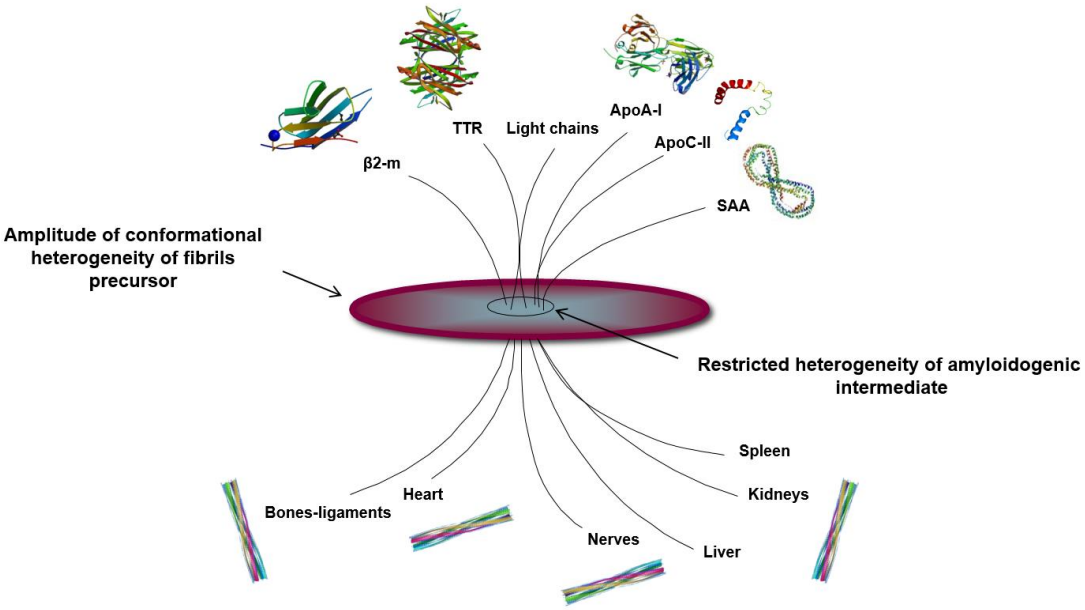

Figure 1. From a heterogeneity of protein precursors to amyloid fibrils

Amyloid diseases can be broadly grouped into:

- Neurodegenerative conditions, in which aggregation occurs in the brain;
- Non neuropathic localized amyloidoses, where the amyloid is restricted to a particular organ or tissue;
- Non neuropathic systemic amyloidoses, in which the "deposits can be present in many or all the viscera, connective tissue, and blood vessel walls, although intracerebral amyloid deposits are never found." (Pepys MB, 2009). About one per thousand deaths in developed countries are associated with systemic amyloidosis.

Localized and systemic amyloidoses can be further grouped into *acquired or hereditary amyloidosis*.

"Acquired amyloidosis arise as a complication of a pre-existing primary disease that either produces an inherently amyloidogenic abnormal protein, or greatly increases the amount of a potentially amyloidogenic normal

protein" (Pepys MB, 2009). The first is, for example, the case of monoclonal immunoglobulin light (L) chains in AL amyloidosis, the latter is represented by β_2-microglobulin (β2-m) in wild type β_2-m (WT β_2-m) amyloidosis or serum amyloid A in AA amyloidosis. Hereditary amyloidoses are associated with mutant genes encoding for variant proteins presenting structural abnormalities, which determine their amyloidogenic potential and represent a group of disorders in constant expansion. To date 36 proteins, listed in table 1, have been recognized as causative agents of different amyloid diseases (Sipe JD et al, 2016).

Table 1. Amyloid fibrils proteins and precursors

Fibril protein	Protein precursor	Target organ	Systemic and/or localized	Acquired or hereditary
AL	Immunoglobulin light chain	All organs usually excluding central nervous system	Systemic Localized	Acquired/hereditary
AH	Immunoglobulin heavy chain	All organs excluding central nervous system	Systemic Localized	Acquired
AA	Serum amyloid A	All organs excluding central nervous system	Systemic	Acquired
ATTR	Wild type transthyretin	Heart mainly in males, ligaments, tenosynovium	Systemic	Acquired
	Variant transthyretin	Peripheral nervous system, autonomic nervous system, heart, eye, leptomeninges	Systemic	Hereditary
Aβ2M	Wild type β2-Microglobulin	Musculoskeletal system	Systemic	Acquired
	Variant β2-Microglobulin	Autonomic nervous system	Systemic	Hereditary
AApoAI	Variant apolipoprotein A I	Heart, liver, kidney, peripheral nervous system, testis, larynx (C-terminal variants), skin (C-terminal variants)	Systemic	Hereditary

AApoAII	Variant apolipoprotein A II	Kidney	Systemic	Hereditary
AApoAIV	Wild type apolipoprotein A IV	Kidney medulla and systemic	Systemic	Acquired
AApoCII	Variant apolipoprotein C II	Kidney	Systemic	Hereditary
AApoCIII	Variant apolipoprotein C III	Kidney	Systemic	Hereditary
AGel	Variant gelsolin	Peripheral nervous system, cornea	Systemic	Hereditary
ALys	Variant lysozime	Kidney	Systemic	Hereditary
ALECT2	Leukocyte chemotactic factor-2	Primarily kidney	Systemic	Acquired
AFib	Variant fibrinogen α	Primarily kidney	Systemic	Hereditary
ACys	Variant cystatin C	Peripheral nervous system, skin	Systemic	Hereditary
ABri	Variant ABriPP	Central nervous system	Systemic	Hereditary
ADan	Variant ADan PP	Central nervous system	Localized	Hereditary
Aβ	Wild type Aβ precursor	Central nervous system	Localized	Acquired
	Variant Aβ precursor	Central nervous system	Localized	Hereditary
AαSyn	α-Synuclein	Central nervous system	Localized	Acquired
ATau	Tau	Central nervous system	Localized	Acquired
APrP	Wild type prion protein	Creutzfeldt-Jacob disease, fatal insomnia	Localized	Acquired
	Variant prion protein	Creutzfeldt-Jacob disease, fatal insomnia, Gerstmann-Straussler-Scheinker syndrome	Localized	Hereditary
ACal	(Pro)calcitonin	C-cell thyroid tumour	Localized	Acquired
AIAPP	Islet amyloid polypeptide	Islets of Langerhans, insulinomas	Localized	Acquired

AANF	Atrial natriuretic factor	Cardiac atria	Localized	Acquired
APro	Prolactin	Pituitary prolactinomas, aging pituitary	Localized	Acquired
AIns	Insulin	Iatrogenic, local injection site	Localized	Acquired
ASPC	Lung surfactant protein	Lung	Localized	Acquired
AGal7	Galectin 7	Skin	Localized	Acquired
ACor	Corneodesmosin	Cornified epithelia, hair follicles	Localized	Acquired
AMed	Lactadherin	Senile aortic, Media	Localized	Acquired
AKer	Kerato-epithelin	Cornea, hereditary	Localized	Acquired
ALac	Lactoferrin	Cornea	Localized	Acquired
AOAAP	Odontogenic ameloblast-associated protein	Odontogenic tumors	Localized	Acquired
ASem1	Semenogelin 1	Vesicula seminalis	Localized	Acquired
AEnf	Enfurvitide	Iatrogenic	Localized	Acquired

Some neurodegenerative or endocrine diseases, not clinically classified as amyloidosis, have also been associated with the presence of intracellular amyloid-like deposits and plaques, which play a crucial role in their pathogenesis (Sipe JD et al., 2016; table 2).

Table 2. Intracellular amyloid protein inclusions

Inclusion name	Protein nature	Site	Associated disease
Lewy bodies	α-synuclein	Neurons intracytoplasmatic	Parkinson's disease
Huntington bodies	PolyQ expanded huntingtin	Neurons intranuclear	Huntington's disease
Hirano bodies	Actin	Neurons	Neurodegenerative disorders
Collins bodies	Neuroserpin	Neurons	Forms of familial presenile dementia
Not specified	Ferritin	Neurons, many different cells	Form of familial neurodegenerative disorder
Neurofibrillary tangles	Tau	Neurons intracytoplasmatic	Alzheimer's disease, fronto-temporal dementia, aging, other cerebral conditions
Aαsyn	α-synuclein	Neurons intracytoplasmatic	Parkinson's disease, other cerebral conditions

1.2 Molecular mechanism of amyloid formation

Several mechanisms, acting independently or in synergy, are responsible for amyloid deposition:

- Some proteins are inherently amyloidogenic and exhibit a tendency to convert into the pathological form and then to aggregate in the form of amyloid fibrils. Wild type transthyretin (WT TTR) amyloidosis is a good example of a protein with inherent tendency to self-assemble into fibrils.
- A single point mutation in the gene encoding for a specific protein can induce the replacement of a single amino acid in the protein sequence thus reducing the conformational stability of the mutant compared to the WT form and promoting aggregation. This mechanism is associated with hereditary amyloidosis.
- The precursor protein may undergo post-translational modification including proteolytic cleavage or oxidation. This is the case of Aβ peptide causing amyloid like plaques in the brain of patients with Alzheimer's disease (Murphy MP & LeVine H, III, 2010).
- The conversion of native conformers into their pathological form can be catalysed by the interaction with misfolded monomers. The prototype of this mechanism is the interaction between prion proteins causing spongiform encephalopathy.
- Some proteins, referred to as natively unfolded proteins, lack a fully structured three-dimensional conformation and are therefore exposed to the risk of self-aggregation. α-synuclein and apolipoproteins are good examples of natively unfolded proteins prone to aggregation.

In addition to the protein amyloidogenic potential other factors that perturb the three-dimensional structure such as a low pH, oxidation, increased temperature, limited proteolysis, metal ions and osmolytes — may act synergistically by shifting the equilibrium toward the partially folded amyloidogenic state (Merlini G & Bellotti V, 2003; Kim YS et al., 2001).

Local micro-environmental conditions can promote the partial unfolding of the native protein thus promoting aggregation, but they can also affect the ultra-structural organization of protein deposits causing them to form either fibrillar

amyloid aggregates or amorphous aggregates (Khurana R et al., 2001). Common components of amyloid deposits, such as glycosaminoglycans and serum amyloid P component (SAP) may exert identical effects by hastening the integration of a soluble polypeptide into a more stable fibril (Merlini G & Bellotti V, 2003). Furthermore fibrillar “seeds” are able to catalyse conformational changes in the soluble protein and they can accelerate the deposition of amyloid during the inflammatory process (Lundmark K et al., 2002; Elliott-Bryant R & Cathcart ES, 1998).

1.3 Composition of amyloid deposits

The analysis of the composition of *ex vivo* amyloid deposits shows that the core of the plaques consists of a major protein component. Aside the amyloid fibril protein, the presence of other ubiquitous components is normally observed. In particular SAP, apolipoprotein E and apolipoprotein A-IV are commonly detected by proteomic mass spectrometry analysis (Vrana JA et al., 2009) and are known as “amyloid signature proteins”.

Here is a list of the common constituents normally identified in amyloid deposits:

- **SAP** (Fig. 2), a plasma glycoprotein belonging to the pentraxin family, synthesized by the liver, which reversibly binds to amyloid (K_d ~ 1μmol/l) in a calcium-dependent fashion, creating a coating, which highly protects the fibrils against proteolysis and confers them resistance to degradation by phagocytosis both *in vivo* and *in vitro (*Tennent GA et al., 1995*)*. The abundance of SAP in the deposits (up to 15% of the total amyloid mass) and its reversible binding to the fibrils make I^{125} radio-labeled SAP an important diagnostic tool for the imaging of amyloid deposits (Pepys MB et al., 1997).

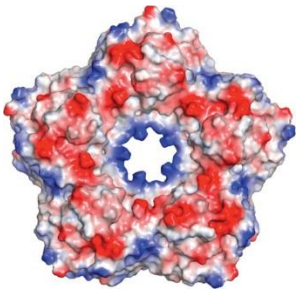

Figure 2. Three-dimensional structure of SAP

(Senior K, 2009)

- **Apolipoprotein E** is common constituent of amyloid plaques although its role in systemic amyloidosis has not yet been identified (Gallo G et al., 1994).
- **Apolipoprotein A-IV** is often found in amyloid deposits and has recently been described as a cause of renal amyloidosis following its deposition in the kidneys (Dasari S et al., 2016).
- **Collagen** (not always present) constitutes a scaffold to which amyloid fibrils adhere and then increase in size (Homma N et al., 1989). Several studies suggest that the interaction with collagen might play an important role in driving the tissue specificity.
- **Proteoglycans,** such as heparan sulphate and dermatan sulphate, act similarly to collagen providing a scaffold for nucleation and fibril growth, but can also protect fibrils against degradation by tightly binding to them. They localize with constitutive elements of extracellular matrix, such as perlecan, laminin, entactin, and collagen IV and contribute to the carbohydrate component of natural amyloid.
- **Metal cations** are implicated in a number of amyloid diseases. Bivalent cations Cu^{2+}, Zn^{2+} and Ni^{2+} have been shown to affect protein conformational transitions and, in stoichiometric amounts, can induce amyloid formation (Jones CE et al., 2004).

1.4 The relation between folding and misfolding

The folding free energy landscape for small proteins can be represented with a funnel-like diagram (Fig. 3), which effectively represents the evolutionary selection of polypeptide sequences able to fold rapidly and reliably towards a unique native state (Watters AL et al., 2007). In the case of larger

polypeptide sequences the surface of the energy landscape appears rougher, allowing the population of partially folded species that may be on or off-pathway to the native fold (Watters AL et al., 2007; Vendruscolo M et al., 2003).

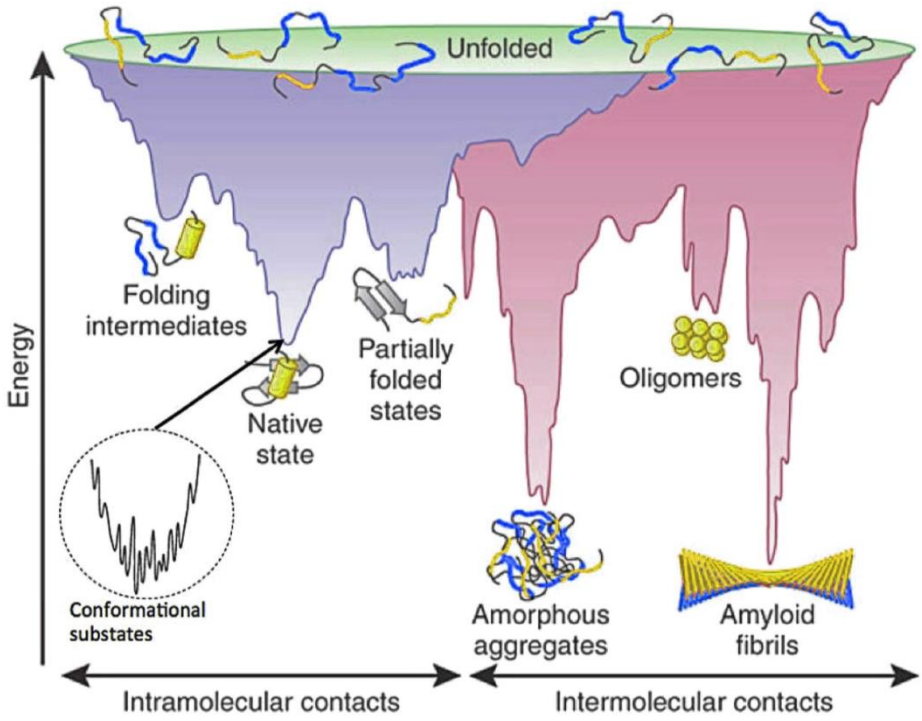

Figure 3. Folding funnel diagram. Representation of the funnel-shaped free-energy landscape (adapted from Rasakatov J & Teplow D, 2017).

Determining the conformation of unfolded states means defining the starting point for protein folding reactions and understanding the role that these species play in a wide variety of biological processes. There also may be the possibility for the polypeptide to acquire an alternative and relatively stable "misfolded state," which is aggregation prone and is energetically favourable having the same, if not lower, minimum energy of the native protein. Many proteins, once secreted, are in dynamic equilibrium with a partially folded conformation, and in this state, they retrace the final part of the folding pathway, ultimately forming either a native or misfolded protein (Brockwell DJ & Radford SE, 2007; McCarney ER et al., 2005).

1.5 Mechanisms of amyloid fibril growth

The molecular mechanism underlying the partial or total unfolding of a protein and subsequent formation of amyloid fibrils *in vitro* is nowadays widely understood thanks to biochemical and kinetics approaches. The pathological pathway taking place *in vivo,* although, appears more complicated and has therefore not yet been clarified. The formation of amyloid fibril is commonly described as a "nucleated growth" mechanism (Naiki H et al., 1997; Pedersen JS et al., 2004) and is characterized by the presence of two distinct phases: a lag phase required for "nuclei" formation followed by a rapid exponential growth phase. Nucleation takes place in the early stages of the amyloid cascade and is a thermodynamically unfavourable stochastic phenomenon, which represents the rate-limiting step of the pathogenic mechanism (Naiki H et al., 1997). It is possible to discriminate between primary and secondary nucleation pathways: primary nucleation consists of an interaction between soluble monomers, whose concentration strongly influences the kinetics of the process, and leads to the formation of small fibrils (Fig. 4 A); secondary processes can be monomer-independent and include different mechanisms such as fibril fragmentation or more complex processes such as surface-catalysed nucleation. In the case of fibril fragmentation the rate of formation of new aggregates only depends on the level of aggregates, while surface-catalysed nucleation might lead to fibril branching and depends on the concentration of both monomeric protein and existing aggregates (Fig. 4 B). Once a nucleus is formed, fibril growth is thought to proceed rapidly by further association of either monomers or oligomers to the end of the existing fibrils in a process referred to as elongation (Naiki H et al., 1997; Pedersen JS et al., 2004). In the presence of high monomer concentration, the conformational rearrangement of the polypeptide subsequent to its binding to the fibril end becomes rate limiting for the overall elongation process making the rate of polymerization largely independent on the monomer concentration (Fig. 4 C; Collins SR et al., 2004). Molecular recycling (Fig. 4 D; Carulla N et al., 2005), consisting of dissociation of molecules from aggregates, also takes place, although the

kinetic rate of this phenomenon appears to be significantly slower than the growth processes in order for fibril growth to occur.

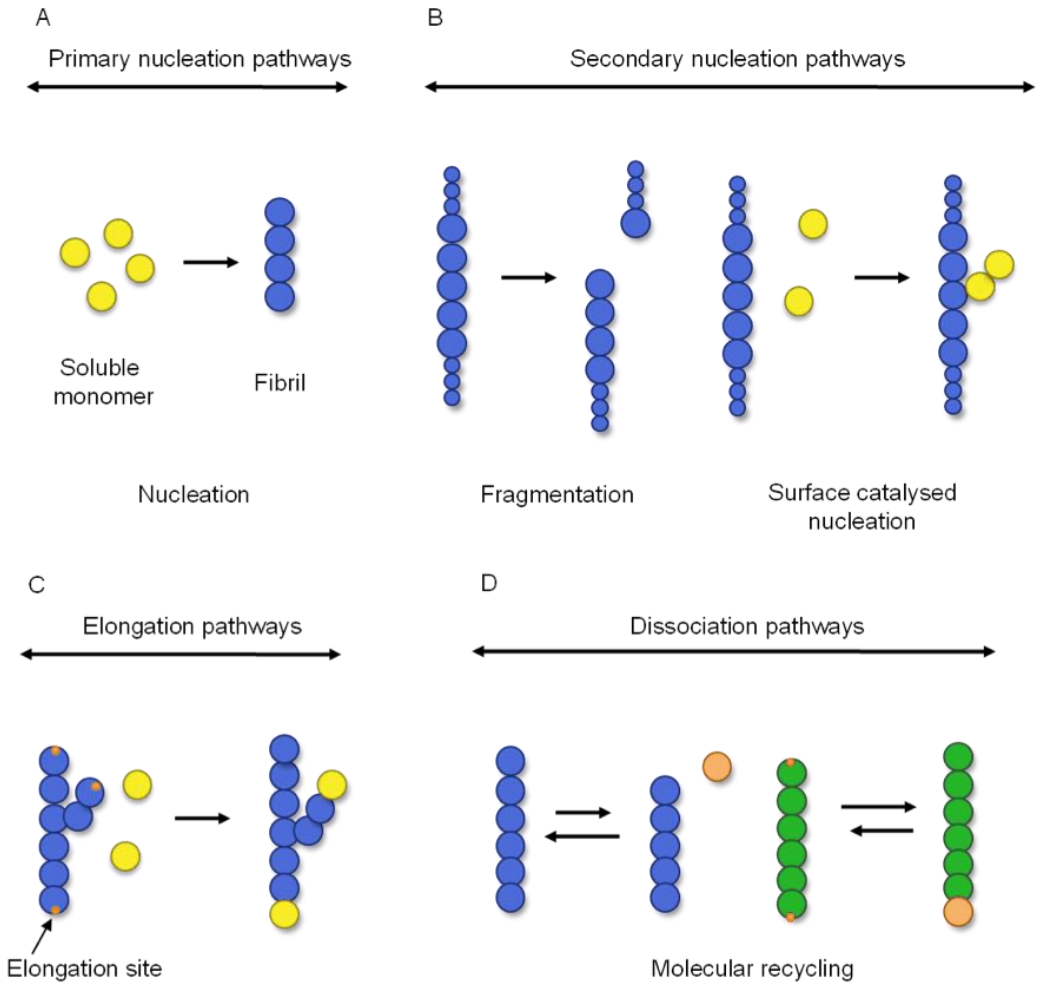

Figure 4. Mechanisms of amyloid fibril growth. (A) Monomer-dependent primary nucleation, **(B)** Monomer-independent secondary nucleation pathways promoting the formation of new aggregates, **(C)** Elongation takes place with addition of new monomers to the fibril ends, **(D)** Molecular recycling: a slow turnover is generated by the constant equilibrium existing between molecules in aggregates and molecules in solution. Figure adapted from Cohen SI et al., 2012 and Carulla N et al., 2005.

As with many other nucleation dependent processes, including crystallization, it is possible to significantly reduce the lag phase preceding aggregation by the addition of preformed fibrillar aggregates to a sample of a protein under aggregation conditions following a procedure referred to as “seeding” (Naiki H et al., 1997; Serio TR et al., 2000). Other parameters such as changes in experimental conditions or the presence of certain types of mutations can also reduce (or eliminate in some cases) the length of the lag phase (Fezoui Y & Teplow DB, 2002). These observations suggest that the lag phase gets shortened and ultimately abolished only when the rate of the aggregation process is no longer limited by the need for nucleation. The absence of a lag phase does not exclude the presence of a nucleated growth mechanism, which might well still operate: it is indeed possible that the time required for fibril growth is sufficiently slow compared to the nucleation process so that the latter represents no longer the slowest step in the conversion of a soluble protein into the amyloid state (Chiti F & Dobson CM, 2006).

Seeding between different protein species, known as cross seeding, is a rare event as demonstrated by several experiments, which showed that when the sequence identity of the protein forming the seeds is lower than 30-40% compared to the species in solution, the efficiency of the seeding effect significantly decreases.

1.6 The structure of amyloid fibrils and factors determining their polymorphism

Several protein precursors, although heterogeneous in structure and function, can ultimately aggregate in the form of amyloid fibrils, which all share the same physico-chemical features and structure. Much information on the structure of amyloid fibrils has been derived by imaging *in vitro* using techniques such as transmission electron microscopy (TEM), atomic force microscopy (AFM) and X-ray fiber diffraction (Serpell LC et al., 2000; Sunde M & Blake C, 1997). In more recent years the technical advance in techniques such as solid-state nuclear magnetic resonance (SSNMR), cryo-electron microscopy (cryo-EM) and Fourier transform infrared spectroscopy

(FTIR) has widely increased the amount of structural information available on the three-dimensional structure of fibrils at an atomic scale resolution. AFM and EM show early pre-fibrillar aggregates as amorphous or micelles. These can then evolve into highly organised structures referred to as protofibrils or protofilaments (Jimenez et al., 1999). Such protofilaments (typically 2–6), each about 2–5 nm in diameter, which twist together to form rope-like fibrillar structures, represent the structural units constituting the fibrils (Fig. 5).

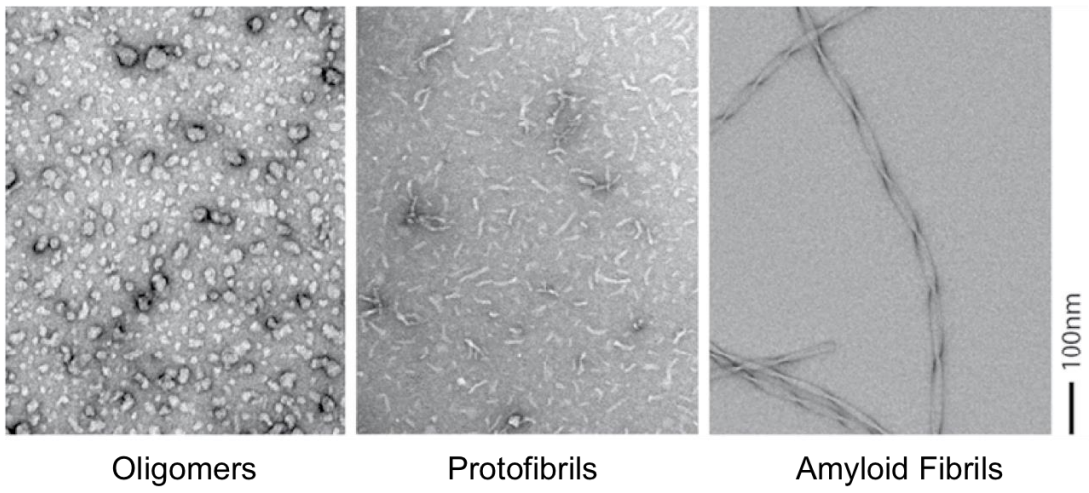

Figure 5. Morphology of fibrillar and pre-fibrillar structures. Negatively stained EM images of oligomers, protofibrils and amyloid fibrils by amyloid β peptide 1-40 are shown (Meinhardt J & Fändrich M, 2009).

Typically, fibrils are 7–13 nm wide or associate laterally to form long ribbons that are 2–5 nm thick and up to 30 nm wide (Serpell LC et al., 2000).

The analysis of the X-ray fiber diffraction pattern (Sunde M & Blake C, 1997) has shown that, within the individual protofilament, the β-strands formed by the polypeptide chain, originated by the whole protein or peptide molecules, run perpendicular to the long axis of the fibril. Several researchers have suggested that a single protofilament comprises four β-sheets, separated by distances of 10 Å. Each molecule within the protofilament contributes four β-strands, with strands one and three forming one parallel β-sheet and with strands two and four forming another parallel β-sheet 10 Å away (Petkova AT et al., 2002; Goldsbury CS et al., 2000; Chiti F & Dobson CM, 2006). Amyloid

fibrils formed by small peptides have helped in the investigation of the cross-ß amyloid structure. X-ray diffraction of this material has shown an intrastrand distance between parallel sheets around 4.8 Å. The distance separating parallel and antiparallel sheets, also called the interstrand distance as it represents the distance between different strands, has instead been calculated around 9.6 Å (Fig. 6 A). Looking down the long axis of the fiber it is possible to observe that the side chains emanating from two sheets are tightly interdigitated, forming a zipper-like interaction referred to as steric-zipper (Fig. 6 B-C), which could explain why different proteins assemble in amyloid fibrils of similar appearance. The differences existing in terms of diameters of the fibrils is associated with the different lengths of the constitutive protein and with the actual number of protofibrils that twist together to form a fibril (Eisenberg D & Jucker M, 2012).

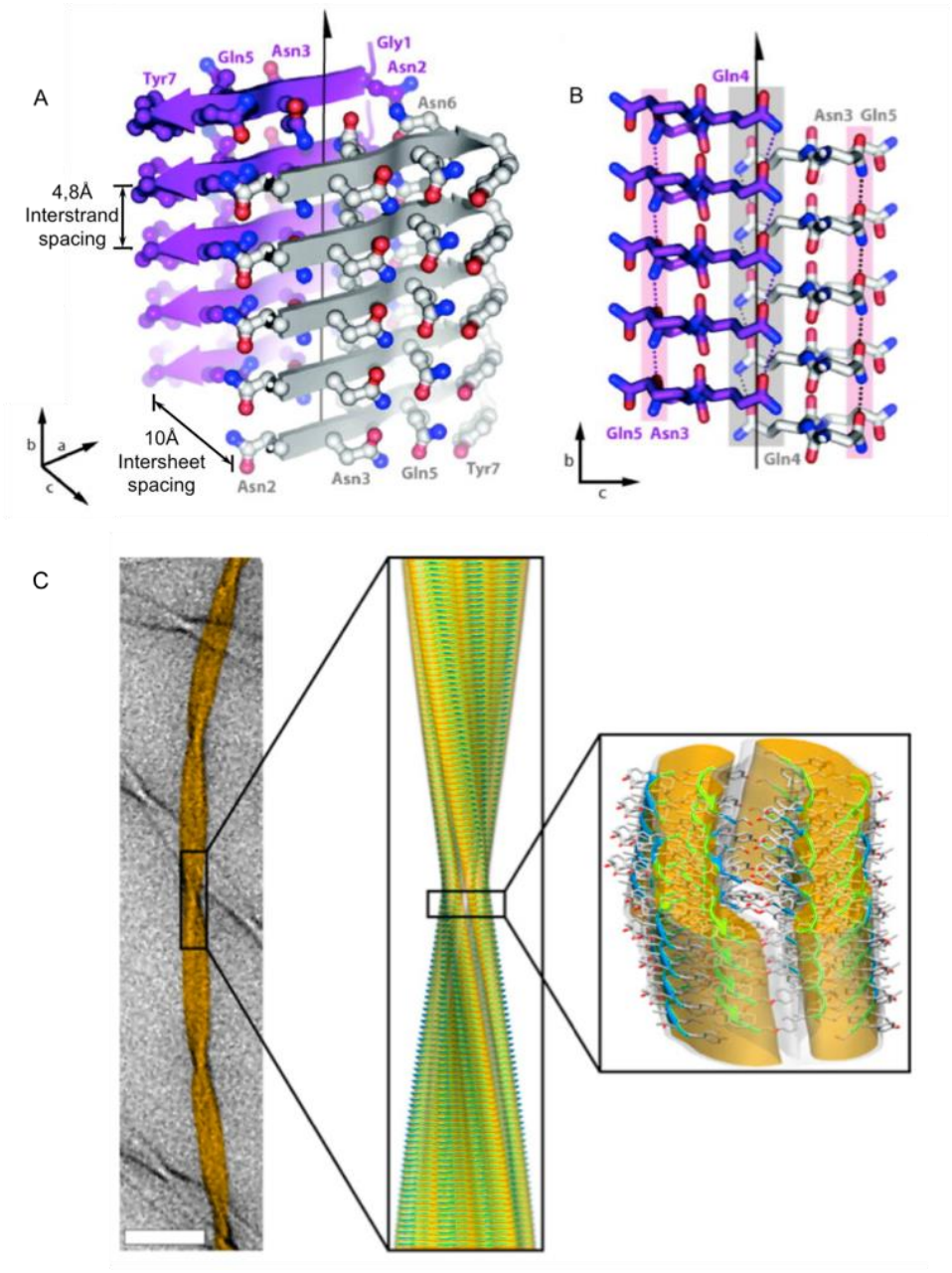

Figure 6. The cross-β amyloid structure (A) The pair-of-sheets structure of the amyloid fibril-forming peptide GNNQQNY. An arrow represents each β-strand's backbone. **(B)** The interdigitation of the sidechains emanating from each sheet is made possible by the vertical shift of one sheet relative to the other. **(C)** Cryo-EM reconstruction of amyloid fibrils originated by TTR 105-115 peptide. The close up clearly shows the steric-zipper motif. Figure adapted from Nelson et al., 2005 and Fitzpatrick et al., 2013.

The presence of the typical cross-β structure is usually identified by the binding of different dyes such as Congo red (CR), Thioflavin-T (ThT) and their derivatives which are thought to form ordered arrays along the lengths of the fibrils, giving rise to specific spectral responses. Upon staining with an alkaline alcoholic CR solution (Puchtler H et al., 1985), the presence of fibrils is uncovered by a characteristic apple-green birefringence under a polarized light microscope (Fig. 7). In the case of ThT, initially described by Naiki and collaborators (Naiki H et al., 1989), the binding to the typical cross-β structure featured in amyloid fibrils causes a conformational change in the ThT molecule, which increases its emission at 480 nm after excitation at 445 nm. Although in some cases non-specific binding has been observed, ThT is commonly used to detect the presence of aggregates *in vitro*.

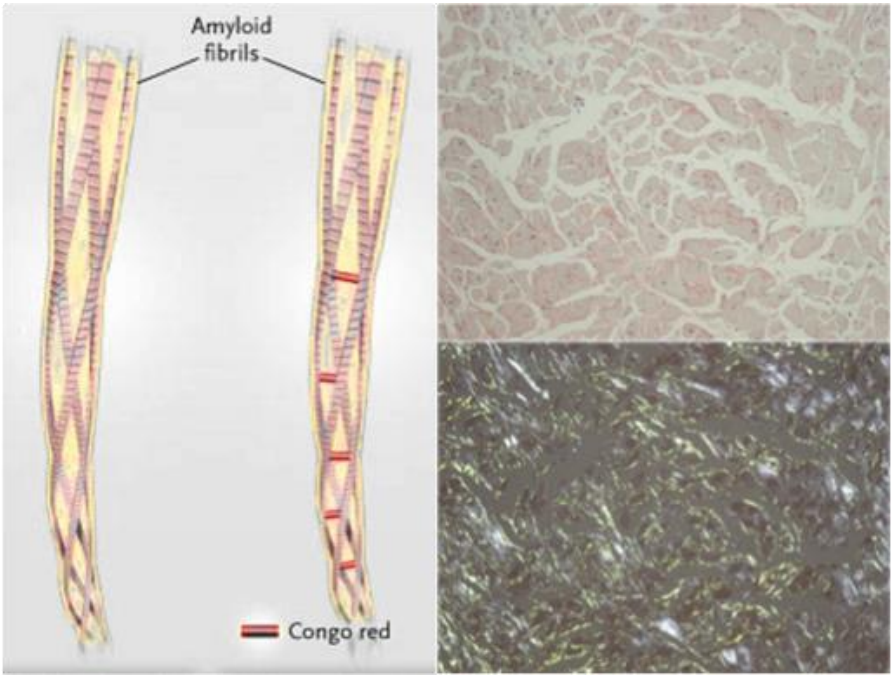

Figure 7. **Congo red mechanism and staining.** Cardiac biopsy from a TTR amyloidosis patient viewed under normal light (top) and polarized light (bottom). Figure adapted from Merlini G & Bellotti V, 2003 and Mangione P et al., 2014.

In conclusion, in order to classify any given protein aggregates as amyloid, three main features need to be displayed:

1. Fibrillar morphology
2. Cross-β structure
3. Characteristic tinctorial properties upon staining with specific dyes.

The fact that we see an heterogeneity in molecular structure, such as the structural positioning of the polypeptide chains within the fibrils (Pedersen JS et al., 2005), is substantially linked to the significant morphological variations that can exist between different fibrils formed from the same peptide or protein. The wide spectrum of structurally different fibrillar aggregates that each protein can form is related to thermodynamic and kinetic factors, which are dominant when the aggregate is being formed (Chiti F & Dobson CM, 2006). Mechanical stress, for example, has been shown to be able to generate fibrils of different molecular structure and/or dimensions even in otherwise identical experimental conditions (Xue WF et al., 2009).

1.7 Amyloid tissue tropism and mechanisms of tissue damage

Which factors drive the specific tissue tropism that different proteins exhibit and why do different mutations of the same protein sometimes lead to different tissue localisation? It is known for example that WT β_2-m preferentially deposits in joints, while the fibrinogen A *α* chain selectively affects the kidneys. It is also known that for example, in familial TTR amyloidosis, individuals with V30M TTR have predominant neuropathic involvement, whereas in individuals expressing the V122I TTR variant cardiomyopathy is the mayor clinical manifestation.

Despite the progress made in the understanding of the disease, in almost every amyloid-related paper we still find the following statement: “the remarkable diversity in organ distribution of amyloid remains one of the most important unsolved problems in amyloid research”.

Aggregation and subsequent deposition of amyloid can take place in the same site of synthesis or it may happen far from the expression site.

There are several factors, which can act favouring the formation of fibrils:

- A high local protein concentration, a short exposure to low pH, increased proteolytic activity as well as the presence of fibril seeds can induce protein aggregation.
- Specific interactions with components of the extracellular matrix, such as tissue glycosaminoglycans and collagen, or cell-surface receptors, such as the receptor for advanced glycation end-products (RAGE), may also determine selective tissue targeting (Stevens FJ & Kisilevsky R, 2000; Yan SD et al., 2000). Furthermore, given that the glycosaminoglycan composition of the extracellular matrix may vary from tissue to tissue, it is possible that this variability influences tissue tropism (Bellotti V et al., 2007).

The mechanism underlying tissue damage is also still being debated: some researchers claim that damaging of tissues and organs is only related to the physical and mechanical stress induced by the presence of the deposits, while others suggest that, in addition to the aforementioned mechanism, the aggregates may also exhibit a cytotoxic effect.

From histological examinations it is evident that the presence of amyloid deposits cause disruption in the tissue structure, which eventually leads to organ dysfunction (Fig. 8). Despite in some cases a prolonged exposure to acquired or hereditary amyloidogenic precursor proteins, the clinical manifestation of the disease only happens when the presence of amyloid deposits becomes demonstrable.

The correlation between total amyloid load and severity of tissue damage differs amongst patients, although, in general, a high amyloid load corresponds with an increased severity of the disease. Clinical data suggest that the stabilisation or reduction of the amyloid burden corresponds to clinical stability or improvement. This observation proves that the presence of amyloid deposits is a necessary condition for the clinical symptoms to manifest (Bjorkman P et al., 1987).

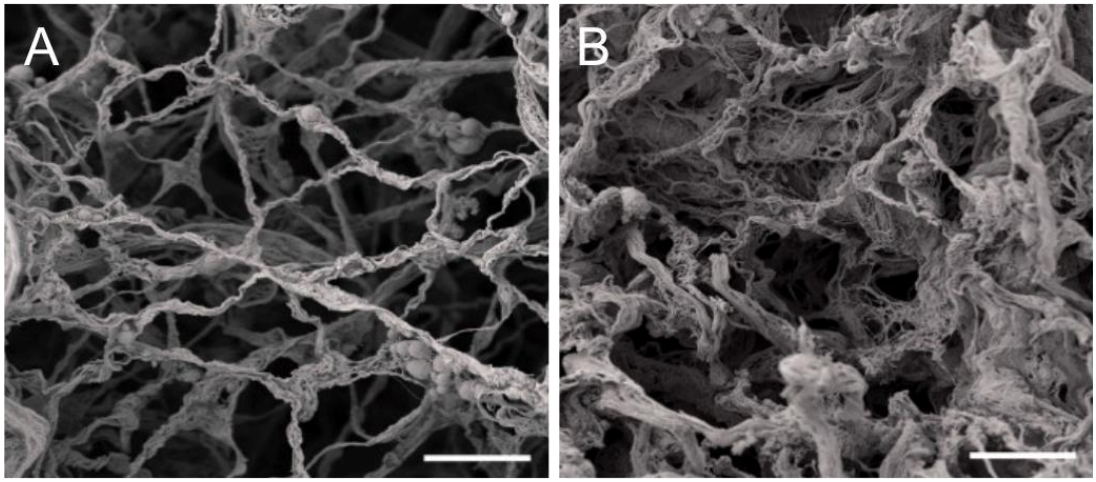

Figure 8. Disruption in the tissue structure caused by amyloid deposition. SEM images of decellularised healthy (A) and amyloidotic (B) mouse liver showing the tissue disruption caused by the presence of amyloid deposits. Scale bar 10 μM. (from Mazza G et al., 2016)

Radford and collaborators have suggested that fragmentation of existing fibrils does not only favour the secondary nucleation pathways, but may also play a role in cytotoxicity. Using fibrils derived from different proteins and fragmenting them to different extents through shaking, they were able to show a correlation between the length of the fibrils and their ability to disrupt cell membrane bilayers and decrease cells viability (Xue WF et al., 2009). Based on these results they have suggested that amyloidogenic precursor proteins, folding intermediates, and protofilaments may exert a cytotoxic effect, which is independent from the amyloid deposits and leads to disease manifestation. Indeed the cytotoxicity of prefibrillar aggregates in recent years has been extensively demonstrated for Aβ (Lambert et al., 1998), TTR (Andersson K et al., 2002), β_2-m (Giorgetti S et al., 2010) and immunoglobulin light chains (Diomede et al., 2014).

The debate is still open and there is no final answer to the question, although it is possible that both amyloid fibrils and prefibrillar species both contribute to tissue damage and disease progression.

1.8 General therapies

The most effective strategy for the treatment of systemic amyloidosis involves the reduction of the levels of amyloid precursor (Merlini G & Bellotti V, 2003). Several studies conducted on AL amyloidosis patients (Comenzo RL et al., 1996; Dember LM et al., 2001) have shown that reduction or elimination of the amyloidogenic clone by chemotherapy improves the function of the affected organs. The same effect has been seen in reactive amyloidosis where the management of the underlying inflammatory disorders can result in regression of the disease.

All the compounds that inhibit the formation of fibril nuclei could prove extremely important in preventing both the deposition of amyloid and in avoiding the cytotoxicity of the soluble oligomers (Findeis MA, 2002; Davis PD et al., 2000). In recent years there has been a growing interest in the design of synthetic peptides that bind natural amyloidogenic peptides preventing further polymerization. Some of these peptides have already been used successfully *in vitro* and in transgenic mice with amyloidosis. Another approach works directly on amyloid deposits targeting the common fibrillar architecture and common protective elements (Pepys MB et al., 2002). Molecules capable of clearing SAP from amyloid deposits or of inhibiting their interaction with glycosaminoglycans have been designed and tested in animal models and clinical trials. Targeting SAP could be a promising strategy as this protein is ubiquitously present in amyloid deposits. Pepys and co-workers have identified a palindromic ligand, named CPHPC, which is able to bind to circulating SAP and induce its decamerization, thus almost completely removing all the circulating protein, without affecting the fraction bound to amyloid fibrils (Pepys MB et al., 2002). The SAP fraction bound to fibrils can then be targeted with a specific monoclonal antibody that localises on the amyloid deposits determining an immune response associated with the recruiting of macrophages and multi-nucleated giant cells (Bodin K et al., 2010). Having removed the circulating SAP, the risk of formation of dangerous immunocomplexes is avoided. The therapy has been tested in both animals and patients affected by systemic amyloidosis, showing

extremely encouraging results (Richards DB et al., 2015; Pepys MB, 2017; Richards DB et al., 2018).

Another innovative approach is immunization against fibrillar proteins in order to increase the clearance of amyloid deposits by increasing the immune response to these aggregates (Merlini G & Bellotti V, 2003).

1.9 Research focus

My PhD studies have been focused on the investigation of the molecular mechanism underlying the conversion of two proteins, TTR and apolipoprotein C-III (apo C-III), from their functional state to pathogenic amyloid fibrils. Thanks to several collaborations I have also had the opportunity to be actively involved in several research projects investigating other amyloidogenic proteins such as ß2-m and α-synuclein, which gave me the opportunity to acquire a general knowledge of the disease and become familiar with different biochemical techniques.

1.10 Transthyretin: roles in human and structure

WT TTR was first identified in 1942 in concentrated cerebrospinal fluid using the Tiselius moving boundary electrophoresis technique (Kabat EA, Moore D, Landow H, 1942) and later by immune-electrophoresis. The presence of WT TTR was soon confirmed in human plasma using several electrophoresis systems based on paper sheet, starch gel, polyacrylamide or reverse-flow electrophoresis.

WT TTR is synthesised by the liver and secreted into the bloodstream, where its concentration is 0.1-0.4 mg/ml (1.8-7.2 µM), depending on factors such as nutritional state, age and sex (lngenbleek T & Young V, 1994). TTR is also synthesised by the choroid plexus and retinal pigment epithelium and then secreted in the cerebrospinal fluid, where the average concentration is 0.017 mg/ml (0.30 µM) and the eye (Jiang X et al., 2001). To a less extent the protein is also synthesised by the α-cells in the Langerhans islets (Jacobsson B et al., 1979). WT TTR was originally called “prealbumin” because it ran faster than albumin on electrophoresis gels, being more anodic than albumin

itself. Its current name originates from its role as thyroxine and retinol transporter.

TTR is in fact the primary carrier of thyroxine in the cerebrospinal fluid, whereas its role as a carrier appears less important in plasma due to the presence of other proteins such as albumin and thyroxine binding globulin (TBG), to which circulating thyroxine almost entirely bind.

TTR is also involved as a carrier of retinol (vitamin A), through its association with retinol-binding protein (RBP) in the blood and the cerebrospinal fluid (Kanai M et al., 1968; Jiang X et al., 2001). The TTR:RBP complex forms in the endoplasmatic reticulum (ER) of the hepatocytes and it exhibits its function in two different ways:

1. It prevents the loss of holo-RBP which, due to its small dimensions (21 kDa), would be excreted by filtration in the kidneys
2. It stabilises the interaction with retinol, thus reducing non-specific release of vitamin A from the complex to receptors other than the target ones.

Measurement of TTR concentration in the blood is also used in medicine as a marker to determine the nutritional status of an individual. Alterations in nutrients supply are quickly counteracted by the visceral compartment and TTR synthesis can be significantly reduced by cytokine-directed orchestration with a redistribution of organ and tissue protein pool (lngenbleek T & Young V, 1994), making it a good indicator of a malnourished patient (Marik PE & Bedigian MK, 1996). Indeed TTR is characterised by a short half-life, although this can sometimes be misleading as its concentration more closely reflects recent dietary intake rather than overall nutritional status (Shenkin A, 2006).

WT TTR is a 55 kDa homotetrameric (Hamilton JA & Benson MD, 2001) protein with a dimer of dimers quaternary structure. Each monomer is a 127-residue polypeptide in which approximately 55% of the amino acids are engaged in the formation of beta sheet structure. Each subunit contains two extended eight-pleated sheets (DAGH and CBEF), each of which comprises four strands (eight in total and named A, B, C, D, E, F, G, and H) with

antiparallel orientation. The structure also contains a short segment of α-helix quaternary structure to which only 5% of the residues contribute. Overall TTR has the shape of a globular protein with a size of 70 Å × 55 Å × 50 Å (Ingenbleek T & Young V, 1994). The crystal structure of this protein was first solved by Blake and collaborators (Blake CC et al., 1978) and is now known to 1.3 Å resolution. Each monomer consists of eight β-strands, named A-H, which are interconnected by loops. A short helix (EF-helix) is located between strands E and F (Palaninathan SK et al., 2012). The β-strands are arranged as a β-sheet sandwich. The core of the protein is generated by the face-to-face interaction of the inner four-stranded β-sheet, formed by strands DAGH, with the outer four-stranded β-sheet, formed by strands CBEF. Two monomers originate a dimer, which is stabilised through H-bonds originated between strands H-H^{I} and F-F^{I}. As a single unit, the TTR dimer is characterised by an inner eight-stranded β-sheet originated by strands DAGHH^{I}G^{I}A^{I}D^{I} and a solvent-exposed outer β-sheet formed by strands CBEFF^{I}E^{I}B^{I}C^{I}. The fully folded TTR homotetramer, characterised by a slight rotation of the dimers in relation to each other along the y axis, originates from the association of two dimers that is mainly stabilised through hydrophobic interactions between loops AB and A^{I}B^{I} as well as loops GH and G^{I}H^{I} (Fig. 9). The folded tetramer is highly stable and possesses an outstanding resistance to most alkaline/acid solutions and denaturating agents.

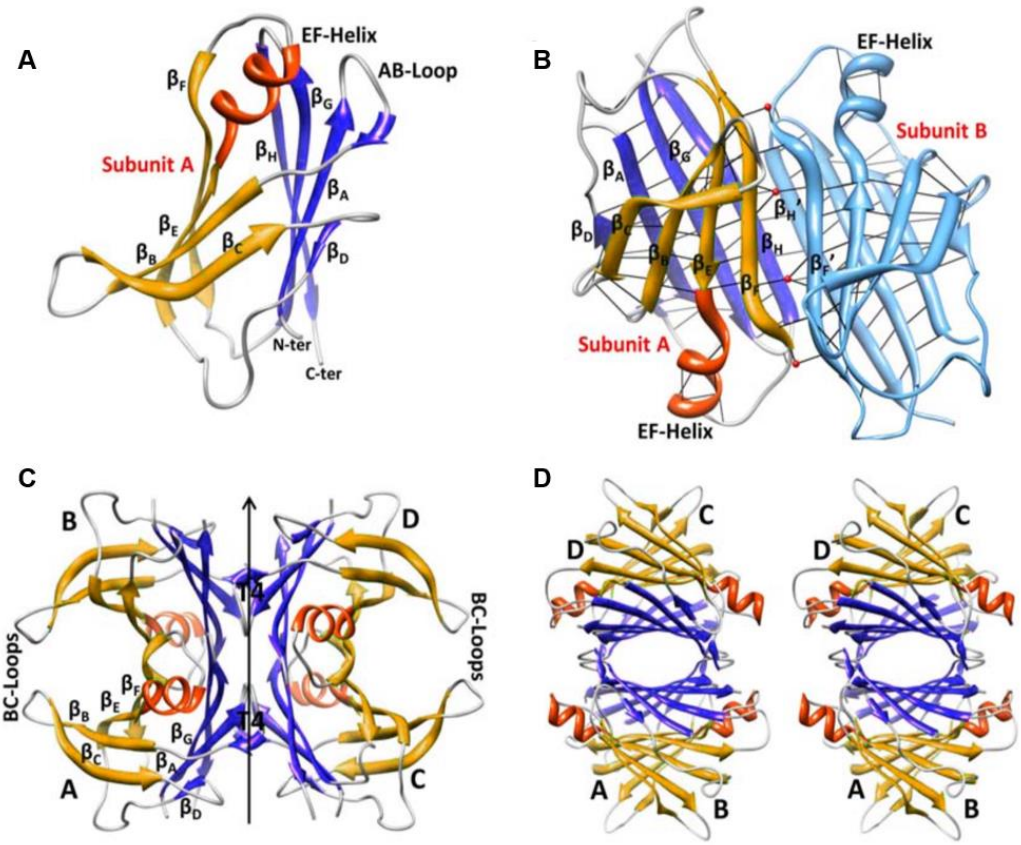

Figure 9. TTR structure. A) TTR monomer with the β-strands indicated. B) TTR dimer. The H-bonds between the strands are shown in black. The red balls indicate water molecules. C) TTR tetramer with the β-strands from one monomer indicated. D) Side view of the TTR tetramer showing the T4 binding pockets and the central channel. For reference, β-sheet DAGHH^{I}G^{I}A^{I}D^{I} is colored in blue, β-sheet CBEFF^{I}E^{I}B^{I}C^{I} is shown in orange and EF-helix in red. Figure adapted from Palaninathan SK, 2012.

Native WT TTR features an open channel whose internal wall is formed by inner sheets and where the two binding sites for thyroid hormones (T4) are located (Wojtczak A et al, 1996; Johnson SM et al, 2005). These binding sites are interrelated by the phenomenon of negative cooperativity, which implies that when one binding site is occupied by a first thyroid molecule, the association constant (K_a) for the second thyroid molecule is drastically reduced (Ingenbleek T & Young V, 1994; Blake CC et al, 1978; Nencetti S &

Orlandini E, 2012). Each T4 binding site is characterised by two symmetric sub-sites, which consist of a small inner binding pocket and a large outer one, comprising three halogen binding pockets named HBP1, HBP2 and HPB3 (Fig. 10), which are defined by the following residues:

- HBP1, the wide outer pocked is formed by residues M13, K15, L17, T106, A108.
- HBP2 comprises residues L17, A108, A109, L110, V121
- HBP3, the inner pocket, is composed by A108, L110, S117 and T119.

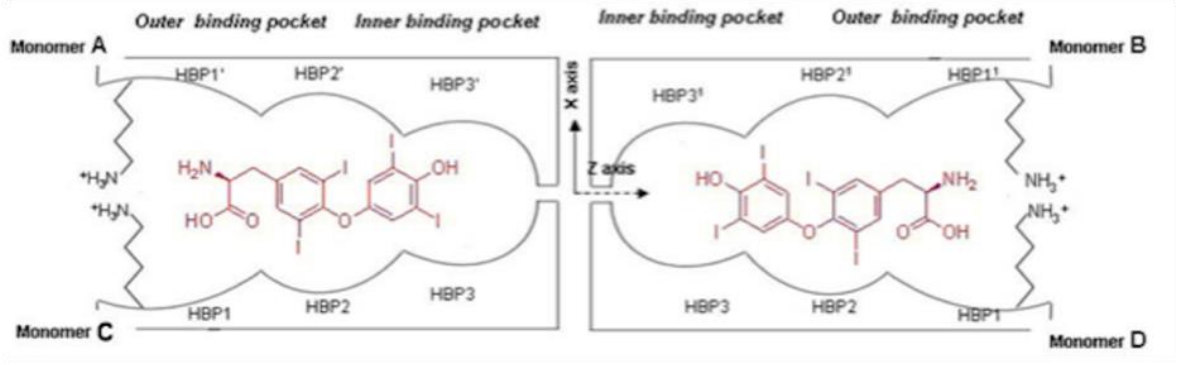

Figure 10. T4 binding site. Schematic representation of the thyroxine binding site showing the outer and inner binding pockets (adapted from Nencetti S & Orlandini E, 2012).

The equimolar interaction with retinol binding protein (RBP), mainly involves the region loop E–α-helix–loop F, even though Leelawatwattana and colleagues have shown that the N-terminal region might also play a role in the formation of the TTR-RBP complex (Leelawatwattana C et al., 2011).
Interestingly, although some minor differences are present, the protein is highly conserved in the animal kingdom, showing the same number of amino acids in the monomer sequence as well as the same tetrameric assembly in several species.

1.11 TTR amyloidosis

Amyloidogenicity is an inherent property of WT TTR, which is responsible for the formation of microscopic and clinically silent amyloid deposits in the heart and blood vessels wall of 10-25% of the population over age 80 (Kolstoe SE et al., 2010; Cornwell GG & Westermark P, 1990; Sletten K et al., 1980). In addition, 77 different sites of mutation have been observed on the TTR gene, encoding for over 100 TTR variants affecting about 10,000 individuals worldwide. These mutations may affect the binding with thyroxine (G6S, A109T TTR) or may not be associated with amyloid deposition (T119M, P102R TTR), although in most cases they determine a reduction of the protein thermodynamic stability and are therefore associated with an increased aggregation propensity in the extracellular space. A complete list including all the TTR variants identified so far is available at http://amyloidosismutations.com/attr.html.

Patients affected by familial diseases are heterozygous, expressing both WT and variant protein, which therefore associate to generate hybrid TTR tetramers, which are less stable than their WT counterparts. This difference in tetramer stability and tendency to dissociate could, according to one of the mechanisms proposed for TTR amyloidogenesis, explain the presence of mainly variant protein in the amyloid deposits of these patients (Dwulet FE & Benson MD, 1983; Dwulet FE and Benson MD, 1984; Wallace et al., 1986; Sekijima et al., 2005; see paragraph 1.13). In recent years familial amyloidosis have become less rare, suggesting an underestimation of these pathologies in the past (Nencetti S & Orlandini S, 2012). Despite the increasing number of reported cases, though, the vast majority of these mutations remain very rare entities (Dwulet FE & Benson MD, 1983; Erikkson M et al., 2009).

Hereditary TTR amyloidosis (ATTR) is fatal within 5-15 years from the diagnosis (Kolstoe S et al., 2010). The clinical phenotype varies depending on the TTR variant involved in the amyloid deposition and ranges from mainly peripheral and autonomic neuropathy to blindness, renal failure and cardiomyopathy (Benson MD, 1989; Westermark P et al., 1990). Also the

severity of disease greatly depends on the variant protein involved, with some mutations causing more aggressive clinical phenotypes in the first or second decade of life, and others being more benign.

Four different type of TTR amyloidosis have been described so far (Table 3):

- WT TTR amyloidosis, previously known as senile systemic amyloidosis (SSA). The name has recently been changed due to younger patients presenting with WT TTR deposition (Sipe JD et al., 2016). This type of amyloidosis is caused by massive cardiac deposition of WT TTR (Ando Y & Suhr OB, 1998), predominantly in males rather than females, causing intractable heart failure. Due to global aging in the population, it is likely that this form of TTR amyloidosis will show an increasing trend in terms of number of patients diagnosed every year.
- Familial amyloid cardiomyopathy (FAC) is caused by different TTR variants, amongst which the most common is the V122I variant where a residue of valine in position 122 is replaced by isoleucine and which is carried by 4% of the African-American population, but is also expressed in African and Afro-Caribbean ethnic groups (Kolstoe SE et al., 2010; Jacobson DR et al., 1997). The clinical phenotype is characterised by the presence of extensive amyloid deposits in the heart. A recent study highlighted a higher incidence of heart failure amongst the carriers of the mutation, although the mortality appeared comparable to that of non-carriers over long-term follow-up (Quarta CC et al., 2015).
- Familial amyloid polyneuropathy (FAP) is an autosomal dominant hereditary amyloidosis whose symptoms, which include polyneuropathy and/or organ dysfunction, manifest between the third and seventh decade, despite the amyloidogenic protein being present at birth (Saraiva MJ, 1991). One of the most common mutations associated with FAP is generated by replacement of valine by methionine at position 30 (V30M TTR). This mutation is commonly found in the Portuguese, Japanese and Swedish population (Saraiva

MJ et al., 1984; Tawara S et al., 1983; Dwulet FE & Benson MD, 1984; Westermark P, 1990; Saraiva MJ, 1995).

- Central nervous system-selective amyloidosis (CNSA), caused by the highly destabilised A25T TTR variant, is less common than TTR systemic amyloidosis possibly because TTR concentration in the CSF is significantly lower than in plasma, thus reducing its tendency to self-assemble.

Table 3. The most common TTR amyloidosis and age of onset (Nencetti S & Orlandini E, 2012)

	Clinical Classification	**Age of Appeareance**	**TTR Type**	**Geographical Area of Impact**
WT TTR amyloidosis	Cardiomyopathy	>60	WT TTR	Worldwide (elderly population)
FAC	Cardiomyopathy	>65	V122I TTR	African-Americans, African, Afro-Caribbean
FAP	Peripheral neuropathy	30-80	V30M TTR	Europe (mainly Portugal and Sweden), Japan
FAP	Peripheral neuropathy and/or cardiomyopathy	>50	Non V30M	Worldwide
CNSA	CNS amyloidosis	<50	A25T, D18G TTR	Worldwide (rare)

TTR amyloidosis, considering both its acquired (WT TTR) and hereditary (TTR variants) forms, represents the second most common form of systemic amyloidosis after AL amyloidosis and the number of people affected by WT TTR amyloidosis is only destined to increase in the next decades due to the overall increase in life expectancy.

1.12 Liver transplant as a therapeutic approach for the treatment of TTR amyloidosis

Considering that the liver represents the major site of TTR synthesis, liver transplantation is an effective therapeutic approach to ameliorate TTR amyloidosis, mainly for FAP patients (Holmgren G et al., 1993). The rationale behind this approach is based on the replacement of a liver containing a mutant TTR gene with a normal gene, thus reducing the mutant TTR levels in the body to < 5% of pre-transplant levels. Although this approach has been generally successful, there have been some rare cases in which the progression of the disease has accelerated following the surgical procedure (Okamoto S et al., 2011). It has also been shown that in some elderly patients, TTR deposition continues even after liver transplantation (Holmgren G et al., 1993; Ando Y et al., 1995). Furthermore, this invasive therapy has not proven successful for the treatment of WT TTR amyloidosis, where there is no mutant protein to be replaced, some forms of FAP, involving mutations other than V30M, and CNSA forms, where TTR is not synthesised by the liver, but from an independent organ (Nencetti S & Orlandini E, 2012). In addition, other elements, such as the fibril composition, play a crucial role in determining the success of this therapeutic approach (see paragraph 1.15).

If we also consider that transplantation needs organs to be transplanted and, in case of a successful operation, the patient has to be treated with immunosuppressive drugs to prevent any immune system reactions, it appears clear why, in the last decade, a great interest has risen in order to find alternative therapeutic strategies for the treatment of these diseases.

1.13 Kelly's widely accepted mechanism of TTR fibrillogenesis and its implications in drug discovery

In 1992 Prof Jeffrey Kelly and collaborators suggested a possible mechanism to describe TTR amyloidogenesis, which was based on *in vitro* experiments performed at non-physiological acidic pH. This mechanism highlights the role of tetramer dissociation as the crucial rate-limiting step in the process leading to fibril formation. Partial unfolding of the monomers, which follows tetramer

dissociation, (Colon W & Kelly JW, 1992; Hammarstrom P et al., 2002; Lai Z et al., 1996; Hursham AR et al., 2004; Sekijima et al., 2005; Quintas A et al., 2001; Foss TR et al., 2005) can then promote further disassembly and formation of soluble oligomers and amyloid fibrils through a favourite thermodynamic downhill process (Fig. 11).

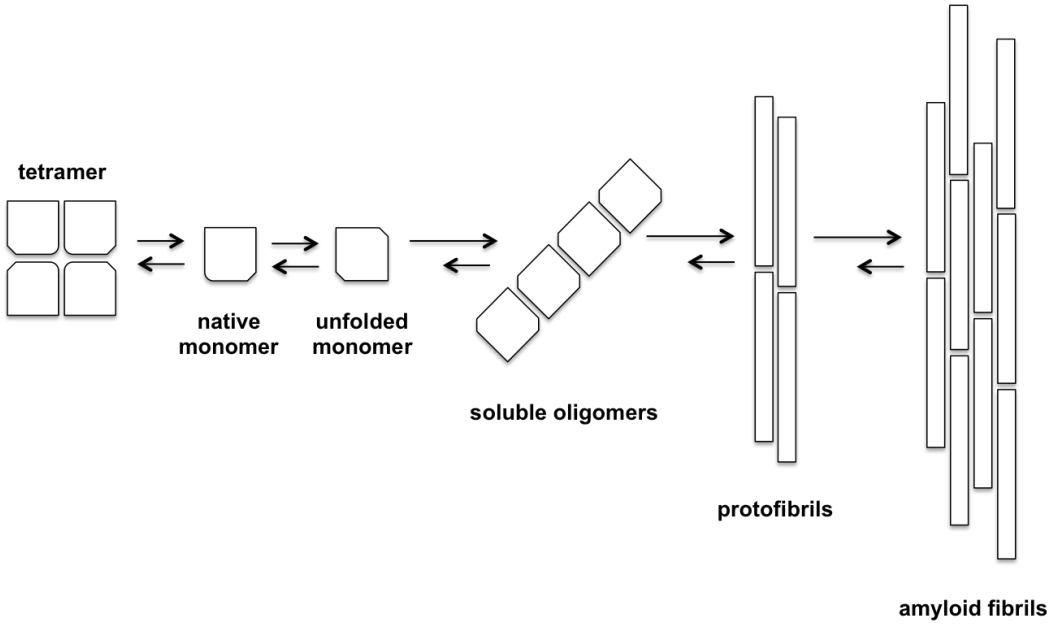

Figure 11. Schematic representation of Kelly's mechanism (adapted from Nencetti S & Orlandini E, 2012).

It has been shown that engineered monomers, which are not amyloidogenic as such, can rapidly aggregate into amyloid-like fibrils if they undergo partial denaturation, such as the one obtained at low pH (Jiang X et al., 2001).

According to this mechanism, the effect of mutations is, usually, the destabilisation of the tetramer, which is associated with an increased velocity of rate-limiting tetramer dissociation and increased rate of fibril formation (Jiang X, 2001; Sekijima Y et al., 2005; Johnson SM et al., 2005; Hurshman AR et al., 2004). Tetrameric WT TTR, although stable (Lai Z et al., 1997), can itself dissociate to form amyloid fibrils as evident in WT TTR amyloidosis.

Although widely accepted, the mechanism does not explain in which compartment, *in vivo*, the protein would be exposed for a long time to low pH, such to induce tetramer dissociation. This mechanism does also not explain

the fact that, as observed in many cases, TTR amyloid fibrils contain proteolytic fragments as main components and not only the full length protein. Furthermore the amyloid-like material obtained in vitro after prolonged incubation at low pH is mostly amorphous and contains only a small proportion of amyloid-like fibrils when analysed by EM and AFM. Congo red staining also suggests low abundance of amyloid fibrils.

Nevertheless, despite these discrepancies between *in vitro* and *in vivo* aggregates, Kelly's mechanism has been generally accepted. It has indeed been the reference method used to investigate the effect of small molecules, analogues of thyroxine, which have been designed and developed to act as inhibitors of TTR amyloidogensis at low pH, following the observation that the natural ligand T4 stabilises the TTR tetramer and reduces its dissociation (see chapter 4).

1.14 Development of new therapeutic strategies

Next to the screening of small ligands, more precisely described in chapter 4, in the past years the use of small interfering RNAs, siRNA (Alnylam) and antisense oligonucleotide, ASOs (Ionis Pharmaceuticals) to knock out hepatic synthesis of TTR (Arsequell G et al., 2012) has been proposed as a possible therapeutic tool.

Both siRNA and ASOs have undergone extensive clinical trials, which showed positive results in terms of suppression of TTR synthesis by blocking the translation of mRNA on the ribosome.

Alnylam developed a double stranded RNA molecule, which specifically matches a sequence located in the non-translated 3^{I} region of TTR mRNA and is able to stop the synthesis of both WT and mutant TTR. The molecules are administered by injection and formulated in lipid nanoparticles, which are captured by the hepatocytes via the LDL receptor. The siRNA are then released in the cytosol of the hepatocytes where they can inhibit TTR mRNA translation on the ribosome. This formulation (ALN-TTR02 or Patisiran) was successful in pre-clinical phase I and II. A phase III study has been completed, showing that the drug is well tolerated by patients with FAP and

causes a concentration-dependent knock-down of TTR production. Prolonged administration of Patisiran induced a 91 % reduction of TTR synthesis in comparison with normal levels and determined an improvement of the polyneuropathy symptoms. As a result of these studies, the drug has been approved for marketing by the FDA (trial NCT02939820).

ASOs, developed by Ionis Pharmaceuticals, are providing similar results with a knockdown of TTR expression >90% in 4 weeks. This drug has undergone a phase III trial to evaluate its safety and toxicity (trial NCT01737398), showing some positive results.

1.15 Role of proteolysis and heterogeneity of TTR amyloid fibrils

Despite being widely accepted, Kelly's mechanism has been debated over the years as it does not take into account the role of post-translational modifications (Westermark P et al., 1996) and, in particular, the role of proteolysis in TTR amyloidosis. Indeed Lundgren's group, analysing the composition of *ex vivo* fibrils, has highlighted in most cases the presence of both full length TTR and a C-terminal fragment, 49-127, originating from proteolytic cleavage of the peptide bond Lys48-Thr49 (Thylén C et al., 2005). The culprit protease responsible for the cleavage has not yet been identified, but the selectivity of the cleavage suggests that it may belong to the class of serine proteases with a specificity similar to trypsin. At the same time Westermark and collaborators have characterised the composition of ex vivo fibrils extracted from WT TTR amyloidosis and FAP patients and have identified two distinct categories (Bergström J et al., 2005; Ihse E et al., 2013), defined as pattern A and pattern B, which are distinguishable from a morphological, histochemical, immunological and structural point of view (Fig. 12).

- Type A fibrils, observed in patients with WT TTR amyloidosis and FAP, show faint color and apple green birefringence upon staining with Congo red (Ihse E et al., 2013). They appear as large nodules in the sub-endocardial, sub-epicardial and myocardial tissue. Interstitial deposits, such as the ones found in blood vessels, are diffuse and homogeneous

and often replace the normal tissue architecture. Ultrastructural analysis using electron microscopy depicts type A fibrils as short and highly packed with a random distribution within the tissue. A close investigation of their composition shows the presence of a high proportion of C-terminal fragments together with the *full length* monomer.

- Type B fibrils, only present in patients with FAP, show intense Congo red staining and birefringence. The fibrils appearance is granular and the localization is the sub-endocardial and sub-epicardial tissue; similar deposits are also found in the walls of the blood vessels. Bundles of fibrils are sometimes found penetrating deeply into cardiac myocytes and appear structured in smaller deposits rather than big homogeneous ones (Bergström J et al., 2005). EM shows long and straight fibrils often aligned parallel to each other and arranged into bundles (Ihse E et al., 2013) that can sometimes deeply penetrate within the myocytes. Such deposits only consist of full length monomeric TTR (Yazaki M et al., 2000; Yazaki M et al., 2003; Cornwell GG et al., 1987; Bergstrom J et al., 2005).

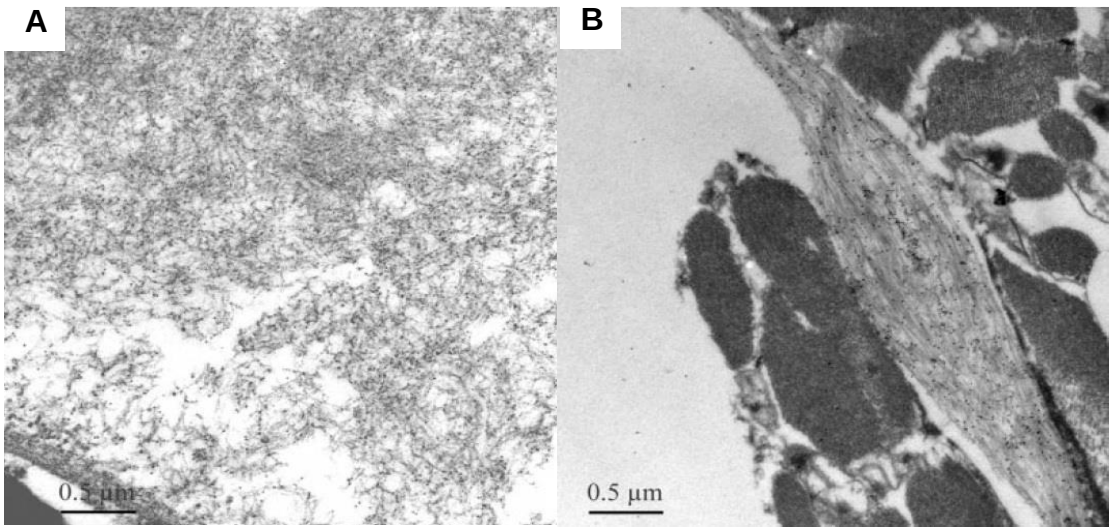

Figure 12. Electron microscopy of TTR fibrils. Different organisation and localisation within the tissue of type A (A) and type B (B) TTR fibrils as shown in electron microscopy. Type A fibrils appear short and highly packed, while type B are long and straight fibrils often aligned parallel to each other and arranged into bundles (images from Bergstrom J et al., 2005).

The presence of truncated fragments in the type A pattern is apparently not influenced by the nature or position of the eventual amino acidic substitution, but it seems to correlate well with the abundance of the cardiac deposits (Ihse E et al., 2008), the increased left ventricular wall thickness, the age of the patients (>50) and the late onset of the disease, being most common in patients affected by WT TTR amyloidosis (Cornwell GG et al., 1987; Cornwell GG et al., 1988; Gustavsson A et al., 1995; Felding P et al., 1985). Furthermore the possible pathogenic role of proteolysis is suggested by the clinical prognosis of patients affected by hereditary TTR amyloidosis who undergo liver transplant in order to replace the production of variant TTR with WT protein. Patients with type A fibrils in their cardiac deposits (Pras M et al., 1984; Pras M et al., 1980; Thylen C et al., 1993; Ando Y et al., 1999) generally show a negative response and an accelerated progression of the disease upon liver transplantation (Gustafsson S *et al*, 2012). The two different patterns might suggest the presence of two distinct mechanism of amyloid formation (Bergstrom J et al., 2005). It is thought that TTR fragmentation takes place locally in the interstitial space before fibrils are formed. Indeed if fragmentation was taking place once the fibrils are formed, also the N-terminal fragment should be found in equal amount in the amyloid deposit.

1.16 First description of the mechano-enzymatic mechanism for TTR amyloidogenesis

The S52P TTR variant has been identified at the UCL Centre for Amyloidosis and Acute Phase Proteins directed by Professor Philip Hawkins and based at the Royal Free Hospital. This variant is associated with the most aggressive clinical phenotype so far described for familial TTR amyloidosis. S52P TTR was identified in an English family and is indeed responsible for a severe form of autosomal-dominant hereditary systemic amyloidosis characterised by early onset (Mangione PP et al., 2014). The patients, who are heterozygous for the specific mutation, developed autonomic dysfunction and polyneuropathy in the third decade, followed by cardiomyopathy, euthyroid

multinodular goiter and sicca syndrome. ^{123}I labelled SAP scintigraphy highlighted the presence of vast amyloid deposits in the liver, spleen, kidneys and adrenal glands, while cardiac function examinations showed an infiltrative restrictive cardiomyopathy with well-preserved ventricular function. Abundant TTR amyloid deposits were found in an endomyocardial biopsy. Immunohistochemistry analysis of *ex vivo* fibrils has identified TTR as the protein responsible for amyloid deposition and subsequent gene sequencing showed that the patients were heterozygous for a mutation, which determines the substitution of a serine residue in position 52 with a proline. Biochemical analysis of the *ex vivo* fibrils classified them as type A (Gustavsson A et al., 1991; Gustavsson A et al., 1995; Bergstrom J et al., 2005) and showed the presence of full length monomers from both variant and WT TTR (Mangione PP et al., 2014) and fragment 49-127 originated only from the variant.

Professor Bellotti's group has characterised the stability of the S52P variant showing that the tetramer was highly destabilised with respect to its WT counterpart as often observed for amyloidogenic variants of TTR. While limited proteolysis analysis performed on WT TTR in the presence of trypsin showed stability against proteolysis, the same analysis performed on the S52P variant showed an enhanced susceptibility to proteolysis with formation of several TTR fragments amongst which the most abundant are 16-127, 49-127 and 81-127 which is a secondary product of digestion. To date no other known amyloidogenic variant has shown the same susceptibility to proteolytic cleavage *in vitro*.

X-ray crystallography did not suggest an increased susceptibility to proteolysis related to structural differences between variant and WT TTR, as their structures appeared almost completely superimposable (Fig. 13). This striking structural similarity, also observed for other TTR variants, could explain the failure of the intracellular quality control system in preventing the release of the variant in the extracellular space (Palanitnathan SK, 2012). The region affected by the mutation, represented by the type 1 β-turn connecting β-sheets C and D, showed a partial loss of the H-bond network.

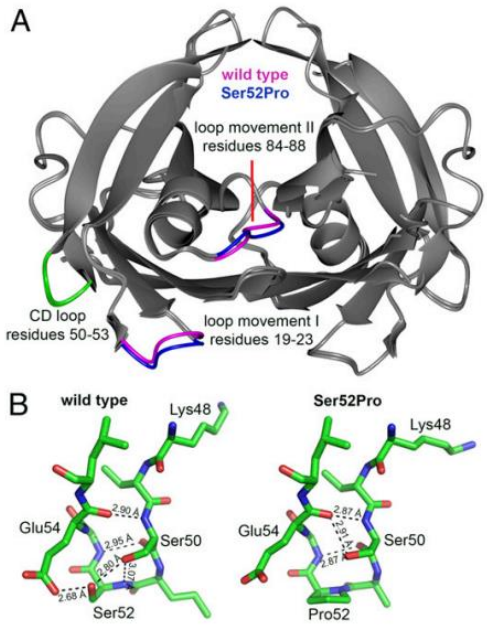

Figure 13. **WT and S52P TTR structural comparison** (A) Structural similarities between WT and S52P TTR. (B) Detail of the H-bond network in the CD loop region. Some bonds are lost due to the substitution of serine 52 with a proline (Mangione PP et al., 2014).

Our group has suggested that the disruption of the H-bond network determines a destabilisation of the CD loop which results in an increased susceptibility to proteolytic cleavage (Mangione PP et al., 2014) and subsequent tetramer destabilisation followed by dissociation and amyloid fibril formation.

It was also shown that proteolysis in not sufficient, although necessary to achieve fibrillogenesis: it is indeed possible to cleave the S52P variant in the absence of shaking, avoiding amyloid formation (like in limited proteolysis experiments). Shaking alone in the absence of proteolysis has given the same result with no aggregation observed. On the other hand, the combination of shaking and proteolysis has been shown to rapidly induce an increase of the ThT emission signal, corresponding to the rapid formation of amyloid fibrils (Fig. 14). The simultaneous presence of proteolysis and

mechanical forces has led to the definition of mechano-enzymatic mechanism for TTR amyloidogenesis.

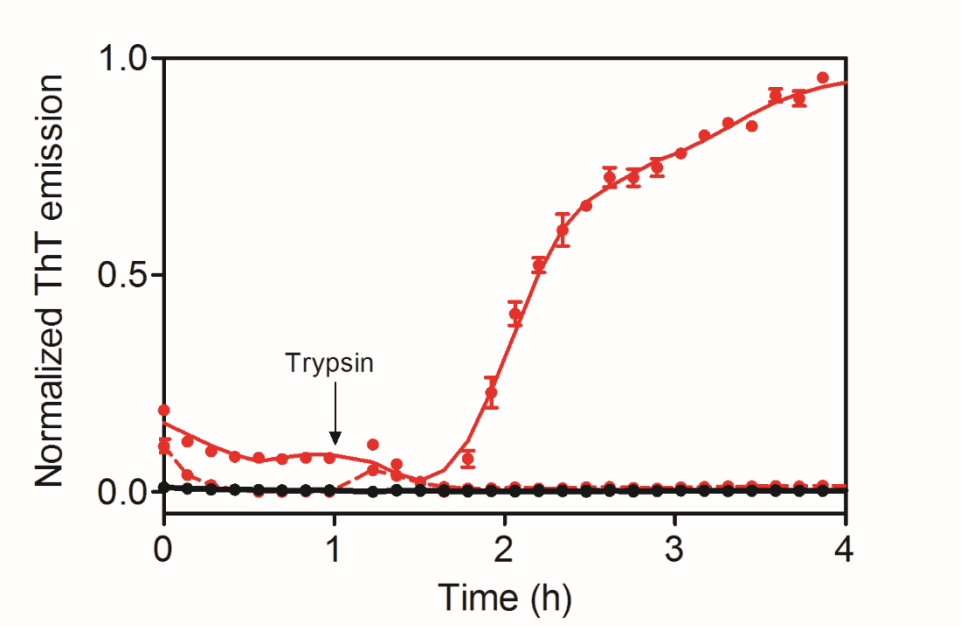

Figure 14. Aggregation of S52P TTR. Fibrillogenesis of S52P TTR in the presence (solid red) and absence (dashed red) of trypsin 5 ng/µl or with agitation only (black) (Mangione PP et al., 2014).

1.17 Mechano-enzymatic cleavage and aggregation of other TTR variants

When I joined Professor Bellotti's group, before starting my PhD, I was actively involved in a series of studies that aimed to find the correct experimental conditions required to achieve cleavage of TTR variants other than S52P.

Since the first experiments performed in 96-well plates, it was clear that no cleavage and subsequent aggregation was taking place, suggesting that forces of higher intensity were necessary to partially unfold the more stable variants and predispose them to proteolysis and aggregation. As previously shown by the Bellotti group on β_2-m (Mangione PP et al., 2013), the role played by hydrophobic-hydrophilic interfaces in promoting aggregation is crucial. Bearing in mind the lesson from β_2-m, we applied the same concept to TTR and increased the air water interface area by moving from 96-well

plates to glass vials in which agitation was generated by a magnetic bar and which were characterised by a much larger air-water interface area. Under these new experimental conditions, aggregation was achieved for several TTR variants, including the WT protein. The variant T119M TTR, which is known to have a stabilising effect on the tetramer and by doing so protects people carrying both the T119M and V30M mutation from developing the polyneuropathy caused by the latter (Hammarström P et al., 2003), was not cleaved even in the presence of forces of higher intensity (Fig. 15).

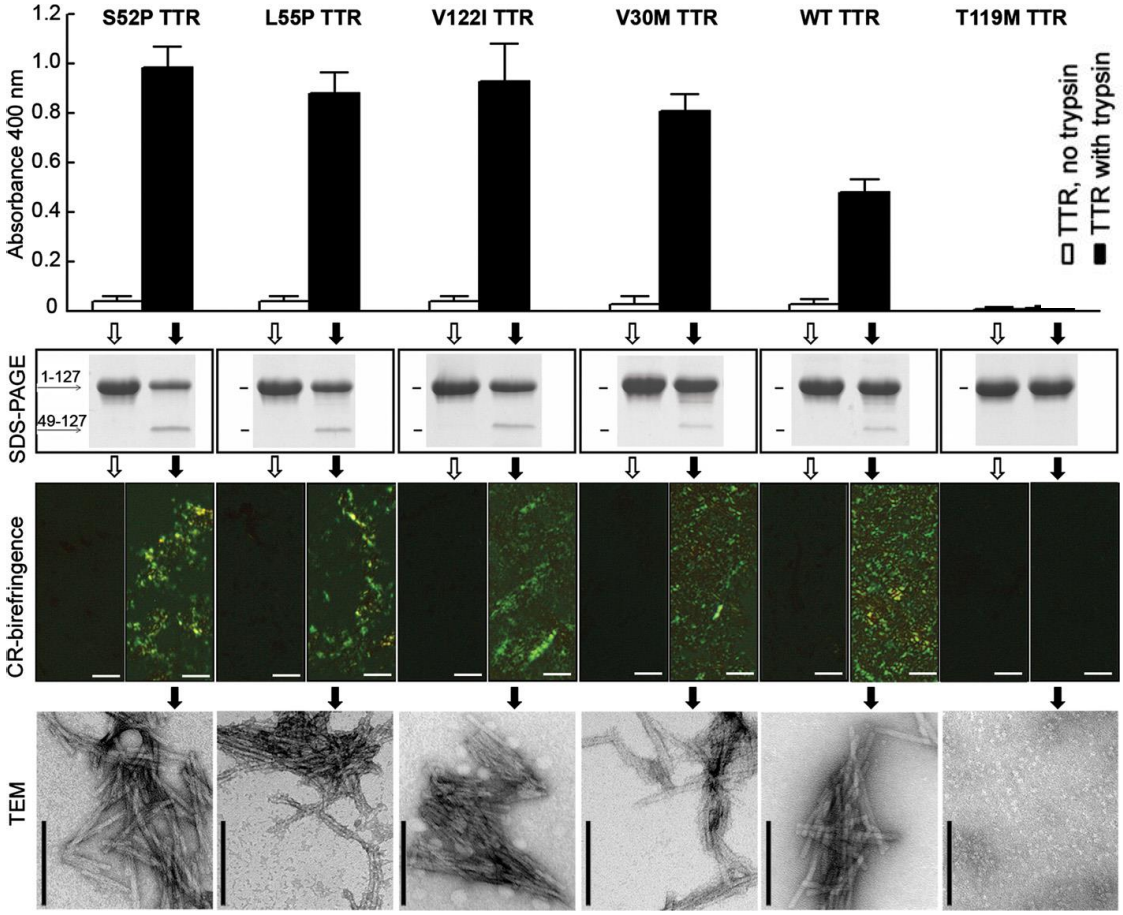

Figure 15. **Fibrillogenesis of amyloidogenic TTR variants.** S52P, L55P, V122I, V30M and WT TTR aggregate in the presence of trypsin under vigorous agitation in the presence of a hydrophobic-hydrophilic interface as monitored by turbidity at 400 nm; selective proteolytic cleavage is shown in the SDS-PAGE. The protective T119M variant did not undergo cleavage or aggregation. Amyloid fibrils formed by all the variants, except T119M TTR, are characterised by light microscopy of CR stained samples under cross-polarised light and EM (Marcoux J et al., 2015).

Interestingly our data showed that different variants exhibited different susceptibility to proteolysis, but no work had been done to try and explain the reasons behind this behavior.
Furthermore, the possibility to obtain genuine amyloid fibrils from several TTR variants, as opposed to mostly amorphous amyloid-like aggregates obtained after long incubation at low pH, stressed the importance of the mechano-enzymatic mechanism as a possible mechanism acting *in vivo*.

1.18 apolipoprotein C-III: functions and structure

Apolipoprotein C-III (apo C-III) is a small protein with a calculated molecular weight of 8754 Da, comprising 79 amino acid residues. It is the most abundant component of the Cs apolipoproteins family (~12 mg/dl plasma). Post translational modifications determine the presence in the plasma of three different isosforms, apo C-III_0, apo C-III_1 and apo C-III_2, characterised by a different number of O-linked sialic acid molecules, indicated by the subscript, attached to threonine 74 (Brewer HB et al., 1974). Interestingly not much is known about the rate of sialylation of apo C-III in diseased patients.
Apo C-III normally circulates in the plasma in association with very low-density lipoproteins (VLDL) and high-density lipoproteins (HDL) (Havel RJ et al., 1973). In recent years its crucial role in the homeostasis of plasma triglycerides has been highlighted and it has been reported as a potential cardiovascular risk factor, suggesting that downregulation of apo C-III expression may have a cardiovasculo-protective effect (Ooi EM et al., 2008).
Although much is still unknown regarding all the roles played by this small exchangeable apolipoprotein, some of its biological functions have been determined and investigated.

Inhibition of lipoprotein lipase activity. Apo C-III has an inhibitory effect on the activity of lipoprotein lipase (LPL), which resides on cell surfaces and normally catalyses the first step of triglyceride-rich lipoprotein lipolysis. The inhibition can take place through three distinct mechanisms involving (I) the displacement of apolipoprotein E (apo E) from the lipid particles or the

induction of structural changes on apo E; (II) the displacement of apolipoprotein C-II (apo C-II), which directly activates LPL, from the lipoprotein surface; (III) the prevention of the interaction between lipoproteins and the negatively charged cell surface. Suggestions have also been made on a possible direct interaction of apo C-III with LPL (Gangabadage CS et al., 2008).

Inhibition of the uptake of triglyceride-rich lipoprotein remnants by the low density lipoprotein (LDL) receptor. This effect appears as a result of the displacement by apo C-III of apo E and apo B from lipoprotein particles, thus impeding the binding to the specific receptor.
As a consequence, triglyceride-rich lipoprotein remnants increase their residence time in the circulation.

Interaction with the high density lipoprotein (HDL) receptor. Apo C-III strongly interacts with the HDL receptor, which normally binds a variety of lipoproteins also including apo E, apo D and apo A-I (Xu S et al., 1997).
It has been shown that apo C-III deficiency correlates well with high levels of plasma HDL cholesterol and a general atheroprotective profile with reduced risk of ischaemic cardiovascular disease (Crosby J et al., 2014; Jorgensen AB et al., 2014).

From a structural point of view in its lipid-free state, apo C-III belongs to the class of the so-called natively unfolded proteins, meaning that it lacks a well-defined secondary and tertiary structure.
When the protein is bound to lipids, on the contrary, it folds and is composed of six amphipathic α-helices, which represent the typical structural motif shared across exchangeable apolipoproteins (Fig. 16).

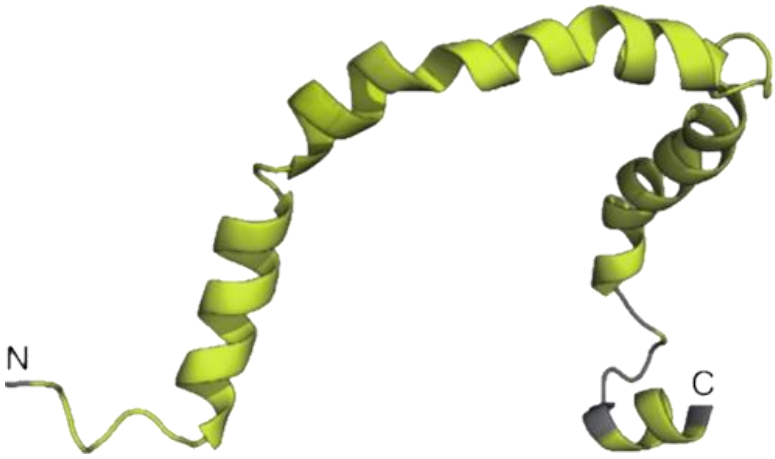

Figure 16. Lipid bound structure of apo C-III. PDB code: pdb2jq3

1.19 apo C-III amyloidosis

The reduced conformational stability associated with the lipid-free state has long been associated with a tendency to self-assembly and generate cross-ß rich insoluble aggregates.

In particular amyloid formation both *in vitro* and *in vivo* has been observed for WT and/or variants of apo A-I (Nichols WC et al., 1988; Booth DR et al., 1995; Booth DR et al., 1996; Genschel J et al., 1998; de Sousa MM et al., 2000; Benson MD et al., 2001; Eriksson M et al., 2009), apo A-II (Benson MD et al., 2001), apo A-IV (Sethi S et al., 2012) and apo C-II (Nasr SH, 2017).

Despite the identification of several mutations on the apo C-III gene (Crosby J et al., 2014), no amyloid deposition associated with apo C-III had previously been described.

Only recently the group led by Professor Sophie Valleix in Paris has identified the first ever amyloidogenic variant of apo C-III, characterised by the substitution in position 25 of an aspartic acid residue with a valine. The mutation was identified in a French family whose members, heterozygous for the mutation, suffered of a severe form of amyloidosis characterised by sicca syndrome in the first place, ultimately developing into hypertension, Raynaud phenomenon and chronic kidney disease with mild proteinuria (Valleix S et

al., 2016). Amyloid deposition, confirmed by SAP scintigraphy and immunohistochemistry, was diffuse and found in several places including salivary glands, heart, bronchi and mainly kidneys. Mass spectrometry analysis revealed the presence of only the variant inside the deposits. The severity of the disease was such that the clinical manifestation was even observed in two patients as early as age 20 years.

Interestingly, the carriers of the mutation showed a 30-50% decrease in the normal apo C-III plasma level, which conferred them overall hypotriglyceridemia, increased plasma levels of HDL-cholesterol and an atheroprotective profile as compared with healthy members of the family not carrying the mutation.

Our group has previously collaborated with Professor Valleix for the characterization of the first amyloidogenic variant of β2-m described in the literature (Valleix S et al., 2012). Thanks to this ongoing collaboration we were involved in the characterization of this newly identified apo C-III variant associated with renal amyloidosis.

1.20 Aims of this thesis

As stated in the title of my PhD project, “Towards the elucidation of pathophysiology of amyloid conversion of globular proteins”, I have focused my research activity on the investigation of the molecular mechanism underlying the conversion of TTR and apo C-III from their soluble functional state to insoluble amyloid fibers using physiological conditions of pH, ionic strength and temperature. As a result of this I have set up bio-compatible methods of fibrillogenesis *in vitro* for both proteins and, in particular for TTR, I have investigated whether small molecules were able to interfere with its fibrillar conversion.

With regards to TTR**,** the discovery of the mechano-enzymatic mechanism underlying TTR amyloidosis (Mangione PP et al., 2014; Marcoux J et al., 2015) has been a big step towards the elucidation of the mechanism of the disease *in vivo*. It has also opened up a completely new scenario in the field of drug discovery as in the past potential inhibitors of TTR amyloidosis were only selected on the basis of their ability to prevent low pH induced aggregation and not on their capacity to prevent mechano-enzymatic mediated fibrillogenesis.

Four main areas have been investigated:

1. Characterization of the molecular mechanism underlying TTR fibrillogenesis including the effect of common constituents of the extracellular matrix and pre-formed amyloid fibrils.
2. Evaluation of the efficacy of putative drugs in inhibiting proteolysis-mediated TTR fibrillogenesis.
3. Investigation of structure and dynamics of TTR by NMR spectroscopy, including the evaluation of the effect of drugs on the protein structure.
4. Identification of the culprit protease responsible for proteolytic cleavage *in vivo*.

With regards to apo C-III my objectives were:

1. To express and purify recombinant WT and variant apo C-III.

2. To characterise the structure and function of the newly identified variant and highlight the differences existing with the non-amyloidogenic WT counterpart.
3. To identify whether amyloid aggregation of the variant apo C-III might occur under physiological conditions.

Chapter 2. Protein expression and purification

2.1 Introduction

For the purpose of the experimental work done for this thesis, I have expressed and purifed both recombinant TTR and apo C-III in *E. coli.*

When I joined the group in 2012, TTR was routinely being purifed according to a purification protocol involving two precipitation steps using ammonium sulphate and three chromatographic steps based on size exclusion chromatography (SEC) and ion exchange chromatography (IEC).

All the experimental data for TTR presented in this thesis, with the exception of the NMR data, were obtained using protein expressed and purified according to this 5-step protocol, which will be defined in this chapter as “method 1”.

In order to perform NMR experiments high concentrations of protein were needed and furthermore, given the size of the protein (55 KDa), deuterium enrinchment was necessary in order to improve the overall quality of the spectra.

Several attempts were made to express ^{2}H, ^{13}C, ^{15}N isotopically labelled TTR according to method 1 by changing the volumes of the flasks/medium used for the expression and/or the induction time, but the resulting yield was very poor in all cases due to low expression levels and the involvement of several purifcation steps where the protein was gradually lost. Potential alternative expression vectors and purification methods were investigated. Professor Trevor Forsyth and his group in Grenoble had previously successfully used a bacterial expression vector (pETM-11) for the expression of ^{2}H ,^{13}C, ^{15}N isotopically labelled TTR with good yield (Yee AW et al., 2016). The plasmid was kindly donated to us and was used to transform BL21 Star (DE3) supercompetent cells, allowing the expression of a sufficient amount of ^{2}H ,^{13}C, ^{15}N isotopically labelled WT TTR, carrying a 6 histidine tag, which could be purified by affinity chromatography and SEC in only 3 steps.

The plasmids encoding for both WT and D25V apo C-III were kindly donated by Professor Philippa Talmud. Recombinant apo C-III was initially expressed and purified under supervision in the laboratory of Professor Philippa Talmud at the UCL Centre for Cardiovascular Genetics where a previous PhD student had successfully developed a strategy for affinity chromatography purification of apo C-III (Liu H et al., 2000).

This expression and purification procedure was then transferred to the UCL Centre for Amyloidosis and Acute Phase Proteins where I carried out my experimental work.

2.2 Materials and methods

2.2.1 Expression and purification of TTR variants – method 1

The selected TTR variant glycerol treated cells were used for protein expression. Cell colonies were inoculated into 2 small tubes each containing 5ml of LB medium (Sigma-Aldrich) with 50 µg/ml of ampicillin (Sigma-Aldrich) and left to grow overnight under shaking at 125 rpm at 37°C. After incubation the 2 colonies were mixed together and 5 ml of the combined culture were inoculated into 2 flasks each containing 1 L of LB medium with ampicillin (50 µg/ml). The flasks were then left shaking at 125 rpm at 37°C until the cell culture reached an optical density of 0.9-1.0 at 600nm; then 1 mM of isopropyl-ß-D-thiogalactopyranoside (IPTG; Sigma-Aldrich) was added to induce protein expression and the cells were left under shaking (125 rpm) at 18°C overnight (~12-15 hours). The following day the cells were centrifuged using a Sorvall RC5C centrifuge equipped with rotor G63 at 3500rpm (3560g) for 30 minutes, then the supernatant was discarded and the resulting pellet was resuspended with the following sonication buffer: 25 mM Tris-HCl (VWR), 2 mM EDTA (Sigma-Aldrich), 0.1 % +Triton (VWR), 0.2 mM phenylmethylsulfonyl fluoride (PMSF, a protease inhibitor; Sigma-Aldrich), pH 8.0. Cells were lysed with one sonication round at 15 microtones amplitude for 15 cycles (each cycle composed of 1 minute on and 1 minute off); sonicated cells were centrifuged using a Sorvall RC5C centrifuge equipped with rotor SLA 1500 at 11,300 rpm (18,000g) for 30 minutes.

The pellet was discarded and the supernatant was treated at 4°C with ammonium sulphate (0.3 g/ml; Sigma-Aldrich) to reach a saturation of 30%. It was then left stirring for at least 15 minutes at 4°C. The sample was centrifuged using a Sorvall RC5C centrifuge equipped with rotor SLA 1500 at 11,300rpm (18.000g) for 30 minutes; the pellet was discarded and the supernatant was treated at 4°C with ammonium sulphate (0.3g/ml) in order to reach a saturation of 60% and was then left stirring for at least 15 minutes. The sample was centrifuged again at 11,300rpm (18,000g) for 30 minutes. The resulting pellet was resuspended into no more than 12 ml of 25 mM Tris-HCl, 100 mM NaCl (VWR), pH 8.0.

The sample was loaded onto a Superdex 75 Hi Load 26/60 Gel Filtration column (GE Healthcare) equilibrated and eluted at 1.5 ml/min with 25mM Tris-HCl, NaCl 100 mM, pH 8.0. The fractions containing the partially purified protein were collected and dialyzed overnight against 5 L of 25 mM Tris-HCl, pH 8.0. The dialyzed protein was then collected and dithiothreitol (DTT; Sigma-Aldrich) was added to reach a concentration of 1 mM. The protein was loaded onto a home-packed Q-Sepharose™ (GE Healthcare) Anion Exchange Column equilibrated with 25 mM Tris-HCl, pH 8.0, and eluted at 6 ml/min using an increasing ionic strength gradient with 25 mM Tris-HCl, 1M NaCl, pH 8.0. The fractions containing the protein were further purified on a Superdex 75 Hi Load 26/60 gel Filtration Column (GE Healthcare) equilibrated and eluted at 1.5 ml/min with 25 mM Tris-HCl, 100 mM NaCl, pH 8.0. The purified protein was then dialyzed for 3 days against water. The final concentration of the dialyzed protein was checked by UV absorbance at 280 nm and a known amount of protein was aliquoted in cryovials for lyophilisation and subsequent storage at -20°C.

Native agarose gel electrophoresis and/or 15% homogeneous SDS-PAGE were used to confirm the presence of the protein in all the chromatographic steps. A gradient 8-18% SDS-PAGE was conducted to confirm the purity of the final sample, which was also tested with mass spectrometry analysis to determine the exact molecular weight and the purity grade.

2.2.2 Transformation of OneShot® BL21 star (DE3) cells with peTM11

One aliquot of OneShot® BL21 Star (DE3) supercompetent E. *coli* cells (Invitrogen) was transformed with the peTM11 plasmid containing the sequence encoding for WT TTR with an additional 6 histidine-tag at the N-terminal. 5-10 µg of plasmid was added, in a volume of 1-5 µl, to a 500 µl cell aliquot. The cells were incubated on ice for 30 minutes before incubation at 42° C for 30 seconds and finally re-incubation on ice for further 2 minutes. 250 µl of SOC medium (2 % tryptone, 0.5 % yeast extract, 10 mM NaCl, 2.5 mM KCl, 10 mM $MgCl_2$, 10 mM $MgSO_4$, and 20 mM glucose) pre-warmed to

37°C was then added and the mixture was incubated at 37°C for 1 hour under stirring (225rpm).

The transformed cells were plated in Petri dishes containing LB medium with 30 µg/ml kanamycin and left growing at 37º C overnight. The following morning a single colony was picked and incubated overnight at 37º C in 5 ml of LB medium containing 30 µg/ml kanamycin.

2.2.3 Glycerol stocks

Stocks of cells were prepared with 850 µl of overnight culture cells and 150 µl of 100% sterile glycerol (Sigma-Aldrich). The glycerol cell treated vials were stored at -80°C.

2.2.4 Expression and purification of ^{2}H ^{13}C ^{15}N WT TTR – method 2

The selected TTR variant glycerol treated cells transformed with the peTM11 plasmid were used for labelled protein expression. Cell colonies were inoculated into a small tube containing 5ml of LB medium (Sigma-Aldrich) with 30 µg/ml of ampicillin (Sigma-Aldrich) and left growing overnight under shaking at 125 rpm at 37°C.

Due to the toxicity of deuterium to cells, several adaptation steps were necessary before proceeding to large scale growth for protein expression. On the morning following the overnight growth incubation 1 ml of the LB culture was inoculated into 5 ml of H-Ross medium (all components dissolved in D_2O (Sigma-Aldrich) and medium brought to final volume in distilled water) and left growing at 37º C. After ~10 hours 1 ml of the cell culture was transferred into 5ml of fresh H-Ross medium. This step was repeated a further 5 times in D-Ross medium (all components dissolved in D_2O and medium brought to final volume in D_2O) for complete adaptation to D_2O.

Table 4. Ross medium composition per litre. All components were prepared in D_2O and filter-sterilised at 0.22 µm under a Envair Class II Microbiological Safety Cabinet. The medium was brought to final volume either in distilled water (H-Ross) or D_2O (D-Ross).

Glucose monohydrate (^{13}C, ^{1}H)	3.41 g
Magnesium sulphate anhydrous	1.2 g
Potassium dihydrogen phosphate	8.7 g
85% phosphoric acid	7.38 g / 4.38 ml
Ammonium chloride (^{15}N)	1.94 g
10M sodium deuteroxide, NaOD (40% w/v)	4 ml
Trace element solution	1 ml
pH was adjusted to 6.8 by addition of 40% w/v NaOD. **The medium was filter sterilised at 0.22 µM and the following components were added:**	
Thiamine-HCl 0.9 mg/ml	10 ml
Kanamicin 50 mg/ml	0.6 ml

The last 5ml of D-Ross culture were used to inoculate a 2 L flask containing 500 ml of D-Ross medium. The cells were left growing at 37º C until the optical density at 600 nm reached 0.5. The temperature was then reduced to 30º C and the cells were left growing until O.D. reached 0.6. The prep was finally induced with 1 mM isopropyl-ß-D-thiogalactopyranoside (IPTG; Sigma-Aldrich) and left growing overnight at 30º C under agitation at 125 rpm. The following day the cells were centrifuged using a Sorvall RC5C centrifuge equipped with rotor G63 at 3500rpm (3560g) for 30 minutes, then the supernatant was discarded and the resulting pellet was resuspended with the following lysis buffer: 20 mM Tris-HCl (VWR), 250 mM NaCl (VWR), 3 mM imidazole (Sigma-Aldrich), 1 tablet of Roche EDTA-free protease inhibitor, pH 8.0. Cells were lysed with one sonication round at 15 microtones

amplitude for 15 cycles (1 minute on and 1 minute off); sonicated cells were centrifuged using a Sorvall RC5C centrifuge equipped with rotor SLA 1500 at 11,300 rpm (18,000g) for 30 minutes. The pellet was discarded and the supernatant was loaded twice at 2 ml/min on a HisTrap FF Crude nickel affinity chromatography column (GE Healthcare) equilibrated in lysis buffer in order to maximise the binding. The column was then washed at 2.5 ml/min with at least 5 column volumes each (25 ml) of washing buffer with different sodium chloride concentrations to remove non-specific bound proteins (Table 5).

Table 5. Washing buffers composition.

Wash buffer 1	20 mM Tris-HCl, 15 mM imidazole, 500 mM NaCl, pH 8.0
Wash buffer 2	20 mM Tris-HCl, 15 mM imidazole, 1 M NaCl, pH 8.0
Wash buffer 3	20 mM Tris-HCl, 15 mM imidazole, 250 mM NaCl, pH 8.0

The protein was finally eluted with 20 mM Tris-HCl, 250 mM NaCl, 250 mM imidazole, pH 8.0. The fractions containing the protein were pooled and dyalised overnight against 5 L of 10 mM Tris-HCl, 50 mM NaCl, 1 mM DTT, pH 7.5. TEV protease (Sigma-Aldrich) 1:100 w/w was added to the dialysis to selectively cleave the 6 histidine-tag. The next morning the dyalised protein was loaded again on the affinity chromatography column to separate it from the cleaved histidine-tag as well as the TEV protease, which is modfied with a 6 histidine-tag to ease its removal. Lacking the tag, the protein was eluted in the unbound fraction, which was then reloaded to ensure maximum purity of the final product. The unbound fraction, containing the protein, was further purified on a Superdex 75 Hi Load 26/60 gel Filtration Column (GE Healthcare) equilibrated and eluted with 25 mM Tris-HCl, 100 mM NaCl, pH 8.0. The purified protein was then dialyzed for 3 days against water. Final concentration of the dialyzed protein was finally checked by UV absorbance at 280 nm and a known amount of protein was aliquoted in cryovials for lyophilisation and subsequent storage at -20°C. A mass

spectrometry analysis was conducted to determine the exact molecular weight, the purity grade and the final level of deuteration.

2.2.5 Apo C-III: site-directed mutagenesis for D to V mutation

Mutagenesis was carried out using the QuickChange kit (Stratagene) to change aspartic acid into valine at position 25 in the WT apo C-III sequence that was engineered into the expression vector pMMHa (~3 kb) which is pAED4 containing the T7 expression cassette of Novagen pET23b. Both primers (Invitrogen Life Technologies) contained the desired mutation.

The sequences of primers were the following:

Forward: 5' CCAAGACCGCCAAGGTTGCACTGAGCAGCG 3'

Reverse: 5' CGCTGCTCAGTGCAACCTTGGCGGTCTTGG 3'

The underlined codon corresponds to nucleotides encoding valine in position 25. The synthesis of the mutated plasmid was performed according to the manufacturer instructions. The PCR mix composition is listed in table 6.

Table 6. PCR mix composition

Mix	Sample A (external primers)
Forward primer (125 ng/µl)	1.25 µl
Reverse primer (125 ng/µl)	1.25 µl
Template plasmid	2 µl
Buffer 10X*	5 µl
dNTPs	1 µl
PfuTurbo™ DNA polimerase (2.5 U/µl)	1 µl

*Buffer 10x: 100mM KCl, 100mM $(NH_4)_2SO_4$, 200mMTrisHCl pH 8.8, 20mM $MgSO_4$, 1% Triton X-100 and 1mg / ml bovine serum albumin.

PCR was performed in a thermocycler using the conditions reported in table 7.

Table 7. PCR conditions

Temperature (°C)	Time (min)	Cycles
95	0.5	1
95	0.5	12
55	1	
68	2	

2.2.6 Selection of mutated plasmid and subsequent transformation into competent cells

The PCR products obtained from the site-direct mutagenesis contained both WT and mutated apo C-III sequence plasmids. To select the mutated plasmid a specific restriction endonuclease, *DpnI*, able to recognise only the methylated, therefore parental, DNA, was used. The enzymatic digestion was carried out by adding 1µl of enzyme *DpnI* (10U /µl) directly to the amplification product that, after agitation and centrifugation for 1 minute at 10,000g was incubated at 37°C for 1 hour. Transformation into Epicurian coli XL1-Blue competent cells was then carried out with the selected mutated plasmid using the heat-shock procedure. These cells produce a specific ligase, which is able to repair the nicked mutated plasmid. The *DpnI* digested DNA (1µl) was added to 50µl of Epicurian coli XL1-Blue cells and on ice for 30 minutes. The mixture was then subjected to heat shock at 42°C for 45 seconds. The cells were subsequently incubated on ice for 2 minutes and then resuspended in 0.5ml of sterile culture medium NZY^+. The medium was prepared with 10g/ L of NZ amine casein hydrolyzate, 5g/L of yeast-extract water-soluble portion of yeast lysate and autoclaved. After sterilization the following compounds were added:

- 5g/L of NaCl,
- 12.5 ml of 1M MgCl2,
- 12.5 ml of 1M MgSO4,

- 10 ml of 2M glucose solution.

The pH of the solution was 7.5. Medium was preheated to 42°C before use; the cells re-suspended in the NZY+ medium were incubated under stirring at 37°C for 1 hour. The cells were spread over agar based plates containing Luria Broth (LB) medium (10g Tryptone, 5g yeast extract and 10g NaCl) with ampicillin (100µg/ml) and incubated at 37°C overnight. The grown colonies were transferred into LB medium to allow their proliferation in solution; the plasmid was then extracted from the bacterial cells with a commercial kit (Quiagen) and subjected to DNA sequencing. The plasmid was then used to transform an aliquot of OneShot® BL21 Star (DE3) supercompetent E. *coli* cells (Invitrogen) using the same procedure described before for TTR.

2.2.7 DNA agarose gel electrophoresis

At the end of each step of the construct preparation, agarose gel electrophoresis was carried out to confirm the presence of the correct amplified PCR or DNA samples. The agarose gel was prepared by dissolving agarose (1-2%, the concentration depending on the size of the sample) in 1X TAE buffer (40mM Tris, 20mM acetic acid glacial, 1mM EDTA, pH 8.0) and adding ethidium bromide (0.5µg/ml). A sample volume of 3µl was loaded in each case along the O'GeneRuler™ 100bp Plus DNA Ladder, ready-to-use standard (Fermentas) that contains a 100bp-3000bp range of DNA length markers. The electrophoresis was carried out in a horizontal electrophoretic chamber with TAE running buffer at room temperature for 45 minutes; amperage was kept constant at 60mA. DNA bands were detected with a transilluminator device.

2.2.8 Expression of recombinant WT and D25V apo C-III

The selected apo C-III variant glycerol treated cells were used for protein expression. Cell colonies were inoculated into 2 small tubes each containing 5ml of LB medium (Sigma-Aldrich) with 100 µg/ml of carbenicillin (Sigma-Aldrich) and left growing overnight under shaking at 125 rpm at 37°C. After incubation the 2 colonies were mixed together and 5 ml of the combined

culture were inoculated into 2 flasks each containing 1 L of SOC medium with carbenicillin (100 µg/ml). The flasks were then left shaking at 125 rpm at 37° C until the cell culture reached an optical density of 0.6 at 600nm; then 1 mM of isopropyl-ß-D-thiogalactopyranoside (IPTG; Sigma-Aldrich) was added to induce protein expression and the cells were left under shaking at 37°C for a further 2 hours. The cells were then centrifuged using a Sorvall RC5C centrifuge equipped with rotor G63 at 3500rpm (3560g) for 30 minutes, then the supernatant was discarded and the resulting pellet was resuspended with the following lysis buffer: 50 mM NaH_2PO_4 (VWR), 10 mM Tris-HCl (VWR), 8 M Urea (VWR), 500 mM NaCl (VWR), pH 8.0. The suspension was then left under moderate shaking (35 rpm) at 4 ºC overnight. The following morning the suspension was sonicated at 15 microtones amplitude for 6 cycles (1 min on and 1 min off) on ice and was then centrifuged at 18,000g for 30 minutes using a Sorvall RC5C centrifuge equipped with rotor SLA 1500. Meanwhile, 2.5 ml of Talon his-tag purification resin (loaded with cobalt) was washed with 10 ml of lysis buffer. The post sonication supernatant was then applied to the Talon his-tag purification resin beads and left shaking at 50 rpm 4 ºC for 2 hours. The suspension was then carefully centrifuged for 2 minutes at 1000 rpm, the supernatant was removed and 10 ml of lysis buffer was added. The operation was repeated another time by adding 4 ml of lysis buffer. The suspension was then poured into a gravity flow chromatography column and allowed to sediment. The column was then washed with 8 ml of lysis buffer before elution with 50 mM NaH_2PO_4 (VWR), 8 M Urea (VWR), 500 mM NaCl (VWR), 500 mM imidazole, pH 8.0. Elution buffer was added in volumes of 2 ml each time and the absorbance of each fraction was monitored at 280 nm with a spectrophotometer. Elution was stopped when the absorbance at 280 nm reached the baseline value. The protein was then dialysed for 3 days against an appropriate buffer (water for the WT, 10 mM ammonium bicarbonate for the variant), the absorbance was checked and 1 mg aliquots were frozen and lyophilised for subsequent storage at -20 ºC.

2.2.9 Expression of recombinant ^{15}N WT and D25V apo C-III

The protein was expressed and purified according to the same protocol presented in the previous paragraph with the only exception that the overnight culture was transferred into 1 L of Cambridge Isotope Laboratories SPECTRA 9 (^{15}N, 98%) medium.

2.3 Results

2.3.1 TTR expression and purification – method 1

The expression of the different TTR variants was carried out following the protocol described in the Material and Methods section. The protein was expressed with an extra N-terminal methionine and extracted from the cells under native conditions. After two steps of ammonium sulphate treatments, the sample was purified using size exclusion chromatography in 25 mM Tris-HCl, 100 mM NaCl, pH 8.0 (Fig. 17).

Fractions containing the protein, as confirmed in a polyacrilamide gel electrophoresis (inset Fig. 17) carried out under denaturing and reducing conditions, were dialyzed overnight against 25 mM Tris-HCl, pH 8.0 in order to remove the NaCl and facilitate further purification steps.

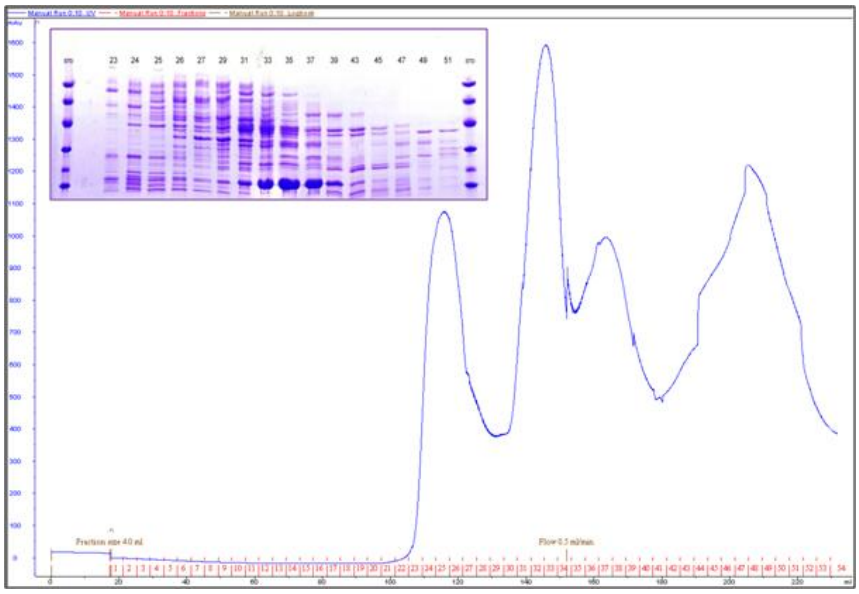

Figure 17. First step of size exclusion chromatography performed on a Superdex 75 Hi Load 26/600 column (GE Healthcare) equilibrated and eluted at 1.5 ml/min with 25 mM Tris-HCl, pH 8.0 containing 100 mM NaCl. Low molecular standards are 97 kDa, 66 kDa, 45 kDa, 30 kDa, 20,1 kDa and 14,4 kDa respectively.

The dialyzed protein was subsequently purified with an anionic exchange chromatography (Fig. 18) and the mobility of protein was checked with a native agarose gel electrophoresis (inset Fig. 18).

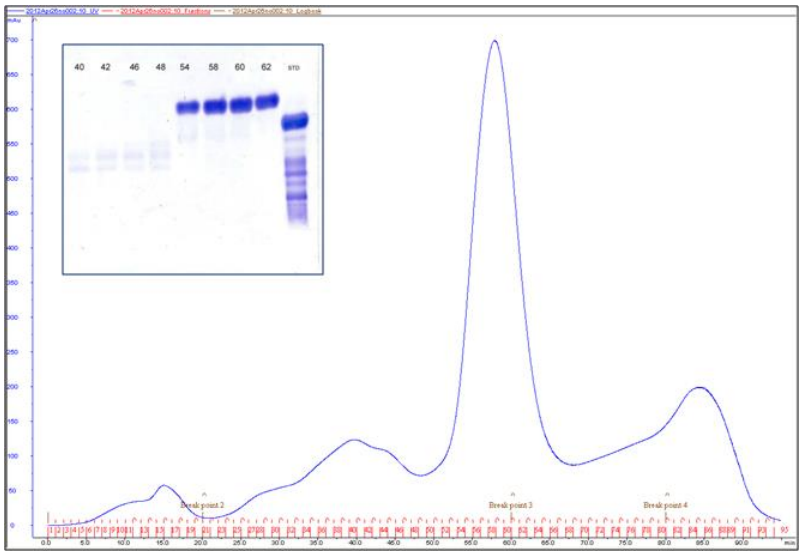

Figure 18. Anion-Exchange chromatography carried out with a Q-Sepharose™ Anion Exchange column eluted as described in the Material and Methods section. Inset shows the electrophoretic mobility of the corresponding chromatographic fractions. Standard is 1/5 diluted human serum.

Anion exchange fractions containing the protein were concentrated in order to be further purified by gel filtration chromatography (Fig. 19), which allowed us to achieve fractions containing a 98% pure protein as confirmed by SDS-PAGE (inset Fig. 19).

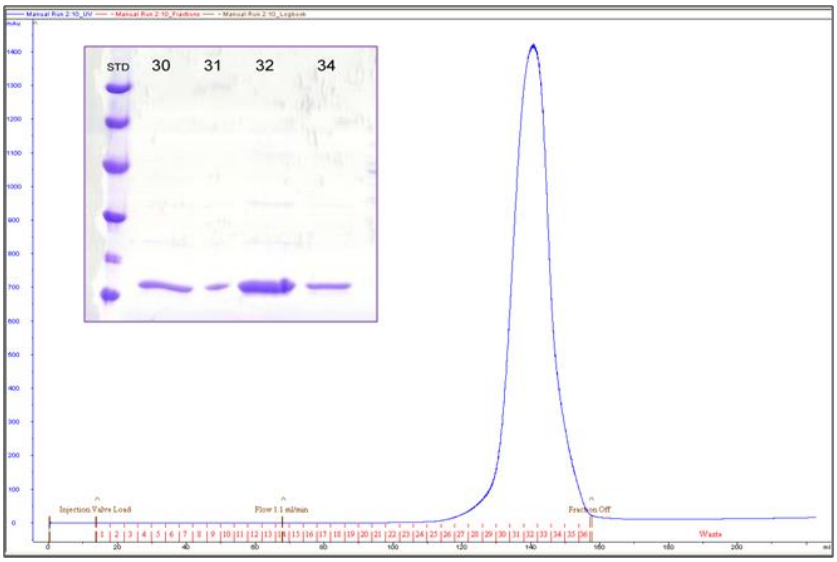

Figure 19. Gel filtration chromatography was conducted as described in the Material and Methods section. The inset shows the SDS_PAGE performed under denaturing and reducing conditions. Low molecular standards are 97kDa, 66kda, 45kDa, 30kDa, 20,1kDa and 14,4kDa respectively.

The exact molecular weight of the different TTR variants was finally checked by electrospray ionization mass spectrometry (Fig. 20) by Dr Graham Taylor and Dr Diana Canetti.

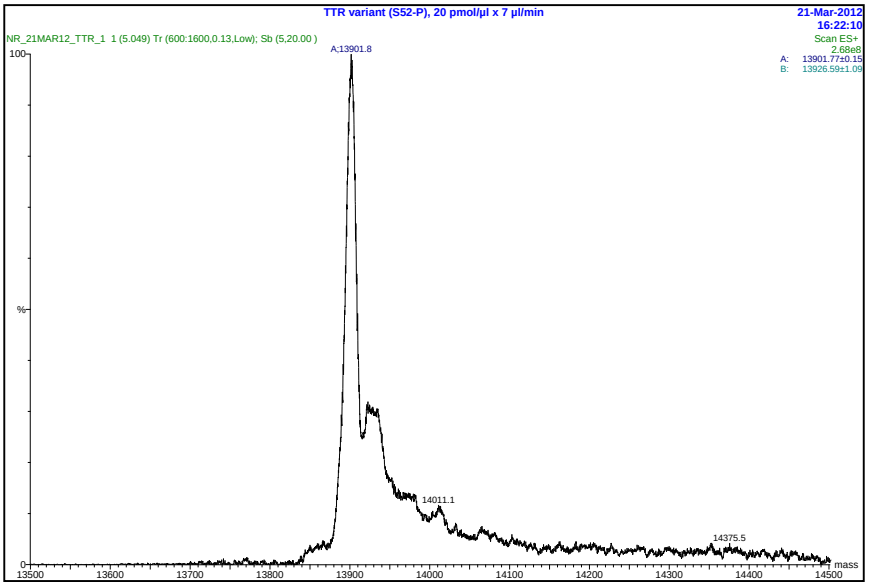

Figure 20. Transformed spectrum of recombinant S52P TTR showing a single major component at Mr of 13,901.8.

2.3.2 Expression and purification of ^{2}H ^{13}C ^{15}N WT TTR – method 2

The protein was expressed using One Shot® BL-21 Star (DE3) supercompetent cells engineered with the peTM11 plasmid containing the cDNA for WT TTR and an extra 6 histidine-tag at the N-terminal. As described in the materials and methods section, the cells were lysed by sonication and then centrifuged. The supernatant was loaded onto a HisTrap FF Crude nickel affinity chromatography column for the first purification step. The fractions containing the protein were dyalised overnight against the gel filtration buffer in the presence of TEV protease (TEV:TTR ratio 1:100 w/w) to remove the 6 histidine-tag. The products of digestion and the TEV protease itself, were removed by loading the dyalised fraction onto the affinity chromatography column once again. The protein was then further purified by size exclusion chromatography on a Superdex 75 Hi Load 26/60 gel filtration column (Fig. 21).

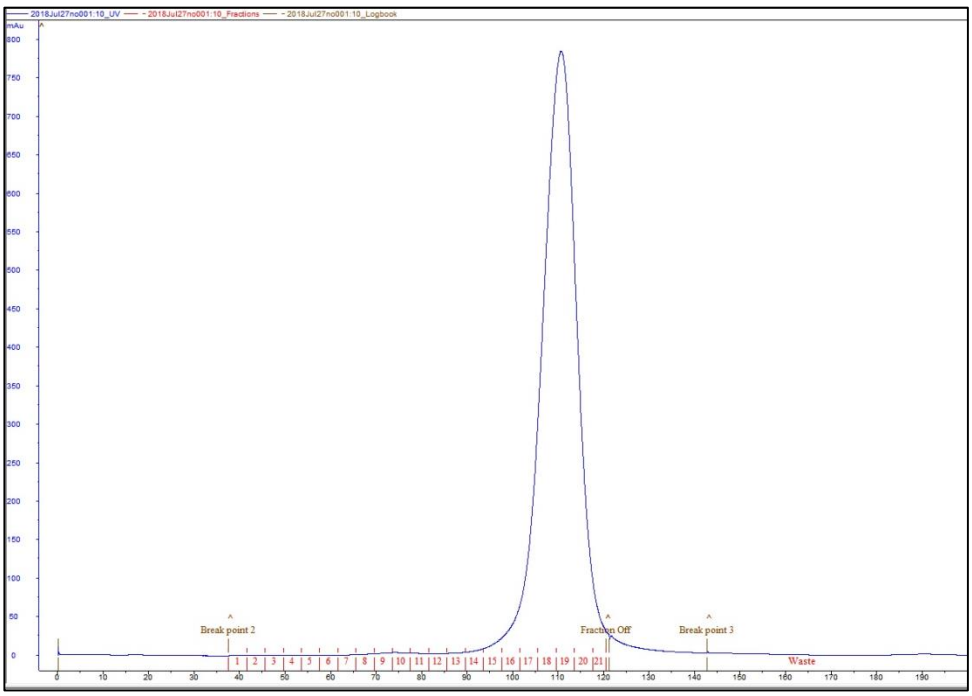

Figure 21. SEC of ^{2}H ^{13}C ^{15}N WT TTR.

The exact molecular weight and the level of deuteration were finally checked by mass spectrometry by Dr Diana Canetti.

2.3.3 Expression of recombinant apo C-III

Apo C-III, both WT and D25V, was expressed using One Shot® BL-21 Star (DE3) supercompetent cells engineered with the pET23b plasmid containing the cDNA for both WT or D25V apo C-III and an extra 6 histidine-tag at the N-terminal. As described in the Materials and Methods section the cells were lysed in 8 M urea by sonication. The protein was then purified by affinity chromatography using a cobalt loaded resin (Talon his-tag purification resin).
The final purity, which appeared ≥ 95%, was checked both by SDS PAGE electrophoresis and electrospray ionization mass spectrometry.
Different buffers had to be used in order to lyophilise the protein and remove the urea, which was present in high concentration from the purification procedure. WT apo C-III appeared stable in water and could sustain a 3 days dialysis procedure without any visible aggregates being formed.
On the contrary the amyloidogenic variant rapidly aggregated in water and was therefore dialysed against 10 mM ammonium bicarbonate, pH 7, where it appeared more stable, prior to lyophilisation.

2.4 Discussion

In general, expression and purification of several TTR variants using the described purification method 1 proved successful, allowing a good protein yield (~50 mg protein from 2 L of cell culture) and a final purity ≥ 95%. The expression of isotopically-labelled ^{2}H ^{13}C ^{15}N WT TTR however, proved extremely challenging using this purification protocol, with a final yield of less than 2 mg per litre of cell culture, which appeared not cost-effective given the amount of protein needed for NMR experiments and the elevated cost of the isotopically labelled reagents used.

The expression vector and purification procedure provided by Professor Trevor Forsyth and his group, were adopted to overcome this issue. Affinity chromatography, made possible by the presence of 6 his-tag, largely increased the yield, allowing the production of ~40 mg ^{2}H ^{13}C ^{15}N WT TTR from 500 ml of cell culture.

The theoretical final deuteration level on non-exchangeable positions, considering that non-deuterated glucose was used, should have reached ~86 % (Leiting et al., 1998). Nevertheless, deuterium-hydrogen exchange took place throughout the whole purification procedure in aqueous buffer thus reducing the expected deuteration level. Mass spec analysis of the sample revealed a protein purity ≥ 95% and a final deuteration level ~65%, which proved sufficient to perform NMR experiments.

Both WT and recombinant apo C-III were successfully expressed with a final protein purity ≥ 95%. The protein was expressed in low levels allowing the purification of ~10 mg of proteins from 2L of starting material. Growth in ^{15}N labelled did not dramatically reduce the final yield allowing the purification of enough WT and variant apo C-III to perform NMR experiments.

Chapter 3. Correlation between susceptibility to proteolysis and protein stability

3.1 Introduction

Several amyloidogenic variant proteins, including TTR variants, have been shown to possess a reduced thermodynamic stability when compared to their WT counterparts. Lysozyme (Booth D et al., 1997), β2-m (Valleix S et al., 2012) and TTR (Mangione PP et al., 2014) are all good examples of proteins in which a single residue substitution can have a dramatic effect in terms of thermodynamic stability and aggregation propensity.

In the mechano-enzymatic mechanism proposed by our group for TTR amyloidogenesis, aggregation is primed by proteolytic cleavage of the peptide bond L48-T49, which dramatically destabilises the TTR tetramer, thus favouring dissociation and subsequent aggregation. Previously published results, obtained in conditions of limited proteolysis (Mangione PP et al., 2014), have highlighted a strong susceptibility to proteolysis exhibited by the S52P TTR variant. The investigation of the thermodynamic stability of S52P TTR revealed that the protein was destabilised with respect to its WT counterpart. Furthermore, the comparison of the X-ray structure of the variant protein with that of WT TTR, has highlighted a partial loss of the local H-bond network around the site of mutation, as a consequence of the S52 to P52 mutation. Such a disruption of the H-bond network would result in an increased flexibility of the CD loop, where the cleavage site is located. It has also been suggested that the destabilisation of the β-turn connecting strands C and D, perturbs the two adjacent strands and increases their flexibility, making the CD loop more accessible to the action of a proteolytic enzyme. Further investigation of the mechano-enzymatic mechanism (Marcoux J et al, 2015) has highlighted a different susceptibility to proteolysis exhibited by different TTR variants, which translated into a different aggregation propensity. Indeed, in order to cleave TTR variants other than S52P, the experimental conditions had to be changed by increasing the area of the hydrophobic-hydrophilic interface and therefore the intensity of the forces acting on the protein (Marcoux J et al., 2015). In the presence of higher

forces, the induced structural perturbations increased the accessibility of the CD loop to the action of the protease, determining cleavage and subsequent aggregation of several TTR variants, with the exception of the protective T119M TTR variant (Marcoux J et al., 2015).
The first goal of my PhD was to investigate the correlation existing between the thermodynamic stability of different TTR variants and their susceptibility to proteolysis.

TTR tetramer stability has been investigated using different approaches including differential scanning calorimetry (DSC; Shnyrov VL et al., 2000), high hydrostatic pressure (HHP; Ferrao-Gonzales AD et al., 2003) and especially urea/guanidine induced denaturation (McCutchen SL et al., 1993; Hammarström P et al., 2001; Hammarström P et al., 2002; Hammarström P et al., 2003). The experimental method applied, the concentration of the protein and the denaturant used influence the final results, therefore the data available in the literature are not always in agreement with each other. For example the stability of the protective T119M variant was estimated by Shnyrov and collaborators to be very similar to that of WT TTR by DSC, while it appeared higher when determined by urea-induced denaturation.
Amongst the different methods described, the tetramer stability of different TTR variants presented in this chapter was determined following the procedure described by Hammarström, Schneider and Kelly in Science (Hammarström P et al., 2001). The method evaluates TTR tetramer stability by exposing the protein to increasing concentrations of guanidine thiocyanate (guanidine-SCN) and monitoring the resulting ratio between folded and unfolded fractions by tryptophan fluorescence. The experimental data can then be analysed according to the Santoro & Bolen equation (Santoro MM & Bolen DW, 1988) in order to obtain information on the stability.
The susceptibility to cleavage and aggregation was tested in two different aggregation conditions. Previous work done on ß2-m by our group (Mangione PP et al., 2013) has highlighted the role played by hydrophobic-hydrophilic interfaces in favouring protein aggregation. In particular, changing

the surface area of such interfaces can quite drastically change the intensity of the forces acting on a protein during an aggregation experiment.

In the first experiment aggregation was carried out in 96-well plates characterised by a diameter of 0.6 cm and a hydrophobic-hydrophilic (air-water) interface area of 0.32 cm^2. Agitation was set to 900 rpm with double orbital shaking.

A second fibrillogenesis experiment was carried out using glass vials with a 1.4 cm diameter and an air-water interface of 1.5 $cm^{2,}$ in which sheer stress was obtained using a magnetic bar agitating at 1500 rpm.

Whether a correlation exists between the experimentally determined stabilities and susceptibility to proteolysis and aggregation is the subject of this chapter.

3.2 Materials and methods

3.2.1 Guanidine-SCN induced denaturation

Several TTR samples were prepared in 50 mM sodium phosphate (VWR), 1 mM EDTA (Sigma-Aldrich), 1mM dithiothreitol (DTT; Sigma-Aldrich) and guanidine-SCN (0 to 3 M with 0.2 M increment between each point; Merck) at a final concentration of 0.2 mg/ml. The final volume was set to 500 µl. The samples were incubated for 24 hours at room temperature (25º C) before tryptophan fluorescence measurement were performed. Spectra were recorded at 25º C using a Perkin Elmer LS55 Luminescence Spectrometer. Excitation was set to 295 nm and the corresponding emission spectra were acquired in the range 310-440 nm. Three accumulations per spectrum were collected.

3.2.2 Determination of midpoint denaturant concentration (C_m)

The ratio between tryptophan fluorescence at 355 nm (unfolded maximum) and 335 nm (folded maximum), as a function of the concentration of denaturant, were analysed using the Santoro & Bolen equation (Santoro MM & Bolen DW, 1988) and fitted to a two-state unfolding transition.

$$yf = \frac{[(\mathrm{yN} + m\mathrm{N}\,[\mathrm{D}]) + (\mathrm{yU} + m\mathrm{U}\,[\mathrm{D}]] * e^{-(\Delta \mathrm{G}^{\circ}/\,\mathrm{RT} + m\mathrm{G}[\mathrm{D}]/\,\mathrm{RT})}}{1 + e^{-(\Delta \mathrm{G}^{\circ}/\,\mathrm{RT} + m\mathrm{G}[\mathrm{D}]/\,\mathrm{RT})}}$$

Where

- yf is the observed fluorescence signal (ratio 355/335).
- yN and yU are the fluorescence signals of the protein in its native and unfolded state, respectively.
- mN and mU are the slopes of the lines corresponding to the pre- and post-transitional regions.
- ΔG is the Gibbs free energy in the absence of denaturant

- R is the ideal gas constant (1.987 cal mol^{-1} K^{-1})
- T is the temperature expressed in K (298.15 K in our case)

The unfolding data were then normalised by calculating the apparent fractions of unfolded protein (Fapp) using the equation reported by Finn and collaborators (Finn BE et al., 1992).

$$fU = \frac{y - yN}{yU - yN}$$

Where

- fU is the fraction unfolded
- y is the ratio between the fluorescence emission intensities at 355 nm and 335 nm, respectively, at a given denaturant concentration
- yN and yU are the values of native and unfolded protein extrapolated form the pre and post transitional baselines.

From the normalised curves the C_m, corresponding to the concentration of denaturant necessary to unfold 50% of the protein in solution, was then extrapolated.

3.2.2 TTR fibrillogenesis in 96-well plate

The selected TTR variant was dissolved 2 mg/ml in PBS, pH 7.4 (Sigma-Aldrich). The protein was then diluted to 1 mg/ml using a 10 µM ThT solution in PBS containing trypsin (Promega Trypsin Gold Mass Spectrometry Grade) to a final enzyme to protein ratio of 1:200 (w/w). The final volume per well was set to 100 µl. The plate was incubated at 37º C in a BMG LABTECH FLUOstar Omega plate reader and subjected to double orbital agitation at 900 rpm. ThT fluorescence emission at 480 nm, following excitation at 445 nm, was monitored every 5 minutes using bottom reading optics. The experiment was stopped when fluorescence reached a stable plateau.

3.2.3 TTR fibrillogenesis in glass vial

The fibrillogenesis samples were prepared dissolving TTR at 1 mg/ml in PBS, pH 7.4 (Sigma-Aldrich). 2 ml per sample were transferred into glass vials characterised by a 1.4 cm diameter and an air-water interface of 1.5 cm^2. Trypsin was added to a final enzyme to protein ratio of 1:200 (w/w). Agitation was generated using a magnetic stir bar rotating at 1500 rpm (IKA magnetic stirrer). Aggregation was followed monitoring the increase in turbidity at 400 nm over time.

3.3 Results

3.3.1 Determination of TTR tetramer stability by guanidine-SCN induced denaturation

Several TTR variants associated with neurological and/or cardiac symptoms, including V30M, V122I, L55P, L111M, I68L and the protective T119M TTR variant, were purified according to the method described in section 2.2.1 of the previous chapter.

The selected variant was incubated in the presence of guanidine-SCN for 24 hours at room temperature to allow complete equilibrium of the unfolding reaction. Tryptophan fluorescence was measured for each of the 16 experimental points by exciting the samples at 295 nm and recording the emission spectra in the range 310-440 nm using a Perkin Elmer LS55 Luminescence Spectrometer.

For all proteins, a progressive reduction of the measured tryptophan emission fluorescence signal, associated with a rearrangement of the protein structure in response to the presence of increasing concentrations of denaturant, was observed for the lower denaturant concentrations. This behaviour was accompanied by a progressive shift of the fluorescence spectra towards the right.

Once a threshold denaturant concentration was reached for each protein, the fluorescence signal slightly increased and a marked shift towards the right was observed. From this point onward, further increase of the denaturant concentration did not induce any shifting. Indeed the fluorescence spectra remained stable, suggesting that complete denaturation had been achieved.

The threshold value of denaturant appeared strongly dependent on the specific variant tested: the more unstable the variant, the less amount of guanidine required to induce denaturation (Fig. 22).

In order to obtain robust data, each experiment was repeated at least three times.

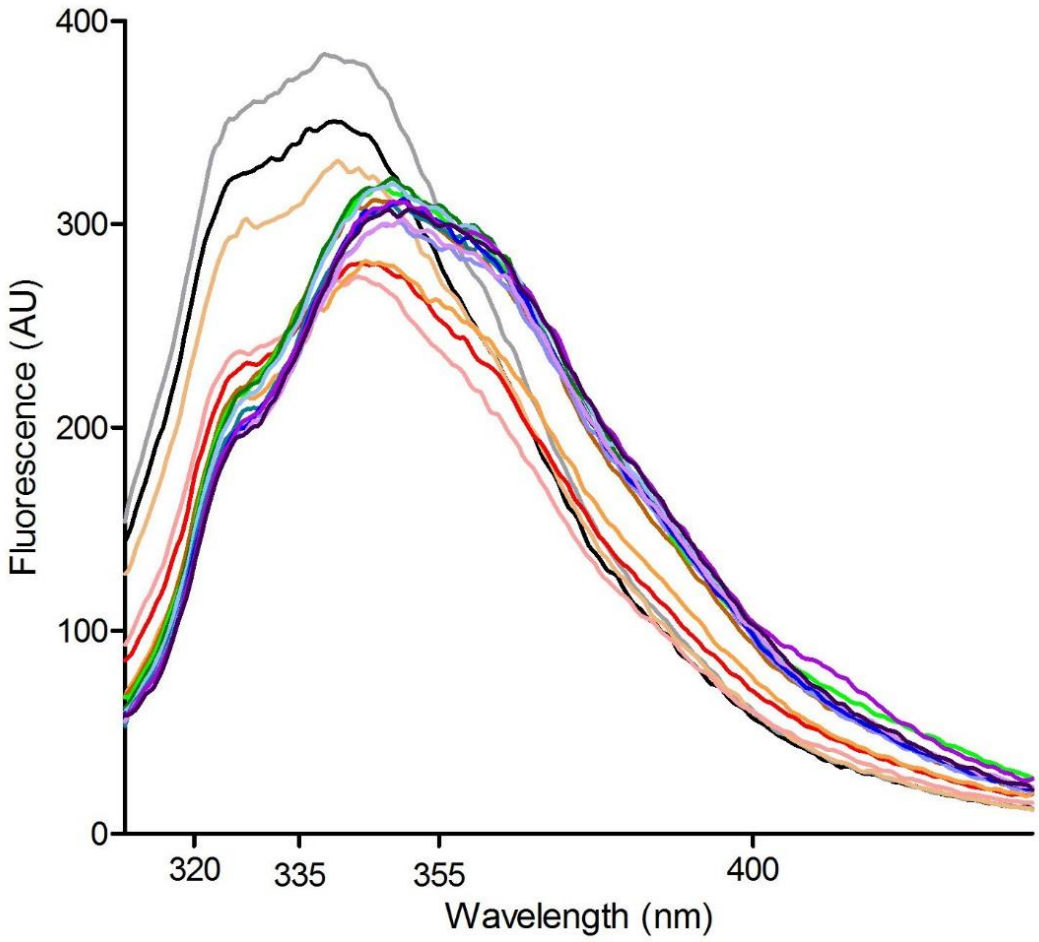

Figure 22. Tryptophan emission fluorescence spectra. Example of tryptophan emission fluorescence spectra for S52P TTR alone (black) and in the presence of 0.2 M (grey), 0.4 M (light orange), 0.6 M (pink), 0.8 (red), 1 M (orange), 1.2 M (brown), 1.4 M (green), 1.6 M (dark green), 1.8 M (light blue), 2 M (blue green), 2.2 M (lilac), 2.4 M (blue), 2.6 M (light violet), 2.8 M (violet) and 3 M (dark violet) guanidine-SCN. Spectra were recorded at 25 °C exciting the sample at 295 and recording emission spectra in the range 310-440 nm with a Perkin Elmer LS55 Luminescence Spectrometer. The final protein concentration was 0.2 mg/ml.

In order to generate the denaturation curves, the ratios between measured tryptophan emission fluorescence at 335 nm, corresponding to the maximum folded, and at 355 nm, corresponding to maximum unfolded, were calculated for each experimental point and analysed using the equation of Santoro and Bolen. The data were then normalised using the equation presented in the section “Materials and Methods”. Analysis and normalisation were performed using the software KaleidaGraph from Synergy (Fig. 23).

Unsurprisingly, the most stable variant was the protective T119M TTR variant, which is known to have a stabilising effect on the tetramer, protecting people carrying both the T119M and V30M mutation from developing familial amyloid polyneuropathy usually caused by the latter (Hammarström P et al., 2003).

The variants I68L and V30M TTR appeared very similar to each other and to WT TTR, whose stability had already been determined by our group (Mangione PP et al., 2014). This similarity in tetramer stability between WT and V30M TTR was in agreement with previously published data (Hurshman Babbes AR et al., 2008).

The variants L55P, V122I and L111M TTR appeared highly destabilised when compared to WT TTR. With respect to S52P TTR, V122I and L55P appeared very similar, while only L111M appeared less stable with a C_m value lower than that previously determined for the S52P TTR variant (Mangione PP et al., 2014).

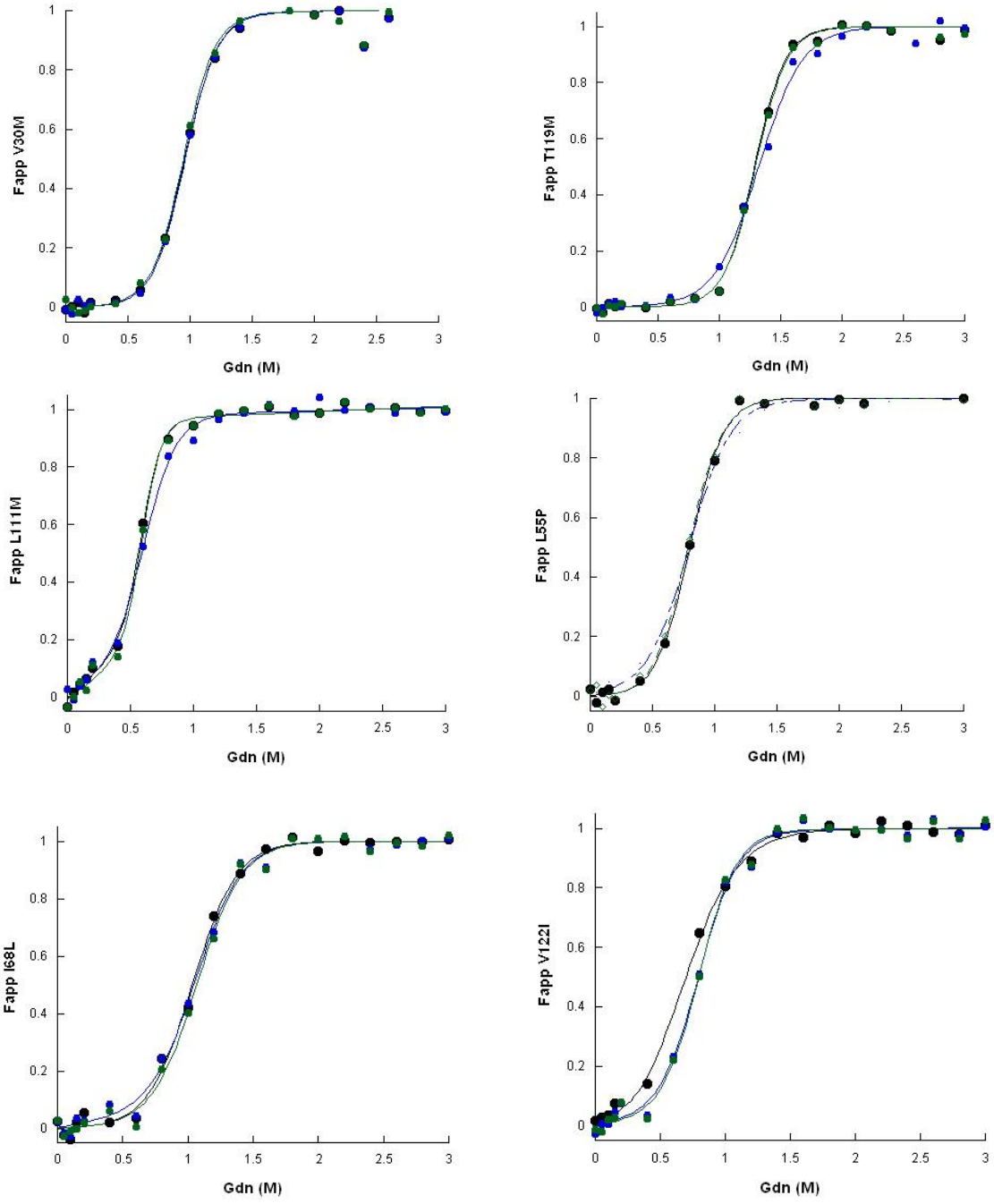

Figure 23. Normalised TTR denaturation curves. Normalised denaturation curves for V30M, T119M, L111M, L55P, I68L and V122I TTR in the presence of guanidine-SCN. Three curves are shown for each variant, representative of three independent experiments. Curves were generated using the software KaleidaGraph. The stability curves for WT and S52P TTR were already published (Mangione PP et al, 2014) and are therefore not presented here.

The midpoint denaturant concentrations for each variant tested, C_m, were extrapolated from the denaturation curves and are reported in table 8.

Table 8. Midpoint denaturant concentrations. Data expressed as mean (SD) of 3 distinct experiments. WT and S52P TTR values are reported for comparison.

TTR variant	**C_m**
WT	1.03 ± 0.02
T119M	1.3 ± 0.02
I68L	1.06 ± 0.02
V30M	0.96 ± 0.01
V122I	0.74 ± 0.1
L55P	0.79 ± 0.01
L111M	0.57 ± 0.02
S52P	0.8 ± 0.06

3.3.2 Evaluation of the aggregation propensity

In parallel with the determination of protein stability, susceptibility to proteolysis and aggregation was investigated. As mentioned in the introduction of this chapter, the mechano-enzymatic mechanism combines the destabilising action of mechanical forces with proteolysis in order to prime TTR aggregation. Indeed, mechanical forces promote partial unfolding, which favours proteolysis. As a result, aggregation rapidly follows due to the combination of the destabilisation of the tetramer induced by the proteolytic cleavage and once again the action of mechanical forces that favour tetramer dissociation.

Two different conditions were selected for fibrillogenesis experiments:

1. Aggregation in 96-well plates under mechano-enzymatic conditions in the presence of trypsin;
2. Aggregation under mechano-enzymatic conditions in glass vials in the presence of trypsin

The areas of the hydrophobic-hydrophilic interfaces for the two systems were respectively 0.32 cm^2 and 1.5 cm^2. The shaking conditions were also different with 900 rpm double orbital for the 96-well plate and 1500 rpm for the glass vial. Our collaborator Professor Ciro Cecconi from the University of Modena (Italy), estimated the total forces acting in the glass vial, accounting for both the contributions of shaking and air-water interface, to be around 20-25 pN. Due to the complexity of the system, a precise quantification of the forces acting on the protein in the 96-well plate system was not possible, although the total forces were estimated to be lower than the threshold value of 20 pN.

It was therefore possible to distinguish between TTR variants that were cleaved and aggregated in the presence of forces < 20 pN and variants, which required higher forces (i.e. > 20 pN) in order to be destabilised and undergo proteolysis and subsequent aggregation.

When aggregation was investigated using a 96-well plates, the ThT signal was completely flat for most of the variants tested, suggesting than no amyloid formation had occurred. However, in the presence of S52P and L111M TTR a positive ThT emission signal was observed, indicating the

formation of amyloid fibrils (Fig. 24). The kinetics of aggregation appeared different between the two variants with a longer lag phase preceding aggregation observed for L111M TTR (~13 hours), when compared to S52P TTR (~ 40 minutes). The kinetics of aggregation also appeared different between the two proteins, with fibrils being formed very rapidly in the presence of S52P TTR and more slowly in the case of L111M TTR. This initial result seemed to contrast with the idea that a lower stability corresponds with an increased propensity to undergo cleavage and aggregation, keeping in mind that the stability of L111M was observed to be lower than that of S52P.

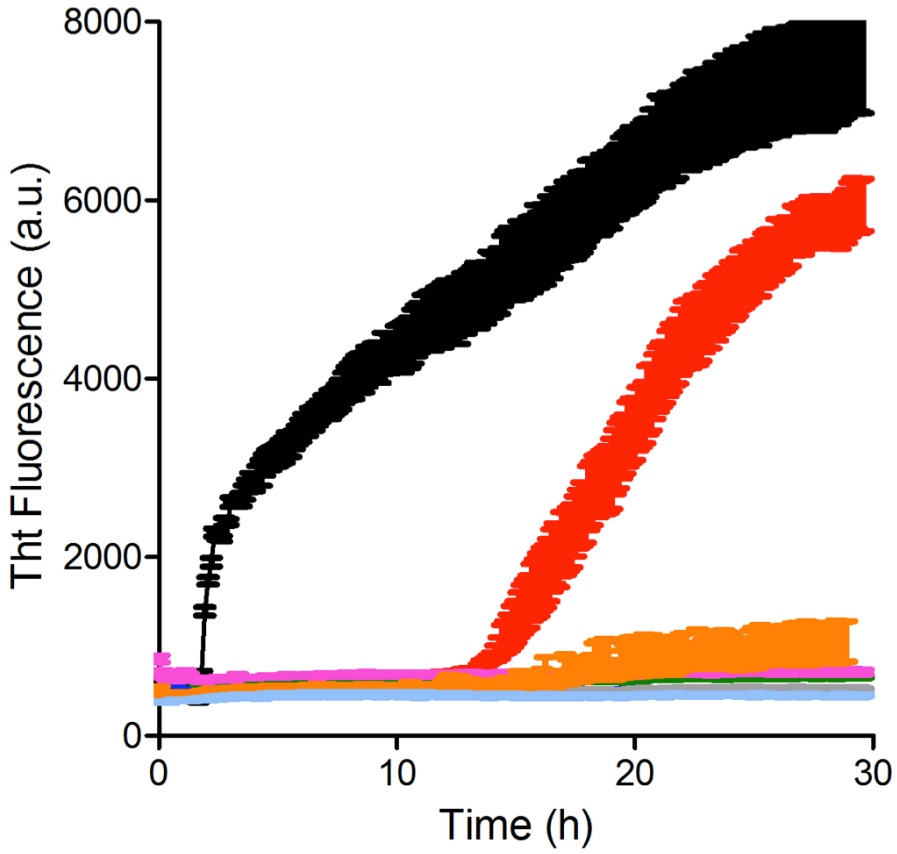

Figure 24. Mechano-enzymatic mediated aggregation of different TTR variants in 96 wells plates. Tht emission fluorescence signal for S52P (black), L111M (red), L55P (green), V30M (pink), WT (blue), V122I (grey), I68L (orange) and T119M (cyan) TTR. Results expressed as mean (SD) of 4 separate experiments.

As previously mentioned, in order to cleave the other TTR variants, the experimental conditions were changed by increasing the forces acting on the protein during aggregation. In the presence of higher forces, all the variants tested, including the WT protein, were cleaved, with the exception of the protective T119M TTR variant. Aggregation was monitored following the increase of turbidity at 400 nm (Fig. 25). As expected from the results obtained using a 96-well plate, both S52P and L111M TTR underwent extensive aggregation in vials. In agreement with the data already published (Marcoux J et al., 2015), L55P and V122I TTR also largely aggregated. V30M, which appeared slightly less stable than the WT protein, aggregated to a lesser extent. For WT TTR, aggregation resulted 50 % lower than that observed for S52P, while I68L TTR aggregated even less. No aggregation was detected for T119M TTR, thus confirming the results previously published.

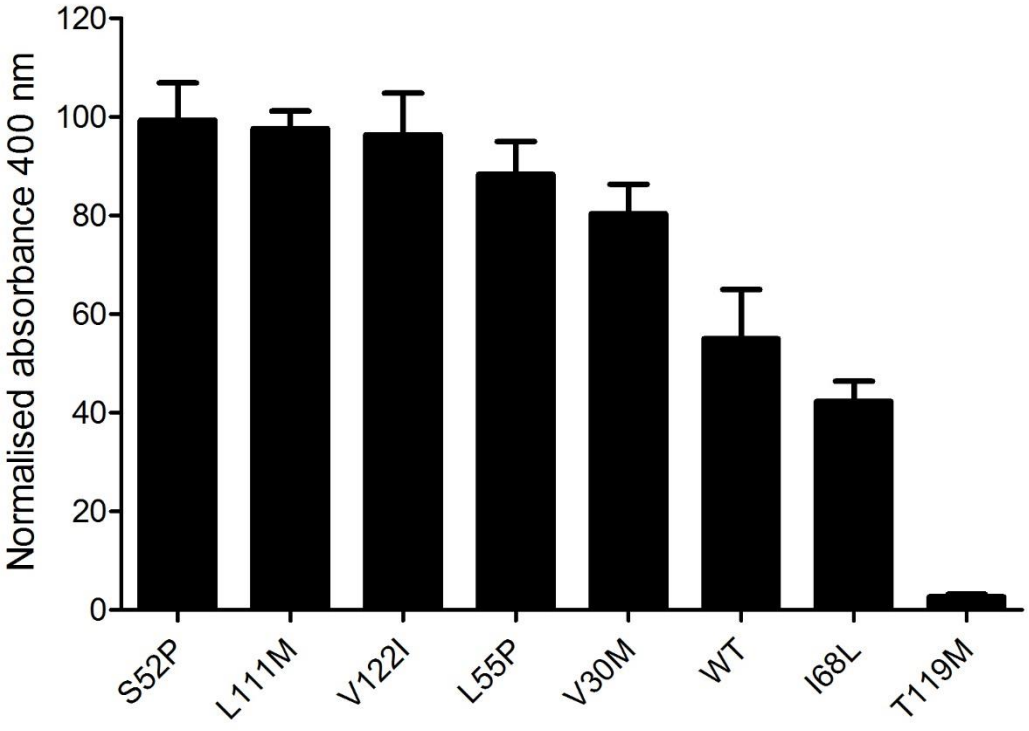

Figure 25. Aggregation of TTR variants in glass vials under mechano-enzymatic conditions. The turbidity at 400 nm after 96 hours of aggregation was normalised to the S52P TTR control sample. Data presented as mean (SD) of three independent experiments.

3.4 Discussion

Denaturation curves were obtained for a series of TTR variants by measuring tryptophan emission fluorescence in the presence of increasing concentrations of guanidine-SCN. The data were analysed and fitted according to the equation of Santoro and Bolen and the midpoint denaturant concentration, C_m, was extrapolated from the denaturation curves for each TTR variant tested. T119M TTR resulted the most stable variant, followed by I68L and WT TTR. L55P, V122I and S52P TTR appeared similarly destabilised when compared to WT TTR. The stability of the V30M variant was estimated to be intermediate between WT and L55P TTR. The most unstable variant appeared to be L111M TTR.

The same variants were then tested for aggregation under two different experimental conditions: one where the overall forces resulted below 20 pN and the other where the calculated forces were above this threshold value. Published data suggest that forces in the range of 5-100 pN are enough to perturb the structure of a native protein like TTR (Cecconi CC et al., 2005; Borgia A et al., 2008), thus increasing the exposure of the proteolytic site to the action of the culprit protease. Only two variants, S52P and L111M TTR, were cleaved in the presence of forces below 20 pN and aggregated showing a different length of the lag phase preceding aggregation. No correlation between the estimated C_m of the two variants and their susceptibility to proteolysis and tendency to aggregate could be observed as the L111M variant appeared less stable, but also less aggregation prone. The data, however, have to be interpreted taking into account the effect induced by the substitution of S52 with P52 described in the introduction. S52P TTR may therefore represent an exception for which the increased susceptibility to proteolysis could be associated with a combination of both reduced stability and increased structural flexibility of the region containing the cleavage site due to the partial loss of the local H-bond network. If we consider the highly unstable L111M variant, forces below 20 pN were sufficient to induce structural perturbations of the protein and promote its cleavage and

aggregation, thus suggesting a correlation between stability and susceptibility to proteolysis and aggregation.

In order to induce aggregation of other variants, the intensity of the forces acting on the protein during fibrillogenesis had to be increased by performing fibrillogenesis experiments in glass vials with a larger hydrophobic-hydrophilic interface surface area (1.5 cm^2 air-water interface). All variants were cleaved and aggregated in these conditions with the exception of the T119M variant, which has been previously reported in the literature as a protective mutation, able to protect carriers from TTR-related polyneuropathy (Hammarström P et al., 2003).

Interestingly, the observed extent of aggregation was different between variants. Indeed, S52P and L111M aggregated under these more harsh experimental conditions as expected. Extensive aggregation was also observed for both V122I and L55P TTR, which had similar stability to S52P with preserved H-bond network around the cleavage site. V30M, for which the estimated C_m appeared lower than that of WT TTR, aggregated to a lesser extent. Finally both WT and I68L, for which the estimated C_m were very similar (1.3 ± 0.02 and 1.06 ± 0.02), resulted as the less aggregation-prone.

Unfortunately, the experimental setup used for aggregation experiments did not allow a fine modulation of the forces, which were either below or above 20 pN, thus not allowing a precise determination of the intensity of the forces necessary to promote partial unfolding for each variant.

As a general conclusion, the data presented show that for the most unstable variants, forces below 20 pN were sufficient to promote structural perturbations and favour proteolysis and aggregation. Forces above this threshold were necessary to obtain the same effect on more stable mutants, which aggregated to different extents on the basis of their thermodynamic stability.

If we combine the aggregation data together with the estimated thermodynamic stabilities, a trend becomes observable (Fig. 26): the lower the stability, the more likely the protein is cleaved and aggregates. These

findings have to be carefully considered when evaluating the effect of small molecules acting as stabilisers. Indeed our data suggest that different TTR variants may respond differently to the stabilisation through small ligands, according to their intrinsic thermodynamic stability. Further considerations on this topic are presented in the following chapters of this thesis.

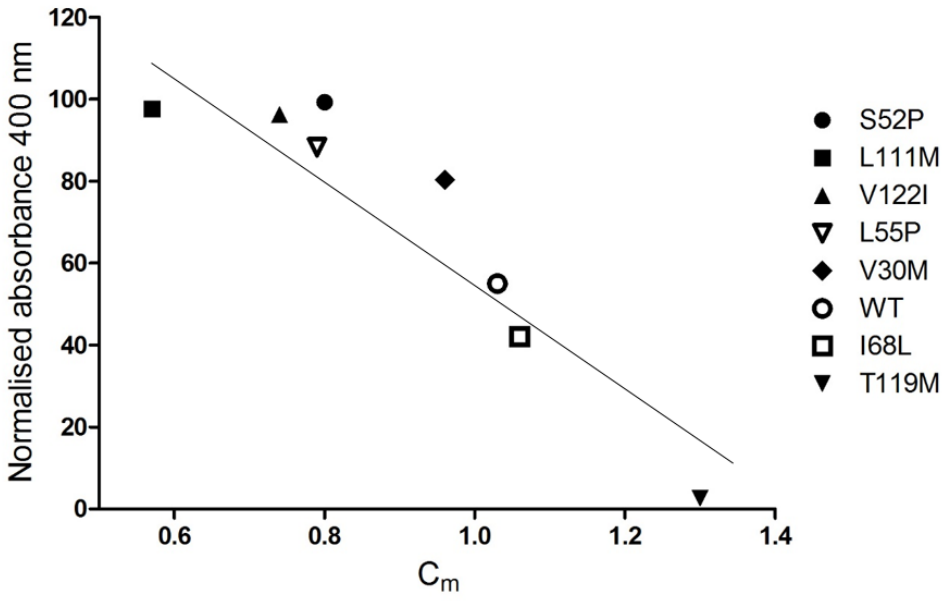

Figure 26. Aggregation propensity and C_m. Normalised absorbance at 400 nm plotted against the estimated C_m of each variant tested. A relation between protein thermodynamic stability and propensity to undergo cleavage and aggregation is observable. The line does not imply the existence of a correlation and was only added to guide the eye.

We are currently developing, together with Jasco Europe, a cuvette-flow system, which would allow a fine tuning of the shear forces acting on the protein and therefore a very precise determination of the relationships existing between forces, unfolding, proteolysis and aggregation.

Chapter 4. Evaluation of the efficacy of TTR stabilisers on the mechano-enzymatic mediated fibrillogenesis

4.1 Introduction

Over the past decade, hundreds of structurally different compounds from chemically different classes have been identified as inhibitors of TTR fibril formation *in vitro* at low pH. Most of the ligands were created using structure-based design principles, while some of them were discovered through focused screening. The evidence that the binding of the thyroid hormone T4 to TTR prevents amyloid fibril formation by stabilisation of the native tetramer and subsequent reduction of tetramer dissociation has prompted the exploitation of small molecule to kinetically stabilise TTR in its native state, over the dissociative transition state (Hammarström P et al, 2003). Unfortunately, though, only a small amount of T4 in plasma is bound to TTR, leaving 99% of WT TTR binding sites in blood unoccupied (Adamski-Werner SL, 2004). Small molecules binding one or both of TTR T4 binding sites could therefore come into play as TTR stabilisers, offering a potential therapeutic alternative to liver transplantation for the treatment of patients with FAP (Coelho T et al, 2012) and a completely new approach for the treatment of other forms of TTR amyloidosis (Hammarström P et al, 2003). Further support for the idea of kinetic stabilisation of the tetramer by means of small molecules comes by the clinical observation that in heterozygous people co-expressing both the trans-suppressor subunit (T119M) and the FAP-associated subunit, V30M (Hammarström P et al, 2003), TTR amyloid disease is prevented due to an increase in the energetic barrier associated with tetramer dissociation.

A large number of small molecules, both natural and synthetic, showing structural similarities with the thyroid hormone T4 were therefore screened by evaluation of the displacement of radioactively labeled T4 from TTR (Nencetti S & Orlandini E, 2012) in search for potential TTR stabilisers. The ability to

inhibit TTR fibril formation *in vitro* at pH 4.4 was then investigated using a standard turbidimetric assay.

With the discovery of the new mechano-enzymatic mechanism for TTR amyloidogenesis (Mangione PP et al., 2014), a completely new evaluation of the ability of these compounds to prevent aggregation became necessary.

During my experimental work I have tested, under mechano-enzymatic conditions, several compounds acting as TTR stabilisers.

Tafamidis. This drug, currently in use for the amelioration of familial amyloid polyneuropathy (FAP), is one of the compounds developed to kinetically stabilise the tetramer and was originally synthesised and developed in Kelly's lab.

From a chemical point of view, the structure of the drug is 2-(3,5-dichlorophenyl)-1,3-benzoxazole-6-carboxylic acid (Fig. 27).

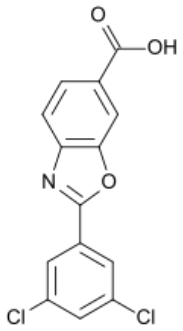

Figure 27. Chemical structure of tafamidis

Tafamidis, administered as its meglumine salt (Vyndaquel®), has completed an 18 month placebo controlled phase II/III clinical trial (Fx-005) (Coelho T et al, 2012) and an 18 month extension study, which provides evidence that this compound (20 mg once daily, now increased to 40 mg) can slow, but not stop, the progression of familial amyloid polyneuropathy (Gundapaneni BK et al, 2018). The results of the clinical trial have led to the approval by the EMA (European Medicine Agency) in 2011 to use the drug for the treatment of stage 1 FAP. Furthermore, in 2013, tafamidis was approved by the *Japanese*

Pharmaceuticals and Medical Devices Agency for the treatment of all stages of FAP (Sekijima Y, 2014). While tafamidis has showed an effect in adult patients with an early stage (stage 1) of FAP (Andrade C, 1952; Coelho T, 1996), its effect on patients with more advanced stages of FAP has not yet been proven (Obici L & Merlini G, 2014). A very recent study, however, suggests that patients treated with tafamidis have a reduced frequency of cardiac complications and urgent hospitalization (data presented at the European Society of Cardiology Congress 2018). The toxicological profile is positive as the drug is well tolerated and shows no relevant side effects as well as a preserved thyroid function (Coelho T et al, 2012). Tafamidis is selectively bound (Kd_1= 2 nM, Kd_2= 154 nM) by TTR (Fig. 13) with negative cooperativity and kinetically stabilises WT and mutant tetramers under mild denaturing conditions, inhibiting amyloidogenesis at acidic pH (Bulawa CE et al, 2012). The delay in the progression of the disease observed in the clinical trials suggests that the drug might exert a similar effect *in vivo*. It has been shown that tafamidis is able to raise the energy barrier for TTR tetramer dissociation and by doing so it decreases fibril formation under physiological conditions, slowing down TTR FAP progression after its onset (Coelho T et al, 2012).

Tolcapone. Repositioning existing drugs licensed for a different therapeutic indication could prove a valid approach to identify new compounds able to inhibit TTR fibrillogenesis. One clear advantage of this approach is the reduced amount of time required to obtain approvals for clinical trials and, eventually, clinical use due to the already known pharmacodynamics, pharmacokinetics and safety profiles. Tolcapone (Fig. 28), an orally active cathecol-O-methyltransferase (COMT) inhibitor authorised in the United States and Europe as an adjunct to levodopa and carbidopa for the treatment of Parkinson's disease, has recently been suggested as a potential inhibitor of TTR fibrillogenesis (Sant'Anna et al, 2016).

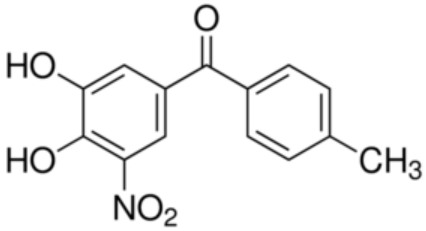

Figure 28. Chemical structure of tolcapone

Tolcapone was shown to specifically bind to TTR, apparently lacking negative cooperativity, and stabilise both WT and mutant TTR variants at low pH, reducing their aggregation, thus preventing TTR-induced cardiotoxicity more effectively than tafamidis (Sant'Anna et al., 2016). However, it is worth noting that despite the high affinity for both binding sites, the maximum stoichiometric ratio achieved in plasma is 1:1. Despite its therapeutic potential, this compound is characterised by an intrinsic toxicity, which could induce severe adverse reactions in patients undergoing treatment on a daily basis.

mds84. The Wolfson Drug Discovery Unit, part of the UCL Centre for Amyloidosis and Acute Phase Proteins, has developed, in collaboration with Glaxo Smith Kline, a palindromic ligand named mds84 that is 2,2'-(4,4'-(heptane-1,7-diylbis(oxy)) bis (3,5-dichloro-4,1-phenylene)) bis (azanediyl) dibenzoic acid (Fig. 29, left). The original aim was to create a compound able to simultaneously bind two TTR molecules, thus creating a condition of rapid clearance of the protein by the reticuloendothelial system. The experimental data, however, suggested that the compound was not linking two TTR tetramers, but, in a one to one stoichiometry, it was surprisingly able to occupy both T4 binding sites in each TTR tetramer molecule with the carbon linker occupying the central channel of the protein.

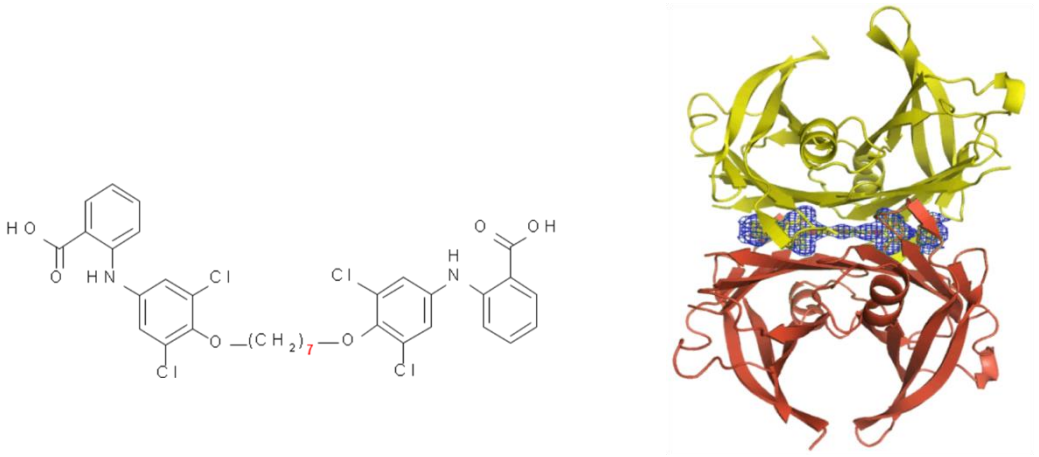

Figure 29. Structure of mds84 and of the mds84-TTR complex. The two identical dimers are shown in yellow and red. Difference electron density is shown in blue (contour 1.5 Å). Image adapted from Kolstoe SE et al, 2010.

The compound proved to bind native TTR irreversibly under physiological conditions. The resulting stabilisation of the tetrameric assembly and inhibition of amyloidogenic aggregation was far more potent than other known ligands tested in the same acidic conditions. X-ray analysis of the TTR–mds84 complex (Fig. 29, right) revealed the chlorinated rings of both head groups in the inner binding site, interconnected by clear electron density corresponding to the 7-carbon linker. This super-stabiliser is orally bio-available and exhibits low inhibitory activity against cyclo-oxygenase (COX) (Kolstoe SE et al, 2010). Furthermore, it is rapidly bound by WT TTR in whole serum and even more avidly by amyloidogenic variants.

The drawback of this molecule is represented by its poor solubility in aqueous buffer, which complicates its development as a potential drug. Nevertheless, it represents a prototype of a class of very promising molecules acting as inhibitors of TTR amyloidogenesis.

Compound A. Although mds84 looked extremely promising, it was lacking some properties necessary to make it a good candidate drug, above all solubility. In collaboration with Glaxo Smith Kline a whole series of bivalent ligands was developed in order to look for more “druggable” molecules retaining the same binding and stabilising properties of mds84. Amongst all, compound A was selected as a lead compound as it showed good binding and stabilising properties, associated with good solubility. Its development was carried on until some adverse reactions were seen in two out of 4 animals in which the drug was tested. Recently, a research project funded by UCL Technology has been awarded to our group in order to look for analogues of compound A lacking the toxicity associated with this molecule. Due to the confidentiality associated with the development of new drugs, both the structure and the name of the compound cannot be disclosed.

V122I TTR, present in 3-4 % of the African and Afro-Caribbean ethnic groups and representing the most prevalent cause of hereditary cardiac amyloidosis (Quarta CC et al., 2015), was used to test the efficacy of the inhibitors listed above as it is carried by a large number of individuals and it shows a behavior in terms of stability and aggregation propensity, which is intermediate between the WT protein and the most aggressive variants.

4.2 Materials and methods

4.2.1 Preparation of drug stock solutions

The compounds were weighed using an analytical scale and dissolved in 99.9 % dimethyl sulfoxide (DMSO; ACROS Organics) to reach a final concentration of 10 mM. These solution were kept at 4 °C protected from light due to the photosensitivity of the compounds.

4.2.2 Mechano-enzymatic fibrillogenesis of V122I TTR in the presence of stabilisers

Lyophilised TTR was dissolved 1 mg/ml (18 μM) in PBS, pH 7.4 (Sigma-Aldrich) and was transferred into glass vials with a diameter of 1.4 cm and an air-water interface corresponding to 1.5 cm^2 that mimicked the hydrophobic surfaces to which the protein is exposed *in vivo*. The stabilisers were tested at 4 different concentrations (9, 18, 36, 72 μM respectively) corresponding to the following drug to TTR ratios: 0.5:1, 1:1, 2:1 and 4:1. Several dilutions of the drug stock solutions were made in order to add the same amount of DMSO to each sample. The same amount of 99.9 % DMSO was added to the control sample without drug. In order to achieve complete binding, the solution was left for 30 min at 37 °C. Following the incubation, trypsin was added to a final concentration of 5 ng/μl. A magnetic stirrer was used to agitate the solution at 1.500 rpm (IKA magnetic stirrer). The samples were left under agitation at 37 °C for 96 hours. Aggregation was monitored by measuring turbidity at 400 nm every 24 hours.

4.2.3 SDS-PAGE electrophoresis

Samples for SDS-PAGE electrophoresis were taken every 24 hours and mixed 1:1 with sample buffer containing sodium dodecyl sulphate (SDS; VWR) and β-mercapto ethanol (VWR) as a reducing agent. The samples were then boiled for 5 minutes and centrifuged for 3 minutes at 10000 rpm. 5 μl of sample was loaded onto a 15% Excel Gel homogeneous SDS-PAGE (polyacrylamide gel 250x110x0.5mm; GE Healthcare). Low molecular weight markers (GE Healthcare) were used as reference.

A constant voltage of 300 V was applied during the run, which was stopped when the front of the solvent reached the cathode. The gel was stained with 0.2 % Coomassie blue (GE Healthcare) dissolved in 45 % methanol (VWR) and 10 % acetic acid (VWR).
The destaining solution used contained methanol and acetic acid in the same proportions used for the Coomassie blue solution.

4.2.4 Quantification of the percentage of uncleaved TTR in solution

Quantification of the electrophoretic bands corresponding to monomeric TTR was carried out using the Quantity One 1-D analysis software from Bio-Rad. The band at time point 0 was considered as 100% of protein in solution and was used to normalise all the other bands within the same experiment.

4.2.5 Congo red staining and scoring of amyloid in the TTR aggregated material

The stock solution was prepared by mixing 3 g of Congo red (Sigma-Aldrich) to 800 ml ethanol (VWR), 200 ml MilliQ water and 20 g NaCl (VWR). The solution was left under stirring for at least 1 hour, filtered with Whattmann paper and activated by adding 1% (v/v) of a 1% NaOH solution (w/v) before staining. TTR aggregated material was obtained by centrifugation of the different samples at the end of the experiment for 20 minutes at 10300 g. The supernatant was removed and the resulting pellet was resuspended in 100 µl of PBS, pH 7.4. 10 µl of sample was pipetted onto a microscopy slide and let dry at room temperature. 2 ml of activated Congo red solution was then placed onto the surface of the slide and left staining for at least 30 minutes. The slides were then washed with MilliQ water, let dry and covered with a coverslip fixed in place with DPX mountant (Sigma-Aldrich). Congo red score was assessed by blind quantification on six slides per each group. The following score was used: 0 (no spot detected), 1 (occasional spots), 2 (green birefringent spots clearly visible and corresponding to the stained spots in the bright field), 3 (surface homogeneously covered by green birefringent material).

4.2.6 Electron microscopy

Transmission electron microscopy analysis was performed using protein samples stained with 2% (w/v) uranyl acetate using a CM120 microscope at 80 keV by Alejandra Carbajal at the Division of Medicine Electron Microscopy Unit, Royal Free Campus, UCL.

4.3 Results

4.3.1 Inhibition of aggregation

Inhibition of the mechano-enzymatic fibrillogenesis was tested in the presence of tafamidis, tolcapone, the experimental bifunctional compound mds84 and compound A, which is a bivalent compound with improved solubility.

As mentioned in the introduction of this chapter, the ability of the different compounds to inhibit aggregation was tested on the V122I TTR variant. Indeed the data presented in chapter 3 identifed this variant as intermediate between the WT protein and the most aggressive variants in terms of stability and aggregation propensity.

Aggregation experiments were carried out at 37º C in PBS, pH 7.4, for 96 hours in the presence of trypsin. A magnetic stirrer provided agitation throughout the whole length of the experiment. ThT, commonly used to detect the formation and/or inhibition of the formation of amyloid fibrils, would have been the best choice to evaluate the activity of the different compounds. However we realised that it could not be used as most of these molecules quenched the ThT emission signal by absorbing in the same wavelength where ThT emits, therefore interfering with results (Fig. 30).

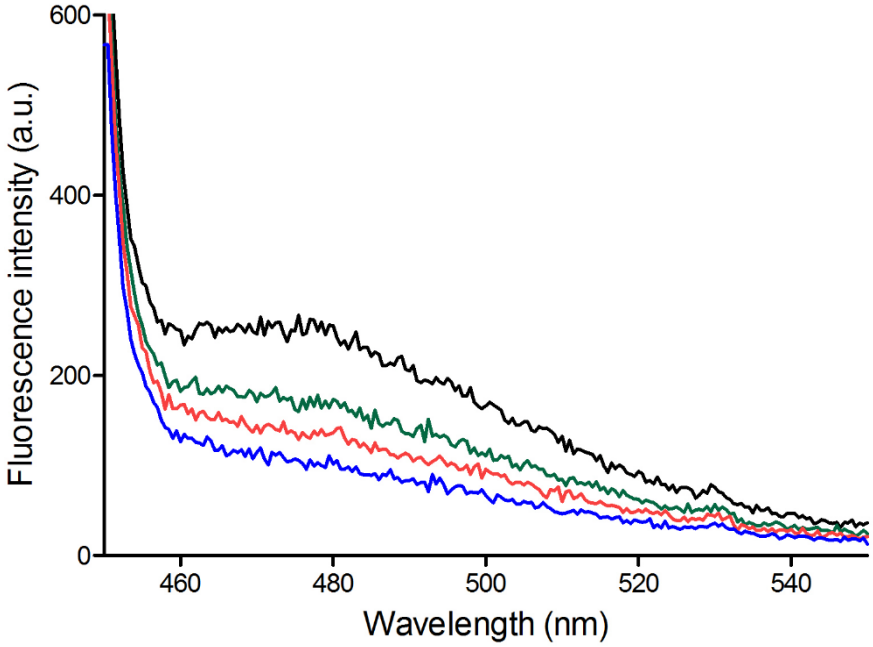

Figure 30. Example of ThT emission fluorescence quenching by tolcapone. Emission fluorescence spectra of a solution of 10 µM ThT and 9 µM S52P TTR fibrils in PBS (black) and in PBS in the presence of 9 µM (green), 18 µM (red) and 36 µM (blue) tolcapone, respectively. The spectra were acquired using a Perkin Elmer LS55 Luminescence Spectrometer. The samples were excited at 445 nm and the emission fluorescence was recorded in the range 450-550 nm with accumulation of three scans.

Turbidity at 400 nm was therefore selected as a way to monitor the formation of insoluble aggregates in solution and was monitored every 24 hours throughout the whole length of the experiment.

The drugs were tested at four different concentrations corresponding to four distinct drug to TTR molar ratios: 0.5:1, 1:1, 2:1 and 4:1. To allow complete binding the solutions containing the protein and the compounds were left for 30 minutes at 37 ºC before trypsin was added.

Figure 31 shows the final turbidity at 96 hours, normalised to the control, which contained only TTR and trypsin without any drug.

Bivalent compounds appeared more effective than their monovalent counterpart, showing better efficacy even at a 0.5:1 ratio. Interestingly,

tolcapone, which lacks negative cooperativity and binds both binding sites with the same affinity, appeared more efficient than tafamidis, showing good inhibition of aggregation in 1:1 ratio. When complete saturation of both binding sites was reached (i.e. in 1:1 ratio for bivalent and 2:1 ratio for monovalent ligands), an almost complete inhibition of fibrillogenesis was achieved for all the compounds tested.

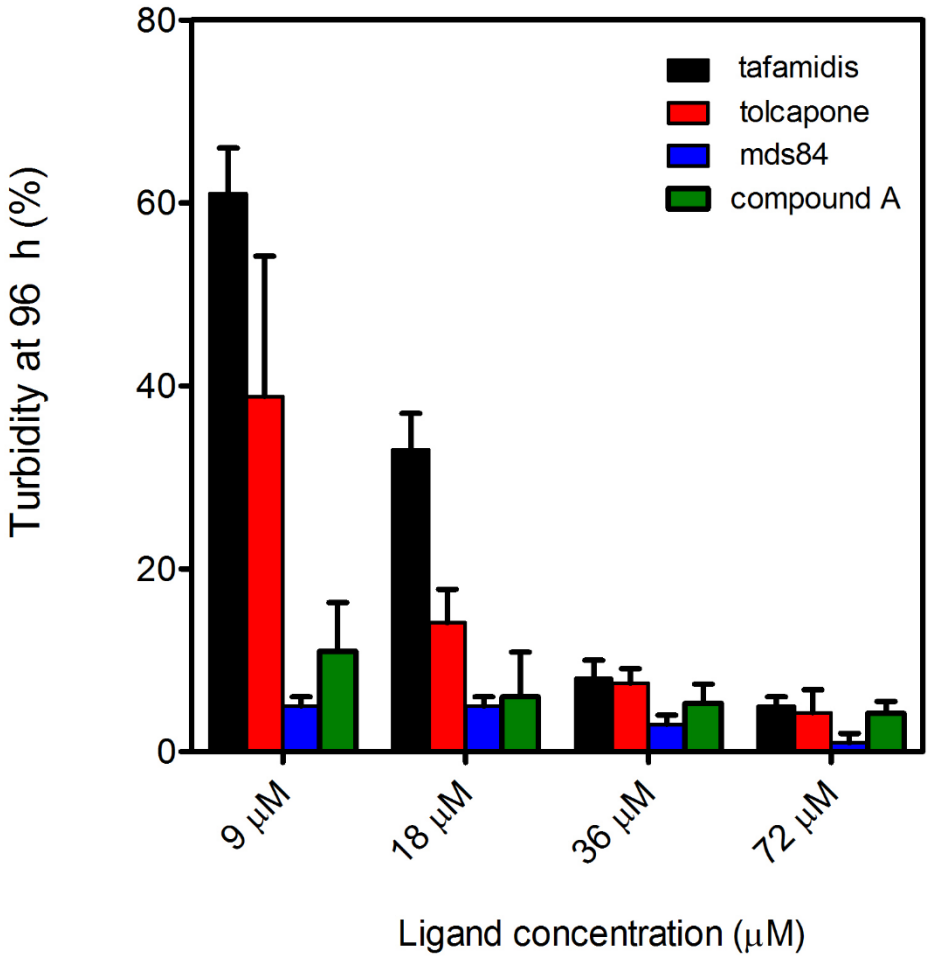

Figure 31. Normalised turbidity at 96 hours in the presence of drugs at different molar ratios. Data presented as mean (SD) of 3 different sets of experiments. The data were normalised to a control sample incubated in the same experimental conditions in the presence of trypsin, without any drug added.

4.3.2 Inhibition of proteolysis

Following the evaluation of the potency of the compounds to inhibit TTR aggregation, investigation of their ability to inhibit proteolytic cleavage of the protein was carried out. At the end of fibrillogenesis, the different samples were analysed by SDS-PAGE under reducing and denaturing conditions. Quantitative analysis of the intensity of the band corresponding to the TTR monomer in SDS-PAGE was performed using the Quantity One 1-D analysis software from Bio-Rad using the rectangular box tool (Fig. 32).

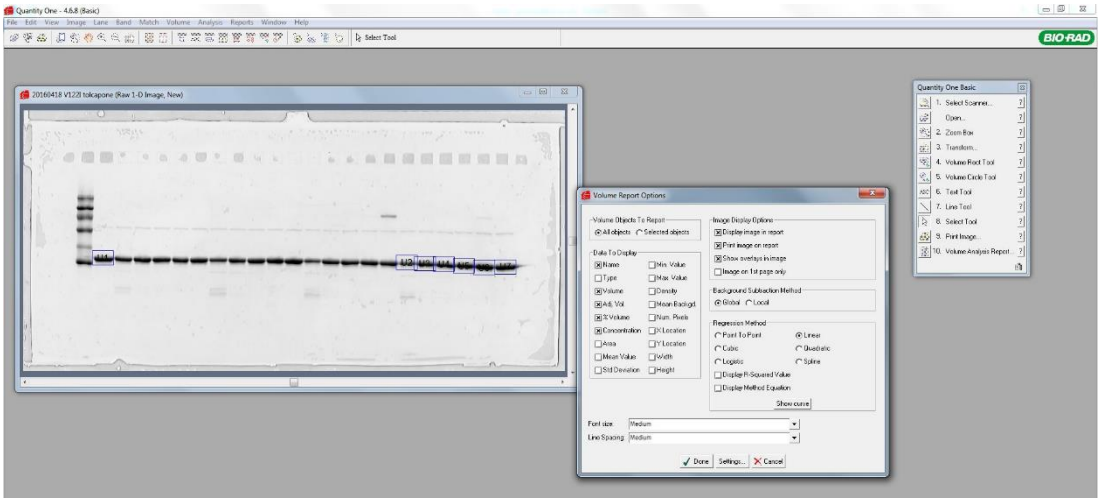

Figure 32. Example of quantification of monomeric TTR electrophoretic bands using the Quantity One 1-D software from Bio-Rad. The rectangular box tool was used to quantify the intensity of the electrophoretic bands. Background correction was set on global.

The intensity of the monomer band at time 0 was compared with the intensity of the same band at the end of the experiment in the presence of different molar ratios of drug, thus retrieving information on the extent of proteolysis, which took place during aggregation. The inhibition of proteolysis correlated well with the inhibition of aggregation as demonstrated by the fact the bivalent compounds were already effective at molar ratios 0.5:1 and 1:1. In

the case of bivalent compounds higher molar ratios were necessary to achieve an almost complete inhibition of proteolysis (Fig. 33).

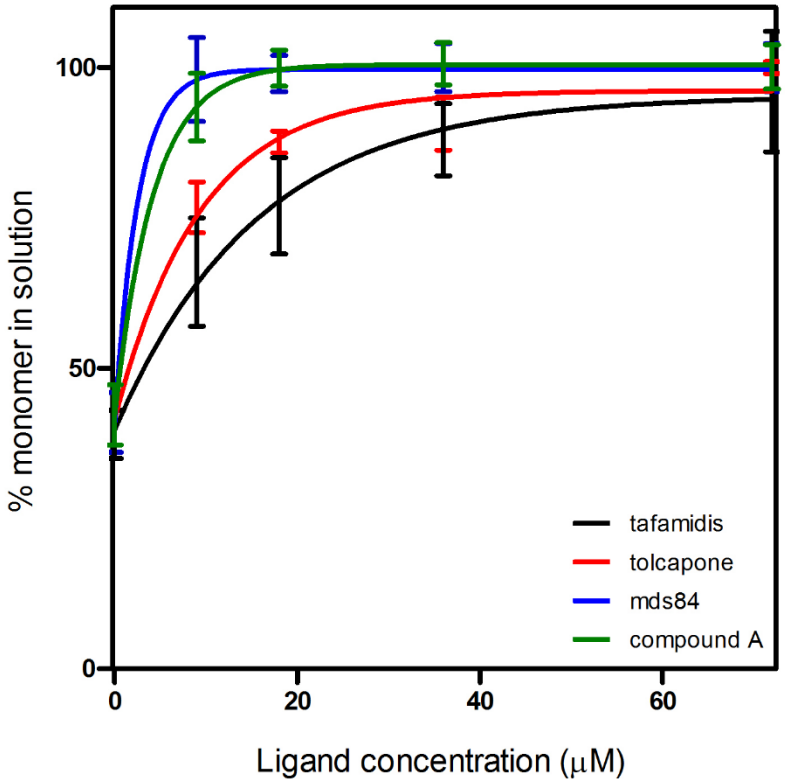

Figure 33. Inhibition of proteolysis by tafamidis (black), tolcapone (red), mds84 (blue) and compound A (green). Data presented as mean (SD) of 3 independent experiments and normalised to the intensity of the TTR band at time 0.

4.3.3 Congo red staining, amyloid score and electron microscopy

Further analysis of the aggregated material was carried out by Congo red staining. At the end of the experiment, the samples were centrifuged for 20 minutes, the supernatant was removed and the pellet resuspended in a volume of 100 µl of PBS.

10 µl of suspension was then placed onto a microscopy slide and stained with Congo red. The samples were then observed under a polarised light microscope (Fig. 34).

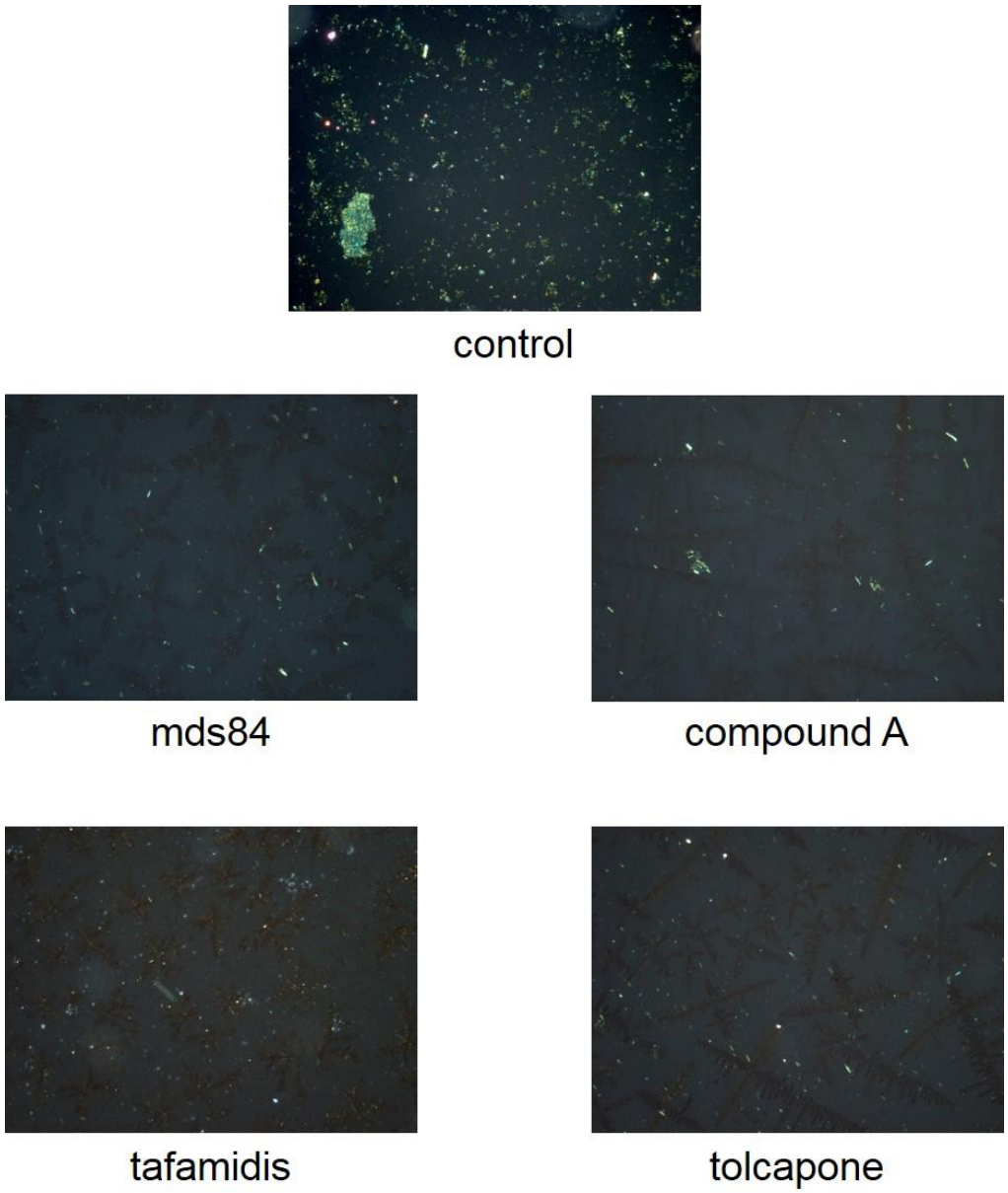

Figure 34. Congo red apple-green birefringence in the presence of fourfold excess of drugs. The control without ligand after 96 hours is shown on top as a reference. Fibrillar amyloid deposits could be detected in all the samples even in the presence of fourfold excess of stabiliser. The images were acquired on a Leica DMLB microscope equipped with a Leica PL Fluotar 10 x/ 0.30 objective using a JVC colour video camera and the Leica IM50 image capture software.

Each slide was given an amyloid score (Fig. 35) using the following criteria:

- 0: no spot detected
- 1: occasional spots
- 2: green birefringent spots clearly visible and corresponding to the stained spots in the bright field
- 3: surface homogeneously covered by green birefringent material

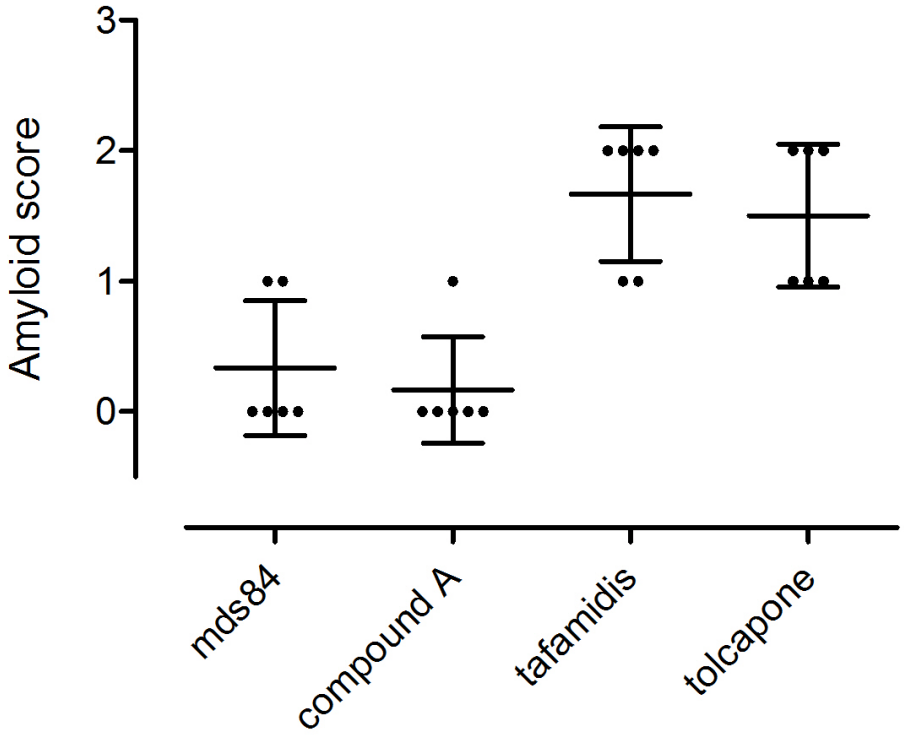

Figure 35. Congo red amyloid score. Congo red score was assessed by blind quantification on six slides per each group.

Electron microscopy analysis performed on the samples containing the highest ligand concentration revealed the presence of amyloid fibrils in all samples, suggesting that the inhibition of aggregation could not be completely stopped, even in the presence of bivalent compounds (Fig. 36).

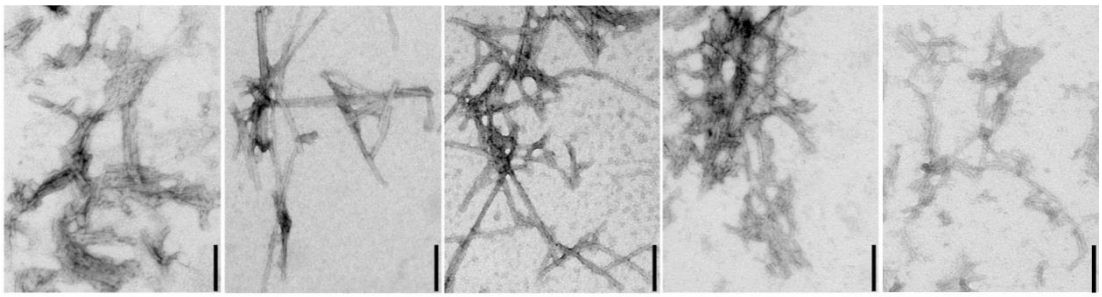

Figure 36. Electron microscopy analysis of the pellet in the presence of different drugs at 72 μM. Left to right: control sample without any drug, mds84, tafamidis, tolcapone, compound A. Scale bar 100 nm.

4.4 Discussion

All the compounds inhibited the formation of amyloid fibrils in a concentration-dependent fashion. At molar ratios of drug to TTR tetramer equal or bigger than 2:1, the different drugs exhibited the same effect with an almost complete inhibition of aggregation (~90%). For molar ratios below 2:1 instead, the two bivalent compounds, mds84 and compound A, proved to be more effective than their monovalent counterparts with tolcapone appearing more effective than tafamidis. A more detailed analysis revealed that at molar ratio of 0.5:1 mds84 reduced fibril formation by approximately 90%, compound A 87%, tolcapone 60% and tafamidis only by 40%. At 1:1 inhibition reached around 60% with tafamidis, ~80% with tolcapone and remained at ~95% with mds84 and compound A. At 2:1 and 4:1 all the compounds inhibited aggregation by approximately 90%. The better efficacy of tolcapone if compared with tafamidis can be explained by its property of not inducing negative cooperativity (Sant'Anna et al., 2016).

In agreement with the turbidity data, all the ligands inhibited proteolysis of TTR in a dose-dependent manner: in the presence of molar ratios of drug to TTR tetramer equal or higher than 2:1, all the compounds exhibited the same effect inducing an almost complete inhibition of the proteolytic digestion. A clear distinction appeared instead at lower molar ratios, where mds84 and compound A proved to be more effective than tolcapone and tafamidis respectively.

A possible explanation for this different behavior can be given by considering the way these compounds interact with the TTR tetramer. In the case of monovalent ligands, such interaction is limited to the two T4 binding pockets.

In the case of the bivalent ligands the binding pockets are occupied, but the central channel is occupied as well. The presence of a carbon linker in the central cavity of the molecule occupies the void volume normally occupied by water molecules and results in the formation of a series of hydrophobic interactions, which possibly stabilise the protein by reducing subunit sliding and inducing some long distance stabilisation of the CD loop, where the proteolytic cleavage takes place.

The central channel could therefore play the role of a third binding pocket, which has never been considered before as possible target of TTR-stabilising ligands (Fig. 37).

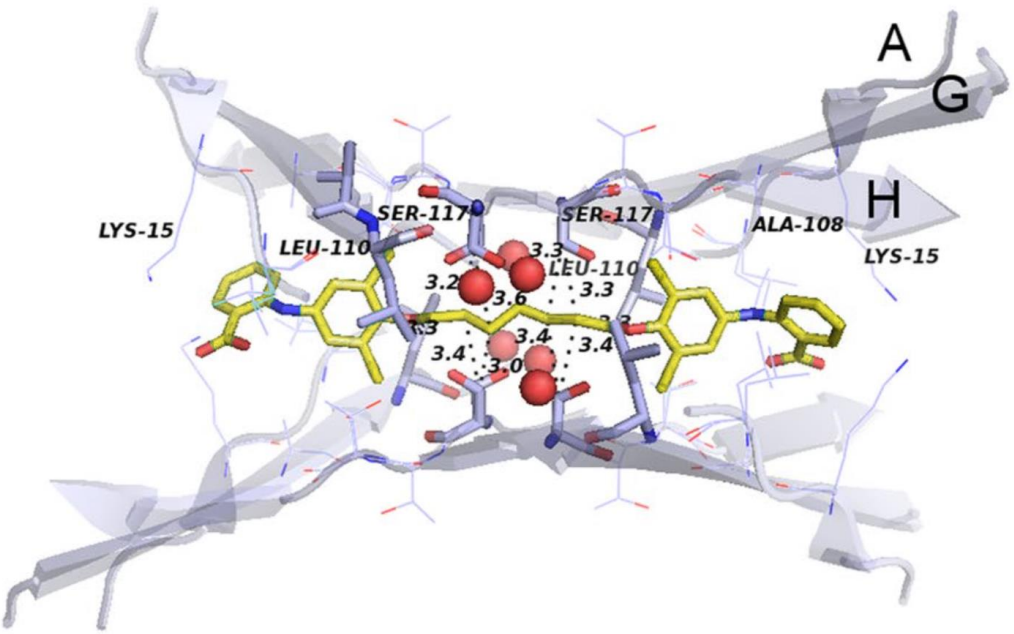

Figure 37. Network of hydrophobic interactions formed by the prototypic bivalent ligand mds84 inside the inner channel (adapted from Verona G et al., 2017).

Even in the presence of large molar excess of tafamidis or tolcapone, with apparent complete inhibition of aggregation, it was possible to detect some insoluble material, which showed the typical apple-green birefringence and was fibrillar when observed in the electron microscope. In the presence of mds84 and compound A only a minimal amount of insoluble material could be detected, but extensive analysis at the polarised microscope revealed the presence of amyloid fibrils.

These final results appear of extreme importance considering the effect that even a minimal amount of amyloid seeds, which we defined *minimal residual*

disease, can have *in vivo* in the development or progression of TTR amyloidosis.

In the light of these results, current clinical trials should be critically analysed. Also the development of new drugs should aim to find compounds able to completely abrogate the formation of even a minimal amount of amyloid fibrils. This is also true for some of the therapies currently exploited to try and treat TTR amyloidosis, which involve the reduction by 90 % or more of TTR hepatic synthesis by the means of antisense oligonucleotides or small interfering RNAs, where even with a very small TTR plasma concentration, the formation of fibrils could still take place.

Chapter 5. NMR as a tool to investigate the structural effects induced by TTR ligands

5.1 Introduction

Established in 1971, the Protein Data Bank (PDB) is a database for the three-dimensional structures of large molecules. It contains almost 300 X-ray structures of WT TTR, TTR variants and TTR complexes, demonstrating how over the last 30 years, crystallography has been widely used to investigate the structure of this protein. Palaninathan (Palaninathan SK, 2012) published a comprehensive review describing the role of X-ray crystallography in the design of inhibitors of TTR fibrillogenesis. However, several times in the paper it is stated that "the crystal structures show no significant conformational changes". In the final remarks the author concludes that "the mutation-induced structural changes and the mechanism of amyloid formation are yet to be elucidated", suggesting that despite the high number of protein structures published, the information that can be derived from them, although powerful in terms of structural data, is not sufficient to fully understand the mechanisms underlying TTR amyloidosis nor the structural changes undergone by the protein upon the binding of small molecules acting as stabilisers. Obtaining clear data on the central channel region also appears challenging, as highlighted by Kolstoe and co-workers who could not detect any electron density whilst investigating the structure of the complex between TTR and 4ajm15, a bivalent compound whose alkyl linker locates inside the inner channel (Kolstoe S et al., 2010).

Our collaborator Dr Matteo Degiacomi at the University of Durham compared the 265 human TTR crystallographic structures available from the PDB database by evaluating their root-mean-square deviation of atomic positions (RMSD) of the TTR monomers and showed that, apart from the F87M/L110M (Palmieri Lde C et al., 2010) and the G53S/E54D/L55D (Karlsson A & Sauer-Eriksson AE, 2007) mutants, no significant differences could be observed (Fig. 38). The first mutant is an engineered TTR monomer in which the introduction of two new amino acids prevents oligomerization into dimers or tetramers by perturbing both the dimer interface and the weak dimer-dimer

interaction (Jiang X et al., 2001) and the latter is another engineered mutant, which shows significant tendency to aggregate *in vitro* (Goldsteins G et al., 1997).

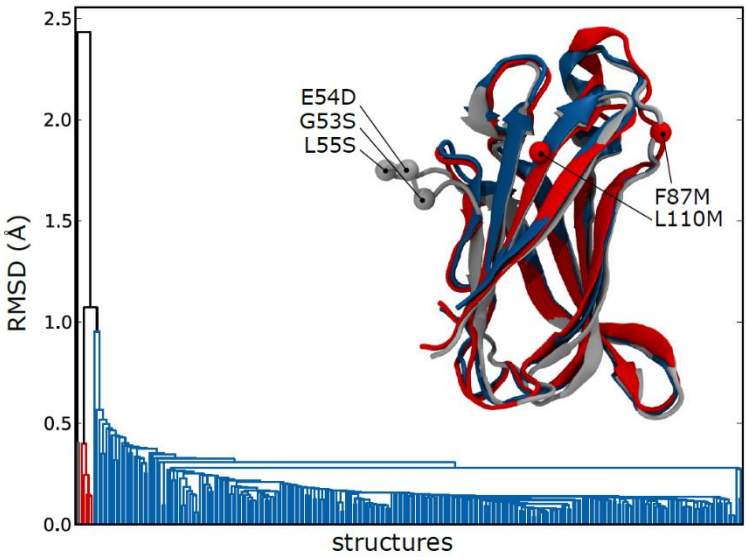

Figure 38. Comparison of TTR X-ray derived structures. The monomers were aligned using the α-carbon atoms common to all structures. The pairwise RMSD of the α-carbons was then calculated and used to cluster the structures using a hierarchical clustering algorithm. Structures were considered to be part of a different cluster if their RMSD was above 1 Å. 258 structures had an RMSD < 0.6 Å (blue, PDB code 1BM7). Only 5 structures of the F87M/L110M mutant at different pH (red, PDB code 3GRG) and 2 structures of the triple mutant G53S/E54D/L55D (gray, PDB code 1G1O) had a difference of more than 1 Å and were therefore clustered apart.

It therefore appears plausible that some structure and dynamics differences existing among the 258 structures analysed are not identified by X-ray crystallography. In fact, the X-ray structure reports the conformation of the protein corresponding to an energy minimum inside the crystal and may only represent a partial view of a more complex set of conformers that may be

present in equilibrium solution. Suggestions on the crucial role played by the dynamics of specific regions of the protein in determining the susceptibility to proteolysis come from the different behaviours observed for distinct TTR variants in the fibrillogenesis experiments presented in chapter 3, and the different protection against proteolysis resulting from the binding of small molecules presented in chapter 4. Indeed, the superior resistance to proteolysis conferred by simultaneous occupancy of both T4 binding sites, in comparison with the effect obtained when only one site is saturated, is a good example of how binding-induced structural changes can have a protective effect towards proteolysis mediated fibrillogenesis.

To address the more complex pattern present in solution in physiological conditions, we used NMR spectroscopy. This technique can be applied to investigate protein structures and dynamics in solution, including those changes induced by pathogenic mutations and ligand binding. In addition, it can also assist in the understanding of the superior efficacy shown by bivalent ligands in comparison with monovalent, for which some considerations have already been presented in the previous chapter. Indeed, one of the key advantages offered by this technique is the ability to investigate protein dynamics in the nanosecond-second timescale. TTR is a 55 kDa protein and is therefore a rather large protein in NMR terms. In fact, the general molecular weight cut off for NMR spectroscopy is around 30 kDa for mono or double labelled proteins (usually ^{15}N and/or ^{13}C). This is due to nuclear spin relaxation effects, including chemical shift anisotropy interaction and dipole-dipole relaxation. Deuterium labelling and the use of appropriate NMR experiments (described in paragraph 5.2.2), though, can overcome this issue making larger proteins suitable candidates for NMR analysis.

Literature review

Some pioneering NMR work on TTR was done by Wemmer and Kelly (Liu K et al., 2000; Liu K et al., 2000; Liu K et al., 2002) who deposited the full assignment of the WT protein at pH 5.75 and used ^{2}H-H exchange to study the stability of the WT tetramer under non-denaturing (pH 5.75) and partial

denaturing conditions (pH 4.5). They showed that at pH 5.75 β-strands A, B, E and G and their interconnecting loops were the most slowly exchanging core of the protein (Liu K et al., 2000), while moving to pH 4.5 β-strands B and E, together with part of β-strand C and F rapidly exchanged with the solvent, thus suggesting a cooperative disruption of half of the β-sandwich that characterises the protein structure (Liu K et al., 2000). In a follow up of this initial work, the same approach was used to investigate the stability of three different TTR isoforms, L55P, V30M and T119M, showing that the two pathogenic mutations induced important destabilisation in the core of the protein, shown by increased ^{2}H-H exchange rate, while enhanced stabilisation was observed for the protein core in the T119M mutation (Liu K et al., 2002). Overall these observations led to the conclusion that destabilisation of the folded state contributes to the amyloidogenicity of TTR, thus supporting the experimental results obtained on TTR fibrillogenesis at low pH. The same ^{2}H-H exchange approach was used to study residue-specific solvent protection factors within the aggregates obtained at pH 4.5 from the Y114C TTR variant (Oloffson A et al., 2004).

Lim and co-workers (Lim KH et al., 2013) utilised a monomeric variant of TTR (F87M/L110M, M-TTR) to investigate the localised structural fluctuation that might predispose the protein to aggregate. They also utilised a triple mutant (F87M/L110M/T119M) in order to compare the data obtained on M-TTR with those obtained with M-T119M TTR, which is the monomeric form of the protective T119M TTR variant. The results suggested that the amyloidogenic state of WT TTR is characterised by a largely native-like CBEF β-sheet conformation, disrupted DAGH β-sheet and structurally perturbed AB loop. The introduction of the mutation in position 119 determines a great reduction of these fluctuations, possibly explaining its stabilising effect *in vivo*. In a follow up paper, by a combination of solid-state and in solution NMR, Lim and colleagues confirmed the data previously published, showing that the soluble amyloidogenic precursor state of TTR contains a native-like CBEF β-structure (Lim KH et al., 2016) and a disrupted DAGH β-sheet.

The M-T119M TTR (F87M/L110M/T119M) structure in solution was solved by Kim and colleagues (Kim JH et al., 2016) who highlighted the sliding of β-strands G and H to a non-native position due to the substitution of T119, whose side chain assumes an outward-pointing position in the WT protein, with M119, whose side chain inserts into the hydrophobic core of monomeric TTR (Kim JH et al., 2016). Apart from the initial work by Wemmer and Kelly, most NMR analyses have been conducted on monomeric forms of the protein, which, although useful to have an insight of the structural fluctuations undergone by the core of the protein, do no resemble its fully folded tetrameric assembly.

Only recently two papers were published by the Wright group on the kinetic analysis of the aggregation pathway at low pH and the effect of pathogenic mutations on the fully folded TTR tetramer (Sun X et al., 2018; Leach BI et al., 2018). A 19F-NMR assay using a trifluoroacetyl probe linked to cysteine 85, in the engineered C10S/S85C TTR variant, that gives distinct shifts for the TTR tetramer and monomeric intermediate was used to directly quantify their populations during the aggregation process and to investigate the kinetics and mechanics of the aggregation pathway of WT and pathogenic mutants of TTR (V30M, L55P, F87A and V122I). Performing experiments at different temperatures and pH 4.4, Sun and co-workers were able to simultaneously investigate the populations of tetrameric TTR, monomeric intermediates and aggregated states, highlighting the critical role played by intersubunit hydrophobic interactions in the stabilisation of the tetramer. They also showed that above 298 K, in their experimental conditions, no soluble oligomers accumulated as the monomeric intermediates rapidly converted into highly-ordered structures.

Analysis of the effect of three pathogenic mutations, V30M, L55P and V122I, showed a number of subtle structural differences between WT and mutant TTR in its tetrameric form. Both V30M and L55P mutations were observed to induce chemical shift perturbations, which propagated from the site of mutation through the β-sheets to the strong dimer interface. The L55P mutation induced structural perturbations in both the DAGH and CBEF β-

sheets and caused a disruption in the hydrogen bond network between strands D and A as well as in strand C, which directly packs against the mutated side chain. Such perturbations propagated through the hydrogen bond network of the CBEF sheet to the strong dimer interface, the CD loop, part of the DE loop and finally the AB loop, which is involved in intermolecular contacts at the level of the weak dimer interface. The V30M substitution mainly affected the CBEF β-sheet, where it perturbed the local hydrogen bond network. Moreover it affected residues both in the E and F strands, which are located in the strong dimer interface. To a lesser extent than for the L55P variant, a minor perturbation was also observed for the DAGH β-sheet. Interestingly, the V122I-induced structural changes were only minor when compared to the WT counterpart and clustered around the site of mutation, from which they propagated to both the strong and the weak dimer interface without inducing major perturbations. Protein dynamics in the millisecond time scale was measured by NMR relaxation dispersion and revealed the existence of a common excited state for all the variants, characterised by an altered structure at the level of both the strong and the weak dimer interfaces.

No literature is available on the structural effects in solution induced by the binding of small molecules to the T4 binding pockets and/or the occupancy of the central region by an aliphatic linker. The data presented in this chapter try to offer a molecular insight on the effects induced on the protein by the binding of the monovalent ligand tafamidis and the bivalent prototypic compound mds84.

5.2 Materials and methods

5.2.1 Methodological approach: considerations on protein structure, deuterium labelling and Transverse Relaxation-Optimised Spectroscopy (TROSY) NMR

It has already been mentioned that usually the molecular weight cut off for NMR spectroscopy of ^{13}C, ^{15}N labelled proteins is ~30 kDa. The molecular weight of TTR is ~55 kDa, which places it above the upper limit of the common size of NMR samples. However, a few considerations have to be made: TTR is a homotetramer, therefore constituted of four identical 127 amino acid long subunits and is characterised by 2,2,2 molecular symmetry, which makes resonances from all subunits equivalent. As a result, despite the presence of 127 * 4 = 508 amino acid residues in the protein, effectively only 127 theoretical peak resonances are observed when an NMR spectrum of TTR is acquired. Considering then that proline residues are not observed, the total number of resonances present in the spectrum becomes 127 - 8 = 119, thus simplifying the analysis of the data, including the full assignment of the protein. In addition to this advantage that strictly derives from the nature of the protein structure, the technical advance in the last 20 years has made it possible to push the boundaries of the molecular weight limit up to 800 kDa or even further, when the correct conditions are met. Undoubtedly, the introduction of high field spectrometers and of cryoprobes has helped in making large proteins suitable samples for NMR spectroscopy experiments, but the parallel development of new technical and experimental strategies appears equally important, in particular the introduction of deuterium labelling and the use of Transverse Relaxation-Optimised Spectroscopy (TROSY). NMR measures the signal of nuclear spins immersed in a homogeneous magnetic field. Such signal is the sum of radio frequencies that have been emitted by the nuclei, in response to a sequence of externally applied radio frequency pulses (Fernandez C & Wider G, 2003). The speed at which the signal decays is inversely proportional to the transverse relaxation time (T_2) and so are the resonance linewidths in the NMR spectrum. For large molecules the transverse relaxation rates of ^{13}C and ^{15}N spins tend to

increase leading to large linewidths and low signal-to-noise ratio. The major source of relaxation is associated with the presence of hydrogen atoms, which cause an efficient distribution of magnetization through the spin system of dipolar coupled protons (spin diffusion; Sattler M and Fesik SW, 1996). The replacement of hydrogen with deuterium eliminates many of the relaxation pathways, thus improving the signal-to-noise ratio. Furthermore the dipolar interaction between ^{13}C or ^{15}N nuclei and an attached proton, which is proportional to the square of the gyromagnetic ratio (ɣ), is significantly reduced when the proton is replaced by a deuteron, given that the gyromagnetic ratio of deuterium is about 6.5 times smaller than that of hydrogen (Sattler M and Fesik SW, 1996; Fig. 39). As a result, the directly attached carbon and H_N T_2 relaxation times are increased.

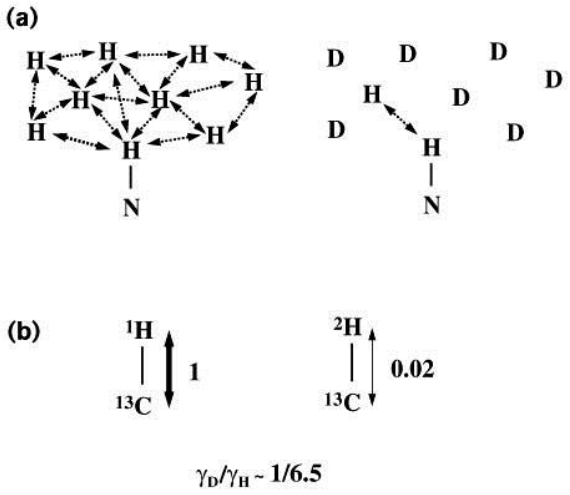

Figure 39. Advantages offered by the use of deuterium labelling. (a) The replacement of hydrogens with deuterium significantly reduces spin diffusion; (b) Due to the reduced gyromagnetic ratio of deuterium, the relaxation times of ^{13}C and ^{15}N spins are greatly increased (figure from Sattler M and Fesik SW, 1996).

In combination with deuterium labelling, TROSY NMR uses spectroscopic means to reduce transverse relaxation by mutual cancellation of relaxation contributions from dipole-dipole relaxation and chemical shift anisotropy (Venters RA et al., 2002). This approach was first described by Pervushin and co-workers in 1997 (Pervushin K et al., 1997). In a typical decoupled ^{1}H-

^{15}N heteronuclear single quantum coherence (HSQC) spectrum, the averaging of the four cross-peak multiplet components observed without decoupling produces one observable peak. As the protein size increases, the spin relaxation introduced by dipole-dipole relaxation and chemical shift anisotropy increases, thus determining different relaxation times for each peak of the multiplet component. As a consequence, while some peaks remain relatively narrow, some others become broad. When decoupling is applied, the averaging of broad and narrow peaks causes a general broadening of the linewidths up to the point when no more signal can be observed. TROSY NMR solves this issue by using phase cycling sequences that cancel out the broad signal components and keep only the narrow component. It can be theoretically shown that TROSY is most effective at high magnetic fields where all the transverse relaxation effects can be nearly completely cancelled for one of the four multiplet components. The ^{2}H-labelling of the protein further suppress the residual linewidth of the TROSY peak due to coupling with remote hydrogens, so that further line narrowing can be achieved. Even though by selecting one specific linewidth about half of the potential signal is lost, in large molecules this is compensated by the slower relaxation and subsequent gain in sensitivity (Fig. 40).

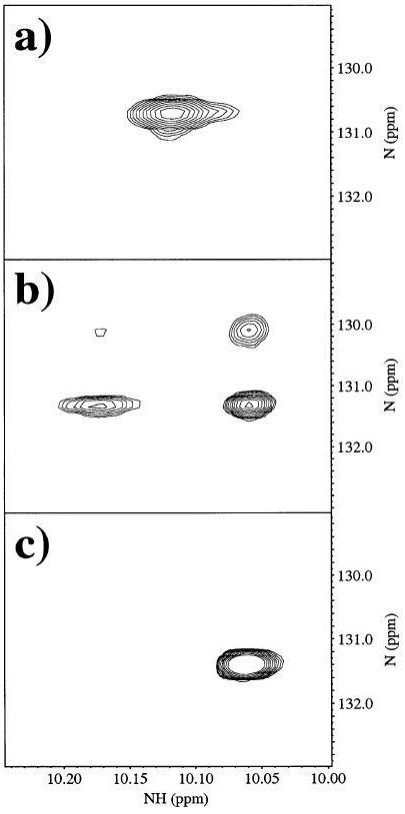

Figure 40. TROSY NMR. (a) The result of decoupling for a ^{1}H-^{15}N HSQC spectrum is a single peak originating from the averaging of the four multiplet peaks obtained without decoupling (b). TROSY NMR takes advantage of phase cycling sequences to cancel out the fast relaxing broader peaks and exclusively select the narrowest one. As a result, despite the loss of part of the overall potential signal, the resulting NMR spectrum is characterised by a single sharp peak (figure from Venters RA et al., 2002).

In order to acquire the high quality NMR spectra of TTR presented in this chapter both deuterium labelling (the protocol for expression in D_2O-enriched medium can be found in paragraph 2.2.4) and TROSY NMR were used.

5.2.2 Assignment of ^{2}H ^{13}C ^{15}N WT TTR

Full assignment of TTR resonance signals was achieved using several triple resonance NMR experiments. The experiments used are now briefly described. A schematic representation is shown in figure 41.

HNCO

This experiment shows the connectivity between the amide of one residue (i) and the carbonyl of the preceding residue (i-1). The magnetisation is transferred from the $^{1}H_N$ of the amide group to the corresponding $^{15}N_H$ and then onto the carbonyl (^{13}CO) of the preceding residue through $^{15}N_H$–^{13}CO J-coupling before being transferred back through the $^{15}N_H$ to the $^{1}H_N$ for detection. HNCO is the most sensitive of all triple resonance NMR experiments.

HN(CA)CO

This experiment shows the connectivity between the amide of one residue (i) and the ^{13}CO of the same residue (i) and the preceding one (i-1). The magnetisation is transferred from the amide $^{1}H_N$ to the corresponding $^{15}N_H$ and then to the $^{13}C\alpha$ of the same residue and the preceding one via $^{15}N_H$-$^{13}C\alpha$ J-coupling. From there via the $^{13}C\alpha$-^{13}CO J-coupling the signal is transferred to the ^{13}CO before being transferred back through the same way onto the $^{1}H_N$ for detection. The chemical shift is only evolved for $^{1}H_N$, $^{15}N_H$ and ^{13}CO, therefore the $^{13}C\alpha$ signal is not detected.

HNCO and HN(CA)CO were used together to assign carbonyls.

HNCA

This experiment shows the connectivity between the amide of one residue (i) and the $^{13}C_{\alpha}$ of the same residue (i) and the preceding one (i-1). The magnetisation is transferred from the amide $^{1}H_{N}$ to the corresponding $^{15}N_{H}$ and then to the $^{13}C_{\alpha}$ of the same residue and the preceding one via $^{15}N_{H}$-$^{13}C_{\alpha}$ J-coupling before being transferred back, via $^{15}N_{H}$, on the $^{1}H_{N}$ for detection.

HN(CO)CA

This experiment selectively shows the connectivity between the amide of one residue (i) and the $^{13}C_{\alpha}$ of the preceding one (i-1). The magnetisation is transferred from the amide $^{1}H_{N}$ to the corresponding $^{15}N_{H}$, then to both the ^{13}CO and the $^{13}C_{\alpha}$ of the preceding residue (i-1) before being transferred back through the same way onto the $^{1}H_{N}$ for detection. The chemical shift is only evolved for $^{1}H_{N,}$ $^{15}N_{H}$ and $^{13}C_{\alpha}$ therefore the ^{13}CO signal is not detected.

HNCA and HN(CO)CA were used together to assign α carbons.

HNCACB

This experiment shows the connectivity between the amide of one residue (i) and both the C_{α} and C_{β} of the same residue (i) and the preceding one (i-1). The magnetisation is transferred from the $^{1}H_{\alpha}$ and $^{1}H_{\beta}$ of both residue i and residue i-1 to the corresponding C_{α} and C_{β} respectively and from the C_{β} to the corresponding C_{α}. The signal then gets transferred to the $^{15}N_{H}$ and then onto the $^{1}H_{N}$ for detection. Because of $^{15}N_{H}$-$^{13}C_{\alpha}$ J-coupling, the signal is also transferred onto the $^{15}N_{H}$ from the $^{13}C_{\alpha}$ of the preceding residue (i-1) therefore for each $^{15}N_{H}$ two C_{α} and C_{β} are visible.

The corresponding experiment HN(CO)CACB to distinguish (i) from (i-1) C_{α} and C_{β}, was attempted but the signal to noise was insufficient to be of any use. Nevertheless, the identification of C_{α} was achieved with the combination of HNCA and HN(CO)CA experiments and the beta carbon resonances were

inferred, taking into consideration that (i) C_β give a more intense cross peak than (i-1) and considering the appropriate shift from the protein sequence.

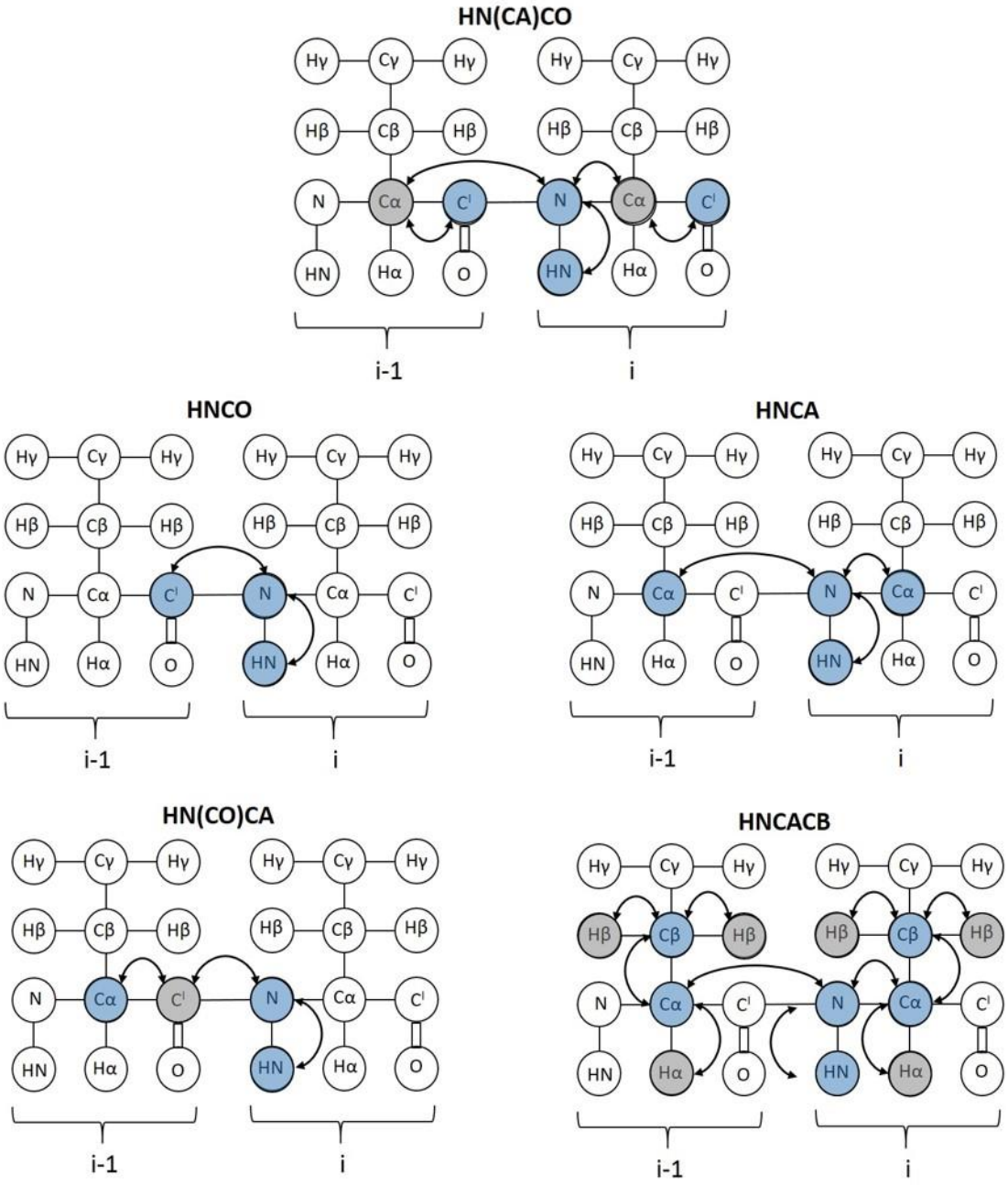

Figure 41. Schematic representation of the three-dimensional NMR experiments used for TTR assignment. Blue indicates atoms for which the signal is evolved. Grey indicates atoms, which get excited during the experiment, but for which the signal is not evolved. Figure prepared using Power Point.

The assignment through 3D NMR experiments exploits the fact that each residue in the protein is linked to the following and preceding ones and the fact that different amino acids have distinct C_α and C_β resonances, some of which are extremely characteristic and can be used as entry points when a protein needs to be assigned from scratch. Table 9 reports typical values for α and β carbons for the 20 amino acids. For example, the resonance for the C_α of glycine is normally around 45 ppm, thus clearly distinguishable from the C_α of all other amino acids. Similar considerations can be made for the C_βs. For example, the resonances for the C_β of serine and threonine residues are typically around 63-69, while for other amino acids the average resonance is around 30-40 ppm (with the exception of alanine for which the C_β resonance is around 19 ppm).

Table 9. Typical resonances of α and β carbons for the 20 amino acids.

Amino acid	C_α	C_β
Gly	45.37	NA
Ala	53.17	18.99
Ser	58.76	63.80
Thr	62.24	69.73
His	56.49	30.23
Trp	57.72	29.96
Cys	59 (ox), 55.4 (red)	40.7 (ox), 28.3 (red)
Gln	56.61	29.18
Glu	57.36	30.00
Met	56.14	32.99
Arg	56.81	30.68
Lys	56.97	32.79
Asn	53.56	38.70
Asp	54.70	40.88
Tyr	58.14	39.31
Phe	58.12	39.95
Leu	55.66	42.30
Val	62.53	32.72
Ile	61.64	38.61
Pro	63.35	31.85

If we consider the pair of experiments HNCA/HN(CO)CA, the first will provide information on both the C_α of residue i and i-1, while the second will only show the C_α of residue i-1. Moving from one amino acid to the previous or following one, a network that links together all the residues and leads to the full assignment of the protein can be created (Fig. 42).

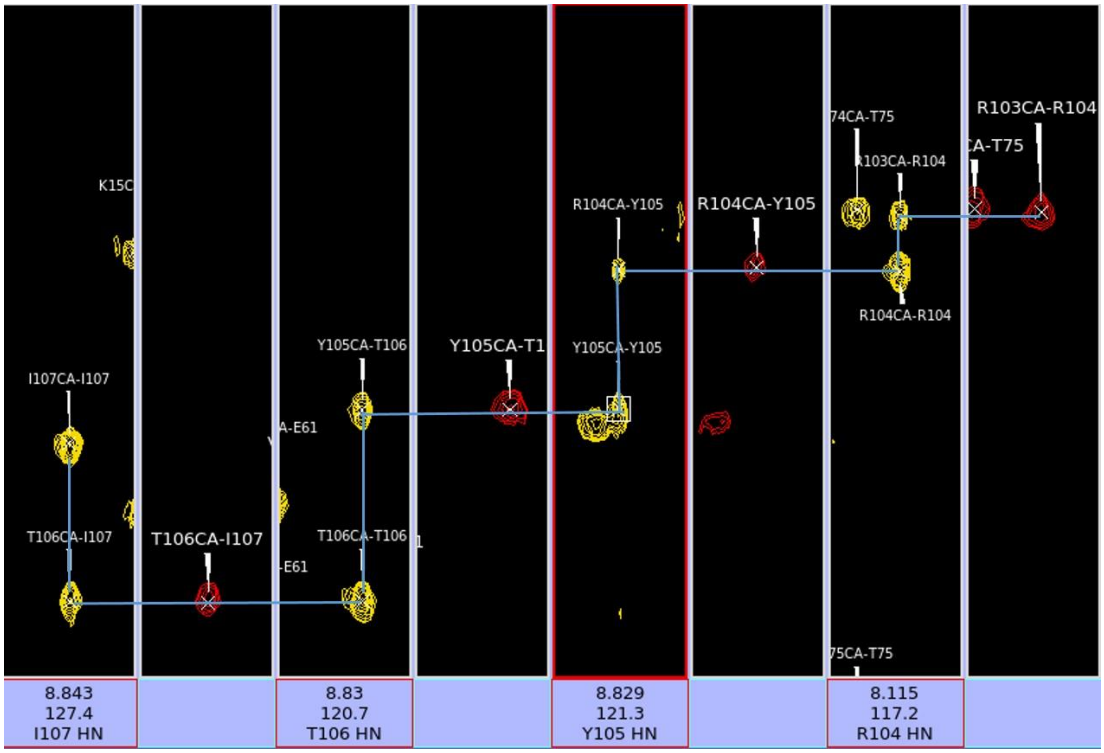

Figure 42. Example of assignment. Assignment of TTR residues I107, T106, Y105 and R104 using the combination of HNCA (yellow) and HN(CO)CA (red) experiments. A network is established between residues located in the backbone of the protein.

The backbone assignment of WT TTR was carried out with the data obtained from the three-dimensional NMR experiments (3D NMR) described above.
Spectra of ^{2}H ^{13}C ^{15}N WT TTR, 50-135 µM, were recorded at 310 K at both pH 7.4 and pH 7 in PBS.
The acquisition parameters are listed in table 10.

Table 10. Acquisition parameters for 3D NMR experiments.

	Number of complex points	Spectral width (ppm) ^{1}H, ^{15}N, ^{13}C
HNCO	3072 x 64 x 64	18, 27, 10
HN(CA)CO	3072 x 64 x 64	18, 27, 10
HNCA	4096 x 50 x 96	18, 27, 30
HN(CO)CA	4096 x 50 x 96	18, 27, 30
HNCACB	4096 x 50 x 96	18, 27, 70

5.2.3 Ligands titration

Tafamidis and mds84 stock solutions were prepared to a final concentration of 10 mM in 99.9 % dimethyl sulfoxide-d_6 (DMSO-D_6; Sigma Aldrich).

^{2}H ^{13}C ^{15}N WT TTR was dissolved in PBS, pH 7.4 at 54.5 µM.

The drug to TTR ratios were 0, 0.5, 1, 1.5 and 2 for tafamidis and 0, 0.5 and 1 for mds84. The titration was followed acquiring ^{1}H-^{15}N TROSY-HSQC spectra for each experimental point (table 11).

Table 11. HSQC acquisition parameters.

	Number of complex points	Spectral width (ppm) ^{1}H, ^{15}N
^{1}H-^{15}N HSQC	2048 x 256	15, 32

In order to confirm the assignment of new peaks arising after the addition of ligands, HNCA spectra were also recorded. 1.5 µl of ligand stock solution was added each time to progressively increase the ligand:TTR ratio. Following this procedure a total of 6 µl DMSO were added to a 600 µl solution containing tafamidis, thus accounting for 1% of the total volume. The effect of 1% DMSO was checked and considered irrelevant.

All spectra were processed with Topspin 3.5 (Bruker Biospin) or NMRPipe (Delaglio F et al., 1995) and analysed in NMRFAM-SPARKY (Lee W et al., 2015). NMR spectra were acquired at 310K with Bruker Avance 700 and 800 MHz NMR spectrometers.

5.3 Results

5.3.1 Assignment of ^{2}H ^{13}C ^{15}N WT TTR

An assignment obtained under different experimental conditions (K_3PO_4 50 mM, NaCl 100 mM, pH 5.75 at 298 K was already deposited in the Biological Magnetic Resonance Bank (BMRB). HSQC spectra of our ^{2}H ^{13}C ^{15}N WT TTR were recorded on a 135 µM sample at 310 K in PBS at both pH 7.0 and pH 7.4.

A set of three-dimensional experiments, including HNCO, HNCA, HN(CO)CA and HNCACB, was used to fully assign the protein.

At pH 7.4 no (or an extremely weak) ^{1}H-^{15}N correlation was observed for residues G4, T5, G6 and K9, C10 in the N-terminal region. Improved correlation was observed at pH 7.0, leading to a complete assignment. Residues H56 and G57, located in the DE loop, were not visible at both pH 7.4 and 7.0. Peaks for F95 and T119, which were partially overlapping with other signals at pH 7.4, became clearly distinguishable at pH 7.0.

While reassigning the protein, two issues with the deposited assignment were found. A mistake was found in the assignment of peaks R103-R104, which had erroneously been labelled as H90-E89 and vice versa.

The assignment of the peak corresponding to A120 was challenging as no ^{1}H-^{15}N correlation was observed when the protein was dissolved in PBS only. Interestingly when 4,4-dimethyl-4-silapentane-1-sulfonic acid (DSS, an NMR reference standard) was added, the signal corresponding to A120 appeared, suggesting an interaction of the reference standard with the protein, most likely at the level of the T4 binding pockets. Upon addition of DSS, chemical shifts involving residues M13, K15 and L17, which define HBP1, were observed as well as the weakening in intensity of some peaks located in strand H at the level of the dimer-dimer interface, in the specific S112, Y114 and S117.

5.3.2 Effect of ligands on TTR

Full assignment of the protein was necessary in order to investigate the effect induced by ligand binding on the protein. The effect of ligands on TTR was monitored recording ^{1}H-^{15}N TROSY-HSQC spectra for each experimental point. In the case of tafamidis 5 different spectra were collected starting with the protein alone and slowly increasing the ligand:protein ratio up to 2:1.

Similarly to T4, tafamidis has as a negative cooperative behaviour that was proven by Bulawa and co-workers (Bulawa CE et al., 2012), and was evidenced by different values of the dissociation constants for the two binding sites (K_{d1}= 2 nm and K_{d2}= 154 nm, respectively). On the basis of these affinity constants, at molar ratio tafamidis:TTR 2:1 and with a protein concentration of 50 μM, all of the TTR molecules present in solution were fully occupied. In the case of the bivalent mds84, instead, only 3 experimental points were necessary as in a 1:1 ratio the ligand fully occupies both binding sites and the inner channel of all the TTR molecules available in solution according to the mechanism described by Kolstoe and collaborators (Kolstoe SE et al., 2010).

Upon progressive addition of ligand, a number of peaks were affected. At a first glance, a slow exchange regime could be hypothesised. In fact, the peaks corresponding to the apo form decreased in intensity and simultaneously those of the holo form appeared and increased. A deeper look, though, interestingly revealed a shift of both the apo and holo form to new positions in the HSQC spectra at molar ratios tafamidis:TTR of 0.5:1 and 1:1. The peaks were therefore classified on the basis of their behaviour into three distinct groups, named I1, I2 and AH.

- I1 was used to classify those peaks for which a decrease in intensity and a shift from the original position was observed for the peak corresponding to the apo (i) form upon binding of tafamidis at ratios 0.5 and 1. In the presence of higher molar ratios of drug (1.5 and 2), such peak completely disappeared. Similarly, the peak corresponding to the holo form (f) appeared in a different position for molar ratios ≤ 1.

The behaviour of residue L55 is representative of peaks belonging to the I1 category.

- Peaks belonging to the category I2, such as S117, were characterised by the disappearance of the peak corresponding to the apo form already at a tafamidis:TTR molar ratios of 0.5 and 1.
- AH was instead used to classify those peaks behaving as expected from a slow exchange regime, for which a progressive transition between the apo and holo form was observed without the formation of intermediates, like in the case of residue D99.

Figure 43 exemplifies the considerations just made by showing the behaviour of residues L55, S117 and D99.

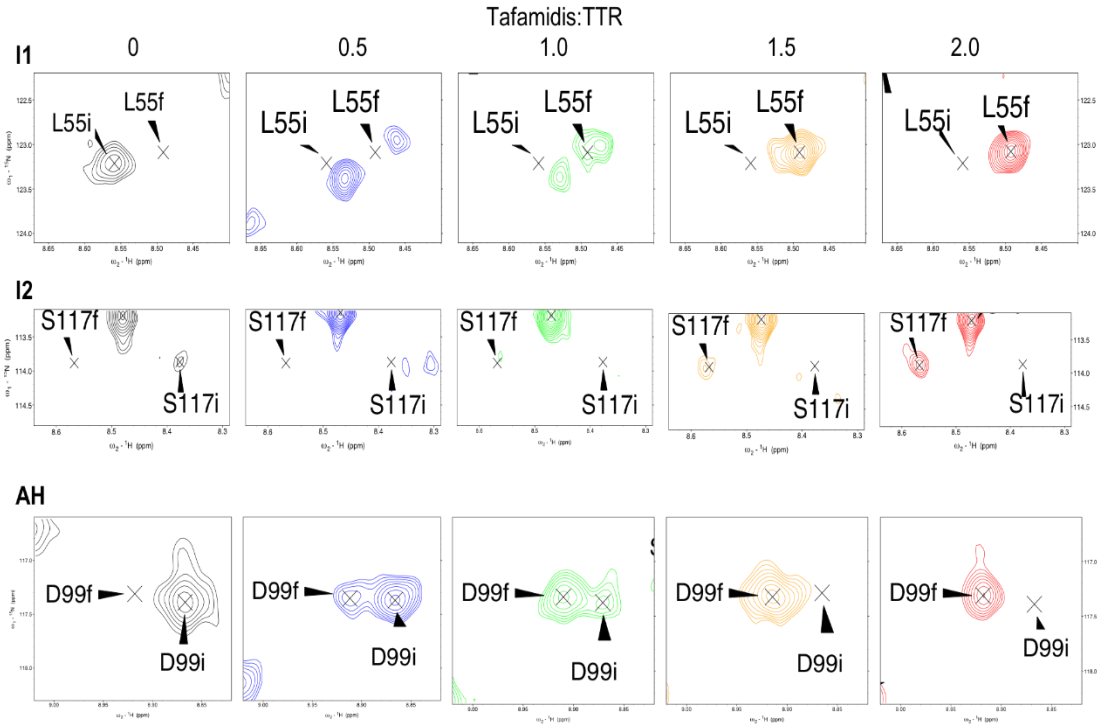

Figure 43. Behaviour of peaks belonging to categories I1, I2 and AH. L55, S117 and D99 are used to exemplify the behaviour of peaks belonging to the different classes. i indicates the initial position, while f indicates the final position at complete saturation.

These observations, in agreement with the previously mentioned negative cooperative effect, suggest that when only one of the two T4 binding sites is occupied, intermediate species, different from the initial and final ones, are present in solution, thus validating the hypothesis of an induced-fit mechanism.

A full list of the peaks classified according to their behaviour in the presence of tafamidis:TTR molar ratios of 0.5 and 1 is presented in table 12 and their localisation on the TTR structure is reported in figure 44. The majority of the peaks interested are located in the dimer interface, but some structural variations were also observed in the outer strand F.

Table 12. WT TTR peaks classified according to their behaviour in the presence of sub-stoichiometric ratios of tafamidis.

I1	I2	AH
13-16, 18-19, 23, 25-27, 33, 50, 53-55, 59, 74-75, 89-90, 92-94, 96, 108-112, 115, 122	17, 21, 88, 114, 117, 118	22, 67, 72, 76, 80, 98-99, 105, 123-124.

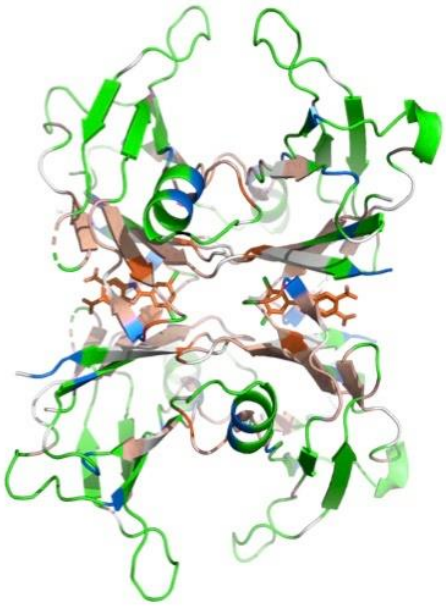

Figure 44. I1, I2 and AH peaks projected onto WT TTR structure in complex with tafamidis. I1 peaks are coloured in light orange, I2 in dark orange and peaks belonging to the AH group in blue.

On the contrary, the binding of mds84, which simultaneously occupies both binding sites, did not originate any intermediate species with all the peaks belonging to the group AH (Fig. 45).

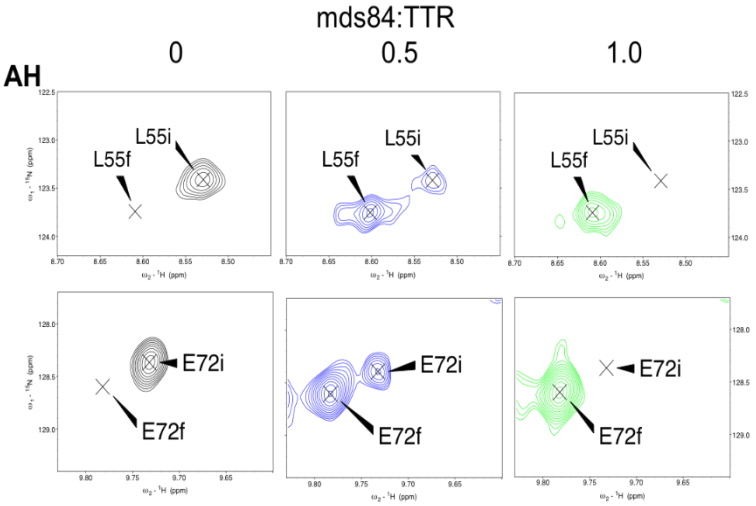

Figure 45. Behaviour of peaks in the presence of mds84. Residues L55 and E72 are shown as examples of the general behaviour observed in the presence of the bivalent ligand.

As already mentioned, in the presence of tafamidis:TTR ratio 2:1 and mds84:TTR ratio 1:1, full occupancy of both binding sites was achieved.

The overlays of the ^{1}H-^{15}N TROSY HSQC spectra for WT TTR in the presence of tafamidis and mds84 at the respective titration endpoints are shown in fig. 47 and 48).

As expected, extensive chemical shift perturbations were observed for both ligands at the level of the dimer-dimer interface (involving β-sheets DAGH of both dimers) in correspondence of the three halogen binding pockets (HBPs): HBP1 formed by M13, K15, L17, T106, A108, HBP2 comprising L17, A108, A109, L110, V121 and the inner pocket HBP3 composed of A108, L110, S117 and T119. Chemical shift perturbation in the presence of the two ligands are shown in figure 46.

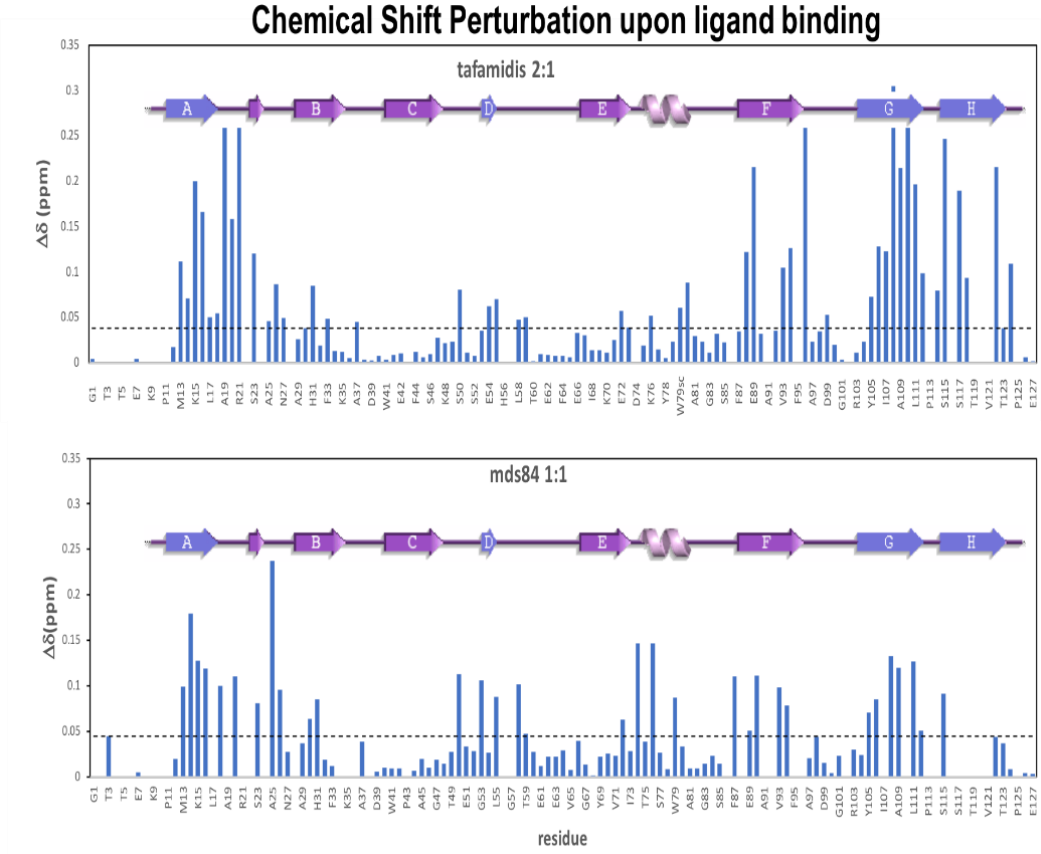

Figure 46. Chemical shift perturbations in the presence of tafamidis (top) and mds84 (bottom).

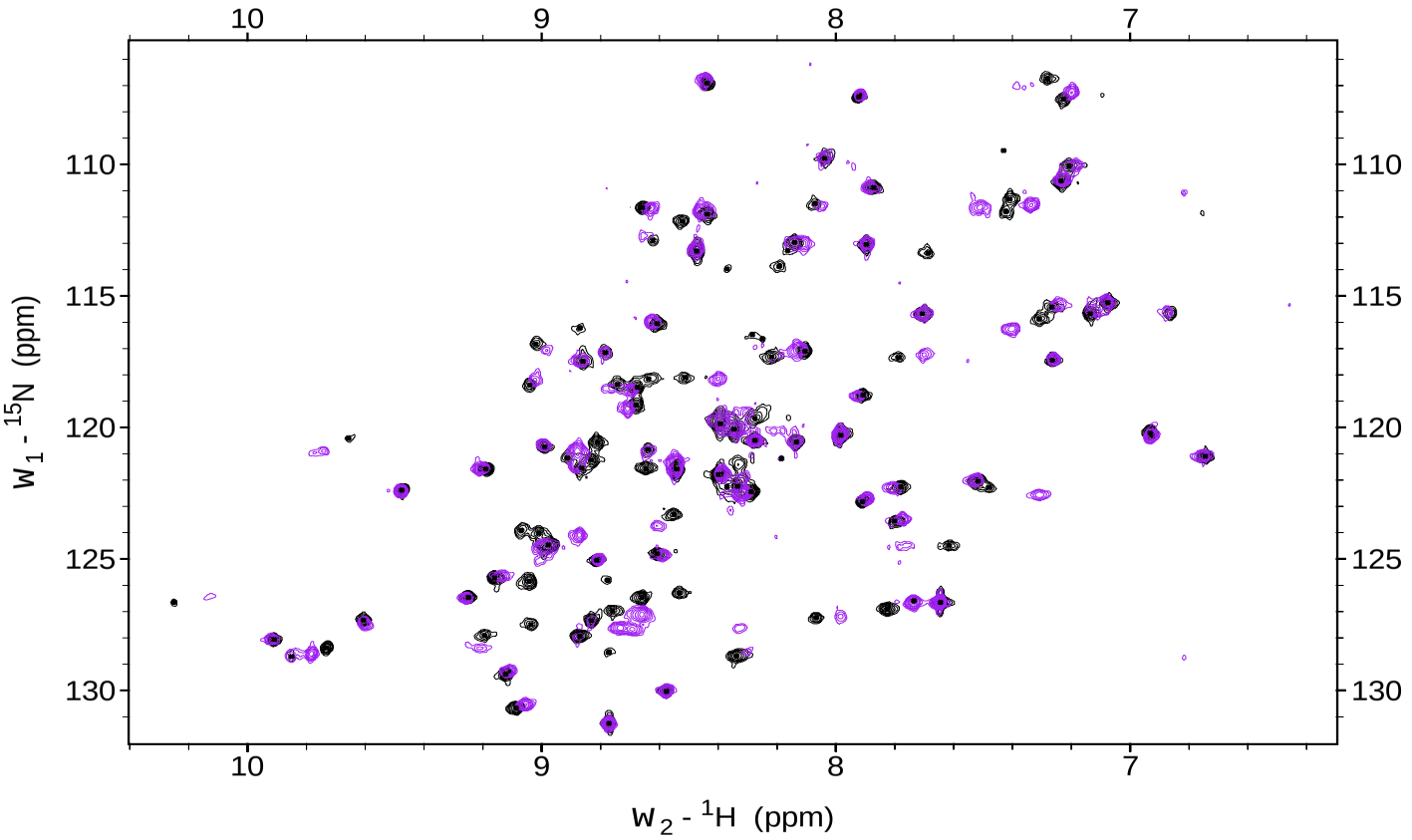

Figure 48. Overlay of ^{1}H-^{15}N TROSY HSQC spectra of ^{2}H ^{13}C ^{15}N WT TTR in the absence (black) and presence (purple) of mds84 in molar ratio 1:1

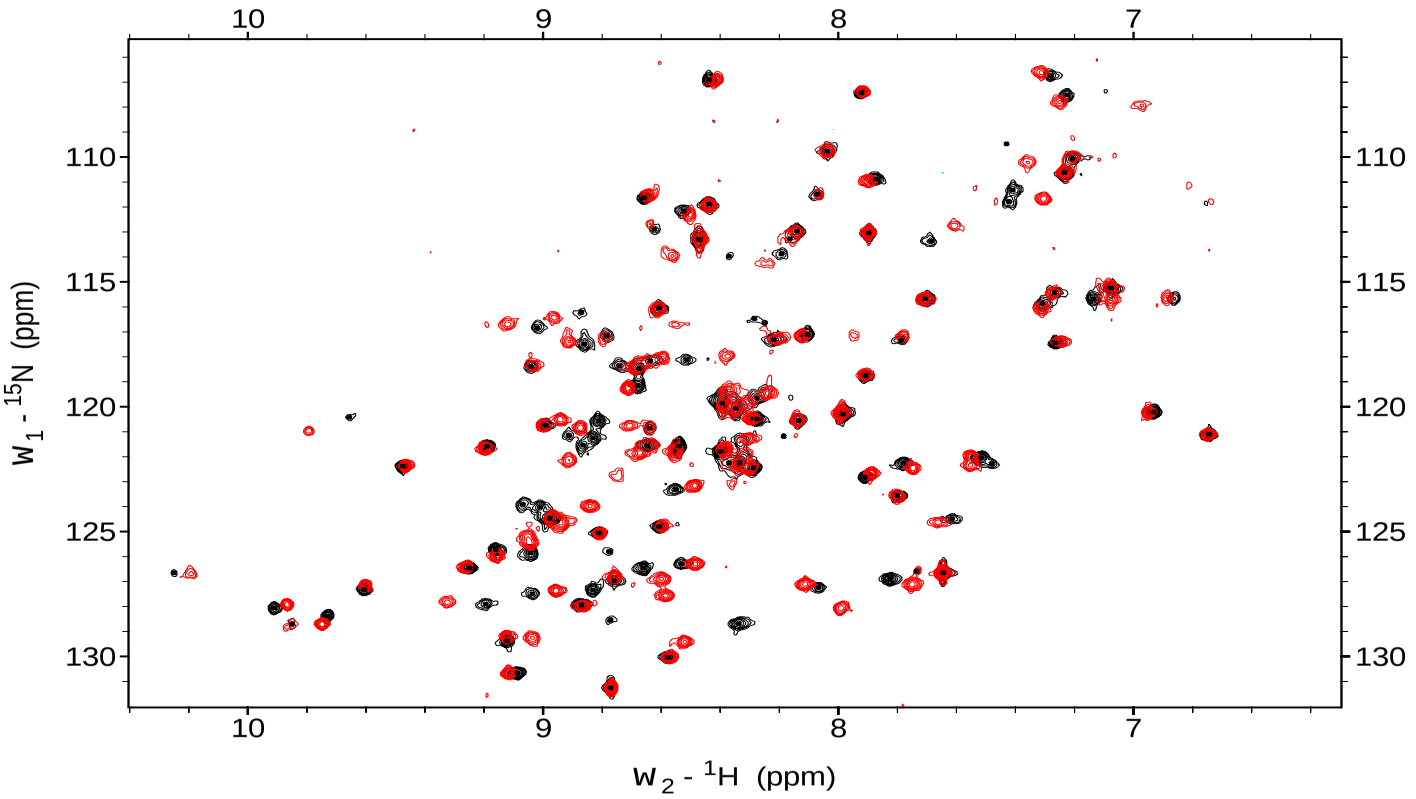

Figure 47. Overlay of ^{1}H-^{15}N TROSY HSQC spectra of ^{2}H ^{13}C ^{15}N WT TTR in the absence (black) and presence (red) of tafamidis in molar ratio 2:1

Full occupancy of both binding sites affected almost all the residues defining the HBPs with the exception of T119, in the presence of both ligands, and V121, in the case of mds84 only. The latter was indeed not observed either in the apo or holo form. While chemical shift perturbations were expected around the binding site, the perturbation of other peaks, located in the outer regions of the protein 12-36 Å far from the HBPs, was not easily predictable.
Strands B, E and F, located in the outer β-sheet, loops AB, CD and DE as well as α-helix H1 were indeed affected by the binding of both ligands. Interestingly, tafamidis only determined a perturbation of loop BC, while loop EH1 was selectively targeted by mds84 (Fig. 49).
Peaks shifting more than 1 standard deviation in loop AB, which is involved in the weak dimer-dimer interface with the loop GH of the opposite chains, were 19-21 for tafamidis and 18, 20, 25 for mds84. A25 is involved in the formation of H-bond with $T49O_{\gamma 1}$ and is subjected to the highest chemical shift perturbation observed in the presence of mds84. The loop CD as well as strands D and E and the α-helix were perturbed by both ligands, even though a stronger effect was achieved when the bivalent ligand was bound.
Both ligands highly affected strand F: for tafamidis, major chemical shift perturbations were observed for residues E89 and T96, which are involved in H-bonding with K76. In the case of mds84, a minimal chemical shift was observed for E89, while the signal for T96 could not be detected. Interestingly, though, K76, which had a minimal perturbation in the presence of tafamidis, was instead highly affected by the binding of mds84. In addition, in the presence of the bivalent ligand, perturbations were also observed for H90 and V93, which face each other. One interesting observation was made for residues K9 and A120, which were not visible in the apo form, but whose resonances appeared clearly when both compounds were bound. Similarly, resonances for A91 and V121, which were lacking in the apo form, were detected, although only when tafamidis was bound. These behaviours could be explained by a reduced exchange rate of the amide with water when a ligand is present, in comparison to the apo form. When mds84 was added, the resonances of 15 residues, distributed in strands A, G, and H at the level

of the dimer interface, in strand F and in loops AB, DE and H1F were lost. This effect was only observed for the bivalent ligand.

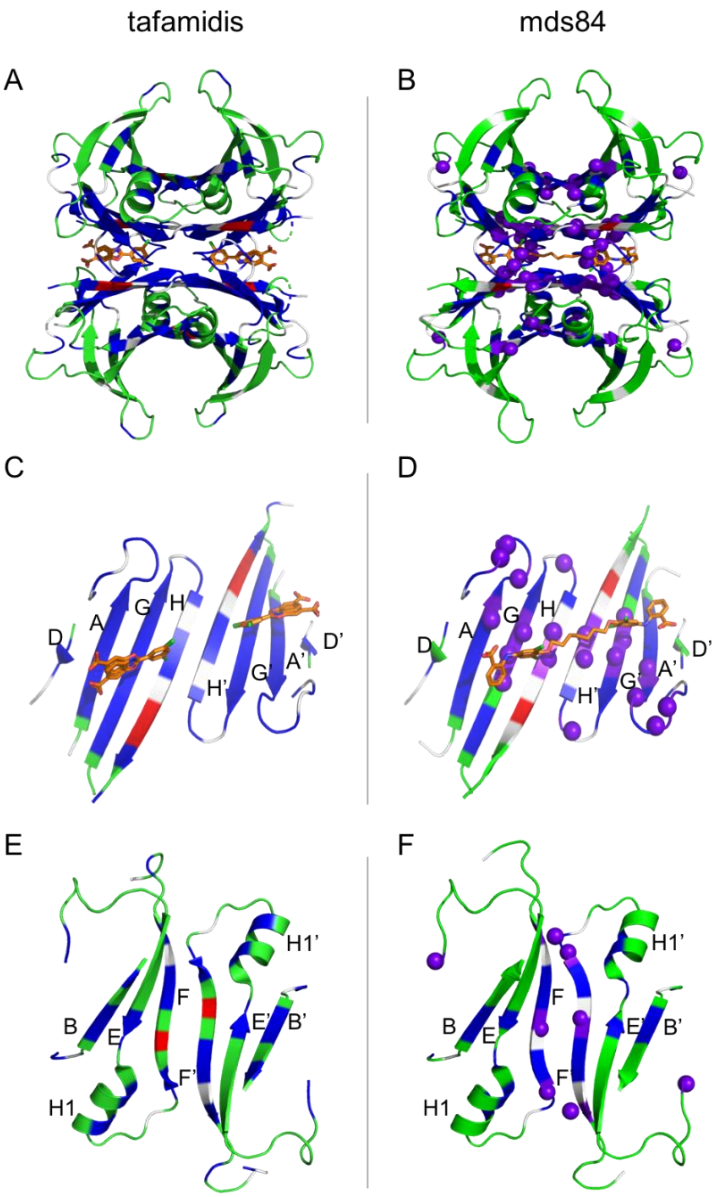

Figure 49. Chemical shift perturbation projected onto the TTR structure. Chemical shifts upon binding of ligands mapped on the structure of TTR in complex with tafamidis (A, C, E; PBD file 3TCT**)** and mds84 (B, D, F; PDB file 3IPE). Residues highlighted in blue shifted more than the average. Red indicates peaks whose resonances were visible only after binding. The purple spheres in the structure with mds84 indicate residues whose resonances could not be detected following ligand binding.

5.4 Discussion

The NMR chemical shift data presented in this chapter give an insight on the structural perturbations originated by the binding of small molecules to the T4 binding pockets.

Given the different experimental conditions used for previous assignment of WT TTR (Liu K et al., 2000), a totally new assignment was obtained at physiological pH in PBS, using a combination of three-dimensional NMR experiments. The analysis of the 3D spectra led to the observation that residues R103, R104 in the deposited assignment had erroneously been labelled as H90, E89 and vice versa. Furthermore, the reassignment of the protein led to the observation that DSS, commonly used to reference NMR spectra, interacts with the protein, likely binding to the T4 binding pocket, and that it is possibly present in the samples used for the deposited assignment in the bio magnetic resonance bank (BMRB) with code 5508.

As discussed in the introduction, despite the large number of X-ray structures available for TTR in the apo form or in complex with ligands, no evident structural variations, such to explain the effect of stabilisers or the amyloidogenic potential of distinct TTR variants had previously been observed.

Even in our specific case, the differences in terms of rmsd of C_α between the X-ray structures of apo TTR and TTR in complex with tafamidis or mds84 appeared modest, in the range of 0.618 and 0.315 Å, respectively, given a small deviation in the FG loop (residues 100-103), as shown in figure 50 .

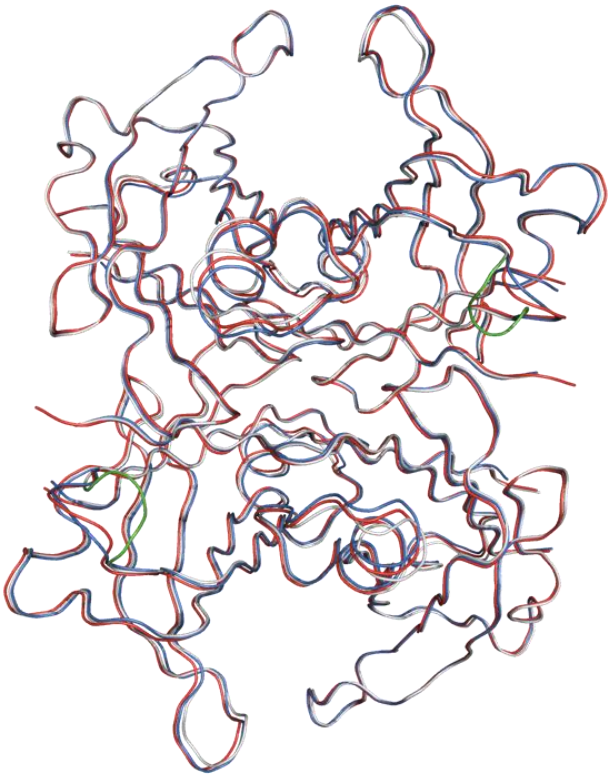

Figure 50. X-ray structures comparison. Superimposition of X-ray structures of apo TTR (red; PDB file 5CN3), TTR in complex with tafamidis (cyan; PDB file 3TCT) and mds84 (grey; PDB code 3IPE). The FG loop on the tafamidis structure is highlighted in green.

On the contrary, NMR allowed the observation of several structural changes induced by the binding of small molecules.

While the binding of mds84 at sub-stoichiometric ratio did not cause any intermediate species to form, as suggested by a normal behaviour typical of a slow exchange regime, the binding of tafamidis in ligand:TTR molar ratios of 0.5 and 1 clearly highlighted the presence of intermediate species in solution. Indeed most of the observable peaks were classified in the I1 and I2 groups, with only a small proportion belonging to the AH group, which is associated with the standard behaviour observed in a slow exchange regime.

As mentioned in chapter 4, tafamidis is bound with negative cooperativity, a phenomenon initially described for the binding of thyroxine to TTR in 1975

(Ferguson RN et al., 1975). Some hypotheses regarding small differences existing between the two sites have been made over the years in an attempt to explain the negative cooperativity effect observed for several ligands. Based on the analysis of the X-ray structures of TTR in complex with ligands, several researchers have suggested the possibility of an asymmetry existing between the two sites, which results in different binding affinity (Neumann P et al., 2001; Tomar D et al., 2012). It has also been suggested that TTR can undergo structural fluctuations, which temporarily make the two sites different. The ligand would then bind one or the other site according to its affinity and by doing so it would affect the conformation of the other binding site, whose affinity for the same molecule would therefore drop (Cianci M et al., 2015; Zanotti G et al., 2017).

The analysis of the ^{1}H-^{15}N correlations in the HSQC NMR spectra acquired in the absence of ligand, did not reveal any evident differences existing between the two binding sites. In the presence of tafamidis in sub-stoichiometric ratios, the formation of intermediate species was instead observed upon occupancy of the first binding site, suggesting some rearrangement taking place on the second binding site, located at the level of the dimer-dimer interface. In 1:1 ratio some effects were also observed in the outer regions of the protein. Of particular interest is the effect induced by full occupancy of both binding sites: as highlighted by the behaviour of peaks belonging to group I1, the conformation of the second binding site changes upon binding of two molecules, thus shifting to a new final position. Therefore, these data support the idea of an allosteric modification of the geometry of the second binding site, when the first one is occupied and might explain the almost 100-fold difference existing between K_{d1} and K_{d2}.

The results obtained at complete saturation are of extreme interest: while chemical shift perturbations were expected around the binding site, the long distance effect observed on the helix, β-sheets BEF and several loops was not predicted. Although the presence of aromatic rings in the ligands modify the chemical shift of nearby amides, such an effect cannot be responsible for the chemical shift perturbation observed for residues located more than 12 Å

from the centres of the rings themselves. Any chemical shift perturbation observed in the outer regions of the protein can therefore only be ascribed to structural reorganization induced by the binding of a ligand.

The appearance of A120 and V121 located in strand H could be explained by a stabilisation of the inter-chain hydrogen bonds between A120 (chain A, C) and Y114 of strand H' (chain B, D) and the intra-protomer hydrogen bond between V121 and T106 located on the opposite strand G.

A striking difference between the mono and bivalent ligand was observed when mds84 was bound, causing the disappearance of 15 amide resonances from the HSQC spectrum. Such effect might be explained with an overall stabilising effect of the bivalent ligand, which changes the protein dynamics to the μs-ms timescale that is unfavourable for investigation by NMR. Although most of the peaks affected are located at the level of the dimer-dimer interface, also the signal relative to residues located in loops AB, DE, H1F and strand D were lost, possibly due to the occupancy of the central channel.

The data shown in the previous chapter highlighted the efficacy of mds84 in preventing both proteolysis and subsequent aggregation. In this light the behaviour of A25 appears of particular interest: it appeared as the most perturbed peak when mds84 was added, while the chemical shift perturbation observed in the presence of tafamidis was just above the average. The reason A25 is so important is that its O is involved in the formation of an H-bond with the side chain of T49, which is located in the hot spot where proteolytic cleavage takes place (peptide bond K48-T49). When first describing the S52P TTR variant, our group highlighted the importance of the H-bond network formed by residues S50, S52 and E54 (Mangione PP et al., 2014). Such network was lost in the variant, due to the substitution of residue 52 with a proline, thus increasing the flexibility of the CD loop and the susceptibility to proteolysis. It is possible that the binding of the bivalent ligand induces a conformational change that favour the strengthening of this cluster of H-bonds, thus decreasing the accessibility to the proteolytic site and conferring a higher protection against mechano-enzymatic mediated

aggregation. It is indeed interesting to note that the chemical shift perturbations observed in this region appear more intense for mds84 than tafamidis. Another interesting effect, observed for both ligands, is the perturbation of residues K76, E89 and T96 that form an inter-chain H-bond network connecting the apexes of two monomers, thus stabilising the dimer. It is also worth noting that no hydrogen bonds connect the dimer-dimer interface with the outer β-sheet. Given that most of the residues pointing in the protein core are of hydrophobic nature, it can be hypothesised that the structural deviations observed in the outer β-sheet are driven by hydrophobic interactions (Fig. 51).

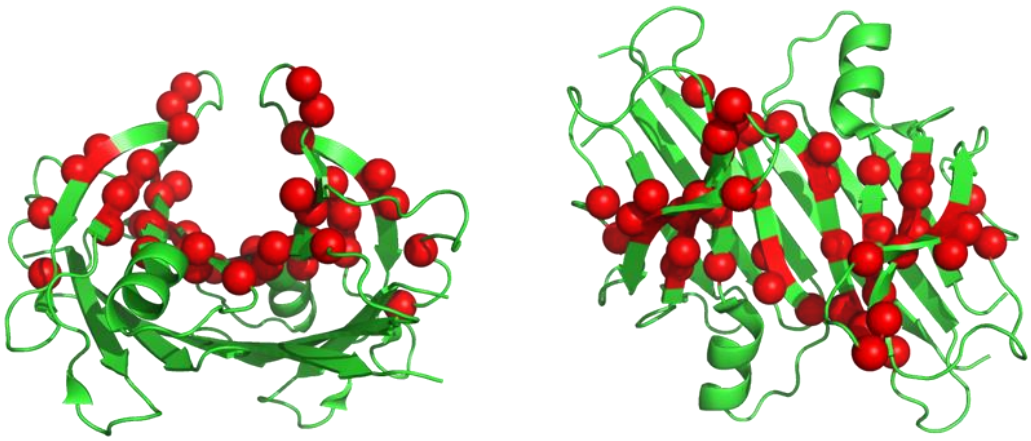

Figure 51. Hydrophobic core. (left) front view and (right) top view of the WT TTR dimer (PDB code 5CN3) in which the hydrophobic residues pointing towards the core of the protein have been highlighted in red.

In conclusion the use of NMR appears extremely promising for the investigation of conformational changes associated with the binding of specific ligands, which are not observable through other techniques, making it an invaluable tool to scrutinise and design new chemical entities acting as TTR stabilisers.

Chapter 6. From in vitro towards the elucidation of the mechanism of TTR amyloidogenesis in vivo

6.1 Introduction

Despite the enormous progress that has been made in reproducing *in vitro* the fibrillar transformation of peptides and proteins, the mechanism that drives the *in vivo* transition of globular proteins from their native functional state to a polymeric fibrillar structure represents an unsolved molecular issue. Solving this is crucial for the understanding of the natural history of amyloid diseases and designing of effective therapies. Moving from pure *in vitro* studies towards the elucidation of the mechanism of a disease *in vivo* represents therefore a crucial step for basic science research. In the amyloid field there has been a continuous attempt over the years to establish aggregation conditions *in vitro*, which could as closely as possible resemble the *in vivo* scenario. For example in the case of ß2-micrglobulin, the pH of the buffers adopted for aggregation experiments has moved from extremely acid to neutral pH in an attempt to move from totally artificial to more biocompatible conditions (Stoppini M & Bellotti V, 2015).

In this attempt to understand the complex biology underlying the amyloid disease and given the extracellular deposition of fibrils, the role of common constituents of the extracellular matrix, such as glycosaminoglycans has been extensively investigated. In particular, the highly charged heparin molecule has previously been described in several papers as an enhancer of amyloid formation by various amyloidogenic proteins including the amyloid-ß peptide (McLaurin J et al., 1999), α-synuclein (Cohlberg JA et al., 2002) and ß2-m (Relini et al., 2008; So M et al., 2017). Different researchers suggest that this sulphate-rich molecule can accelerate the rate of fibrillogenesis by offering charged surfaces to amyloidogenic proteins and inducing partial misfolding that predispose them to aggregation.

At the same time, since its first description by Naiki and collaborators in 1997, the effect of preformed fibrils has been widely accepted and described in several papers. A seeding effect is also observed *in vivo,* where the process of amyloid deposition is drastically accelerated once the first *nuclei*

have formed and deposited in the extracellular matrix, leading to the clinical manifestation of the disease.

It has been shown that a large number of amyloidogenic proteins can be seeded *in vitro* in order to accelerate or sometimes induce fibril formation. A PubMed search gives hundreds of results, showing the effect of seeding on proteins such as ß2-micrglobulin (Natalello A et al., 2016), tau (Mirbaha H et al., 2018), lysozyme (Krebs MR et al., 2004) and many others.

Only recently there has been the first report of seeding effect on TTR at low pH using *ex vivo* cardiac fibrils (Saelices L et al., 2018).

The first part of this chapter is focused on the evaluation of the effect of heparin and seeds on the newly identified mechano-enzymatic mechanism described by our group (Mangione PP et al., 2014; Marcoux J et al., 2015). In contrast with the generally accepted mechanism of fibrillogenesis (Colon W & Kelly JW, 1992), which involves a long incubation at non physiological pH, the mechano-enzymatic mechanism allows the formation of genuine amyloid fibrils by several TTR variants, including the WT protein, at physiological pH in the presence of shear stress and proteolysis.

Although the mechano-enzymatic mechanism effectively describes a plausible pathway leading to amyloid fibril formation, it does not fully resemble the *in vivo* scenario since trypsin was used in the original set up designed *in vitro*.

Indeed trypsin, even though effective *in vitro* in priming TTR amyloidogenesis by selective proteolysis of the loop interconnecting strands C and D, is unlikely to represent the culprit protease responsible for proteolysis of TTR *in vivo* as it is uniquely synthesised by the liver and, once secreted, it is compartmented in the small bowel lumen. Considering that TTR is a circulating plasma protein, it is extremely likely that the enzyme associated with the formation of the amyloidogenic fragment is located in the extracellular matrix and/or in the plasma.

As a consequence of this first part of my work, the second part of this chapter mainly focuses on the strategy adopted to identify a pathophysiologically plausible serine-protease responsible for cleavage *in vivo,* taking advantage

of the MEROPS database (Rawlings ND et al., 2016), which is a manually annotated database with information on more than 4000 peptidases classified according to families and clans.

From a pool of potential candidates, we were able to identify plasmin, on the basis of its structural similarity with trypsin, which proved able to prime TTR amyloidogenesis *in vitro* in the same fashion as trypsin under mechano-enzymatic conditions. The effects of heparin and seeds were also confirmed in the presence of the newly identified enzyme.

Finally, in order to resemble as much as possible the mechanism in vivo, we have designed an *in vitro* assay that recapitulates not only the activation of plasmin, but the entire pathway in which plasminogen-plasmin activation is just one of the several intermediate steps. This activation pathway *in vivo* is ubiquitous and constantly activated and is therefore fully consistent with a possible key role played in TTR amyloidogenesis.

The atomic force images shown in this chapter were acquired by Dr Annalisa Relini at the University of Genoa, Italy.

6.2 Materials and methods

6.2.1 S52P TTR fibrillogenesis in the presence of heparin

Samples of recombinant S52P TTR, 100 µl at 1 mg/ml in PBS, pH 7.4 containing 10 µM ThT, were incubated at 37 °C in Costar 96-well black plates in the presence of trypsin (enzyme:substrate ratio of 1:200) and 0.1 mg/ml heparin (Sigma-Aldrich). The plate was sealed with clear sealing film and subjected to 900 rpm double-orbital shaking. Bottom fluorescence was recorded at 500 s intervals (BMG LABTECH FLUOstar Omega).

6.2.2 S52P TTR fibrillogenesis in the presence of seeds

Samples of recombinant S52P TTR, 100 µl at 1 mg/ml in PBS, pH 7.4 containing 10 µM ThT, were incubated at 37 °C in Costar 96-well black plates in the presence of trypsin (enzyme:substrate ratio of 1:200) and 0.1 mg/ml of preformed S52P TTR *in vitro* fibrils. The plate was sealed with clear sealing film and subjected to 900 rpm double-orbital shaking. Bottom fluorescence was recorded at 500 s intervals (BMG LABTECH FLUOstar Omega).

6.2.3 MEROPS database search

MEROPS database (http://www.ebi.ac.uk) contains information on more than 4000 peptidases classified according to families and clans. The residues belonging to the proteolytic substrate are named Pn---P4-P3-P2-P1-||-P1'-P2'-P3'-P4'---Pm' where the || sign represents the scissile bond. The substrate specificity was based on the frequency of Lys in position P1 in the substrates reported in the database.

6.2.4 Evaluating proteolytic activity in the presence of D-Val-Leu-Lys 4-nitroanilide dihydrochloride peptide

Specificity for the C-terminal end of lysine of the database-identified enzymes was evaluated using the D-Val-Leu-Lys 4-nitroanilide dihydrochloride peptide (Sigma-Aldrich), following the instructions provided by the manufacturer, by monitoring absorbance at 405 nm using a BMG LABTECH FLUOstar Omega plate reader.

6.2.5 Proteolysis of S52P TTR and fibrillogenesis

Samples of recombinant S52P TTR, 100 µl at 0.5 mg/ml in PBS, pH 7.4 containing 10 µM ThT, were incubated at 37 °C in Costar 96-well black-wall plates in the presence of a protease; either plasmin, trypsin, thrombin, proteinase K, chymotrypsin kallikrein-related peptidase 12 or tryptase alpha, using an enzyme/substrate ratio of 1:50. The plate was sealed with clear sealing film and subjected to 900 rpm double-orbital shaking. Bottom fluorescence was recorded at 500 s intervals (BMG LABTECH FLUOstar Omega).

6.2.6 Effect of α2-antiplasmin on TTR fibril formation

Recombinant S52P TTR in 200 µl volumes at 1 mg/ml in 20 mM Tris-HCl at pH 7.5, containing 150 mM NaCl, 5 mM CaCl2, 10 µM ThT, was incubated at 37°C in sealed Costar 24- well black-wall plates, together with 20 ng/µl of plasmin and α2-antiplasmin at 0.09, 0.18, 0.36 and 0.72 µM. A sample without α2-antiplasmin was used as control. The selected inhibitor concentrations corresponded to molar ratios to plasmin of 0.25:1, 0.5:1, 1:1 and 2:1, based on an average molecular weight of 55 kDA for plasmin. The plate was subjected to 900 rpm double orbital shaking and ThT fluorescence emission was monitored using a BMG LABTECH FLUOstar Omega plate reader. Data were normalized to the ThT signal at plateau reached in the samples without the plasmin inhibitor. All experiments were conducted in triplicate.

6.2.7 Preparation of S52P TTR amyloid seeds in the presence of plasmin

S52P TTR fibrillar seeds were prepared in 96-well black-wall plate containing 200 µl of 1 mg/ml S52P TTR and plasmin at an enzyme:substrate ratio (w/w) of 1:50 in 20 mM Tris-HCl, 150 mM NaCl, 5 mM $CaCl_2$, 10 µM ThT pH 7.5 at 37 °C. The plate was sealed with clear sealing film and subjected to 900 rpm double-orbital shaking. Bottom fluorescence was recorded in a BMG LABTECH FLUOstar Omega. Aliquots of the final ThT positive material were

stained with alkaline alcoholic Congo red and examined under high intensity cross polarised light. Samples were also examined by negative transmission electron microscopy (TEM).

6.2.8 Effect of plasmin on pre-formed S52P TTR fibrillar seeds

After quantification by bicinchoninic acid protein assay kit (Pierce), 200 µl aliquots of fibrils at 0.1 mg/ml per well were further monitored in a sealed Costar 96-well black-wall plate in the presence and in the absence of 4 ng of plasmin in 20 mM Tris-HCl, 150 mM NaCl, 5 mM $CaCl_2$, 10 µM ThT pH 7.5 at 37 °C and agitation as above. Bottom ThT fluorescence was monitored at 500 s intervals as usual in a multimode-plate reader in three replicate test and control wells.

6.2.9 Fibrillogenesis of other TTR variants and WT TTR

Fibrillogenesis of a number of TTR isoforms including S52P, V30M, L55P, V122I, WT and T119M TTR was carried out in a sealed Costar 24-well black-wall plate subjected to a 900 rpm double orbital shaking using 500 µl of solution at 1 mg/ml of TTR in 20 mM Tris-HCl containing 150 mM NaCl, 5 mM $CaCl_2$, 10 µM ThT, pH 7.5 at 37 °C in the presence of 20 ng/ml of plasmin. ThT fluorescence emission was monitored over time until it reached a plateau. All experiments were conducted in triplicate.

6.2.10 Effect of seeds on plasmin-mediated fibrillogenesis by S52P TTR

ThT emission in the 96-well black-wall plate containing 200 µl at 1 mg/ml S52P TTR and plasmin at an enzyme:substrate ratio (w/w) of 1:50 was monitored in three replicates in the presence and in the absence of 0.1 mg/ml S52P TTR fibrils prepared as described above. All the reactions were conducted in 20 mM Tris-HCl, 150 mM NaCl, 5 mM $CaCl_2$, 10 µM ThT pH 7.5 at 37 °C. The plate was sealed with clear sealing film and subjected to 900 rpm double-orbital shaking. Bottom fluorescence was recorded at 500 s intervals (BMG LABTECH FLUOstar Omega). Data were normalised to the highest value of ThT signal after subtraction of the seeds related fluorescence intensity.

6.2.11 Effect of heparin on plasmin-mediated fibrillogenesis by S52P TTR

Samples of recombinant S52P TTR, 100 µl at 1 mg/ml in 20 mM Tris-HCl at pH 7.5, containing 150 mM NaCl, 5 mM CaCl2, 10 µM ThT, were incubated at 37 °C in Costar 96-well black-wall plates in the presence of plasmin (enzyme:substrate ratio of 1:50 w/w) and 0.1 mg/ml heparin (Sigma-Aldrich). The plate was sealed with clear sealing film and subjected to 900 rpm double-orbital shaking. Bottom fluorescence was recorded at 500 s intervals (BMG LABTECH FLUOstar Omega).

6.2.12 Effect of seeds on plasmin-mediated fibrillogenesis by S52P TTR

Samples of recombinant S52P TTR, 100 µl at 1 mg/ml in 20 mM Tris-HCl at pH 7.5, containing 150 mM NaCl, 5 mM CaCl2, 10 µM ThT, were incubated at 37 °C in Costar 96-well black plates in the presence of plasmin (enzyme:substrate ratio of 1:50 w/w) and 0.1 mg/ml S52P *in vitro* fibrils. The plate was sealed with clear sealing film and subjected to 900 rpm double-orbital shaking. Bottom fluorescence was recorded at 500 s intervals (BMG LABTECH FLUOstar Omega).

6.2.13 Formation of clot, fibrinolysis and/or fibril formation

A two-stage procedure was set up for clot formation (I), fibrinolysis and/or fibril formation (II). All experiments were conducted in Costar 96-well black–wall plates at 37 °C using a multimode plate reader (BMG LABTECH FLUOstar Omega) to monitor either changes in turbidity at 350 nm or ThT emission fluorescence. Fibrin polymerisation was initiated by adding thrombin (0.5 NIH U/ml) to 1 µM human fibrinogen in 20 mM Tris-HCl, pH 7.5 containing 150 mM NaCl and 5 mM $CaCl_2$ (buffer A) using a total volume of 100 µl per well. Change in turbidity at 350 nm was recorded to monitor clot formation every 20 s. After turbidity had reached a stable level (~30 min), 100 µl of buffer A containing tPA (2 x 0.027 µM), plasminogen (2 x 1 µM) and TTR (2 x 18 µM) were gently layered on top of the fibrin polymer. The plate was then sealed with clear sealing film and subjected to 900 rpm double-

orbital shaking. Turbidity at 350 nm was measured at 500 s intervals at 37 °C. Blank subtraction and a correction based on the volume per well and the microplate dimensions was selected to normalise all absorption values to 1 cm path length. The two-stage procedure was performed in the presence of 10 µM ThT. Bottom fluorescence was recorded every 20 s for 30 min in stage I; after addition of tPA, plasminogen and TTR in stage II, the ThT signal was monitored at 500 s intervals for 20 h. SDS-homogenous 15 % PAGE (GE Healthcare) under reducing conditions was carried out to analyse protein composition before and after enzyme treatment with fluid agitation. Pellets harvested at the end of stage II were further analysed by TEM, light microscopy after alkaline alcoholic Congo red staining as described above and atomic force microscopy (AFM).

6.2.14 Atomic force microscopy

Atomic force microscopy was performed by Dr Annalisa Relini in Genoa, Italy. Briefly, the aggregated material obtained at the end of phase II was resuspended in water and diluted 100-fold. 10 µl aliquots were deposited on freshly cleaved mica and dried under mild vacuum. Samples in which no pellet was present were diluted, deposited and dried as described above, but were rinsed with water to remove excess of salts. Tapping mode AFM images were acquired in air using a Multimode scanning probe microscope equipped with an “E” scanning head (maximum scan size, 10 µm) and driven by a Nanoscope V controller (Digital Instruments, Bruker). Single beam uncoated silicon cantilevers (type OMCL-AC160TS, Olympus and TESPA_V2, Bruker) were used. The drive frequency was between 260 and 310 kHz; the scan rate was 0.25– 0.5 Hz.

6.3 Results

6.3.1 Effect of heparin on S52P TTR mechano-enzymatic aggregation

The effect of heparin was tested on trypsin-mediated S52P TTR fibrillogenesis at physiological pH and temperature.

100 µl of protein at 18 µM concentration were incubated at 37º C in 96 wells plate in PBS, pH 7.4 in the presence of trypsin 5 ng/µl (trypsin: TTR ratio 1:200 w:w), heparin (100 µg/ml) and ThT 10 µM.

The sample was shaken at 900-rpm double orbital in a BMG FluoStar plate reader (BMG Labtech). The aggregation was measured by monitoring the ThT emission signal at 480 nm after excitation at 445 nm.

In order to exclude the possibility of heparin making ThT positive peptides/aggregates or promoting aggregation in the absence of proteolysis, control samples with only TTR and heparin or heparin and trypsin alone were included.

Two main heparin-induced effects, which agree with the data available in the literature, could be observed: the highly charged glycosaminoglycan promoted TTR amyloidogenesis and induced a shortening of the lag phase associated with the nucleation phase as well as an increased final yield in terms of amyloid fibrils as indicated by the higher intensity of the ThT emission signal at plateau. No ThT signal could be detected when heparin and trypsin were incubated together, suggesting that no ThT positive peptides/aggregates were formed. Furthermore, heparin alone was not sufficient to promote aggregation, confirming the importance played by proteolysis in priming the fibrillogenesis through selective cleavage and tetramer destabilisation (Fig. 52).

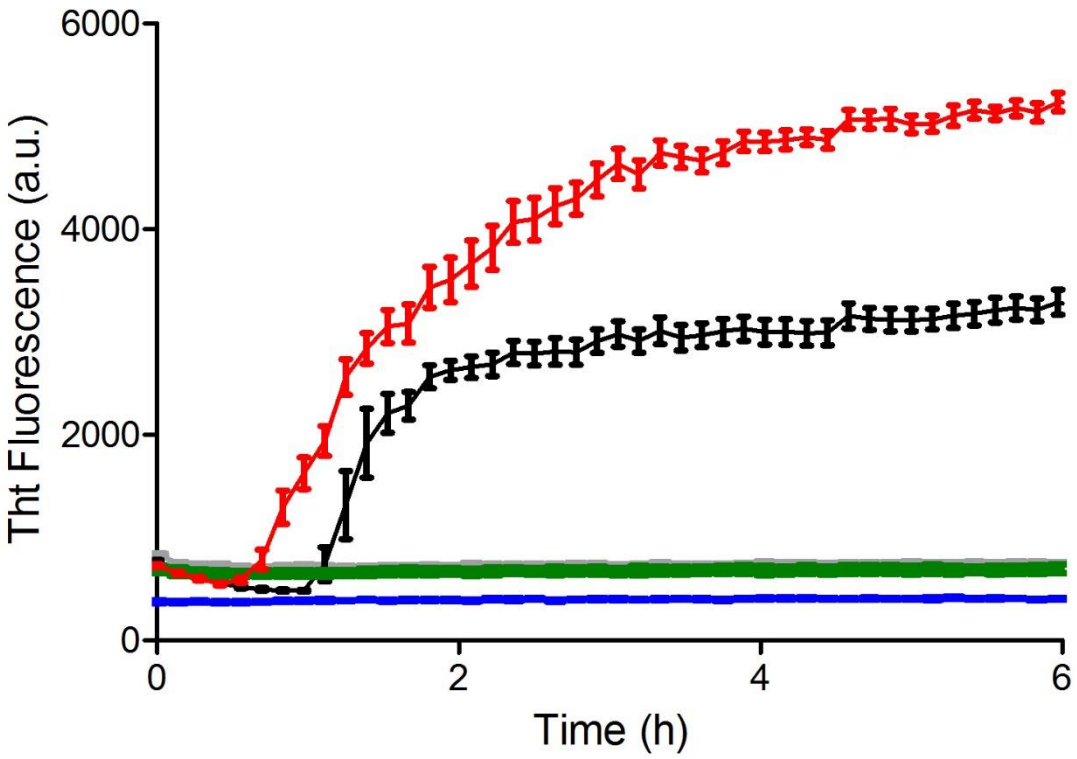

Figure 52. Effect of heparin on S52P TTR fibrillogenesis. ThT emission fluorescence at 480 nm of S52P TTR alone (grey), S52P TTR in the presence of heparin (green), S52P TTR in the presence of trypsin 1:200 (black) and S52P TTR in the presence of both trypsin and heparin (red). A control sample with trypsin and heparin (blue) was included. Samples were subject to 900 rpm double orbital shaking at 37º C. Results expressed as mean (SD) of 3 independent experiments.

6.3.2 Effect of seeds on S52P TTR fibrillogenesis

The effect of preformed recombinant S52P fibrils was tested on S52P TTR fibrillogenesis *in vitro*.

S52P TTR at different concentrations (18 µM, 9 µM, 4.5 µM, 2.25 µM and 1.125 µM respectively) was incubated in 96 wells plates at 37 ˚C in the presence of 10 µM ThT, 900 rpm double orbital agitation, 0.1 mg/ml of S52P TTR preformed fibrils and trypsin in a constant enzyme to protein ratio (1:200 w/w). A set of samples in the same experimental conditions, but without any preformed fibrils added was run in parallel.

The experiment was left to proceed until a stable plateau of the ThT emission signal was reached (Fig. 53).

The addition of seeds in the system caused a shortening of the lag phase, normally required for nucleation, suggesting that the critical concentration of full length and truncated TTR necessary for nucleation of fibrils was reached from the very start of the experiment and induced an acceleration of the fibrillogenesis even at lower TTR concentrations.

Due to the strong dependency of fluorescence on temperature, the samples were incubated at 37 ºC and the ThT emission signal was recorded for 30 minutes before trypsin was added. Following this procedure allowed a flat ThT baseline, which was necessary in order to perform further analysis on the total amount of amyloid fibrils formed in the presence and absence of seeds.

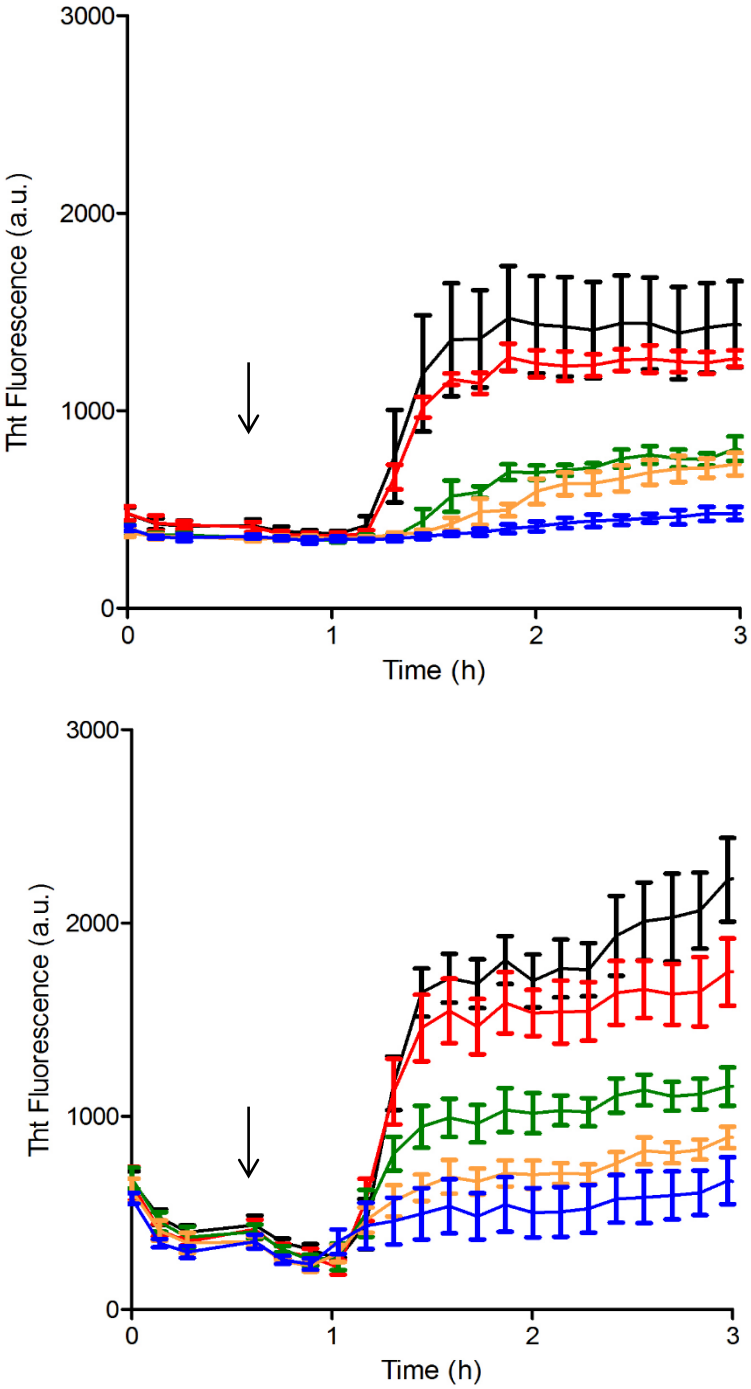

Figure 53. **Effect of seeds**. S52P TTR fibrillogenesis at different concentrations in the presence of a constant trypsin to protein ratio (1:200) in the absence (top) and presence (bottom) of seeds (0.1 mg/ml) monitored by ThT fluorescence emission at 480 nm over time. S52P TTR concentrations: 18 μM (black), 9 μM (red), 4.5 μM (green), 2.25 μM (yellow), 1.125 μM (blue).The signal recorded without seeds was subtracted from the data obtained in the presence of seeds. The arrow indicates the addition of trypsin.

In the absence of seeds a progressive delay in the onset of fibrillogenesis could be observed with the decrease of the protein concentration in solution. Such delay was completely absent in the presence of seeds, suggesting a strong effect in promoting aggregation even at low protein concentrations. Indeed all the samples behaved in the same in terms of length of the lag phase. The shortening of the lag phase becomes more evident by plotting the length of the lag phase against the concentration of the protein (Fig. 54).

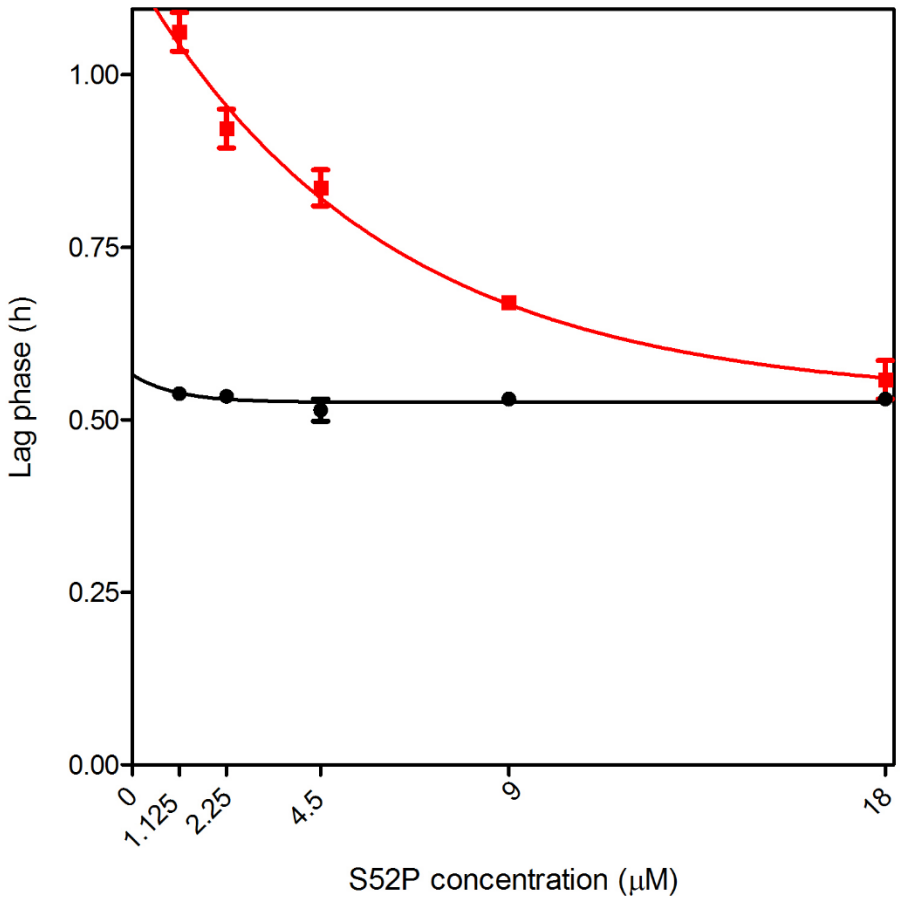

Figure 54. TTR concentration plotted against length of the lag phase. Schematic representation of the behavior of the lag phase in the absence (red) or presence (black) of seeds. The lag phase was determined considering the addition of trypsin to the solution as time 0. Trypsin was added 30 minutes after the beginning of the experiment (indicated by an arrow in the previous figure).

The difference in terms of intensity of ThT emission before and after aggregation was analysed and the intensity of such signal was used as a quantitative parameter to evaluate the amount of amyloid fibrils formed during the aggregation process.

The two sets of samples appeared significantly different in terms of total yield of amyloid fibrils formed. For every TTR concentration tested, the total amount of amyloid aggregates formed resulted about 1/3 more for the samples in which seeds were added at the start of the experiment (Fig. 55).

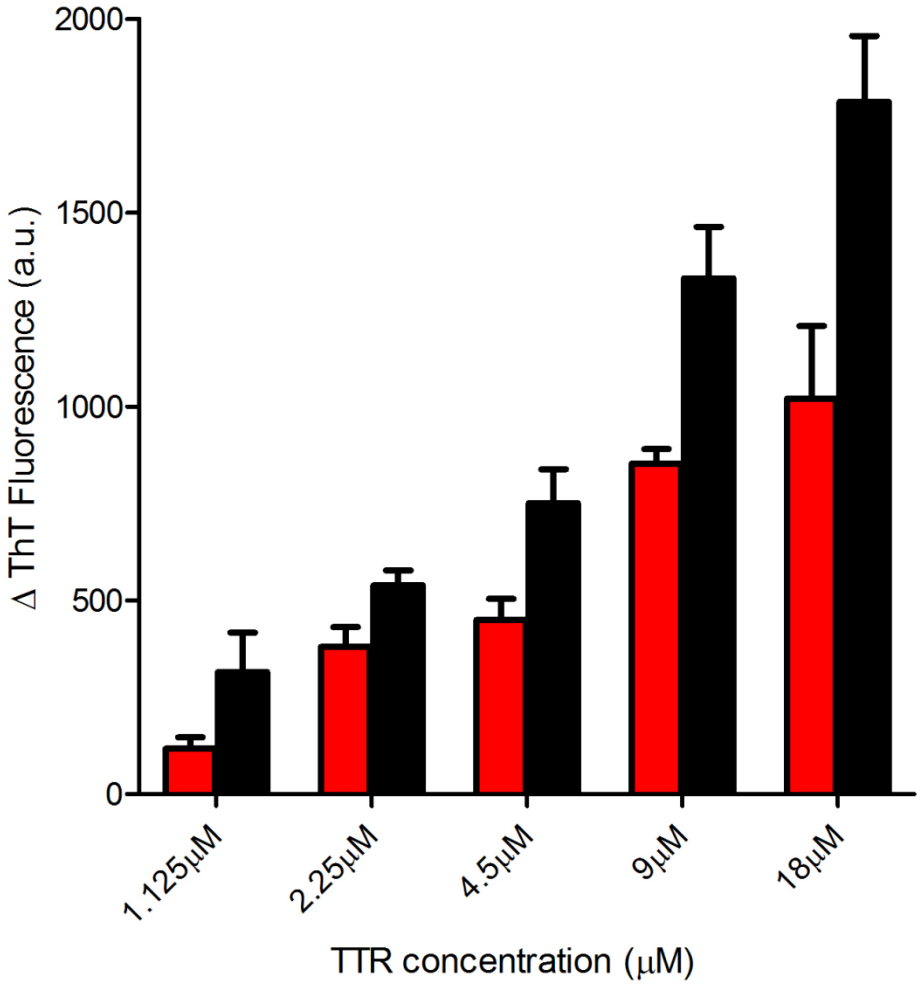

Figure 55. Difference in ThT emission signal before and after aggregation. The histograms represent the difference in terms of quantum fluorescence before and after aggregation has occurred in the absence (red) and presence (black) of seeds for the different TTR concentrations tested. Data expressed as mean (SD) of three different experiments.

6.3.3 Search for the putative enzyme in the MEROPS database

Peptidases were specifically identified in the MEROPS database amongst those able to cleave at the C-terminal end of lysine in the substrate (position P1). Amongst the initial 344 proteases showing the same specificity as trypsin and wider tissue localization, only 75 fulfilled the requisites of being human and with an extracellular localisation according to the UNIPROT protein database. Within this group, the majority belonged to the Serine Chymotrypsin like and metallopeptidase types (Table 13).

To further reduce the number of potential candidates, only those enzymes which had specificity for lysine in P1 higher than 30% were considered. Only four potential candidates were left after this strict selection: trypsin, tryptase alpha, kallikerein-related peptidase 12 and plasmin (Table 14).

Trypsin appeared as the most specific enzyme with specificity for lysine in P1 around 60%. As mentioned in the introduction, though, it was excluded due to its selective localization in the small bowel lumen, which is not compatible with a proteolytic event expected to take place in plasma. On the contrary, despite a reduced specificity, all the other enzymes identified were secreted and interestingly, apart from kallikrein-related peptidase 12 for which no structural information has been reported yet, they shared structural similarity with trypsin.

Table 13. Summary of the human extracellular proteases identified in the MEROPS database considering lysine in position P1 of the substrate.

Clan	Family	Type	Number
A	A01	Asp_pepsin_like	3
C	C01	Cys_papain_like	1
MA	M01	Aminopeptidase_like	2
MA	M10	metallopeptidase	14
MA	M12	astacin_like	7
MA-MC	M13-M43	neprilysin_like; carboxypeptidase	7
PA	S01	Ser_Chymotrypsin_like	38
SB	S08	Ser_subtilisin_like	2
SR	S60	Ser_lactoferrin	1
Total			**75**

Table 14. Peptidases with specificity for lysine in position P1 higher than 30%.

Enzymes	Specificity for Lys in P1 (%)	Primary Localization
S01.151 trypsin 1	60	intestinal tract
S01.143 tryptase alpha	56	lung, stomach, spleen, heart and skin
S01.020 kallikrein-related peptidase 12	55	salivary glands, stomach, uterus, trachea, prostate, thymus, lung, colon, brain, breast, and thyroid
S01.233 plasmin	45	plasma and many other extracellular fluids

6.3.4 Mechano-enzymatic S52P TTR fibrillogenesis in the presence of the identified enzymes

Before any aggregation experiment was started, the three selected enzymes were screened using a simple yet effective colorimetric assay, which is based on cleavage of the D-Val-Leu-Lys 4-nitroanilide dihydrochloride peptide. If the enzyme specifically recognises the C-terminal end of the lysine residue, 4-nitroanilin is released from the tripeptide in the solution determining a progressive change in colour, which can be detected over time at 405 nm using a spectrophotometer. This initial screening was necessary as in some cases the producers did not specifically test for preserved enzymatic activity after the purification and could therefore not guarantee that the enzyme was actually fully functional. Plasmin, kallikrein-related peptidase 12 and tryptase alpha were all able to cleave at the C-terminal of lysine with similar kinetics (Fig. 56)

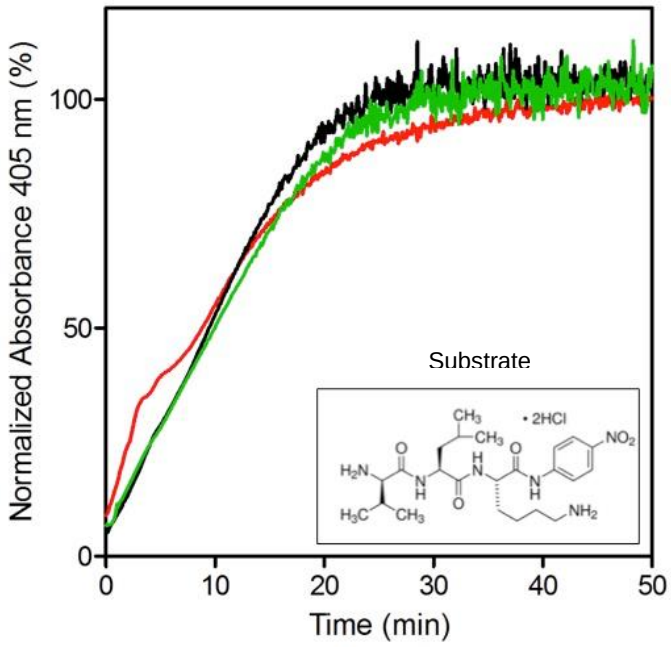

F**igure 56. Evaluation of selective enzymatic activity.** Plasmin (black), tryptase alpha (red) and kallikrein-related peptidase 12 (green) activity was tested by following the release of 4-nitroanilin from the D-Val-Leu-Lys 4-nitroanilide dihydrochloride peptide (inset) at 405 nm over time using a BMG LABTECH FLUOstar Omega. The curves were normalised to 100% of 4-nitroanilin released at the end of the experiment.

Once the activity was confirmed, the three enzymes were tested on S52P TTR to see whether they could induce proteolysis-mediated fibrillogenesis.

S52P TTR was selected, as it is a very unstable variant, which is easily cleaved and was therefore the best choice to rapidly screen the effect of the proteases. 100 µl of protein at 0.5 mg/ml (9 µM tetramer) were incubated in a 96 well plate at 37 ºC in the presence of plasmin, tryptase alpha or kallikrein-related peptidase 12 in ratio 1:50. The plate was then shaken at 900 rpm with double orbital movement. Aggregation was monitored by ThT emission at 480 nm (final ThT concentration in the sample 10 µM).

Tryptase alpha, although active on the peptide, did not trigger TTR amyloid conversion and the ThT emission signal remained flat throughout the length of the experiment. On the contrary, both plasmin and kallikrein-related peptidase 12 induced amyloid fibril formation, even though the latter had a very modest activity (Fig. 57).

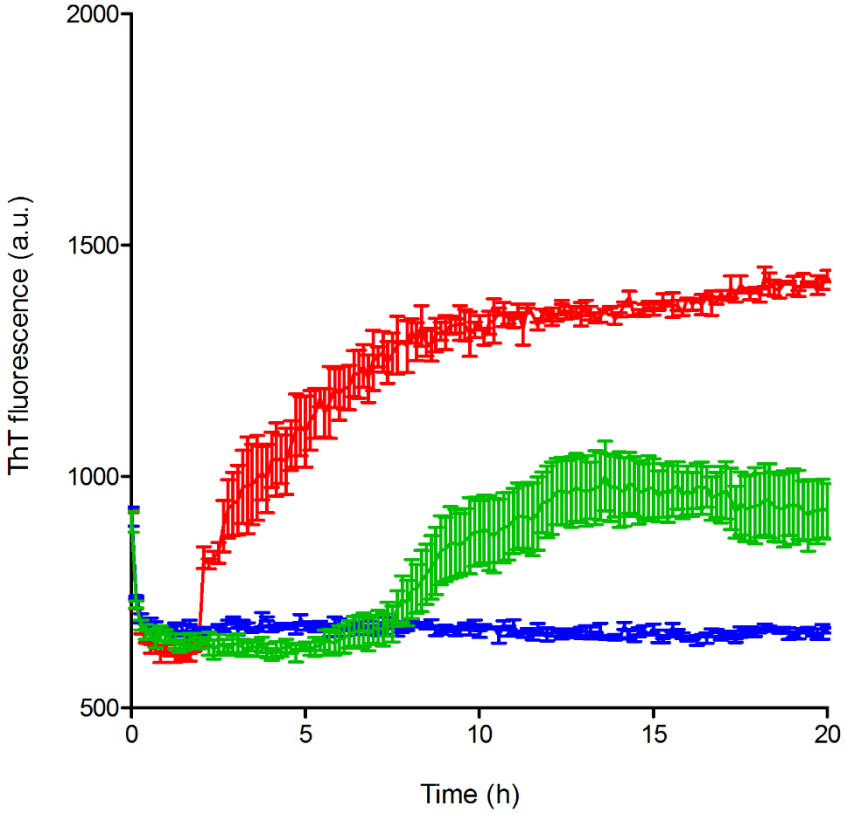

Figure 57. Aggregation of S52P TTR in the presence of plasmin, tryptase alpha and kallikrein-related peptidase 12. Tht emission signal for plasmin (red), kallikrein related peptidase 12 (green) and tryptase alpha (blue) was recorded at 480 nm after excitation at 445 nm every 500 s. Aggregation was followed until the signal reached a plateau. Data presented as mean (SD) of 3 different experiments.

As a control, in order to confirm that a close correlation exists between enzyme specificity and subsequent TTR fibrillogenesis, other enzymes with different substrate specificity such as thrombin, chymotrypsin and proteinase K were tested in the same experimental conditions used for plasmin, kallikrein-related peptidase 12 and tryptase alpha. Once again ThT emission was used to follow the aggregation over time. The enzyme to protein ratio adopted was 1:50 for all the proteases. All of them proteolysed TTR to a different extent, but none of them triggered TTR fibrillogenesis, confirming that not proteolysis in general, but specific cleavage at the C-terminal of lysine is essential in order to promote aggregation (Fig. 58).

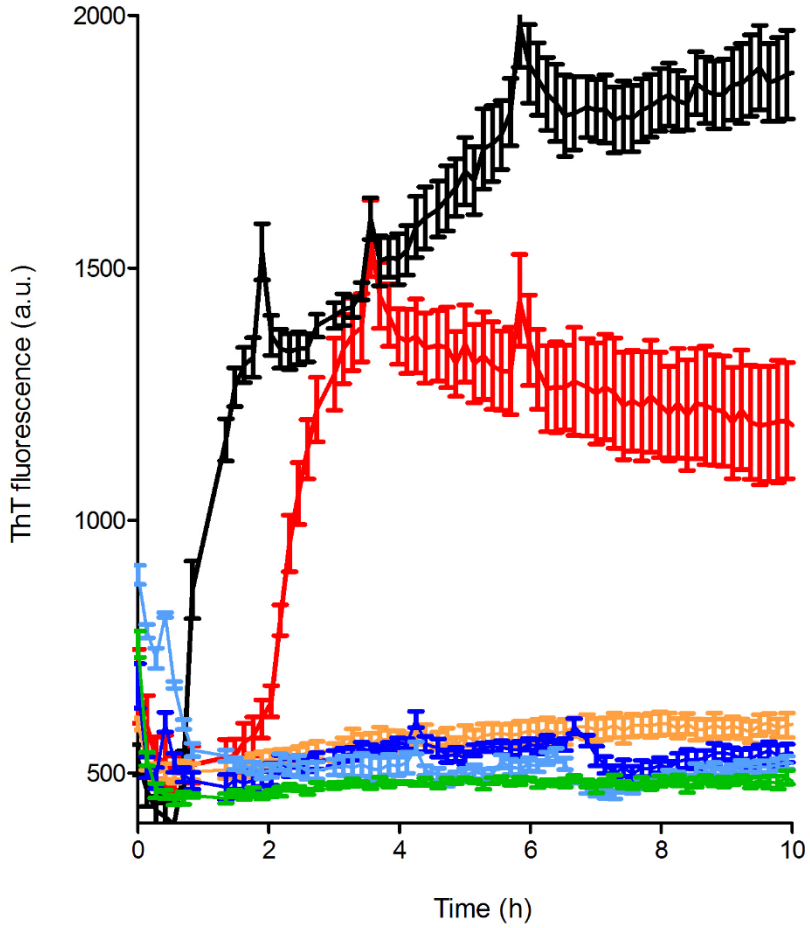

Figure 58. Non-specific enzymes did not trigger amyloid formation. ThT emission signal for S52P TTR in the presence of thrombin (green), chymotrypsin (orange) and proteinase K (blue). Trypsin (black), plasmin (red) and S52P TTR alone (light blue) are included for reference. Results presented as mean (SD) of three replicates.

The results obtained strongly implicated plasmin as a candidate to be the possible putative enzyme responsible for proteolytic cleavage of the peptide bond Lys48-Thr49 of TTR *in vivo*. Plasmin appeared less active than trypsin as indicated by the lower intensity of the ThT emission signal at plateau and the longer lag phase preceding the growth phase.

These observations are consistent with the SDS PAGE analysis of the sample after fibrillogenesis, which highlighted the formation of less

amyloidogenic TTR fragment 49-127 the presence of plasmin if compared to the trypsin treated sample. Electron microscopy analysis as well as Congo red staining of the aggregated material confirmed the presence of genuine amyloid fibrils comparable to those previously obtained through trypsin-mediated fibrillogenesis (Fig. 59).

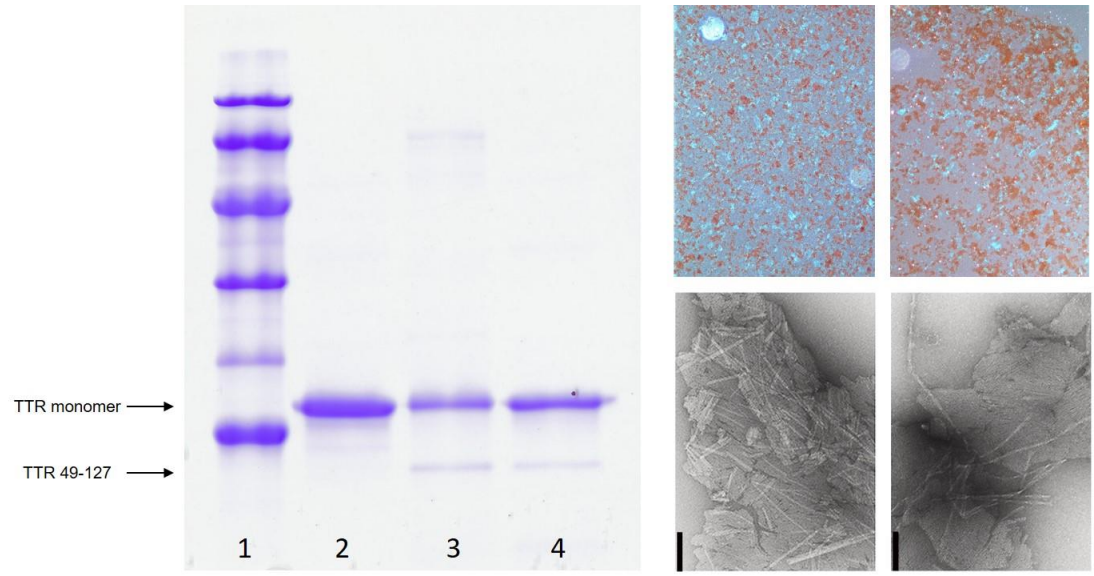

Figure 59. Comparison between aggregates formed in the presence of trypsin and plasmin. SDS 15% PAGE analysis of the aggregated material after fibrillogenesis. Lane 1: marker proteins (14.4, 20.1, 30.0, 45.0, 66.0 and 97.0 kDa); lane 2: S52P TTR, time 0; lane 3: in vitro S52P TTR fibrils in the presence of trypsin; lane 4: *in vitro* S52P TTR fibrils with plasmin. Congo red staining of aggregate obtained in the presence of trypsin (top left) or plasmin (top right). Negatively stained transmission electron micrographs of S52P TTR amyloid fibrils formed in the presence of trypsin (bottom left) or plasmin (bottom right).

6.3.5 Effect of α2-antiplasmin on plasmin mediated S52P fibrillogenesis

The effect of α2-antiplasmin, a natural inhibitor of plasmin, was tested on S52P TTR fibrillogenesis.

Full-length plasminogen (Glu-plasminogen) comprises 791 residues and seven domains: an N-terminal Pan-apple domain (PAp), 5 kringle domains (KR1-5) and the serine protease domain (SP), which contains the active site. The natural activation process of the zymogen into plasmin involves a structural rearrangement and the proteolytic cleavage of the peptide bond Arg561-Val562 located into the so-called activation loop (Law RH et al., 2013). Following its activation, plasmin can then be further proteolysed to a different extent on its kringle domains. The enzyme used for the fibrillogenesis experiment was purchased from Sigma-Aldrich and was purified from human plasma. The manufacturer provided information on the molecular weight of the protein, which, due to different extent of proteolysis during its activation *in vivo*, appeared very heterogeneous in the range 86-24 KDa. An average molecular weight of 55 KDa was therefore considered in order to establish the correct molar ratios α2-antiplasmin:plasmin for the inhibition experiments.

Plasmin-mediated fibrillogenesis was carried out as before, but 0.09, 0.18, 0.36 and 0.72 μM α2-antiplasmin was added, corresponding to molar ratios to plasmin of 0.25:1, 0.5:1, 1:1 and 2:1.

Aggregation was monitored by ThT fluorescence emission until the control sample, incubated with plasmin in the absence of inhibitor reached a plateau (Fig. 60).

In a molar ratio of 0.25:1, α2-antiplasmin approximately halved the ThT emission signal by inhibiting plasmin activity. The aggregation was already completely abrogated at molar ratio 0.5:1 and the ThT signal remained flat at higher molar ratios suggesting that no amyloid fibrils were formed.

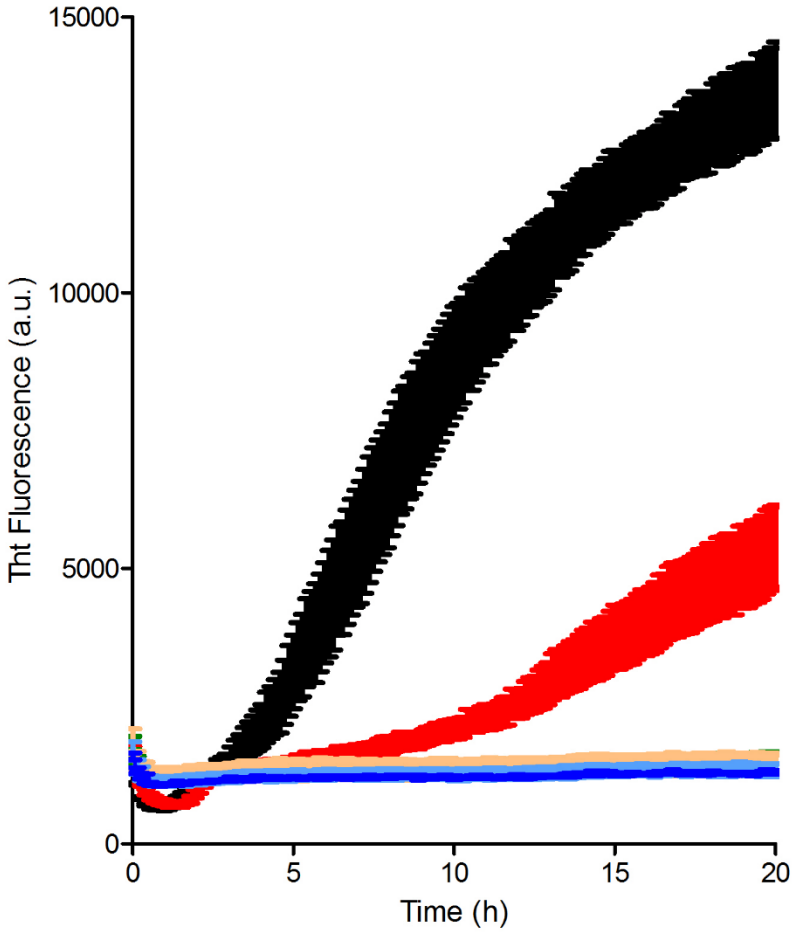

Figure 60. α2-antiplasmin inhibits plasmin-mediated fibril formation by S52P TTR. S52P TTR in the presence of plasmin (black), α2-antiplasmin 0.25:1 (red), α2-antiplasmin 0.5:1 (yellow), α2-antiplasmin 1:1 green) and α2-antiplasmin 2:1 (blue) in PBS at 37 ºC under vigorous agitation at 900 rpm . TTR alone (light blue) is shown for reference. The aggregation was stopped when the ThT signal reached a plateau. Data presented as mean (SD) of three replicates.

6.3.6 Effect of plasmin on TTR amyloid fibrils

It has been suggested that plasmin might play an important protective role against Alzheimer's disease by digesting Aß amyloid fibrils (Tucker HM et al., 2000). We decided to investigate whether plasmin exhibits the same effect on TTR amyloid fibrils *in vitro*. The digestion of TTR pre formed fibrils was monitored by ThT emission fluorescence. If ThT is added to a suspension containing amyloid fibrils, the dye will bind to the fibrils and a corresponding emission signal will be detected. If the fibrils are not degraded, the emission signal will remain constant over time. On the contrary, if the fibrils are degraded the ThT will decrease over time as the total amount of amyloid decreases. This principle was used to investigate the eventual digestion of the aggregates by plasmin.

In vitro amyloid fibrils were prepared following the standard aggregation protocol in a plate reader under agitation with S52P TTR dissolved 1 mg/ml in 20 mM Tris-HCl, pH 7.5, containing 150 mM NaCl and 5 mM $CaCl_2$ and plasmin added in ratio 1:50. $CaCl_2$ was added to increase both plasmin stability and activity. Precise quantification of the final aggregated material was obtained using a commercial bicinchoninic acid protein assay kit (Pierce). 200 µl of fibrils at a final concentration 0.1 mg/ml were then incubated at 37 ºC in Tris-HCl buffer in the presence of 10 µM ThT, 4 ng of plasmin and subjected to 900 rpm double orbital shaking.

Under continuous agitation a very slow decay in the fluorescence intensity was observed both in the presence and in the absence of plasmin (Fig. 61). This behavior can be explained as a result of the rearrangement of the macro-assembly of fibrils, which took place during the experiment independently of the presence of the enzyme.

Interestingly while native TTR showed susceptibility to cleavage by plasmin in the presence of mechanical forces, TTR amyloid fibrils were completely resistant to degradation by plasmin under the same experimental conditions.

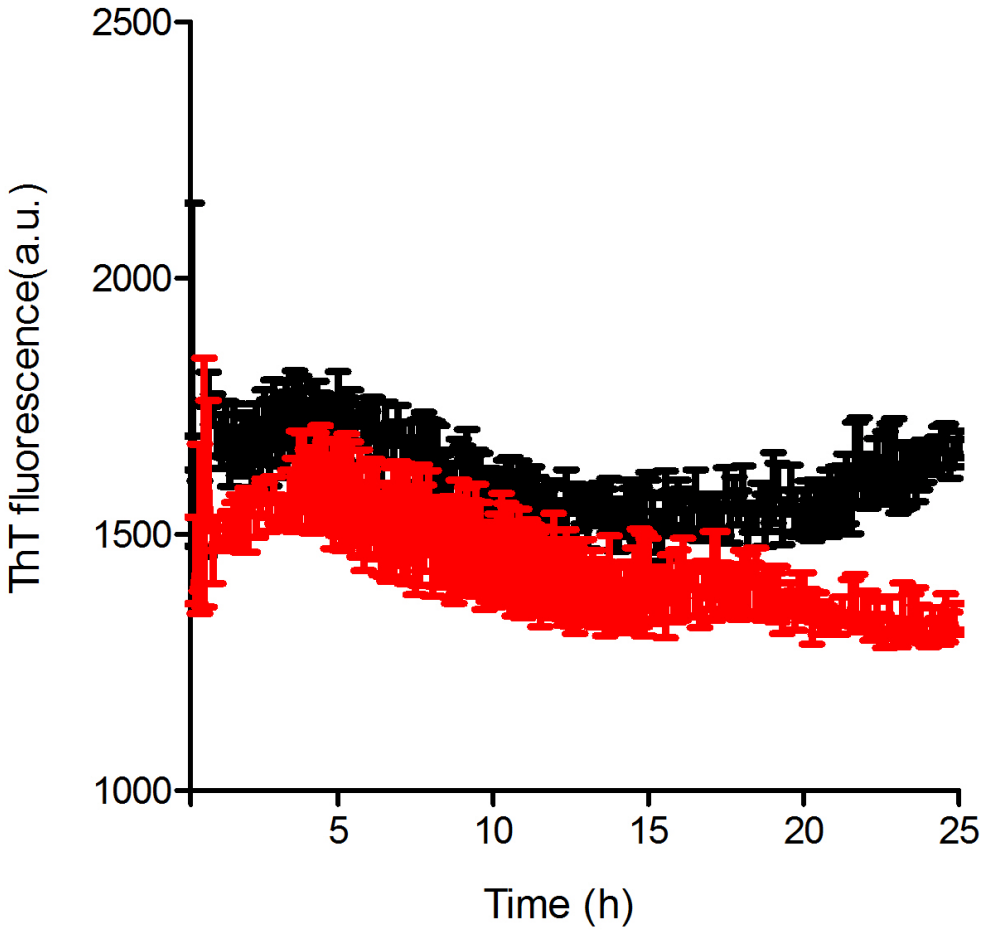

Figure 61. Effect of plasmin on S52P TTR in vitro fibrils. ThT emission signal of 0.1 mg/ml S52P fibrils in the presence (red) and absence (black) of plasmin 1:50. Tht fluorescence at 37 ºC under shaking at 900 rpm was monitored every 500s. Results presented as mean (SD) of three replicates.

6.3.7 Plasmin-mediated cleavage of other TTR variants

As initially done with trypsin when the mechano-enzymatic mechanism was further investigated (Marcoux J et al., 2015), it became crucial to investigate the effect of plasmin on TTR variants other than the highly unstable S52P variant. Fibrillogenesis of other variants including V122I, V30M, L55P, T119M and WT TTR was tested under mechano-enzymatic conditions in the presence of plasmin.

Due to the higher thermodynamic stability of the other TTR variants, the aggregation protocol had to be modified in order to increase the intensity of the forces acting on the protein during aggregation. Following on from the experimental work previously published (Marcoux J et al., 2015), the strategy adopted was to increase the hydrophobic-hydrophilic interface by switching from 96-well plates to 24-well plates and increase the volume added to each well to 500 µl.

All the amyloidogenic TTR variants tested, as well as WT TTR, were cleaved by plasmin in this *in vitro* mechano-enzymatic system and they all formed genuine amyloid fibrils. In terms of amyloid fibrils yield, the data agreed with those previously published in the presence of trypsin. S52P TTR aggregated the most and was followed by V122I, V30M and L55P TTR while WT TTR aggregated to a much lower extent. As expected, the stabilising T119M TTR variant did not aggregate at all (Fig. 62). This difference in terms of amyloid yield correlates with the early onset and severity of the clinical phenotype associated with the amyloidogenic variants in comparison with the late onset and slow progression associated with WT TTR. T119M TTR is a well-known protective mutation co-expressed in some people carrying the V30M mutation, which prevents them from developing V30M-related polyneuropathy by super stabilisation of the TTR tetramer (Hammarström P et al., 2003)

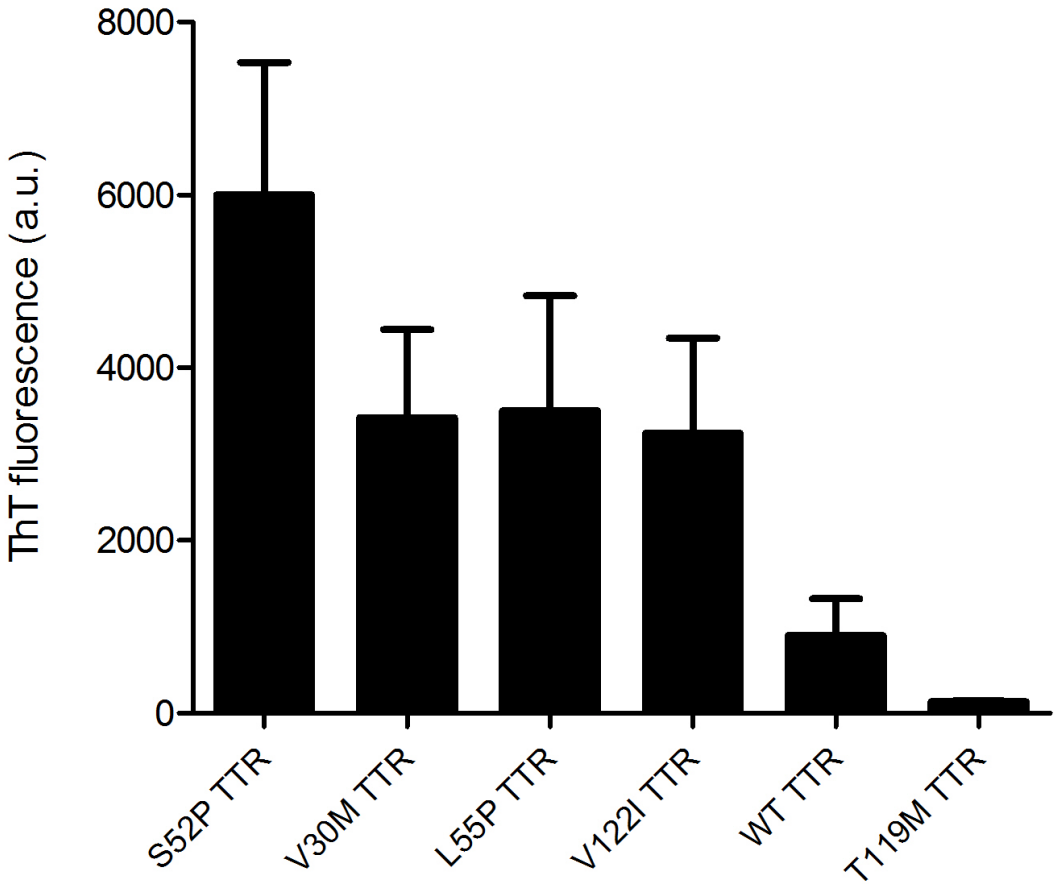

Figure 62. Cleavage of other TTR variants by plasmin. V122I, V30M, L55P and WT TTR were cleaved by plasmin (plasmin:TTR ratio 1:50) under mechano-enzymatic conditions. The samples were tested in triplicate. Data presented as mean (SD).

6.3.8 Effect of heparin and seeds on plasmin-mediated S52P TTR fibrillogensis

The effect of heparin and seeds, already tested in the presence of trypsin, was investigated on plasmin-mediated S52P TTR fibrillogenesis.

TTR was dissolved 1 mg/ml in 20 mM Tris-HCl, pH 7.5, containing 150 mM NaCl and 5 mM $CaCl_2$. Heparin was added in the same concentration used before at 0.1 mg/ml. Plasmin was added in a protease to TTR ratio of 1:50.

200 µl were transferred into a 96-well plate and were subjected to 900 rpm double orbital shaking at 37 ºC. Aggregation was monitored by ThT emission fluorescence at 480 nm following excitation at 445 nm (Fig. 63).

To a different extent, the effects of heparin on plasmin-mediated fibrillogenesis were similar to those observed in the presence of trypsin even though the shortening of the nucleation phase appeared less pronounced than in the presence of trypsin. The aggregation was enhanced when heparin was present as indicated by the higher intensity of the ThT fluorescence signal.

The effect of seeds was also investigated in the presence of plasmin. As previously observed in the presence of trypsin, TTR amyloid fibrillogenesis mediated by plasmin under mechano-enzymatic conditions was accelerated by the presence of preformed TTR amyloid fibrils, which substantially abrogated the lag phase and produced a higher final yield (Fig. 64)

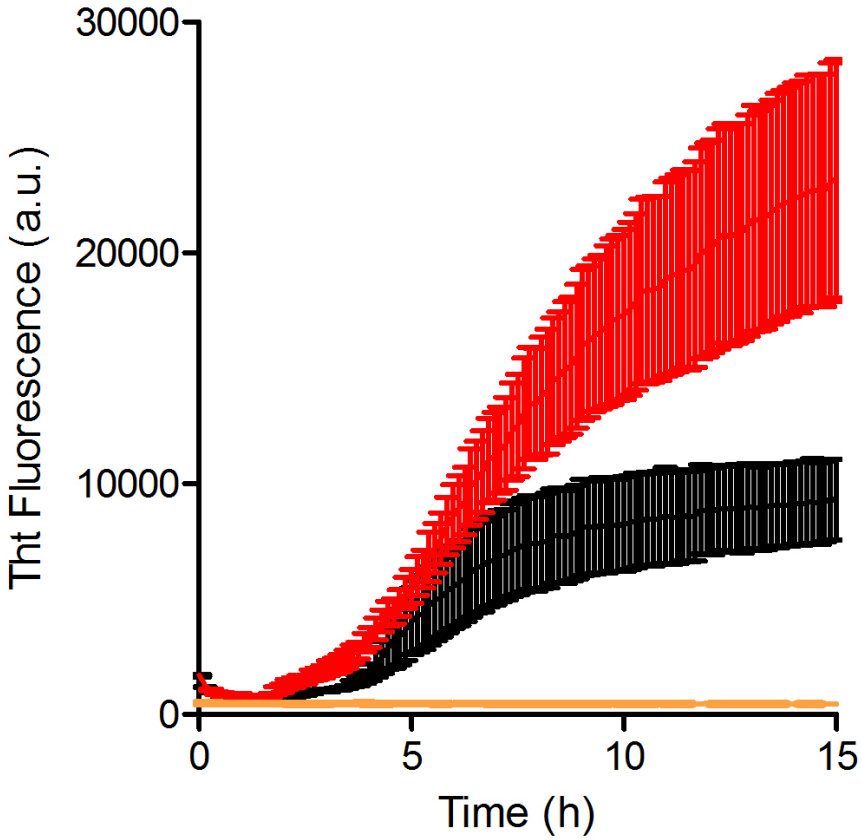

Figure 63. Effect of heparin on plasmin-mediated S52P TTR fibrillogenesis. ThT emission signal curves for S52P in the presence of plasmin (black), S52P in the presence of both plasmin and heparin (red) and heparin in the presence of plasmin (orange). Data presented as mean (SD) of three replicates.

.

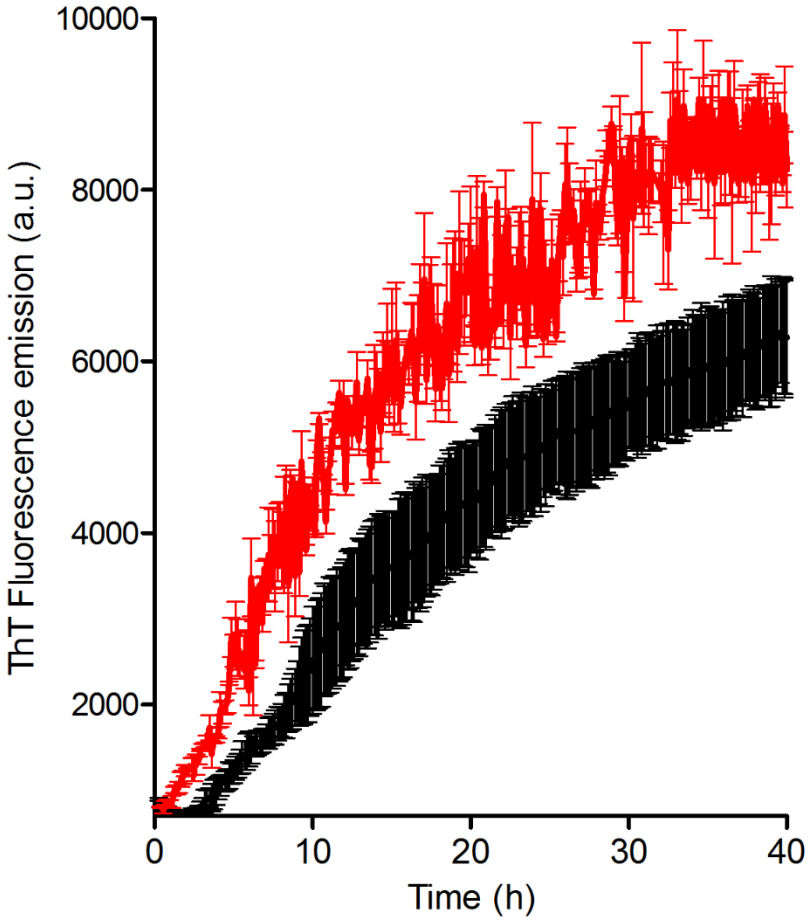

Figure 64. Effect of seeds on plasmin-mediated S52P TTR fibrillogenesis.

ThT fluorescence emission curves for S52P TTR in the presence of plasmin (black) and in the presence of plasmin and seeds (red). Data presented as mean (SD) of three replicates.

6.3.9 Linking *in vitro* and *in vivo*: from fibrin to fibril formation

In an attempt to make the model closer to the *in vivo* conditions, the fibrillar conversion of TTR was studied in an *in vitro* system mimicking the environment in which two major phases of the dynamic process characterised by the formation of clot and amyloid take place. Fibrinolysis of the *in vitro* model fibrin clot was initiated in the presence of either S52P TTR or the stabilising T119M variant. A control sample without TTR was included. The process of polymerisation and depolymerisation was monitored by measuring both the non-specific spectrophotometric turbidity at 350 nm and the specific spectrofluorimetric signal of the complex ThT-fibrils at 480 nm following excitation at 445 nm. The experiment was divided into two phases: clot formation (phase I) and clot dissolution/fibril formation (phase II).

Turbidity

In phase I, fibrinogen was converted into fibrin under the action of thrombin. The formation of clot was associated with a rapid increase in turbidity (Fig 65 A, top left). Tissue plasminogen activator (tPA), plasminogen and TTR were then carefully layered on top of the clot. tPA promoted the activation of plasminogen into plasmin, which started to dissolve the clot as normally happens in the physiological process of coagulation and fibrinolysis. The clot lysis was visualised by a rapid decrease in turbidity in phase II.

Two divergent spectroscopic profiles characterised phase II (Fig. 65 A, top right), depending on which TTR variant was layered on top of the clot. In the presence of the highly unstable S52P TTR variant, a decrease in turbidity following the dissolution of the clot was observed although this was then followed by a sharp rise in light scattering associated with the formation of TTR insoluble aggregates.

On the contrary, when the stabilising T119M TTR was added, only a drop in turbidity, associated with clot dissolution, was observed and this was not followed by any sharp increase in light scattering since this TTR variant is resistant to cleavage and fibrillogenesis as shown in figure 65, thus

confirming the data reported by Marcoux J and collaborators (Marcoux J et al., 2015).

ThT emission fluorescence

In parallel, the same process was monitored by ThT emission fluorescence. In phase I the signal remained completely flat, indicating that the presence of the fibrin clot did not interfere in any way with the ThT emission signal (Fig. 65 A, bottom left).

Once again two different behaviours were observed in phase II. When the pathogenic S52P TTR variant was added, the ThT emission signal rapidly increased as a consequence of the formation of ThT positive amyloid fibrils. On the contrary, in the presence of the super stable T119M TTR variant, the signal remained completely flat as only clot dissolution took place and no amyloid fibrils were formed (Fig. 65 A, bottom right).

At the end of the experiment, the different samples were collected and sent to our collaborator Dr. Annalisa Relini in Genoa in order to analyse them by atomic force microscopy.

Different structural features were observed in the presence of the pathogenic S52P or the stable T119M variant TTR (Fig. 65 B). Fibrillar structures compatible with the size of mature amyloid fibrils were indeed observed in the sample containing S52P TTR. This longer fibrils were observed emerging from a thick layer of shorter fibrillar structures, confirming that extensive fibrillation occurred in this sample. No fibrillar material was observed both in the presence of T119M TTR and in the absence of any TTR variant. These samples only contained globular structures, both arranged in short chains and isolated, corresponding to small aggregates of fibrin.

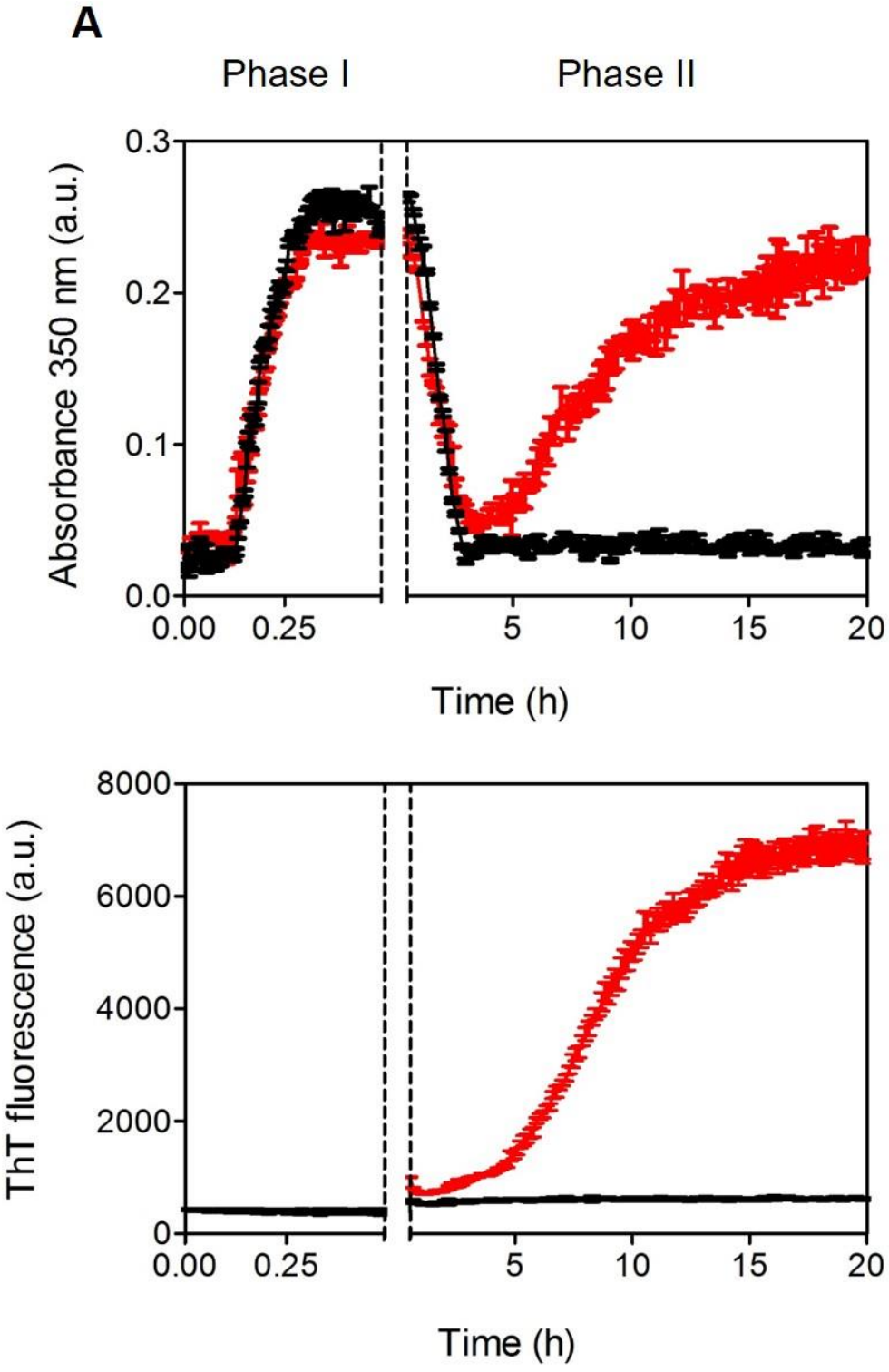
A
Phase I
Phase II
Absorbance 350 nm (a.u.)
0.3
0.2
0.1
0.0
0.00
0.25
5
10
15
20
Time (h)
ThT fluorescence (a.u.)
8000
6000
4000
2000
0
0.00
0.25
5
10
15
20
Time (h)

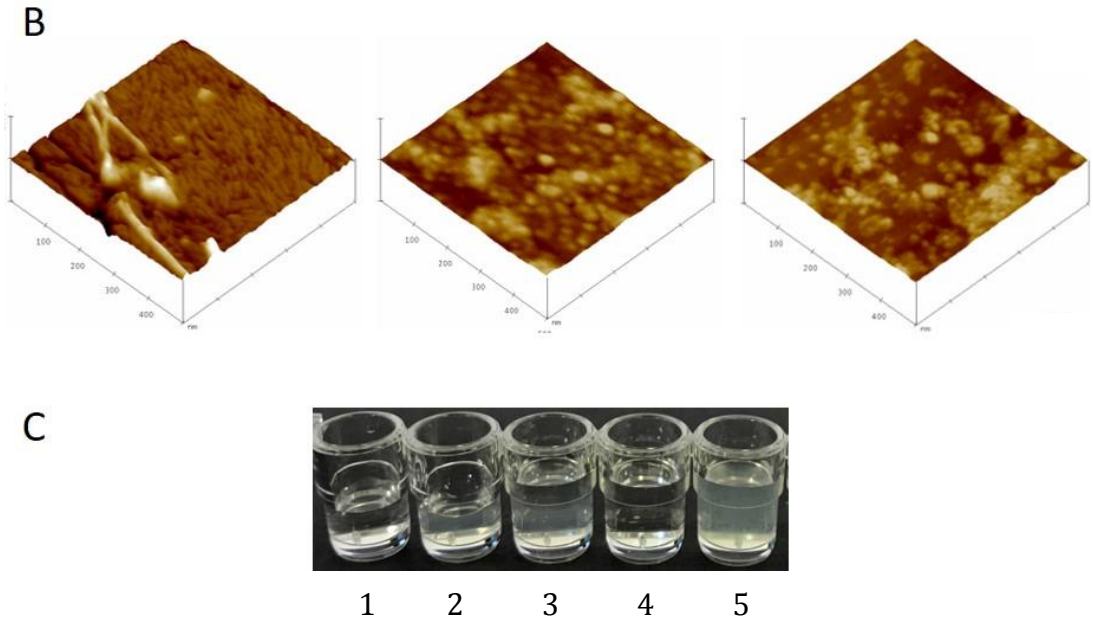

Figure 65. From fibrin to fibril formation. (A) Clot formation and dissolution/fibril formation monitored by generic spectrophotometric turbidity at 350 nm (top) and amyloid specific ThT emission fluorescence (bottom) in the presence of S52P TTR (red) and T119M TTR (black). The gap between phase I and the beginning of phase was ~1 min. The control sample in which TTR was not added behaved similarly to the sample containing T119M and is therefore not shown. (B, left to right) Surface plots of topographic tapping mode AFM images of the final material obtained in the presence of S52P TTR, T119M TTR and in the absence of any TTR isoforms. (C, left to right) Picture of wells containing: (1) fibrinogen and thrombin before the clot is formed; (2) fibrin clot; (3) TTR, tPA and plasminogen layered over the clot; (4) fibrinolysis in the presence of T119M TTR; (5) fibrinolysis in the presence of S52P TTR with turbidity caused by insoluble amyloid fibrils.

6.4 Discussion

The processes involved in the misfolding of native precursors, the formation of amyloid fibrils and the anatomical localisation of amyloid deposition *in vivo*, are still unknown for TTR as well as for other types of systemic amyloidosis (Pepys MB, 2009).

The aggregation-enhancing effect showed by heparin both in the presence of trypsin and plasmin highlights the importance that the composition of the extracellular matrix might play in inducing partial unfolding and subsequent local deposition of amyloidogenic proteins. The observed shortening of the lag phase may, in fact, be explained by heparin-induced partial unfolding of TTR, which predisposed the protein to proteolysis and subsequent aggregation. The increased amyloid yield is instead associated with the stabilisation of the fibrillar aggregates by heparin.

Pre-formed fibrils had a dramatic effect on TTR aggregation both in the presence of trypsin and plasmin. The final amyloid yield was significantly higher when seeds were added, thus indicating a more effective incorporation of amyloid precursors into the fibrils. This effect resulted in a shortening of the lag phase preceding aggregation as shown when S52P TTR aggregation was monitored at different concentrations, but in the presence of a constant trypsin to TTR ratio.

All the experimental work performed by our group in recent years has been focused on the hypothesis that mechano-enzymatic mechanism can be involved in the in vivo pathogenic pathway leading to amyloid fibril formation by TTR. As mentioned in the introduction, it is very unlikely that trypsin, despite being extremely effective in priming TTR amyloidogenesis, could represent the enzyme responsible for proteolysis *in vivo,* therefore the crucial question about the culprit protease responsible for proteolytic cleavage *in vivo* has always been open. A bioinformatics approach allowed the identification of three possible enzymes and the data presented in this chapter on the efficacy of plasmin to trigger amyloid formation by TTR *in vitro* strongly suggest it as a plausible candidate. Several proteolytic enzymes were tested and proved completely inefficient in triggering amyloid formation

in vitro. Plasmin provided the essential selectivity of cleavage and triggered TTR fibrillogenesis, which was characterised by classical kinetic phases of nucleation and elongation. Plasmin-mediated fibrillogenesis determined the formation of genuine amyloid fibrils, which share structural similarities with *ex vivo* TTR amyloid fibrils. Other than plasmin, only kallikrein-related peptidase 12 produced an increase in the ThT signal associated with amyloid formation by S52P TTR, which is the most unstable and amyloidogenic TTR variant described so far. Kallikrein-related peptidase 12, however, was not considered as it has a very transient activity *in vivo* and its effect *in vitro* was characterised by a long lag phase and a very modest final amyloid yield.

In comparison to trypsin, plasmin showed a lower activity, which could not only be explained on the basis of an inferior specificity for the substrate (45% against 60%). Once activated, plasmin undergoes extensive self-digestion, which could contribute to a reduction of its activity and a consequent delay in the formation of the first amyloid nuclei necessary to initiate the whole aggregation process. Several amyloidogenic TTR variants, including the WT protein were all cleaved by plasmin to a different extent, replicating the results previously published for trypsin. On the contrary, the protective T119M variant proved resistant to the action of the enzyme.

Interestingly plasmin is ubiquitously and continuously activated *in vivo* as it plays important physiological roles in fibrinolysis and haemostasis, cell migration, tissue remodelling, wound healing, angiogenesis and degradation of extracellular matrix (Law RH et al., 2013), where TTR deposition takes place. The possible *in vivo* scenario of plasmin-mediated TTR fibrillogenesis involves activation of plasminogen to plasmin by tPA within the clot and by urokinase plasminogen activator (uPA) in the extracellular matrix. Stochastic cleavage of the TTR tetramer by plasmin may initiate aggregation by providing the critical concentration of full length and truncated TTR necessary for nucleation. The results obtained in the presence of seeds suggest that once nucleation has occurred, the elongation of fibrils can then proceed even in the presence of low concentrations of amyloid precursors. *In vivo* plasmin activity has to be finely tuned by balancing the activity of activators, such as

tPA and uPA, and inhibitors, such as α2-antiplasmin and plasminogen activator inhibitor. In this delicate balance, the conditions for cleavage of TTR may happen rarely, but there may also be some external events influencing the plasminogen-plasmin activation pathway. For example, the intensity of normal physical activity is known to increase fibrinolytic activity (Weiss C et al., 1998). Increased physical activity is also known to increase the heart rate and activity as well as increase the mechanical stress associated with movement in places like the carpal tunnel or the spine, where TTR deposition is often observed. The importance of mechanical stress in favouring structural perturbations and promoting cleavage and aggregation has been discussed in chapter 2.

Interestingly Ishiguro and collaborators (Ishiguro K et al., 2018) have observed increased level of plasmin-α2-antiplasmin inhibitor complex in patients with AL amyloidosis, who show a tendency to bleed due to the activation of fibrinolysis. Proteolysis is not exclusive to TTR amyloidosis, but is a common feature of other forms of amyloidosis including ß2-m dialysis related amyloidosis and indeed AL amyloidosis suggesting that an imbalance in the plasminogen-plasmin system might be involved to a different extent in the pathogenesis of several amyloid diseases. This hypothesis emphasises the importance that several factors may play in determining individual susceptibility to familial and acquired forms of TTR amyloidosis. Such factors may also dramatically affect the manifestation of the disease and determine its natural history including progression and tissue distribution of amyloid deposition.

Chapter 7. Structure, function and aggregation propensity of the novel amyloidogenic D25V apolipoprotein C-III variant

7.1 Introduction

As mentioned in the general introduction, the D25V apo C-III variant was the first ever apo C-III variant described for having an association with amyloid deposition.

Apo C-III, as well as other lipoproteins, belongs to the group of intrinsically unstructured proteins, which are characterised by a lack of stable tertiary structure when existing in a lipid-free state under physiological conditions (Dyson HJ & Wright PE, 2005; Dunker AK et al., 2008). Despite the lack of a well-defined structure these proteins can readily fold following the interaction with other macromolecules. Indeed, intrinsically unstructured proteins are highly dynamic and constantly switch back and forth between the folded and the unfolded state. It is this transient permanence in the unfolded state which, as discussed in the introduction, may lead to the self-assembly into pre-fibrillar intermediates and finally insoluble amyloid fibrils.

This chapter focuses on the biochemical, functional and structural studies performed on the D25V apo C-III variant in an attempt to understand the molecular basis of its tendency to form amyloid fibrils *in vitro*, thus allowing the speculation on the processes occurring *in vivo*.

Following successful protein expression of both WT and variant apo C-III, the experimental work was organised into three main research areas:

1. Structural characterization of the variant in comparison with the WT protein by NMR spectroscopy. All NMR experiments were performed and analysed together with Dr Chris Waudby from the UCL Institute of Structural and Molecular Biology.
2. Functional comparison between WT apo C-III and D25V apo C-III with particular focus on the lipid binding properties and the inhibitory activity on lipoprotein lipase (LPL). In order to perform LPL inhibition

experiments I visited the lab of Prof Gunilla Olivecrona at the University of Umea, Sweden.

3. Investigation of the aggregation propensity of the variant in physiological buffer. Several techniques including ThT fluorescence, Congo red UV-vis spectroscopy and circular dichroism were used in this part of the project.

7.2 Materials and Methods

7.2.1 NMR spectroscopy

NMR spectra were acquired at 315 K, using a 700-MHz BrukerAvance III spectrometer equipped with a TXI cryoprobe. WT and D25V apo C-III were dissolved in 10 mM sodium acetate (pH 5.0), 180 mM SDS, 10 % D_2O (Gangabadage CS et al., 2008) to a final concentration of 0.5 mM (~3 mg/ml). ^{1}H-^{15}N HSQC and nuclear overhauser effect spectroscopy (NOESY)-HSQC were used for peak assignment. ^{1}H-^{15}N TRACT experiments were used to determine the theoretical hydrodynamic radii of both WT and D25V apo C-III in solution. The data were processed using NMRFAM-SPARKY.

7.2.2 Interaction with DMPC multilamellar vesicles

Interaction of recombinant WT and D25V apo C-III with dimyristoylphosphatidylcholine (DMPC) multilamellar vesicles (De Pauw M et al., 1995) was followed by monitoring the decrease in turbidity of DMPC liposomes at 325 nm as a function of time at 30 °C (Liu H et al., 2000) in 10 mM Tris-HCl buffer pH 8.0 containing 150 mM NaCl, 8.5% KBr, 0.01% NaN_3 and 0.01% EDTA using a 1 cm path length quartz cell in a Jasco V-650 spectrophotometer equipped with a Peltier temperature controller. The DMPC vesicles were obtained by sonication of the phospholipid for 3 cycles of 7 min at 37 °C. The lipid to protein ratio was set to 2:1. The lipid/protein association was expressed as percentage of the turbidity of DMPC vesicles in the absence of apo C-III. The lipid-binding properties of the two apo C-III isoforms were determined from the curves by evaluating the time required to reduce the absorbance at 325 nm by 50% of its initial value.

7.2.3 Native agarose gel electrophoresis

The electrophoretic mobility of native WT and D25V apo C-III in the presence and absence of DMPC was analysed using 1 % medium electroendosmosis agarose gel dissolved in 70 mM barbiturate-sodium barbiturate buffer, pH 8.6 containing 2 mM calcium lactate. 3 µl of sample were loaded onto the gel. Fivefold diluted human plasma in 2 % bromophenol blue solution was used

as marker for protein electrophoretic mobility. Electrophoresis running conditions: 20 V/cm^{-1} in a water-thermostated chamber at 10 °C. The gel was fixed for 15 min in a 15 % acetic acid solution containing 1 % picric acid, pressed overnight, dried and stained with Coomassie Blue.

7.2.4 Circular dichroism in the presence of sodium dodecyl sulphate (SDS)

Far-UV CD spectra were acquired for both WT and D25V apo C-III using a Bio-Logic MOS-500 spectrometer at 25 °C. Apo C-III was dissolved 1 mg/ml in PBS, pH 7.4. Several samples were prepared by diluting an SDS stock solution in PBS to the following final concentrations: 0; 0.2; 0.3; 0.4; 0.5; 0.6; 0.7; 0.8; 0.9; 1; 1.5 mM respectively. 100 µl of protein were then added to each sample in order to reach a final volume of 200 µl and a final protein concentration of 0.5 mg/ml (50 µM). The CD spectra were recorded in the range 195-250 nm using a step of 0.25 nm and averaging of 3 acquisitions. The acquisition period was set to 1s. All spectra were blank subtracted. Mean residue ellipticity was calculated taking into consideration the sample concentration and its molecular weight.

7.2.5 Inhibition of lipoprotein lipase activity

The catalytic activity of bovine LPL, in the presence of either WT or D25V apo C-III, was measured using an emulsion with the same composition as Intralipid 10% (Fresenius-Kabi, Sweden) containing ^{3}H triolein as substrate (Bengtsson-Olivecrona G & Olivecrona T, 1992). The composition of the incubation medium contained: 2 % (v/v) of the emulsion, 0.1 M NaCl, 60 mg/ml BSA, 0.15 M Tris-HCl, pH 8.5, and 16.7 U/ml heparin. Before addition of bovine LPL (0.25 mg/ml) in a final 200 ml mixture, the medium was pre-incubated with or without each apo C-III sample for at least 10 min. After 30 min incubation under agitation at 25 °C, 2 ml of isopropanol, heptane and 1 M H_2SO_4 (40:48:3:1) and 0.5 ml of water were added in order to stop the reaction. Free fatty acids were extracted using sequential centrifugations in glass tubes for 3 min at 2,580 g to obtain two phases. Following the first

centrifugation, 800 ml of the upper phase were transferred to other vials containing alkaline ethanol. 3 ml of heptane were added and the sample was mixed and centrifuged again. After removal of the upper phase, 3 ml of heptane were mixed into the lower phase, which was then centrifuged following the same procedure described above. The supernatant was removed and 800 ml of the lower phase were transferred to a vial containing 2 ml of scintillation liquid to count radioactivity and quantify the ^{3}H free fatty acids (nmol*ml/min). The LPL activity was then expressed as percentage of the enzyme activity in the absence of apo C-III.

7.2.6 Prediction of β-sheet content

Prediction of the β-sheet content for WT and D25V apo C-III was calculated using the Garnier-Osguthorpe-Robson (GOR) method version IV (Garnier J et al., 1996).

7.2.7 Prediction of aggregation-prone regions

Prediction of the aggregation-prone regions was calculated using the Zyggregator method (Tartaglia GG et al., 2008).

7.2.8 Change in secondary structure monitored by CD spectroscopy

Far-UV CD spectra were acquired using the same parameters described in paragraph 8.2.5. The protein was dissolved in PBS, pH 7.4 at a concentration of 1 mg/ml (100 µM). Spectra were acquired at 37 °C at 0, 0.5, 4 and 6 hours respectively. CD measurements were combined with the fibrillogenesis experiments described in the next paragraph.

7.2.9 Apo C-III fibrillogenesis in physiological buffer under agitation

Fibrillogenesis experiments were performed in standard quartz cells stirred at 1,500 rpm (IKA magnetic stirrer) at 37 °C in PBS, pH 7.4 at a protein concentration of 100 µM. Aggregation was carried out without seeds of preformed fibrils and monitored following the increase of turbidity at 350nm.

ThT fluorescence emission of the protein aggregate suspension was measured at the end of the aggregation.

7.2.10 ThT fluorescence emission

ThT fluorescence emission at 480 nm following excitation at 445 nm was measured for each apo C-III isoform at the end of fibrillogenesis on a 10 µl aliquot of protein sample added to 490 µl of PBS, pH 7.4, in the presence of 10 mM ThT.

7.2.11 Transmission electron microscopy (TEM) and atomic force microscopy (AFM)

Transmission electron microscopy analysis was performed using protein samples stained with 2% (w/v) uranyl acetate using a CM120 microscope at 80 keV by Alejandra Carbajal at the Division of Medicine Electron Microscopy Unit, Royal Free Campus, UCL.

AFM analysis was carried out by Dr Annalisa Relini at the University of Genoa, Italy, on 10 µl of fibrillar sample incubated on a freshly cleaved mica substrate for 5 min, then rinsed and dried. AFM measurements were performed in tapping mode with a Multimode Scanning Probe Microscope driven by a Nanoscope IV controller (Digital Instruments, Bruker), using single-beam uncoated silicon cantilevers (type OMCL-AC160TS, Olympus). The drive frequency was between 290 and 320 kHz, the scan rate was between 0.5 and 0.8 Hz. Scan size is 1.2 mm.

7.2.12 Congo red UV-vis spectroscopy

Congo red UV-vis spectroscopy (Klunk WE et al., 1989) was performed on the aggregated material coming from fibrillogenesis experiments. At the end of the experiment the sample was pelletted for 15 mins at 10000 g. The total amount of aggregate was calculated by difference between the total initial concentration and the concentration of soluble protein present in the supernatant at the end of the experiment. The pellet was resuspended at 1

mg/ml, 50 µl were mixed with 450 µl of a 10 µM solution of Congo Red in PBS and left 15 mins at room temperature before recording the UV trace.

7.2.13 Congo red staining

Congo red staining was performed as described in paragraph 4.2.5

7.3 Results

7.3.1 Structural characterization by NMR spectrosocopy

A full assignment of the wild protein was already available (*BioMagResBank database accession number 15268)* and published by Gangabadage and colleagues (Gangabadage CS et al., 2008). In the experimental conditions selected, due the presence of 180 mM SDS, the protein is thought to assume its fully folded state, characterised by the presence of six amphipathic α-helices. WT apo C-III was prepared in the same conditions previously published and a good quality ^{1}H-^{15}N HSQC spectrum was obtained (Fig. 66 left). The available assignment was used as a template to assign all the peaks of our recombinant WT protein, which appeared identical to the published one. D25V apo C-III was then prepared in the same conditions and a ^{1}H-^{15}N HSQC spectrum of similar quality to the WT one was obtained (Fig. 66, right).

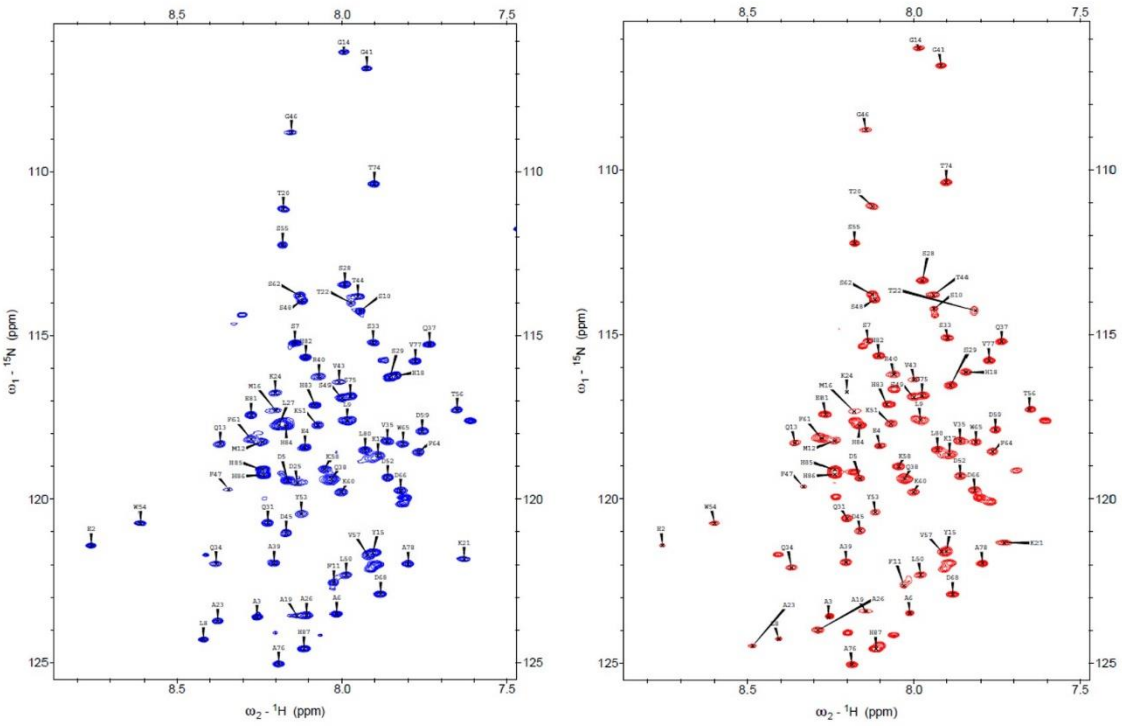

Figure 66. ^{1}H-^{15}N HSQC spectra of WT (blue) and D25V (red) apo C-III. Spectra were acquired at 315 K on a 700-MHz BrukerAvance III spectrometer equipped with a TXI cryoprobe on a 0.5 mM protein sample in 10 mM sodium acetate (pH 5.0), 180 mM SDS, 10 % D_2O.

A nuclear overhauser effect spectroscopy (NOESY)-HSQC spectrum was then recorded in order to reassign perturbed residues located around the mutation site, which could not directly be assigned by simple comparison with the WT apo C-III ^{1}H-^{15}N HSQC spectrum. Gangabadage and colleagues had already shown the formation of α-helical structure for the WT protein. NOESY-HSQC was helpful to confirm the presence of α-helical structure in case of the D25V variant also. Indeed, the presence of sequential NOEs from the H_α atom of residue i to the H_N atom of residues i+1/i+3, typical of the α-helical secondary structure, was observed, (Fig. 67).

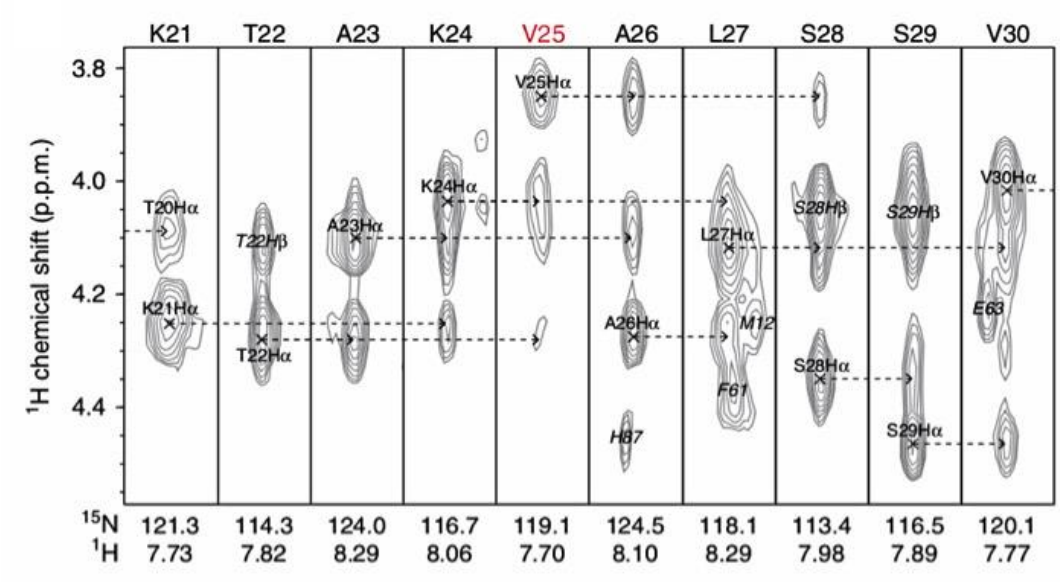

Figure 67. Typical NOEs associated with the α-helical structure. ^{1}H strips from the NOESY-HSQC spectrum of D25V apo C-III. Sequential NOEs from the H_α atom of residue i to the H_N atom of residue i+1/i+3 are highlighted by the dashed arrows

The ^{1}H-^{15}N HSQC spectra of WT and variant apo C-III appeared almost completely superimposable and only peaks located near the site of mutation showed significant chemical shifts (Fig. 68).

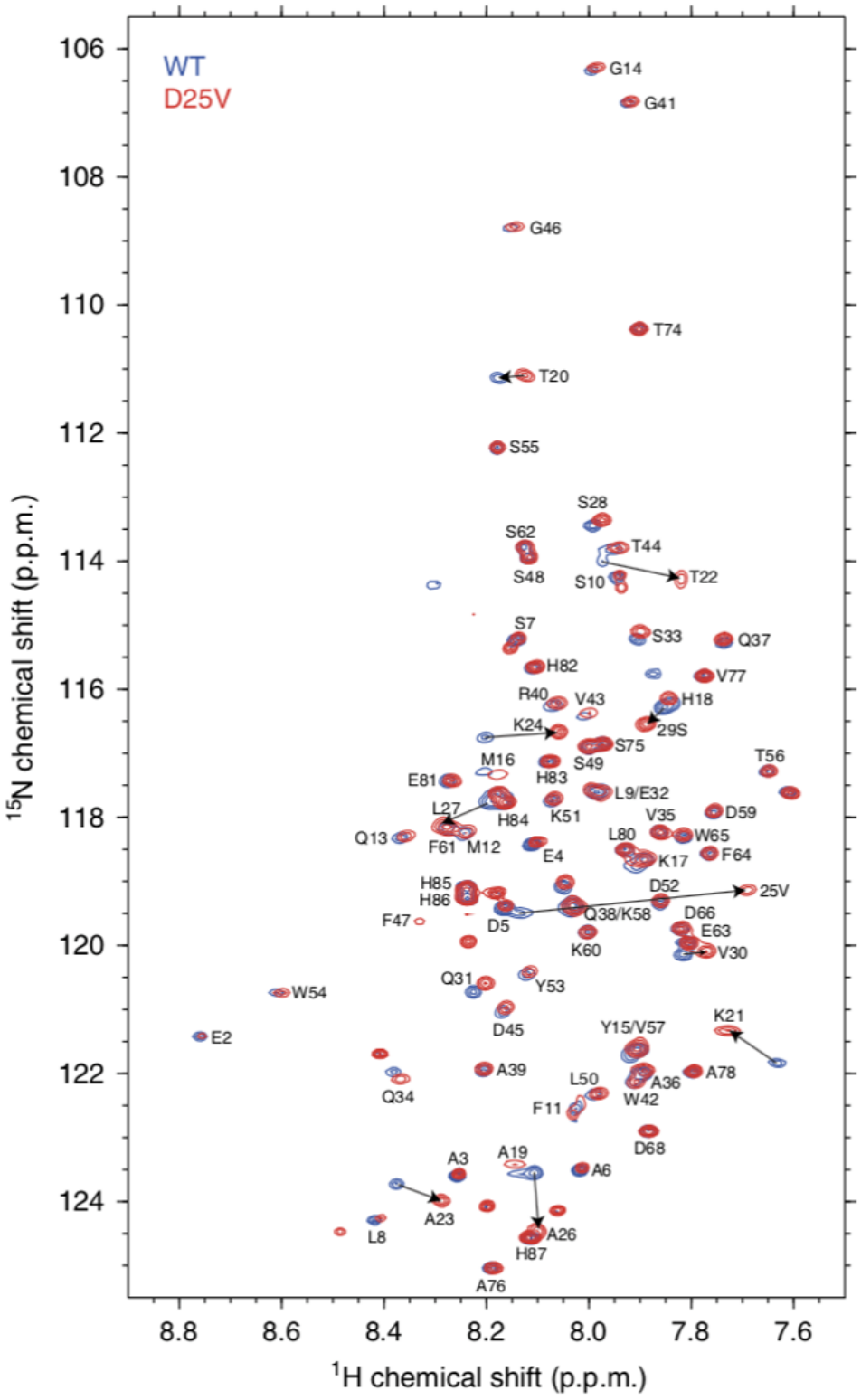
WT
D25V
106
108
110
112
114
116
118
120
122
124
^{15}N chemical shift (p.p.m.)
8.8
8.6
8.4
8.2
8.0
7.8
7.6
^{1}H chemical shift (p.p.m.)
G14
G41
G46
T74
T20
S55
S28
S62
T44
S48
S10
T22
S7
S33
Q37
H82
V77
R40
V43
H18
K24
29S
S75
M16
S49
T56
E81
H83
L9/E32
L27
H84
K51
V35
D59
Q13
F61
M12
L80
W65
E4
K17
F64
H85
H86
D52
25V
F47
D5
Q38/K58
D66
E63
K60
V30
Q31
Y53
W54
D45
Y15/V57
K21
E2
A39
L50
A36
A78
Q34
W42
F11
D68
A3
A19
A6
A23
L8
A26
H87
A76

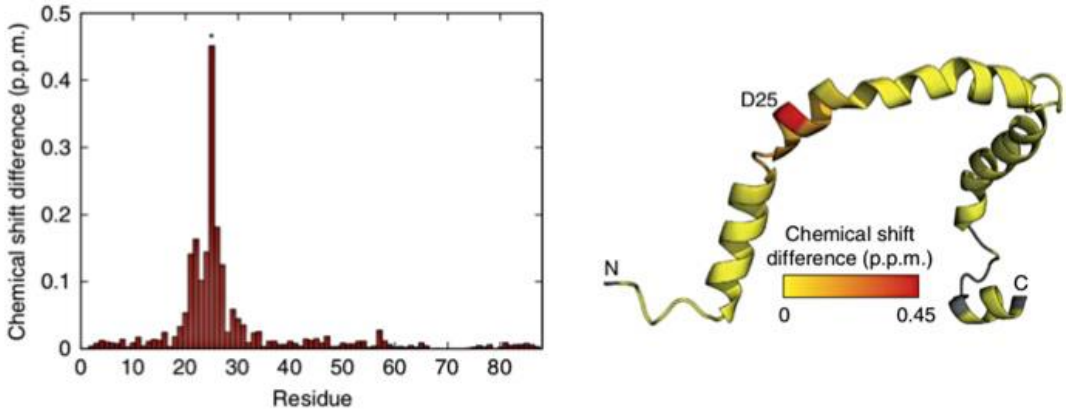

Figure 68. Superimposition of ^{1}H-^{15}N HSQC spectra of WT and D25V apo C-III and amide chemical shift differences. (previous page) The two ^{1}H-^{15}N HSQC spectra appeared almost completely superimposable apart from residue 25 and some peaks located in proximity of the site of mutation. The black arrows indicate large chemical shifts from the WT spectrum. The spectra were recorded at 315 K, using a 700-MHz BrukerAvance III spectrometer equipped with a TXI cryoprobe. (left) Amide chemical shift differences between WT and D25V apo C-III. Residue 25 is indicated with an asterisk. (right) Plotting the amide chemical shift differences onto the apo C-III structure (PDB code pdb2jq3) clearly highlighted the clustering of chemical shifts around the mutation site.

The rotational correlation time (T_c), which in folded proteins usually correlates to a good approximation with the molecular weight (Lee D et al., 2006), was determined for both WT and D25V apo C-III using ^{1}H-^{15}N TROSY for rotational correlation times (TRACT) experiments. Based on the TROSY technique, introduced in chapter 6, ^{1}H-^{15}N TRACT enables highly efficient measurements of the effective rotational correlation times in biological macromolecules by suppressing the influence of dipole–dipole (DD) relaxation by remote protons in backbone ^{15}N–^{1}H moieties as well as relaxation contributions from chemical exchange (Lee D et al., 2006). The measurement of T_c was used to estimate the Stokes radii (R_s) of the two

proteins (i.e. is the radius of a sphere with the same hydrodynamic properties experimentally determined).

In good agreement with the mild differences observed in ^{1}H-^{15}N HSQC spectra, the two proteins appeared almost identical with estimated Stokes radii (R_S) of 20.3 ± 0.6 Å and and 19.6 ± 0.2 Å for WT and D25V apo C-III respectively, which correlated with the expected radius for a folded protein of ~10 KDa.

In conclusion, NMR results evidenced a substantial structural identity between WT and variant apo C-III in their folded state. The relatively modest number of chemical shifts observed, apart from the expected ones around the mutation site, the identical Stokes radii and the results of NOESY-HSQC experiment suggested that the mutation Asp-Val was well tolerated and the protein could reach a properly folded state in the presence of ligands.

7.3.2 Lipid binding in the presence of DMPC multilamellar vesicles

The structural information obtained by NMR spectroscopy suggested that both proteins could fold correctly upon interaction with lipid-like micellar structures. However whether they could bind lipid particles with the same efficacy was still unknown.

An experimental set up for the determination of apo C-III lipid binding properties had already been described by Liu and collaborators (Liu H et al., 2000). The assay was based on the spectrophotometric determination of the decrease in turbidity at 325 nm following the interaction of apo C-III with DMPC liposomes at 30 °C.

The DMPC vesicles were prepared by sonication (8.2.2) and used within 24 hours to avoid the risk of disruption of the micellar structures. Following sonication the lipid suspension appeared cloudy and an intense absorbance could be detected at 325 nm.

The protein was then added and a real time measurement of the absorbance at 325 nm was followed with a spectrophotometer for 15 minutes. Upon binding of the protein, the vesicles became soluble as demonstrated by the

progressive decrease of the turbidity signal. By the end of the experiment the suspension had clarified.

Binding to DMPC multilamellar vesicles could be observed for both WT and D25V apo C-III, although the time required by the latter to reduce the absorbance at 325 nm to 50 % of its original value resulted 168.7 ± 8.1 s against 114.7 ± 4.2 s required by the WT. These results suggested that the mutation may cause a less efficient binding as already observed for other apo C-III variants (Liu H et al., 2000). Moreover at equilibrium the absorbance at 325 nm was decreased by approximately 85-90 % of its original value in the presence of the WT, while the decrease was approximately 70% in the presence of the variant, suggesting a different extent of interaction (Fig. 69).

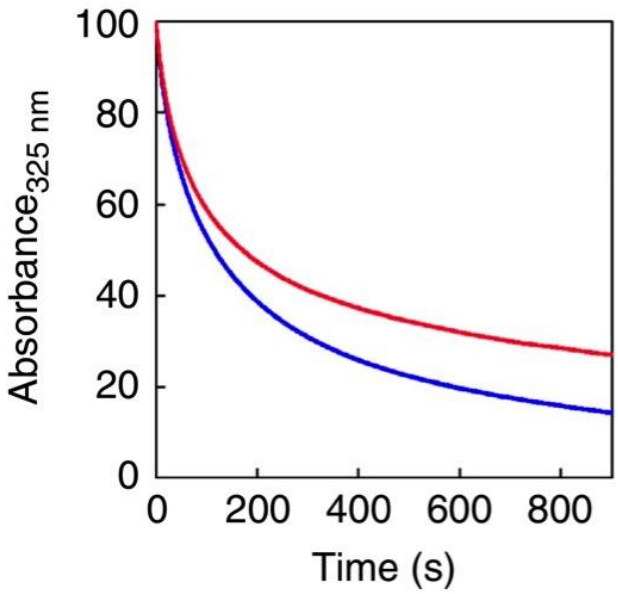

Figure 69. WT (blue) and D25V (red) apo C-III binding to DMPC liposomes. Absorbance at 325 nm was monitored in real time with a spectrophotometer for 15 minutes at 30 °C. Apo C-III/lipid ratio was 2:1 (w/w). The binding curves shown are representative of three independent experiments and expressed as percentage of the initial absorbance of the vesicles at 325 nm. The time required to reduce by 50% the initial signal at 325 nm. t50% was 114.7 ± 4.2 s and 168.7 ± 8.1 s for WT and D25V respectively.

The change in motility in native gel electrophoresis, however, showed that at equilibrium, even the variant was fully integrated in the lipid vesicles. Interestingly, the solubility of the variant that in the absence of lipids was very poor and caused precipitation at the site of deposition was rescued once the protein was bound to the lipid particles, suggesting that, *in vivo*, aggregation could indeed take place when the protein is in the lipid-free unfolded state (Fig. 70).

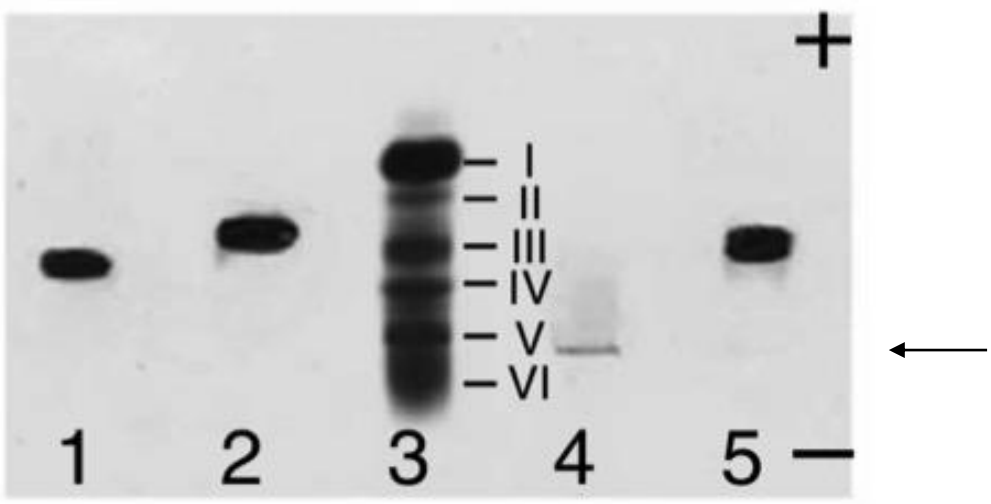

Figure 70. Native gel electrophoresis of WT and D25V apo C-III in complex with DMPC vesicles. 1) WT apo C-III alone 2) WT apo C-III in complex 2:1 with DMPC liposomes 3) marker 4) D25V apo C-III 5) D25V apo C-III in complex 2:1 with DMPC liposomes. The marker was human plasma diluted 1:5 in 2 % bromophenol blue. The major plasma components are highlighted: albumin (I), α-1 antitrypsin (II), haptoglobin (III), transferrin (IV), fibrinogen (V) and γ-globulin (VI). The arrow indicates the site of deposition

7.3.3 Circular dichroism in the presence of SDS

In order to further investigate the binding properties of the protein, the folding of the protein in the presence of SDS was investigated by circular dichroism spectroscopy. Study of the folding in the presence of SDS by CD spectroscopy had previously been successfully used for α-synuclein (Gosh D et al., 2013).

Several samples containing the same amount of protein and increasing concentrations of SDS were prepared in PBS, pH 7.4. The final SDS concentrations were 0; 0.2; 0.3; 0.4; 0.5; 0.6; 0.7; 0.8; 0.9; 1; 1.5 mM respectively. The CD spectra were recorded in the range 195-250 nm using a step of 0.25 nm between experimental points. Averaging of three distinct recordings was used. Spectra were acquired at 30 °C.

The concentration of both proteins was checked with a spectrophotometer by measuring the absorbance at 280 nm (molar extinction coefficient 19480) and was adjusted to 0.5 mg/ml before the different samples in the presence of SDS were prepared. Interestingly the CD spectra in the absence of SDS suggested that the variant was less structured than its WT counterpart. It is worth noting that for practical reasons, the concentration of SDS used was below the critical micellar concentration (8.2 mM) therefore the lipid-like particles obtained under these conditions were less structured than those obtained with DMPC. Nevertheless, upon binding to SDS particles, a progressive increase of the specific α-helix signals at 222 and 208 nm was observed for both proteins, suggesting that the interaction and subsequent folding was less efficient for the variant in comparison with the WT (Fig. 71). These results appeared in line with what was already observed in the presence of DMPC, where a different reduction in turbidity was observed between WT and variant.

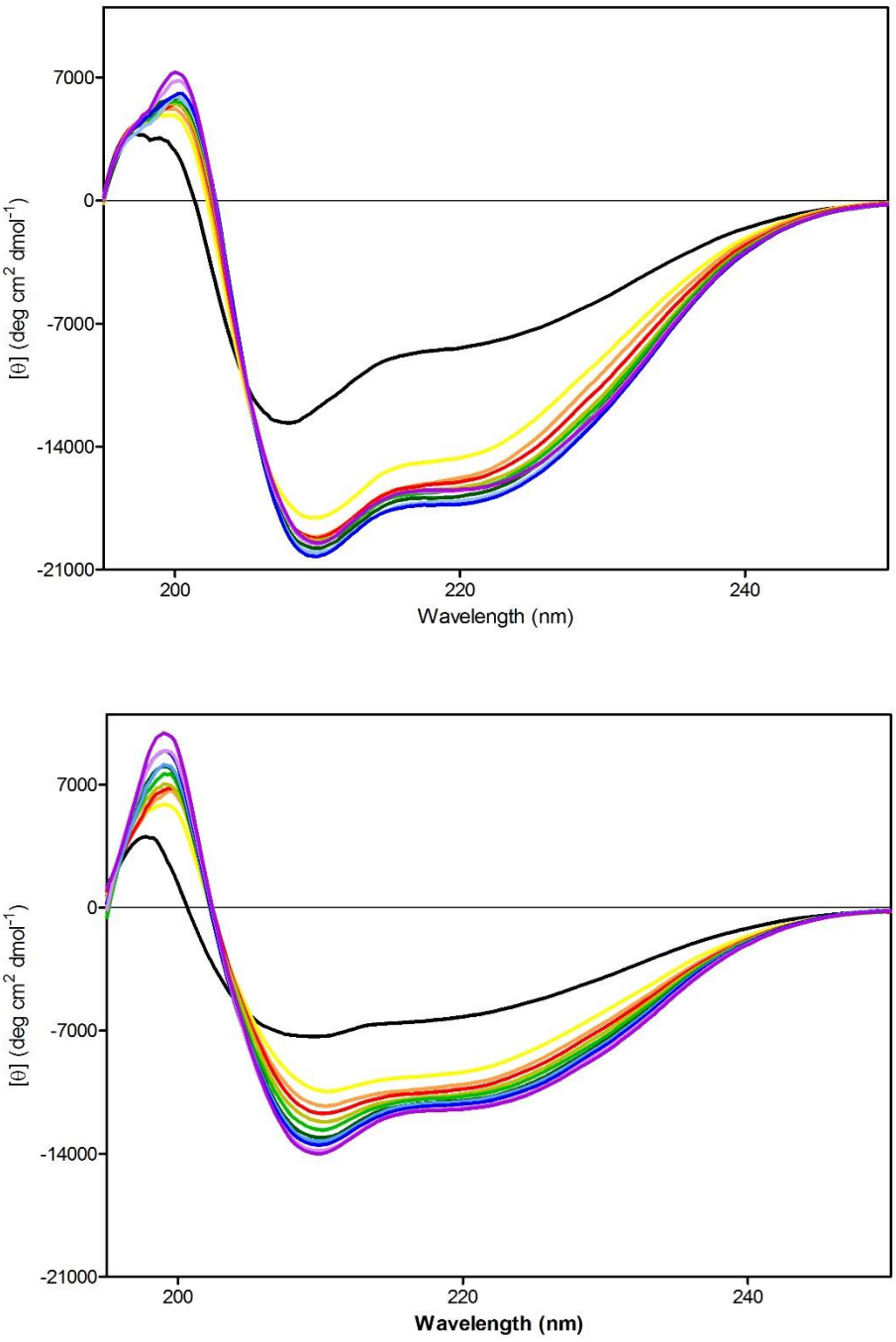

Figure 71. CD spectroscopy of apo C-III in the presence of SDS. CD spectra were recorded at 30 °C on a Bio-Logic MOS-500 spectrometer in the range 195-250 nm using 3 accumulations and 0.25 nm step. WT (top) and D25V apo C-III (bottom) spectra in the presence of 0 (black), 0.2 (yellow), 0.3 (orange), 0.4 (red), 0.5 (brown), 0.6 (light green), 0.7 (dark green), 0.8 (light blue), 0.9 (blue). 1 (violet) and 1.5 mM (purple) SDS. Data expressed as mean residue ellipticity calculated considering concentration and molecular weight of the sample.

7.3.4 Inhibition of LPL activity

In order to further characterise the variant from a functional point of view, its ability to inhibit lipoprotein lipase *in vitro* was evaluated. In order to do so, I spent a week in the laboratory directed by Professor Gunilla Olivecrona at the University of Umea, Sweden. Professor Olivecrona was the first to describe the methodology to evaluate inhibition of LPL (Bengtsson-Olivecrona G & Olivecrona T, 1992) and her laboratory is the only one in the world performing this assay which is based on the evaluation of the release of ^{3}H labelled fatty acids from triolein by LPL in the presence of different concentrations of apo C-III.

Either WT or D25V apo C-III were added to the ^{3}H triolein emulsion at 5 different concentrations: 2.5, 3.75, 5, 6.25 and 7.5 µM respectively. After 10 minutes LPL was added to start the reaction, which was carried out for 30 minutes at room temperature before being stopped by the addition of H_2SO_4 in combination with isopropanol and heptane. The free fatty acids that have been hydrolysed were extracted with a series of sequential centrifugations and phase separations. The final product of these separation steps contained the ^{3}H labelled free fatty acids, which were quantified by radioactivity count.

LPL activity was then expressed as nmol of product formed for ml of starting solution per minute.

A progressive decrease of LPL activity was detected in response to increasing concentrations of apo C-III. No significant difference could be observed between WT and variant, indicating that the mutation did not affect in any way the inhibitory activity on LPL (Fig. 72).

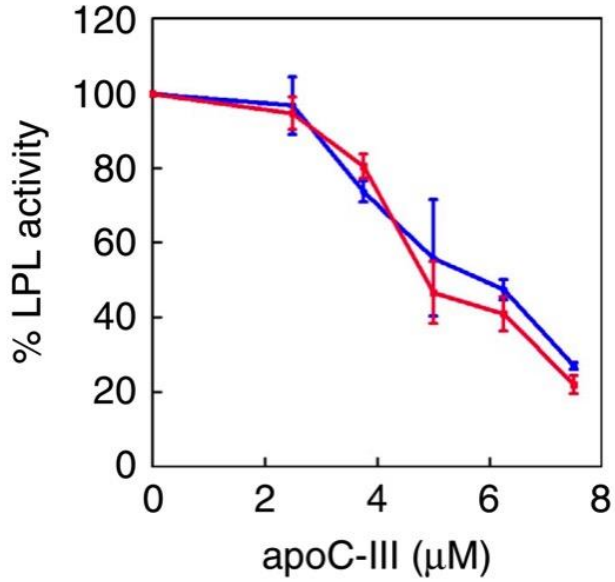

Figure 72. Inhibtion of LPL activity. WT (blue) and D25V apo C-III (red) exhibited the same inhibitory activity on LPL. Data expressed as mean (SD) of three independent experiments. LPL activity expressed as percentage of the activity measured in the absence of apo C-III.

7.3.5 Prediction of β-sheet content and aggregation prone regions

Several algorithms are available to predict the α-helical or β-sheet content of a protein on the basis of its sequence. For example, a sequence of large aromatic residues and/or β-branched amino acids is likely to be found in β-sheet. The Garnier-Osguthorpe-Robson (GOR) method takes into account all of these parameters and gives as an output a "map" of the α or β propensity plotted against the protein sequence.

The GOR method was used to predict the β propensity of both WT and D25V apo C-III (Fig. 73) and showed that, due to the substitution of a charged aspartic acid with an hydrophobic valine, the variant had an increased propensity to assume a β-sheet conformation around the site of mutation. No other differences were predicted for the rest of the sequence.

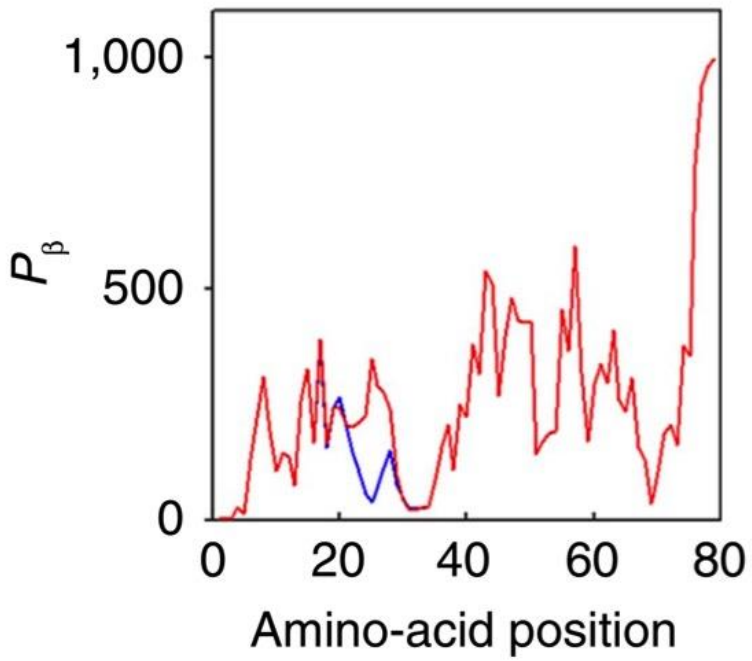

Figure 73. Prediction of the β-sheet content. WT (blue) and D25V apo C-III (red) β-sheet content was predicted using the GOR method. An increased propensity to assume β-sheet conformation was suggested around the site of mutation.

The Zyggregator method, developed by Tartaglia and colleagues in Cambridge, predicts from the amino acid sequence the aggregation propensity of a protein considering parameters such as α and β propensity, hydrophobicity, charge, hydrophobic patterns, gatekeepers and local stability. The aggregation propensity of both WT and D25V apo C-III was predicted using the software available at http://www-vendruscolo.ch.cam.ac.uk/zyggregator.php.

The predicted effect of the mutation was an increased aggregation propensity for the variant in comparison with WT apo C-III (Fig. 74).

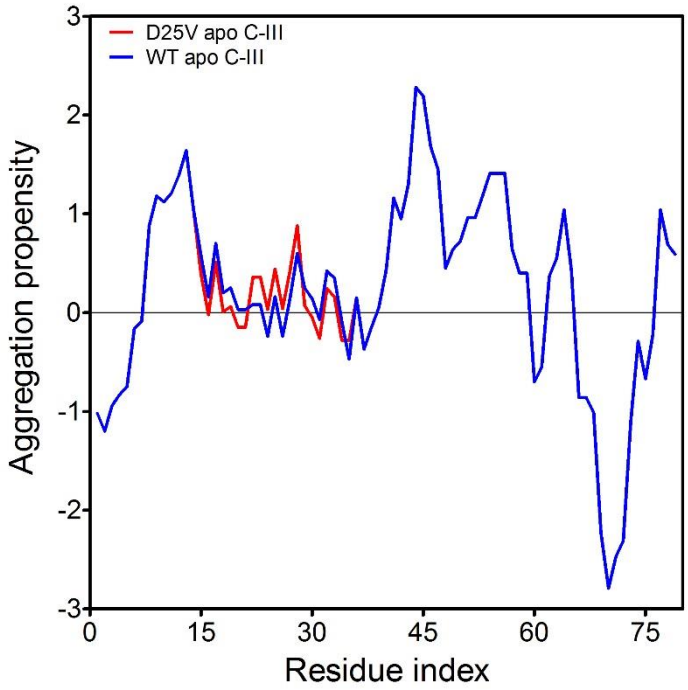

Figure 74. Aggregation propensity predicted by the Zyggregator method. D25V apo C-III (red) showed an increased aggregation propensity around the mutation site when compared to WT apo C-III (blue).

7.3.6 Fibrillogenesis in physiological buffer

The predictions suggested an increased tendency to form β-sheet secondary structure, which correlated well with the predicted higher aggregation propensity. The precipitation at the site of deposition in native gel electrophoresis and the difference in the CD spectra in the absence of SDS seemed to confirm at least the second prediction on the aggregation propensity. The overall structural similarity observed by NMR spectroscopy in the lipid bound state and the capacity to interact with lipid-like particles, although to a different extent than WT apo C-III, indicated that the maximal difference between the two proteins existed in the lipid-free state. Fibrillogenesis was therefore performed in PBS, pH 7.4, in the presence of 100 µM either WT or D25V apo C-III. The temperature was set to 37 °C and the sample was subjected to mechanical agitation by the mean of a magnetic bar rotating at 1500 rpm (IKA magnetic stirrer). Aggregation was followed by monitoring the increase in turbidity at 350 nm (Fig. 75). WT apo C-III did not aggregate throughout the experiment and the solution appeared clear by the end of it. On the contrary the variant rapidly aggregated and reached a plateu around 2.5 hours after the start of the experiment, to which point the sample appeared cloudy. Our data suggest that the mutation causes a reduced affinity and therefore we can speculate that *in vivo* the percentage of variant in lipid-free state might increase. The mechanism of fibrillogenesis in vivo could therefore be determined by two synergistic factors: increased free form and reduced threshold for aggregation.

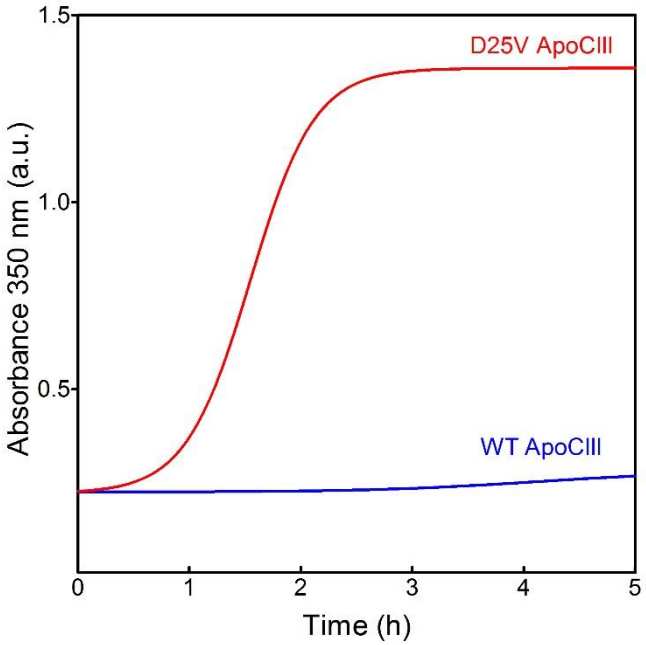

Figure 75. Fibrillogenesis in physiological buffer. WT (blue) and D25V apo C-III (red) aggregation was followed monitoring the increase of turbidity at 350 nm with a spectrophotometer. Rapid aggregation was observed for the variant. Data presented are representative of three replicates.

In parallel with turbidity measurements, CD spectra for both WT and variant apo C-III were recorded in order to monitor the structural transitions undergone by the proteins during the aggregation experiment. Spectra were recorded at 0, 0.5, 4 and 6 hours respectively (Fig. 76). In agreement with the turbidity measurements the CD spectra recorded for WT apo C-III remained identical over time, confirming that the protein did not undergo any structural change whilst exposed to perturbing conditions. On the contrary for the variant a shift toward a β-sheet prominent content was already observed after 30 minutes in total agreement with the aggregation data.

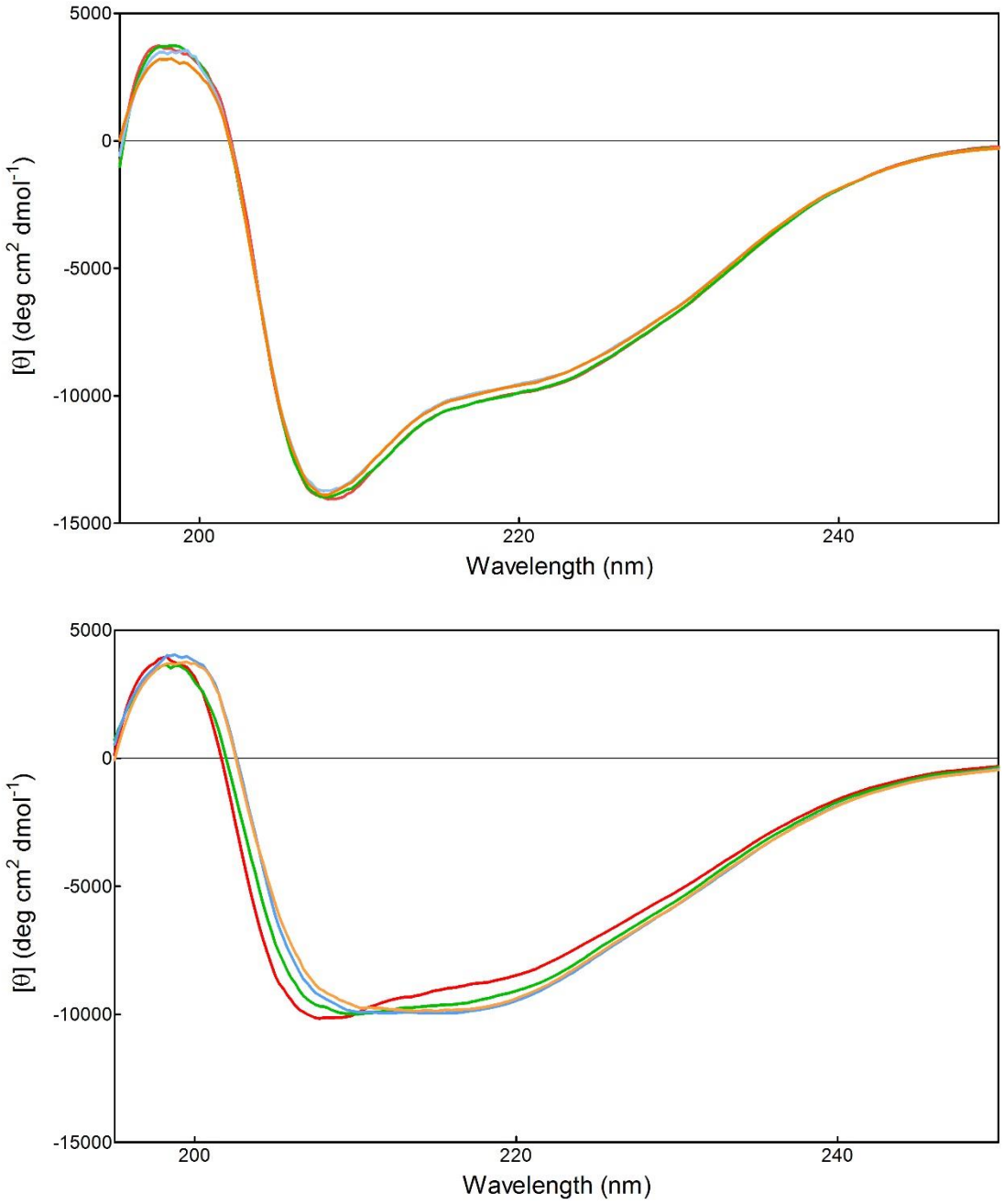

Figure 76. CD spectra of apo C-III samples during aggregation. (top) WT apo C-III and (bottom) D25V apo C-III spectra recorded at 0 (red), 0.5 (green), 4 (light blue0 and 6 hours (orange) respectively. CD spectra were recorded at 37 °C on 200 µl of the aggregation sample using a Bio-Logic MOS-500 spectrometer. A rapid change toward β-sheet conformation was observed for the variant.

To confirm the amyloid nature of the aggregate, ThT emission fluorescence was measured at the end of the fibrillogenesis experiment.

10 µl of sample were mixed with 490 µl of a 10 µM solution of ThT in PBS and the emission fluorescence at 480 nm was measured with a spectrofluorometer following excitation at 445 nm. Only D25V apo C-III was ThT positive, confirming the presence of amyloid fibrils in the sample. Further confirmation of the fibrillar nature of the aggregate came from both electron microscopy and atomic force microscopy performed by Alejandra Carbajal in London and Dr Annalisa Relini in Genoa, Italy, on the pellet obtained after centrifugation (Fig. 77).

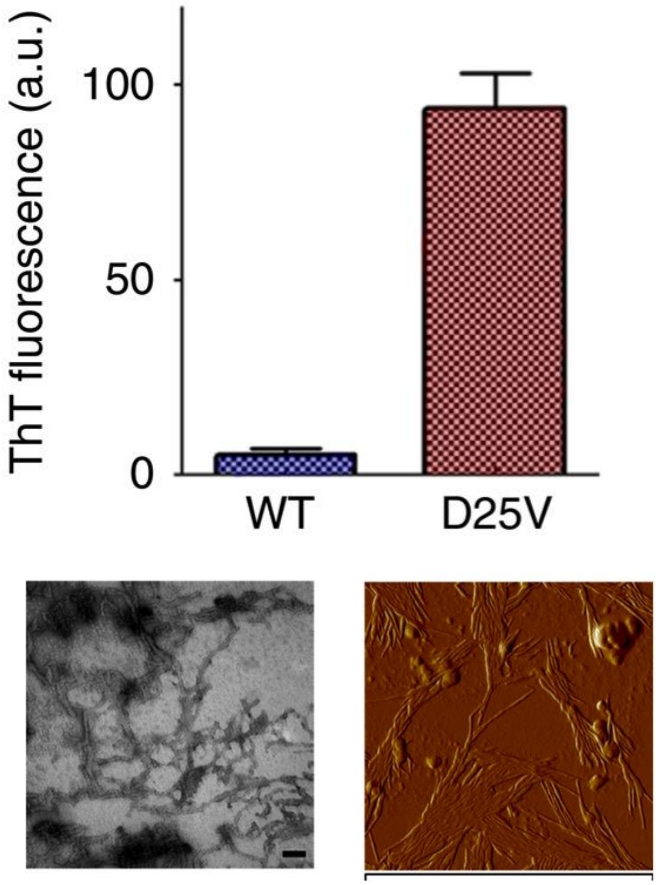

Figure 77. ThT, EM and AFM analysis of the apo C-III samples. ThT results presented as mean (SD) of three separate experiments. Both EM and AFM confirmed the fibrillar nature of the aggregate.

Congo red staining and Congo red UV-vis spectroscopy were performed to add another proof of the presence of amyloid fibrils. As described in the general introduction, Congo red exhibits a characteristic apple-green birefringence under polarised light if amyloid fibrils are present. The interaction between the dye and the fibrils can also be monitored by UV-vis spectroscopy as described by Klunk and colleagues (Klunk WR et al., 1989).

Congo red UV-vis absorbance spectrum is characterised by a maximum of absorbance around 480 nm. When Congo red is bound to amyloid fibrils, the Congo red/amyloid fibrils spectrum shifts toward the right and the maximum of absorbance can be recorded at 540 nm. 50 µl of a 1 mg/ml solution of D25V fibrils were mixed with 450 µl of a 10 µM solution of Congo red in PBS. In order to allow full binding, the solution was left for 15 minutes at room temperature.

In the meanwhile UV-vis spectra for Congo red alone and apo C-III fibrils alone were recorded. Following the 15 minutes incubation, a spectrum was recorded for Congo red/apo C-III fibril complex (Fig. 78).

A clear shift towards the right with a new maximum of absorbance at 540 nm was detected, confirming once more the presence of genuine amyloid fibrils in the D25V apo C-III sample. The same analysis could not be performed for WT apo C-III as no pellet was obtained after centrifugation.

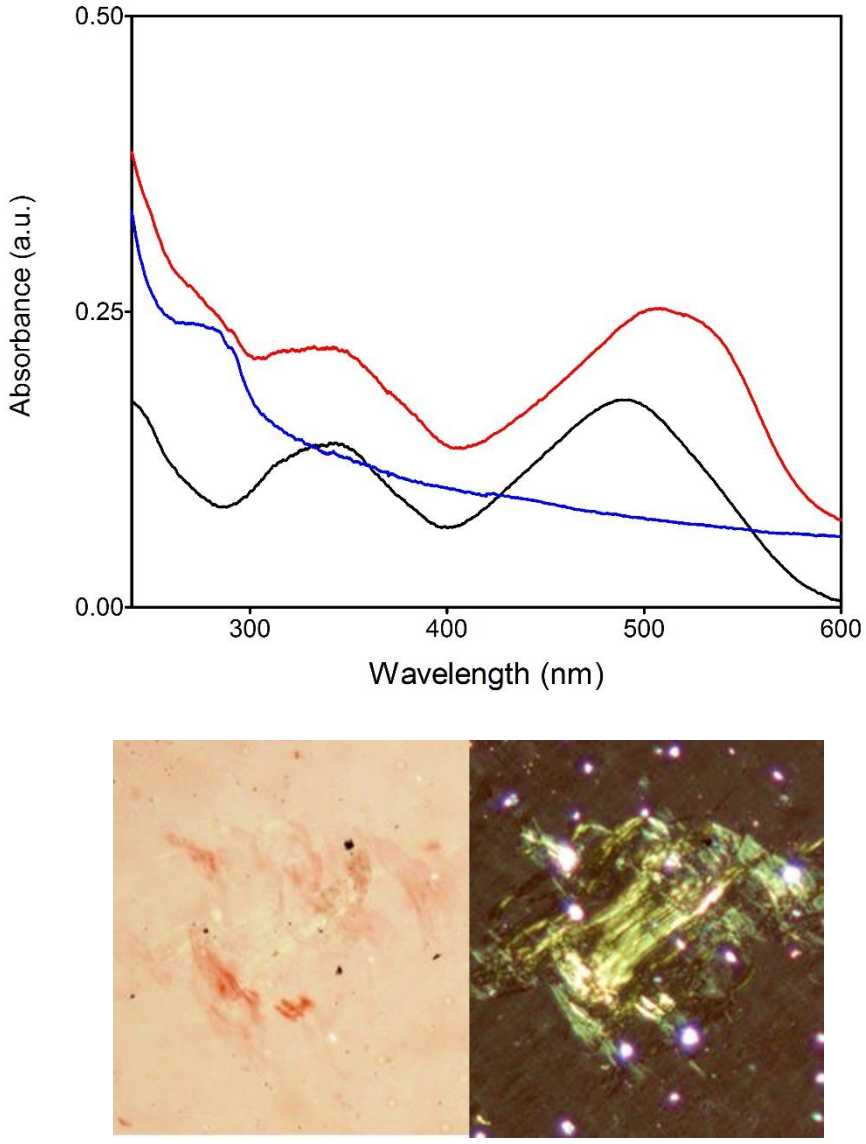

Figure 78. Congo red UV-vis spectroscopy and staining. (top) Spectra for Congo red 10 µM alone (black), D25V apo C-III fibrils alone (blue) and Congo red/fibril complex (red). The maximum of absorbance around 480 nm for Congo red alone shifted to 540 nm when the dye was in complex with D25V apo C-III fibrils. (bottom) Congo red staining was performed on the aggregated material obtained from fibrillogenesis experiments. Upon light polarization, the typical apple-green birefringence was observed.

7.4 Discussion

The results presented in this chapter offer an insight on the structural and functional characterization of the first described amyloidogenic mutation of apo C-III, characterised by the substitution Asp to Val in position 25, together with the investigation of its aggregation propensity in physiological buffer.

NMR was used to investigate the structural differences existing between WT and variant in their lipid-bound state. The ^{1}H-^{15}N HSQC spectra appeared very similar and significant chemical shifts could be observed only within a few residues from the mutation site. NOESY-HSQC showed that the α-helical conformation was preserved despite the mutation. Determination of the rotational correlation time (T_c) by ^{1}H-^{15}N TRACT experiments and subsequent calculation of the theoretical Stokes radius did not reveal any difference between the two proteins.

The lipid-binding properties were investigated both in the presence of DMPC and SDS. Some differences could be observed with D25V apo C-III reducing the turbidity of DMPC liposomes to a less extent that its WT counterpart (70 % against 85-90% respectively) and requiring more time to reduce by 50 % the initial turbidity (168.7 ± 8.1 s and 114.7 ± 4.2 s respectively). These results suggest that the interaction with lipid particles is partially impaired by the presence of the mutation, although at equilibrium also the variant was fully integrated in the liposomes and its solubility was rescued. In agreement with the data collected in the presence of DMPC, SDS-induced α-helical conformation was observed for both proteins by far-UV CD spectroscopy, confirming the structural data obtained by NMR. The extent of interaction with SDS was reduced for the variant, which appeared extensively less structured than the WT protein in the absence of any lipid-like molecules. No difference was observed in terms of inhibition of LPL activity supporting the results previously published on another variant designed in silico, D25N apo C-III, for which the change in charge associated with unmodified hydrophobicity did not interfere with the inhibitory effect on LPL activity (Larsson M et al., 2013). In conclusion, the two proteins appeared similar from a structural and

functional point of view in their lipid-bound state. On the contrary, they appeared significantly different in the lipid-free state.

Sequence-based predictions of the β-sheet content as well as of the aggregation propensity suggested for the variant an increased propensity to acquire β-sheet conformation and undergo aggregation. Indeed rapid aggregation was observed when the protein was incubated under shaking conditions in physiological buffer. The presence of amyloid fibrils in the aggregate was confirmed by several different approaches including ThT emission fluorescence, electron microscopy (EM), atomic force microscopy Congo red staining and Congo red UV-vis spectroscopy. It is worth noting that aggregation of WT apoC-III into polymeric ordered structures in the shapes of triangles, squares and loops, following a 3 days incubation under shaking in physiological buffer, was previously reported (de Messieres M et al., 2014). No resemblance exists between these structures and the genuine amyloid fibrils obtained with the D25V variant, although a structural transition similar to the one followed by CD spectroscopy was also observed for the WT protein, thus not implying any amyloidogenicity *in vivo*.

The nature of the protein, constantly transitioning between the lipid-free and the lipid-bound state, could be crucial in the understanding of the mechanism of fibrillogenesis *in vivo*. It is indeed possible that due to its strong instability in physiological buffer, the variant can rapidly aggregate and form fibrils when the concomitance of lipid-free state and right environmental conditions is present. The imbalance in the WT/variant ratio observed *in vivo* could be explained by the preferential incorporation of the variant only in the amyloid deposits and a potential partial impairment of secretion by the intracellular quality control. This would be in line with the observations made for some of the amyloidogenic variants of apo A-I for which the same unbalance was found (Marchesi M et al., 2011).

Chapter 8. Conclusions and future work

The work presented in this thesis is focused on the characterisation of the molecular mechanism underlying the transition of two different amyloidogenic proteins from their soluble functional state to insoluble amyloid fibrils in conditions of pH, ionic strength and temperature that resemble the physiological environment *in vivo* as closely as possible.

When I started my research project, the mechano-enzymatic mechanism for TTR amyloidogenesis had just been discovered on the very unstable S52P TTR variant (Mangione PP et al., 2012). It was then validated as a general mechanism on other TTR variants, including the WT protein (Marcoux J et al., 2014). The results previously published clearly highlighted a different susceptibility to proteolysis exhibited by distinct variants, which translated in a different propensity to aggregate. It was not known whether this difference could correlate with the thermodynamic stability of each variant. The overall stability of each variant was therefore determined from denaturation curves obtained at different concentrations of guanidine-SCN. The tendency to aggregate, which is strongly based on the susceptibility to proteolysis, was instead studied in two distinct experimental conditions characterised by different intensity of the forces acting on the protein during cleavage and subsequent aggregation. The results show a correlation between forces applied, thermodynamic stability, susceptibility to proteolysis and aggregation. We need to consider that, *in vivo*, the mechanical forces originated by the extracellular flow can be extremely high in certain organs, including the heart where TTR deposition commonly occurs. A clear quantification of the total forces acting *in vivo* in the heart is not simple. Dokos and his group have estimated (Dokos S et al, 2000, 2002) the forces acting in the ventricles of the heart, showing that they have similar intensity, if not higher, to that present in our experimental condition, also considering the contribution coming from the mechanical contraction associated with the organ function. It is therefore more than plausible that the forces acting *in vivo* are sufficient to destabilise TTR (either WT or variant), thus predisposing

it to proteolysis and aggregation. The less stable the variant, the lower the intensity of the forces required to induce partial unfolding.

The role played by ubiquitous components of the extracellular matrix has not yet been clarified (Stoppini M & Bellotti V, 2015). Further characterisation of the mechano-enzymatic mechanism was carried out testing the effect of heparin on S52P TTR aggregation. As already observed for other amyloidogenic proteins such as β2-m (Relini et al., 2008; So M et al., 2017), aggregation was strongly accelerated and enhanced when the glycosaminoglycan was present, highlighting the role that common constituents of the extracellular matrix may play in driving tissue specific amyloid deposition.

The aggregation-enhancing effect of seeds has to be carefully considered when imagining the possible scenario *in vivo* (Fig. 79). We can envisage an initial situation in which, in the absence of seeds, proteolysis followed by the release of amyloidogenic fragments can take place. Indeed, in these initial stages, the equilibrium could point towards the complete digestion of the fragments, rather than amyloid deposition. It is plausible that at any given time, a certain proportion of fragments escape digestion, thus reaching a critical concentration suitable for a crucial nucleation event. Our data suggest that the scenario would then drastically change with the equilibrium rapidly shifting towards amyloid deposition as the process would be accelerated by the elongation of fibrils nuclei.

In this light, the efficacy of treatments aiming to reduce the level of circulating TTR, such as siRNAs and ASOs, has to be carefullly evaluated. The presence of amyloid deposits in the tissues of the treated patients, even if minimal, could be enough to favour further deposition, independently of the concentration of the protein precursor, thus only delaying the progression of the disease rather completely stopping it.

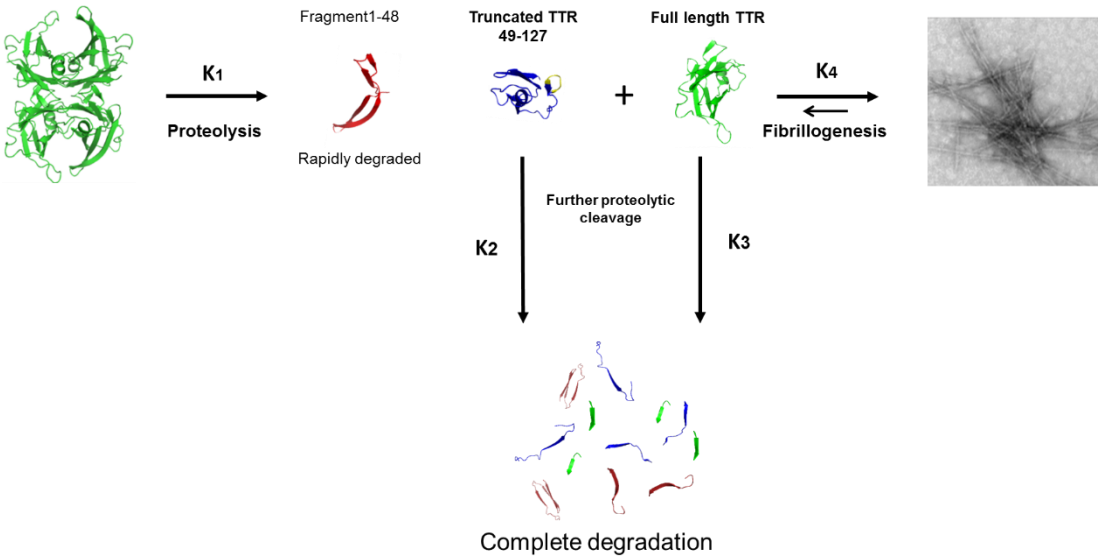

Figure 79. TTR amyloid formation. Schematic representation of the model proposed for amyloid formation by TTR. k_1, k_2, k_3 and k_4 represent the kinetics constants regulating the different steps. The presence of seeds would shift the equilibrium towards the formation of amyloid fibrils by increasing k_4, thus reducing k_2 and k_3, associated with complete digestion of both TTR monomers and fragments.

Even though trypsin effectively cleaves TTR and promotes its fibrillogenesis *in vitro*, one of the open questions about the mechano-enzymatic mechanism has always been the identity of the culprit protease responsible for proteolysis *in vivo*. A bioinformatics approach was used to identify a pool of possible candidate proteases andfrom these, we demonstrated experimentally that plasmin can promote TTR fibrillogenesis in a similar fashion to trypsin, leading to the formation of genuine amyloid fibrils.

Plasmin is ubiquitously expressed and it is involved in the remodelling of the extracellular matrix as well as fibrinolysis. If we consider that these two events are constantly taking place in the body, the possibility that plasmin represents the enzyme responsible for cleavage *in vivo* is real.

Using an experiment combining clot formation and plasminogen activation in the presence of TTR, we suggest a possible connection existing between the

physiological pathway of fibrinolysis and the pathological process of fibril formation.

The mechano-enzymatic mechanism offers a new challenge in terms of inhibition of aggregation by the mean of small ligands. In this mechanism, two physically different events affect the protein: partial unfolding and proteolysis. Separately, these two events, have been extensively studied and dissected for their role in promoting amyloidogenesis of globular proteins. The novelty of the observations reported in this thesis lies in the demonstration that local unfolding caused by bio-mechanical forces allows the action of specific proteases. Unfolding and proteolysis cannot therefore be considered as separate events, but have to be considered as integrated multiple steps at the origin of amyloid conversion of globular proteins. Compounds able to stabilise TTR, such as tafamidis, designed as drugs to treat and prevent systemic TTR amyloidosis, have been identified exclusively by their capacity to inhibit TTR dissociation and aggregation induced by low pH *in vitro*. However, even with apparently complete pharmacological stabilisation of circulating TTR, the clinical benefit observed so far is limited to modest slowing of the progression of peripheral neuropathy. The data presented in chapter 4 highlight the superior efficacy exhibited by bivalent ligands that are able to simultaneously occupy both T4 binding sites at 1:1 molar ratio, over monovalent ligands, such as tafamidis. Even when apparent complete inhibition of aggregation is obtained, a careful analysis of the material obtained after aggregation highlights the presence of some amyloid aggregates that we can define as “minimal residual disease material”, which also has to be carefully considered in the light of the considerations made on the effect of seeds. The superiority showed by bivalent ligands can be explained not only by the simultaneous occupancy of both binding sites, but also by the occupancy of the central cavity of the TTR molecule.

The results obtained in solution by NMR spectroscopy provide an insight on the molecular rearrangement taking place when ligands are bound to the protein and which are not observable by other techniques, including X-ray

crystallography. Indeed, the long distance effect observed when the ligands are bound, has never been described before. The results suggest that these structural variations, affecting the outer regions of the protein, might be driven by hydrophobic interactions involving residues located in the core of the protein. Furthermore, the results obtained at substoichiometric ratios of tafamidis offer some hints on the negative cooperativity exhibited by monovalent ligands, which cannot be fully explained by the analysis of the X-ray data so far available.

According to the NMR data, the superior efficacy shown by the bivalent compound mds84 seems to be associated with the stabilisation of the local H-bond network in the CD loop, where the cleavage site is located. Upon binding the loop becomes more rigid, thus reducing its accessibility to the action of the protease. These results could have a strong implication on drug discovery, highlighting a potential central role played by NMR in the development of more effective TTR stabilisers able to fully prevent TTR cleavage and aggregation.

The molecular abnormalities causing the amyloid conversion of globular proteins are frequently hidden in the dynamic states that these macromolecules can transiently visit. NMR is therefore an irreplaceable technique for the investigation into amyloidogenesis. We have also used this technique to study another amyloidogenic protein, apo C-III, that we have identified, for the first time as amyloidogenic in humans. The results presented here show substantial structural similarity between WT apo C-III and the amyloidogenic D25V apo C-III variant in their lipid-bound form. Indeed, NMR data of both proteins in complex with SDS show minor chemical shift perturbations located around the site of mutation and no disruption of the α-helical conformation was observed as a consequence of the mutation.

Lipid binding and inhibition of LPL activity were also evaluated, but no macroscopic differences were highlighted.

Sequence-based bioinformatics analysis revealed an increased tendency to form β-sheet secondary structure and to undergo aggregation.

Indeed, when moving to conditions of physiological pH, ionic strength and temperature, the variant showed a strong tendency to rapidly aggregate in the form of typical amyloid fibrils. This process was associated with a progressive shift towards a more prominent β-content, as shown by CD measurement.

Future work

Future work would include the screening and development of new bivalent TTR stabilisers able to completely inhibit the formation of amyloid fibrils, including the so called “minimal residual disease” that normally escapes the classical procedures used to monitor amyloid formation *in vitro*. This would involve the evaluation of their ability to stop mechano-enzymatic fibrillogenesis as well the evaluation of their effect on the protein structure by NMR spectroscopy.

Further characterisation of the mechano-enzymatic mechanism could also by achieved by NMR spectroscopy, with particular attention on the investigation, at atomic resolution, of the structural modifications following protein cleavage.

It would also be extremely interesting to further characterise the relationship between protein stability and susceptibility to proteolysis with a precise quantification of the forces necessary to promote the aggregation of each variant. We envisage that different variants could respond differently to the binding of specific ligands as recently shown by Klimtchuk and co-workers (Klimtchuk et al., 2018), who highlighted the lack of effect shown by diflunisal in protecting proteolytic cleavage of the CD loop in the E51_S52dup variant. Other data obtained by our group and not presented in this thesis indicate a lack of effect of several TTR stabilisers in inhibiting S52P TTR fibrillogenesis, while better results are obtained when WT TTR is tested.

We therefore suggest the idea of tailored medicine, according to which the treatment should be strictly related to the specific misfolding dynamics of every single variant.

Bibliography

Adamski-Werner SL, Palaninathan SK, Sacchettini JC, Kelly JW (2004). Diflunisal analogues stabilize the native state of transthyretin. Potent inhibition of amyloidogenesis. J Med Chem 47(2):355-74.

Andersson K, Olofsson A, Nielsen EH, Svehag SE, Lundgren E (2002). Only Amyloidogenic Intermediates of Transthyretin Induce Apoptosis. Biochemical and Biophys Res Commun 294.2: 309-14.

Ando Y, Tanaka Y, Nakazato M, Ericzon BG, Yamashita T, Tashima K, SakashitaN, Suga M, Uchino M, Ando M (1995). Change in variant transthyretin levels in patients with familial amyloidotic polyneuropathy type I following liver transplantation. Biochem Biophys Res Commun 211(2):354-358.

Ando Y, Suhr OB (1998). Autonomic dysfunction in familial amyloidotic polyneuropathy (FAP). Amyloid 5(4):288-300.

Ando Y, Ando E, Ohlsson P-I, Olofsson A, Sandgren O, Suhr O, Terazaki H, Obayashi K, Lundgren E, Ando M, Negi A (1999). Analysis of transthyretin (TTR) forms of amyloid fibrils in familial amyloidotic polyneuropathy (Met30). Amyloid 6(2):119-123.

Andrade C (1952). A peculiar form of peripheral neuropathy; familiar atypical generalized amyloidosis with special involvement of the peripheral nerves. Brain 75(3):408-427.

Arsequell G, Planas A (2012). Methods to Evaluate the Inhibition of TTR Fibrillogenesis Induced by Small Ligands. Curr Med Chem 19(15):2343-2355.

Bellotti V, Nuvolone M, Giorgetti S, Obici L, Palladini G, Russo P, Lavatelli F, Perfetti V, Merlini G (2007). The Workings of the Amyloid Diseases. Annals of Medicine 39.3: 200-07.

Bengtsson-Olivecrona G, Olivecrona T (1992). In Lipoprotein Analysis-A Practical Approach. Oxford Univ.

Benson MD (1989). Familial amyloidotic polyneuropathy. Trends Neurosci 12(3):88– 92.

Benson MD, Liepnieks JJ, Yazaki M, Yamashita T, Hamidi Asl K, Guenther B, Kluve-Beckerman B (2001). A new human hereditary amyloidosis: the result of a stop-codon mutation in the apolipoprotein AII gene. Genomics 72(3):272-7.

Bergsröm J, Gustavsson A, Hellman U, Sletten K, Murphy CL, Weiss DT, Solomon A, Olofsson BO, Westermark P (2005). Amyloid deposits in transthyretin-derived amyloidosis: Cleaved transthyretin is associated with distinct amyloid morphology. J Pathol 206(2):224-232.

Bjorkman PJ, Saper MA, Samraoui B, Bennett WS, Strominger JL, Wiley DC (1987). The Foreign Antigen Binding Site and T Cell Recognition Regions of Class I Histocompatibility Antigens. Nature 329.6139: 512-18.

Blake CC, Geisow MJ, Oatley SJ, ReÂrat B, Rerat C (1978). Structure of prealbumin: secondary, tertiary and quaternary interactions determined by Fourier refinement at 1.8 Å. J Mol Biol 121:339-356.

Bodin K, Ellmerich S, Kahan MC, Tennent GA, Loesch A, Gilbertson JA, Hutchinson WL, Mangione PP, Gallimore JR, Millar DJ, Minogue S, Dhillon AP, Taylor GW, Bradwell AR, Petrie A, Gillmore JD, Bellotti V, Botto M,

Hawkins PN, Pepys MB (2010). Antibodies to human serum amyloid P component eliminate visceral amyloid deposits. Nature 468:93-97.

Booth DR, Tan SY, Booth SE, Hsuan JJ, Totty NF, Nguyen O, Hutton T, Vigushin DM, Tennent GA, Hutchinson WL, et al. (1995). A new apolipoprotein Al variant, Trp50Arg, causes hereditary amyloidosis. QJM 88:695–702.

Booth DR, Tan SY, Booth SE, Tennent GA, Hutchinson WL, Hsuan JJ, Totty NF, Truong O, Soutar AK, Hawkins PN, et al. (1996). Hereditary hepatic and systemic amyloidosis caused by a new deletion/insertion mutation in the apolipoprotein AI gene. J Clin Invest 97:2714–2721.

Booth DR, Sunde M, Bellotti V, Robinson CV, Hutchinson WL, Fraser PE, Hawkins PN, Dobson CM, Radford SE, Blake CC, Pepys MB (1997). Instability, unfolding and aggregation of human lysozyme variants underlying amyloid fibrillogenesis. Nature 385(6619):787-93.

Borgia A, Williams PM, Clarke J (2008). Single-molecule studies of protein folding. Annu Rev Biochem 77: 101–125.

Brewer HB Jr, R Shulman, P Herbert, R Ronan, K Wehrly (1974). The complete amino acid sequence of alanine apolipoprotein (apo C-III), an apolipoprotein from human plasma very low density lipoproteins. J Biol Chem 249:4975-4984.

Brockwell DJ, Radford SE (2007). Intermediates: ubiquitous species on folding energy landscapes. Curr Opin Struct Biol 17(1):30-37.

Bulawa CE, Connelly S, Devit M, Wang L, Weigel C, Fleming JA, Packman J, Powers ET, Wiseman RL, Foss TR, Wilson IA, Kelly JW, Labaudinière R

(2012). Tafamidis, a potent and selective transthyretin kinetic stabilizer that inhibits the amyloid cascade. Proc Natl Acad Sci USA 109(24):9629-9634.

Carulla N, Caddy GL, Hall DR, Zurdo J, Gairí M, Feliz M, Giralt E, Robinson CV, Dobson CM. Molecular Recycling within Amyloid Fibrils. Nature 436.7050: 554-58.

Cecconi C, Shank EA, Bustamante C, Marqusee S (2005). Direct observation of the three-state folding of a single protein molecule. Science 309:2057 – 2060.

Chiti F, Dobson CM (2006). Protein misfolding, functional amyloid, and human disease. Annu Rev Biochem 75:333-366.

Cianci M, Folli C, Zonta F, Florio P, Berni R, Zanotti G (2015). Structural evidence for asymmetric ligand binding to transthyretin. Acta Crystallogr D Biol Crystallogr 71(Pt 8):1582-92.

Coelho T (1996). Familial amyloid polyneuropathy: new developments in genetics and treatment. Curr Opin Neurol 9(5):355-359.

Coelho T, Maia LF, Martins da Silva A, Cruz MW, Planté-Bordeneuve V, Lozeron P, Suhr OB, Campistol JM, Conceiçao I, Schmidt H, Trigo, Kelly JW, Labaudiniere R, Chan J, Packman J, Wilson A, Grogan DR (2012). Tafamidis for transthyretin familial amyloid polyneuropathy: a randomized, controlled trial. Neurology 79(8):785-92.

Cohen SI, Vendruscolo M, Dobson CM, Knowles TP (2012). From macroscopic measurements to microscopic mechanisms of protein agg regation. J Mol Biol 421(2-3):160-71.

Cohlberg JA, Li J, Uversky VN, Fink AL (2002). Heparin and other glycosaminoglycans stimulate the formation of amyloid fibrils from α-synuclein in vitro. Biochemistry 41:1502–1511.

Collins SR, Douglass A, Vale RD, JS Weissman (2004). Mechanism of Prion Propagation: Amyloid Growth Occurs by Monomer Addition. PLoS Biology 2.10: E321.

Colon W, Kelly JW (1992). Partial denaturation of transthyretin is sufficient for amyloid fibril formation in vitro. Biochemistry 31(36):8654-8660.

Comenzo RL, Vosburgh E, Simms RW, Bergethon P, Sarnacki D, Finn K, Dubrey S, Faller DV, Wright DG, Falk RH, Skinner M (1996). Dose-intensive melphalan with blood stem cell support for the treatment of AL amyloidosis: one-year follow-up in five patients. Blood 88(7):2801-2806.

Connelly S, Choi S, Johnson SM, Kelly JW, Wilson IA (2010). Structure-based design of kinetic stabilizers that ameliorate the transthyretin amyloidoses. Curr Opin Struct Biol 20: 54–62.

Cornwell GG 3rd, Westermark P (1980). Senile Amyloidosis: A protean manifestation of the aging process. J Clin Pathol 33(12):1146-1152.

Cornwell GG 3rd, Sletten K, Olofsson BO, Johansson B, Westermark P (1987). Prealbumin: its association with amyloid. J Clin Pathol 40(2):226-231.

Cornwell GG 3rd, Sletten K, Johansson B, Westermark P (1988). Evidence that the amyloid fibril protein in senile systemic amyloidosis is derived from normal prealbumin. Biochem Biophys Res Commun 154(2):648-653.

Crosby J, Peloso GM, Auer PL, Crosslin DR, Stitziel NO, Lange LA, Lu Y, Tang ZZ, Zhang H, Hindy G, Masca N, Stirrups K, Kanoni S, Do R, Jun

G, Hu Y, Kang HM, Xue C, Goel A, Farrall M, Duga S, Merlini PA, Asselta R, Girelli D, Olivieri O, Martinelli N, Yin W, Reilly D, Speliotes E, Fox CS, Hveem K, Holmen OL, Nikpay M, Farlow DN, Assimes TL, Franceschini N, Robinson J, North KE, Martin LW, DePristo M, Gupta N, Escher SA, Jansson JH, Van Zuydam N, Palmer CN, Wareham N, Koch W, Meitinger T, Peters A, Lieb W, Erbel R, Konig IR, Kruppa J, Degenhardt F, Gottesman O, Bottinger EP, O'Donnell CJ, Psaty BM, Ballantyne CM, Abecasis G, Ordovas JM, Melander O, Watkins H, Orho-Melander M, Ardissino D, Loos RJ, McPherson R, Willer CJ, Erdmann J, Hall AS, Samani NJ, Deloukas P, Schunkert H, Wilson JG, Kooperberg C, Rich SS, Tracy RP, Lin DY, Altshuler D, Gabriel S, Nickerson DA, Jarvik GP, Cupples LA, Reiner AP, Boerwinkle E, Kathiresan S (2014). Loss-of-function mutations in APOC3, triglycerides, and coronary disease. N Engl J Med 371(1):22-31.

Dasari S, Amin MS, Kurtin PJ, Vrana JA, Theis JD, Grogg KL, Alexander MP, Nasr SH, Fervenza FC, Leung N, Sethi S (2016). Clinical, biopsy, and mass spectrometry characteristics of renal apolipoprotein A-IV amyloidosis. Kidney Int 90(3):658-64.

Davis PD, Raffen R, Dul LJ, Vogen MS, Williamson KE, Stevens JF, Argon Y (2000). Inhibition of amyloid fiber assembly by both BiP and its target peptide. Immunity 13:433-42.

de Messieres M, Huang RK, He Y, Lee JC (2014). Amyloid triangles, squares and loops of apolipoprotein C-III. Biochemistry 53(20):3261-3.

De Pauw M, Vanloo B, Weisgraber K, Rosseneu M (1995). Comparison of lipid-binding and lecithin:cholesterol acyltransferase activation of the amino- and carboxyl-terminal domains of human apolipoprotein E3. Biochemistry 34:10953–10966.

de Sousa MM, Vital C, Ostler D, Fernandes R, Pouget-Abadie J, Carles D, Saraiva MD (2000). Apolipoprotein AI and transthyretin as components of amyloid fibrils in a kindred with apoAI Leu178His amyloidosis. Am J Pathol 156:1911–1917.

Dember LM, Sanchorawala V, Seldin DC, Wright DG, LaValley M, Berk JL, Falk RH, Skinner M (2001). Effect of dose-intensive intravenous melphalan and autologous blood stemcell transplantation on AL amyloidosis-associated renal disease. Ann Intern Med 134(9 Pt 1):746-753.

Diomede L, Rognoni P, Lavatelli F, Romeo M, del Favero E, Cantù L, Ghibaudi E, di Fonzo A, Corbelli A, Fiordaliso F, Palladini G, Valentini V, Perfetti V, Salmona M, Merlini G (2014). A Caenorhabditis elegans-based assay recognizes immunoglobulin light chains causing heart amyloidosis. Blood 123(23):3543-52.

Dunker AK, Silman I, Uversky VN, Sussman JL (2008). Function and structure of inherently disordered proteins. Curr Opin Struct Biol 18:756.

Dyson HJ, Wright PE (2005). Intrinsically unstructured proteins and their functions. Nat Rev Mol Cell Biol 6:197–208.

Dwulet FE, Benson MD (1983). Polymorphism of human plasma thyroxine binding prealbumin. Biochem Biophys Res Commun 114(2):657-662.

Dwulet FE, Benson MD (1984). Primary structure of an amyloid prealbumin and its plasma precursor in a heredofamilial polyneuropathy of Swedish origin. Proc Natl Acad Sci USA 81(3):694-698.

Eisenberg D, Jucker M (2012). The Amyloid State of Proteins in Human Diseases. Cell 148.6:1188-203.

Elliott-Bryant R, Cathcart ES (1998). Amyloid enhancing factor and dietary transmission in accelerated amyloid A amyloidosis. Clin Immunol Immunopathol 88:65-9.

Eriksson M, Schönland S, Yumlu S, Hegenbart U, von Hutten H, Gioeva Z, Lohse P, Büttner J, Schmidt H, Röcken C (2009). Hereditary apolipoprotein AI-associated amyloidosis in surgical pathology specimens: identification of three novel mutations in the APOA1 gene. J Mol Diagn 11:257–262.

Eriksson M, Büttner J, Todorov T, Yumlu S, Schönland S, Hegenbart U, Kristen AV, Dengler T, Lohse P, Helmke B, Schmidt H, Röcken C (2009). Prevalence of germline mutations in the TTR gene in a consecutive series of surgical pathology specimens with ATTR amyloid. Am J Surg Pathol. 33(1):58-65.

Felding P, Fex G, Westermark P, Olofsson BO, Pitkänen P, Benson L (1985). Prealbumin in Swedish patiens with senile systemic amyloidosis and familial amyloidotic polyneuropathy. Scand J Immunol 21(2):133-140.

Ferguson RN, Edelhoch H, Saroff HA, Robbins J, Cahnmann HJ (1975). Negative cooperativity in the binding of thyroxine to human serum prealbumin. Preparation of tritium-labeled 8-anilino-1-naphthalenesulfonic acid. Biochemistry 14(2):282-9.

Fernández C, Wider G (2003). TROSY in NMR studies of the structure and function of large biological macromolecules. Curr Opin Struct Biol 13(5):570-80.

Ferrao-Gonzales AD, Palmieri L, Valory M, Silva JL, Lashuel H, Kelly JW, Foguel D (2003). Hydration and packing are crucial to amyloidogenesis as revealed by pressure studies on transthyretin variants that either protect or worsen amyloid disease. J Mol Biol 328:963–974.

Fezoui Y, Teplow DB (2002). Kinetic studies of amyloid beta-protein fibril assembly. Differential effects of alpha-helix stabilization. J Biol Chem 277:36948–54.

Findeis MA (2002). Peptide inhibitors of beta amyloid aggregation. Curr Top Med Chem 2:417-23.

Finn BE, Chen X, Jennings PA, Saalau-Bethell SM, Matthews CR (1992) in Protein Engineering (Rees AR, Sternberg MJE and Wetzel R, eds) 167–189, IRL Press at Oxford University Press, Oxford

Fitzpatrick AW, Debelouchina GT, Bayro MJ, Clare DK, Caporini MA, Bajaj VS, Jaroniec CP, Wang L, Ladizhansky V, Müller SA, MacPhee CE, Waudby CA, Mott HR, De Simone A, Knowles TP, Saibil HR, Vendruscolo M, Orlova EV, Griffin RG, Dobson CM (2013). Atomic structure and hierarchical assembly of a cross-β amyloid fibril. Proc Natl Acad Sci USA 110(14):5468-73.

Foss TR, Wiseman RL, Kelly JW (2005). The pathway by which the tetrameric protein transthyretin dissociates. Biochemistry 44(47):15525–15533.

Gallo G, Wisniewski T, Choi-Miura NH, Ghiso J, Frangione B (1994). Potential role of apolipoprotein E in fibrillogenesis. Am J Pathol 145(3):526-530

Gangabadage CS, Zdunek J, Tessari M, Nilsson S, Olivecrona G, Wijmenga SS (2008). Structure and dynamics of human apolipoprotein CIII. J Biol Chem 283(25):17416-27.

Garnier J, Gibrat JF, Robson B (1996). GOR method for predicting protein secondary structure from amino acid sequence. Methods Enzymol 266:540–553.

Genschel J, Haas R, Pröpsting MJ, Schmidt HH (1998). Apolipoprotein A-I induced amyloidosis. FEBS Lett 430:145–149.

Ghosh D, Mondal M, Mohite GM, Singh PK, Ranjan P, Anoop A, Ghosh S, Jha NN, Kumar A, Maji SK (2013). The Parkinson's disease-associated H50Q mutation accelerates α-Synuclein aggregation in vitro. Biochemistry 52(40):6925-7.

Gillmore JD, Hawkins PN (2013). Pathophysiology and treatment of systemic amyloidosis. Nat Rev Nephrol 9(10):574-86.

Giorgetti S, Raimondi S, Pagano K, Relini A, Bucciantini M, Corazza A, Fogolari F, Codutti L, Salmona M, Mangione P, Colombo L, De Luigi A, Porcari R, Gliozzi A, Stefani M, Esposito G, Bellotti V, Stoppini M (2010). Effect of Tetracyclines on the Dynamics of Formation and Destructuration of β2-Microglobulin Amyloid Fibrils. J Biol Chem 286(3):2121-31.

Goldsbury CS, Wirtz S, Müller SA, Sunderji S, Wicki P, Aebi U, Frey P (2000). Studies on the in vitro assembly of a beta 1-40: implications for the search for a beta fibril formation inhibitors. J Struct Biol 130(2-3):217–231.

Goldsteins G, Andersson K, Olofsson A, Dacklin I, Edvinsson A, Baranov V, Sandgren O, Thylén C, Hammarstrom S, Lundgren E (1997). Characterization of two highly amyloidogenic mutants of transthyretin. Biochemistry 36(18):5346-52.

Gundapaneni BK, Sultan MB, Keohane DJ, Schwartz JH (2018). Tafamidis delays neurological progression comparably across Val30Met and non-

Val30Met genotypes in transthyretin familial amyloid polyneuropathy. Eur J Neurol 25(3):464-468.

Gustafsson S, Ihse E, Henein MY, Westermark P, Lindqvist P, Suhr OB (2012). Amyloid fibril composition as a predictor of development of cardiomyopathy after liver transplantation for hereditary transthyretin amyloidosis. Transplantation 93(10):1017-1023.

Gustavsson A, Engstrom U, Westermark P (1991). Normal transthyretin and synthetic transthyretin fragments form amyloid-like fibrils in vitro. *Biochem Biophys Res Commun* 175: 1159–64.

Gustavsson Å, Jahr H, Tobiassen R, Jacobson DR, Sletten K, Westermark P (1995). Amyloid fibril composition and transthyretin gene structure in senile systemic amyloidosis. Lab Invest 73(5):703-708.

Hamilton JA, Benson MD (2001). Transthyretin: a review from a structural perspective. Cell Mol Life Sci 58:1491-1521.

Hammarström P, Jiang X, Deechongkit S, Kelly JW (2001). Anion shielding of electrostatic repulsions in transthyretin modulates stability and amyloidosis: insight into the chaotrope unfolding dichotomy. Biochemistry. 40(38):11453-9.

Hammarström P, Schneider F, Kelly JW (2001). Trans-suppression of misfolding in an amyloid disease. Science 293(5539):2459-62.

Hammarstrom P, Jiang X, Hurshman AR, Powers ET, Kelly JW (2002). Sequence-dependent denaturation energetics: A major determinant in amyloid disease diversity. Proc Natl Acad Sci USA 99(Suppl4):16427–16432.

Hammarstrom P, Sekijima Y, White JT, Wiseman RL, Lim A, Costello CE, Altland K, Garzuly F, Budka H, Kelly JW (2003). D18G transthyretin is monomeric, aggregation prone, and not detectable in plasma and cerebrospinal fluid: a prescription for central nervous system amyloidosis? Biochemistry 42:6656–6663.

Havel RJ, Kane JP, Kashyap ML (1973). Interchange of apolipoproteins between chylomicrons and high density lipoproteins during alimentary lipemia in man. J Clin Invest 52:32–38.

Holmgren G, Ericzon BG, Groth CG, Steen L, Suhr O, Andersen O, Wallin BG, Seymour A, Richardson S, Hawkins PN (1993). Clinical improvement and amyloid regression after liver transplantation in hereditary transthyretin amyloidosis. Lancet 341(8853):1113–1116.

Homma N, Gejyo F, Isemura M, Arakawa M (1989). Collagen-binding affinity of beta-2-microglobulin, a preprotein of hemodialysis-associated amyloidosis. Nephron. 53(1):37-40.

Hurshman AR, White JT, Powers ET, Kelly JW (2004). Transthyretin aggregation under partially denaturing conditions is a downhill polymerization. Biochemistry 43(23):7365-7381.

Hurshman Babbes AR, Powers ET, Kelly JW (2008). Quantification of the thermodynamically linked quaternary and tertiary structural stabilities of transthyretin and its disease-associated variants: the relationship between stability and amyloidosis. Biochemistry 47(26):6969-84.

Ihse E, Ybo A, Suhr O, Lindqvist P, Backman C, Westermark P (2008). Amyloid fibril composition is related to the phenotype of hereditary transthyretin V30M amyloidosis. J Pathol 216(2):253-261.

Ihse E, Rapezzi C, Merlini G, Benson MD, Ando Y, Suhr OB, Ikeda S, Lavatelli F, Obici L, Quarta CC, Leone O, Jono H, Ueda M, Lorenzini M, Liepnieks J, Ohshima T, Tasaki M, Yamashita T, Westermark P (2013). Amyloid fibrils containing fragmented ATTR may be the standard fibril composition in ATTR amyloidosis. Amyloid 20(3):142-150.

Ingenbleek Y, Young V (1994). Transthyretin (prealbumin) in health and disease: nutritional implications. Annu Rev Nutr 14:495-533.

Ishiguro K, Hayashi T, Yokoyama Y, Aoki Y, Onodera K, Ikeda H, Ishida T, Nakase H (2018). Elevation of Plasmin-α2-plasmin Inhibitor Complex Predicts the Diagnosis of Systemic AL Amyloidosis in Patients with Monoclonal Protein. Intern Med 57(6):783-788.

Jacobson DR, Pastore RD, Yaghoubian R, Kane I, Gallo G, Buck FS, Buxbaum JN (1997). Variant-sequence transthyretin (isoleucine 122) in late-onset cardiac amyloidosis in black Americans. N Engl J Med 336(7):466-473.

Jiang X, Smith CS, Petrassi HM, Hammarstrom P, White JT, Sacchettini JC, Kelly JW (2001). An engineered transthyretin monomer that is nonamyloidogenic, unless it is partially denatured. Biochemistry 40:11442–11452.

Jiménez JL, Guijarro JI, Orlova E, Zurdo J, Dobson CM, Sunde M, Saibil HR. Cryo-electron Microscopy Structure of an SH3 Amyloid Fibril and Model of the Molecular Packing. EMBO Journal 18.4 (1999): 815-21.

Johnson SM, Wiseman RL, Sekijima Y, Green NS, Adamski-Werner SL, Kelly JW (2005). Native state kinetic stabilization as a strategy to ameliorate protein misfolding diseases: A focus on the transthyretin amyloidoses. Acc Chem Res 38(12):911-921.

Jones CE, Abdelraheim SR, Brown DR, Viles JH (2004). Preferential copper (2+) coordination by His96 and His111 induces beta-sheet formation in the unstructured amyloidogenic region of the prion protein. J Biol Chem 279(31):32018-32027

Jorgensen AB, Frikke-Schmidt R, Nordestgaard BG, Tybjaerg-Hansen (2014). A Loss-of-function mutations in APOC3 and risk of ischemic vascular disease. N Engl J Med 371:32–41.

Kabat EA, Moore D, Landow H (1942). An electrophoretic study of the protein componentis in cerebrospinal fluid and their relationship to the serum proteins. J Clin Invest 21(5):571-577.

Kanai M, Raz A, Goodman DS (1968). Retinol-binding protein: the transport protein for vitamin A in human plasma. J Clin Invest 47(9):2025-2044.

Karlsson A, Sauer-Eriksson AE (2007). Heating of proteins as a means of improving crystallization: a successful case study on a highly amyloidogenic triple mutant of human transthyretin. Acta Crystallogr Sect F Struct Biol Cryst Commun 63(Pt 8):695-700.

Khurana R, Gillespie JR, Talapatra A, Minert LJ, Ionescu-Zanetti C, Millett I, Fink AL (2001). Partially folded intermediates as critical precursors of light chain amyloid fibrils and amorphous aggregates. Biochemistry 0:3525-35.

Kim YS, Cape SP, Chi E, Raffen R, Wilkins-Stevens P, Stevens FJ, Manning MC, Randolph TW, Solomon A, Carpenter JF (2001). Counteracting effects of renal solutes on amyloid fibril formation by immunoglobulin light chains. J Biol Chem 276:1626-33.

Kim JH, Oroz J, Zweckstetter M (2016). Structure of Monomeric Transthyretin Carrying the Clinically Important T119M Mutation. Angew Chem Int Ed Engl 55(52):16168-16171.

Klimtchuk ES, Prokaeva T, Frame NM, Abdullahi HA, Spencer B, Dasari S, Cui H, Berk JL, Kurtin PJ, Connors LH, Gursky O (2018). Unusual duplication mutation in a surface loop of human transthyretin leads to an aggressive drug-resistant amyloid disease. Proc Natl Acad Sci USA 115(28):E6428-E6436.

Klunk WE, Pettegrew JW, Abraham DJ (1989). Quantitative evaluation of congo red binding to amyloid-like proteins with a beta-pleated sheet conformation. J Histochem Cytochem 37(8):1273-81.

Kolstoe SE, Mangione PP, Bellotti V, Taylor GW, Tennent GA, Deroo S, Morrison AJ, Cobb AJ, Coyne A, McCammon MG, Warner TD, Mitchell J, Gill R, Smith MD, Ley SV, Robinson CV, Wood SP, Pepys MB (2010). Trapping of palindromic ligands within native transthyretin prevents amyloid formation. Proc Natl Acad Sci USA 107(47):20483-20488.

Krebs MR, Morozova-Roche LA, Daniel K, Robinson CV, Dobson CM (2004). Observation of sequence specificity in the seeding of protein amyloid fibrils. Protein Sci 13(7):1933-8

Lai Z, Colón W, Kelly JW (1996). The acid-mediated denaturation pathway of transthyretin yields a conformational intermediate that can self-assemble into amyloid. Biochemistry 35(20):6470-82.

Lai Z, Colon W, Kelly JW (1996). The acid-mediated denaturation pathway of transthyretin yields a conformational intermediate that can self-assemble into amyloid. Biochemistry 35(20):6470-6482.

Lambert MP, Barlow AK, Chromy BA, Edwards C, Freed R, Liosatos M, Morgan TE, Rozovsky I, Trommer B, Viola KL, Wals P, Zhang C, Finch CE, Krafft GA, Klein WL (1998). Diffusible, nonfibrillar ligands derived from Aβ1-42 are potent central nervous system neurotoxins. Proc Natl Acad Sci USA 95 (1998):6448–6453.

Larsson M, Vorrsjo E, Talmud P, Lookene A, Olivecrona G (2013). Apolipoproteins C-I and C-III inhibit lipoprotein lipase activity by displacement of the enzyme from lipid droplets. J Biol Chem 288:33997–34008.

Law RH, Abu-Ssaydeh D, Whisstock JC (2013). New insights into the structure and function of the plasminogen/plasmin system. Curr Opin Struct Biol 23(6):836-41.

Leach BI, Zhang X, Kelly JW, Dyson HJ, Wright PE (2018). NMR Measurements Reveal the Structural Basis of Transthyretin Destabilization by Pathogenic Mutations. Biochemistry 57(30):4421-4430.

Lee D, Hilty C, Wider G, Wüthrich K (2006). Effective rotational correlation times of proteins from NMR relaxation interference. J Magn Reson 178(1):72-6. Epub 2005 Sep 26.

Lee W, Tonelli M, Markley JL (2015). NMRFAM-SPARKY: enhanced software for biomolecular NMR spectroscopy. Bioinformatics 31(8):1325-7.

Leiting B, Marsilio F, O'Connell JF (1998). Predictable deuteration of recombinant proteins expressed in Escherichia coli. Anal Biochem 265(2):351-5.

Leelawatwattana L, Praphanphoj V, Prapunpoj P (2011). Effect of the N-terminal sequence on the binding affinity of transthyretin for human retinol-binding protein. FEBS J 278(18):3337-47.

Lim KH, Dasari AK, Hung I, Gan Z, Kelly JW, Wemmer DE (2016). Structural changes associated with transthyretin misfolding and amyloid formation revealed by solution and solid-state NMR. Biochemistry 55(13):1941-4.

Lim KH, Dasari AKR, Ma R, Hung I, Gan Z, Kelly JW, Fitzgerald MC (2017). Pathogenic mutations induce partial structural changes in the native β-Sheet structure of transthyretin and accelerate aggregation. Biochemistry 56(36):4808-4818.

Lim KH, Dyson HJ, Kelly JW, Wright PE (2013). Localized structural fluctuations promote amyloidogenic conformations in transthyretin. J Mol Biol 425(6):977-88.

Liu H, Labeur C, Xu CF, Ferrell R, Lins L, Brasseur R, Rosseneu M, Weiss KM, Humphries SE, Talmud PJ (2000). Characterization of the lipid-binding properties and lipoprotein lipase inhibition of a novel apolipoprotein C-III variant Ala23Thr. J Lipid Res 41:1760-71.

Liu K, Cho HS, Hoyt DW, Nguyen TN, Olds P, Kelly JW, Wemmer DE (2000). Deuterium-proton exchange on the native wild-type transthyretin tetramer identifies the stable core of the individual subunits and indicates mobility at the subunit interface. J Mol Biol 2000 303(4):555-65.

Liu K, Cho HS, Lashuel HA, Kelly JW, Wemmer DE (2000). A glimpse of a possible amyloidogenic intermediate of transthyretin. Nat Struct Biol 7(9):754-7.

Liu K, Kelly JW, Wemmer DE (2002). Native state hydrogen exchange study of suppressor and pathogenic variants of transthyretin. J Mol Biol 320(4):821-32.

Lundmark K, Westermark GT, Nystrom S, Murphy CL, Solomon A, Westermark P (2002). Transmissibility of systemic amyloidosis by a prion-like mechanism. Proc Natl Acad Sci USA 99:6979-84.

Mangione PP, Esposito G, Relini A, Raimondi S, Porcari R, Giorgetti S, Corazza A, Fogolari F, Penco A, Goto Y, Lee YH, Yagi H, Cecconi C, Naqvi MM, Gillmore JD, Hawkins PN, Chiti F, Rolandi R, Taylor GW, Pepys MB, Stoppini M, Bellotti V (2013). Structure, folding dynamics, and amyloidogenesis of D76N β2-microglobulin: roles of shear flow, hydrophobic surfaces, and α-crystallin. J Biol Chem 288(43):30917-30.

Mangione PP, Porcari R, Gillmore JD, Pucci P, Monti M, Porcari M, Giorgetti S, Marchese L, Raimondi S, Serpell LC, Chen W, Relini A, Marcoux J, Clatworthy IR, Taylor GW, Tennent GA, Robinson CV, Hawkins PN, Stoppini M, Wood SP, Pepys MB, Bellotti V (2014). Proteolytic cleavage of Ser52Pro variant transthyretin triggers its amyloid fibrillogenesis. Proc Natl Acad Sci USA 111(4):1539-1544.

Marchesi M, Parolini C, Valetti C, Mangione P, Obici L, Giorgetti S, Raimondi S, Donadei S, Gregorini G, Merlini G, Stoppini M, Chiesa G, Bellotti V (2011). The intracellular quality control system down-regulates the secretion of amyloidogenic apolipoprotein A-I variants: a possible impact on the natural history of the disease. Biochim Biophys Acta 1812:87–93.

Marcoux J, Mangione PP, Porcari R, Degiacomi MT, Verona G, Taylor GW, Giorgetti S, Raimondi S, Sanglier-Cianférani S, Benesch JL, Cecconi C, Naqvi MM, Gillmore JD, Hawkins PN, Stoppini M, Robinson CV, Pepys MB, Bellotti V (2015). A novel mechano-enzymatic cleavage mechanism underlies transthyretin amyloidogenesis. EMBO Mol Med 7(10):1337-49.

Marik PE, Bedigian MK (1996). Refeeding hypophosphatemia in critically ill patients in an intensive care unit. A prospective study. Arch Surg 131(10):1043-1047.

Mazza G, Simons JP, Al-Shawi R, Ellmerich S, Urbani L, Giorgetti S, Taylor GW, Gilbertson JA, Hall AR, Al-Akkad W, Dhar D, Hawkins PN, De Coppi P, Pinzani M, Bellotti V, Mangione PP (2016). Amyloid persistence in decellularized liver: biochemical and histopathological characterization. Amyloid 23(1):1-7.

McCarney ER, Kohn JE, Plaxco KW (2005). Is there or isn't there? The case for (and against) residual structure in chemically denatured proteins. Crit Rev Biochem Mol Biol 40(4):181-189.

McCutchen SL, Colon W, Kelly JW (1993). Transthyretin mutation Leu-55-Pro significantly alters tetramer stability and increases amyloidogenicity. Biochemistry 32:12119–12127.

McLaurin J, Franklin T, Zhang X, Deng J, Fraser PE (1999) Interactions of Alzheimer amyloid β peptides with glycosaminoglycans. Eur J Biochem 266:1101–1110.

Meinhardt J, Fändrich M (2009). Structure of amyloid fibrils. Pathologe. 30(3):175-81.

Merlini G, Bellotti V (2003). Molecular mechanisms of amyloidosis. N Engl J Med 349(6):583-596.

Mirbaha H, Chen D, Morazova OA, Ruff KM, Sharma AM, Liu X, Goodarzi M, Pappu RV, Colby DW, Mirzaei H, Joachimiak LA, Diamond MI (2018). Inert and seed-
competent tau monomers suggest structural origins of aggregation. Elife 7.

Miroy GJ, Lai Z, Lashuel HA, Peterson SA, Strang C, Kelly JW (1996). Inhibiting transthyretin amyloid fibril formation via protein stabilization. Proc Natl Acad Sci USA 93:15051-15056.

Murphy MP & LeVine H, III (2010). Alzheimer's Disease and the β-Amyloid Peptide. J Alzheimers Dis. 19(1): 311.

Naiki H, Higuchi K, Hosokawa M, Takeda T (1989). Fluorometric determination of amyloid fibrils in vitro using the fluorescent dye, thioflavin T1. Anal Biochem 177(2):244-9.

Naiki H, Hashimoto N, Suzuki S, Kimura H, Nakakuki K, Gejyo F (1997). Concentration-dependent inhibitory effects of apolipoprotein E on Alzheimer's beta-amyloid fibril formation in vitro. Biochemistry36(20):6243-50.

Nasr SH, Dasari S, Hasadsri L, Theis JD, Vrana JA, Gertz MA, Muppa P, Zimmermann MT, Grogg KL, Dispenzieri A, Sethi S, Highsmith WE Jr, Merlini G, Leung N, Kurtin PJ (2017). Novel Type of Renal Amyloidosis Derived from Apolipoprotein-CII. J Am Soc Nephrol 28(2):439-445.

Natalello A, Mangione PP, Giorgetti S, Porcari R, Marchese L, Zorzoli I, Relini A, Ami D, Faravelli G, Valli M, Stoppini M, Doglia SM, Bellotti V, Raimondi S (2016). Co-fibrillogenesis of Wild-type and D76N β2-microglobulin: THE CRUCIAL ROLE OF FIBRILLAR SEEDS. J Biol Chem 291(18):9678-89.

Nelson R, Sawaya MR, Balbirnie M, Madsen AØ, Riekel C, Grothe R, Eisenberg D (2005). Structure of the cross-beta spine of amyloid-like fibrils. Nature 435(7043):773-8.

Nencetti S, Orlandini E (2012). TTR Fibril Formation Inhibitors: Is there a SAR? Curr Med Chem 19(15)2356-2379.

Neumann P, Cody V, Wojtczak A (2001). Structural basis of negative cooperativity in transthyretin. Acta Biochim *Pol,* 48(4):867-75.

Nichols WC, Dwulet FE, Liepnieks J, Benson MD (1988). Variant apolipoprotein AI as a major constituent of a human hereditary amyloid. Biochem Biophys Res Commun 156:762–768.

Obici L, Merlini G (2014). An overview of drugs currently under investigation for the treatment of transthyretin-related hereditary amyloidosis. Expert Opin Investig Drugs. (9):1239-51.

Okamoto S, Zhao Y, Lindqvist P, Backman C, Ericzon BG, Wijayatunga P, Henein MY, Suhr OB (2011). Development of cardiomyopathy after liver transplantation in Swedish hereditary transthyretin amyloidosis (ATTR) patients. Amyloid 18(4):200-5.

Olofsson A, Ippel JH, Wijmenga SS, Lundgren E, Ohman A (2004). Probing solvent accessibility of transthyretin amyloid by solution NMR spectroscopy. J Biol Chem 279(7):5699-707.

Ooi EM, Barrett PH, Chan DC, Watts GF (2008). Apolipoprotein C-III: understanding an emerging cardiovascular risk factor. Clin Sci 114:611–624.

Palaninathan SK (2012). Nearly 200 X-ray crystal structures of transthyretin: what do they tell us about this protein and the design of drugs for TTR amyloidoses? Curr Med Chem 19(15):2324-42.

Palmieri Lde C, Lima LM, Freire JB, Bleicher L, Polikarpov I, Almeida FC, Foguel D (2010). Novel Zn2+-binding sites in human transthyretin: implications for amyloidogenesis and retinol-binding protein recognition. J Biol Chem 285(41):31731-41.

Pedersen JS, Christensen G, Otzen DE (2004). Modulation of S6 fibrillation by unfolding rates and gatekeeper residues. J Mol Biol 341:575–88.

Pedersen JS, Dikov D, Flink JL, Hjuler HA, Christiansen G, Otzen D (2005). The changing face of glucagon fibrillation: structural polymorphism and conformational imprinting. J Mol Biol 355:501–23.

Pepys MB, Booth DR, Hutchinson WL, et al. (1997). Amyloid P component: a critical review. Amyloid 4:274-295.

Pepys MB (2009). A molecular correlate of clinicopathology in transthyretin amyloidosis. J Pathol 217:1-3.

Pepys MB (2017). Immunotherapeutic clearance of systemic amyloid deposits by antibodies to serum amyloid P component. Amyloid 24(sup1):5-6.

Pepys MB, Herbert J, Hutchinson WL, Tennent GA, Lachmann HJ, Gallimore JR, Lovat LB, Bartfai T, Alanine A, Hertel C, Hoffmann T, Jakob-Roetne R, Norcross RD, Kemp JA, Yamamura K, Suzuki M, Taylor GW, Murray S, Thompson D, Purvis A, Kolstoe S, Wood SP, Hawkins PN (2002). Targeted pharmacological depletion of serum amyloid P component for treatment of human amyloidosis. Nature 417:254-9.

Pervushin K, Riek R, Wider G, Wüthrich K (1997). Attenuated T2 relaxation by mutual cancellation of dipole-dipole coupling and chemical shift anisotropy indicates an avenue to NMR structures of very large biological macromolecules in solution. Proc Natl Acad Sci USA 94(23):12366-71.

Petkova AT, Ishii Y, Balbach JJ, Antzutkin ON, Leapman RD, Delaglio F, Tycko R (2002). A structural model for Alzheimer's beta-amyloid fibrils based

on experimental constraints from solid state NMR. Proc Natl Acad Sci USA 99(26):16742-16747.

Pras M, Franklin EC, Prelli F, Frangione B (1981). A variant of prealbumin from amyloid fibrils in familial polyneuropathy of Jewish origin. J Exp Med 154(3):989- 993.

Pras M, Prelli F, Franklin EC, Frangione B (1983). Primary structure of an amyloid prealbumin variant in familial polyneuropathy of Jewish origin. Proc Natl Acad Sci USA 80(2):539-542.

Puchtler H, Waldrop FS, Meloan SN (1985). A review of light, polarization and fluorescence microscopic methods for amyloid. Appl Pathol 3(1-2):5-17.

Quarta CC, Buxbaum JN, Shah AM, Falk RH, Claggett B, Kitzman DW, Mosley TH, Butler KR, Boerwinkle E, Solomon SD (2015). The amyloidogenic V122I transthyretin variant in elderly black Americans. N Engl J Med. 372(1):21-9.

Quintas A, Vaz DC, Cardoso I, Saraiva MJ (2001). Tetramer dissociation and monomer partial unfolding precedes protofibril formation in amyloidogenic transthyretin variants. J Biol Chem 276(29):27207-27213.

Ranlov I, Alves IL, Ranlov PJ, Husby G, Costa PP, Saraiva MJ (1992). A Danish kindred with familial amyloid cardiomyopathy revisited: identification of a mutant transthyretin-methionine111 variant in serum from patients and carriers. Am J Med 93:3–8.

Raskatov JA, Teplow DB (2017). Using chirality to probe the conformational dynamics and assembly of intrinsically disordered amyloid proteins. Sci Rep 7(1):12433.

Rawlings ND, Barrett AJ, Finn R (2016). Twenty years of the MEROPS database of proteolytic enzymes, their substrates and inhibitors. Nucleic Acids Res 44:D343-D350.

Relini A, De Stefano S, Torrassa S, Cavalleri O, Rolandi R, Gliozzi A, Giorgetti S, Raimondi S, Marchese L, Verga L, Rossi A, Stoppini M, Bellotti V (2008). Heparin strongly enhances the formation of beta2-microglobulin amyloid fibrils in the presence of type I collagen. J Biol Chem 283(8):4912-20.

Richards DB, Cookson LM, Barton SV, Liefaard L, Lane T, Hutt DF, Ritter JM, Fontana M, Moon JC, Gillmore JD, Wechalekar A, Hawkins PN, Pepys MB (2018). Repeat doses of antibody to serum amyloid P component clear amyloid deposits in patients with systemic amyloidosis. Sci Transl Med10(422).

Richards DB, Cookson LM, Berges AC, Barton SV, Lane T, Ritter JM, Fontana M, Moon JC, Pinzani M, Gillmore JD, Hawkins PN, Pepys MB (2015). Therapeutic Clearance of Amyloid by Antibodies to Serum Amyloid P Component. N Engl J Med 373(12):1106-14.

Saelices L, Chung K, Lee JH, Cohn W, Whitelegge JP, Benson MD, Eisenberg DS (2018). Amyloid seeding of transthyretin by ex vivo cardiac fibrils and its inhibition. Proc Natl Acad Sci U S A. pii: 201805131.

Sant'Anna R, Gallego P, Robinson LZ, Pereira-Henriques A, Ferreira N, Pinheiro F, Esperante S, Pallares I, Huertas O, Almeida MR, Reixach N, Insa R, Velazquez-Campoy A, Reverter D, Reig N, Ventura S (2016). Repositioning tolcapone as a potent inhibitor of transthyretin amyloidogenesis and associated cellular toxicity. Nat Commun 7:10787.

Santoro MM, Bolen DW (1988) Unfolding free energy changes determined by the linear extrapolation method. 1. Unfolding of phenylmethanesulfonyl α-chymotrypsin using different denaturants. Biochemistry 27(21):8063–8068.

Saraiva MJ, Birken S, Costa PP, Goodman DW (1984). Amyloid fibril protein in familial amyloidotic polyneuropathy, Portuguese type. Definition of molecular abnormality in transthyretin (prealbumin). J Clin Invest 74(1):104-119.

Saraiva MJ (1991). Recent advances in the molecular pathology of familial amyloid polyneuropathy. Neuromuscolar Disord 1(1):3-6.

Saraiva MJ (1995). Transthyretin mutations in health and disease. Hum Mutat 5(3):191-196.

Sattler M, Fesik SW (1996). Use of deuterium labeling in NMR: overcoming a sizeable problem. Structure 4(11):1245-9.

Senior K (2009). Could SAP depletion stabilize Alzheimer disease? Nat. Rev. Neurol. doi:10.1038/nrneurol.2009.67.

Sekijima Y, Wiseman RL, Matteson J, Hammarström P, Miller SR, Sawkar AR, Balch WE, Kelly JW (2005). The biological and chemical basis for tissue-selective amyloid disease. Cell 121(1):73-85.

Sekijima Y (2014). Recent progress in the understanding and treatment of transthyretin amyloidosis. J Clin Pharm Ther 39(3):225-33.

Serio TR, Cashikar A, Kowal AS, Sawicki GJ, Moslehi JJ, Serpell L, Arnsdorf MF, Lindquist SL (2000). Nucleated conformational conversion and the replication of conformational information by a prion determinant. Science 289:1317–21.

Serpell LC, Sunde M, Benson MD, Tennent GA, Pepys MB, Fraser PE (2000). The protofilament substructure of amyloid fibrils. J Mol Biol 300(5):1033-1039.

Sethi S, Theis JD, Shiller SM, Nast CC, Harrison D, Rennke HG, Vrana JA, Dogan A (2012). Medullary amyloidosis associated with apolipoprotein A-IV deposition. Kidney Int 81(2):201-6.

Shenkin A (2006). Serum prealbumin: Is it a marker of nutritional status or of risk of malnutrition? Clin Chem 52(12):2177-9.

Shnyrov VL, Villar E, Zhadan GG, Sanchez-Ruiz JM, Quintas A, Saraiva MJ, Brito RM (2000). Comparative calorimetric study of non-amyloidogenic and amyloidogenic variants of the homotetrameric protein transthyretin. Biophys Chem 88:61–67.

Sipe JD (1992). Amyloidosis. Annu. Rev. Biochem. 61:947-75.

Sipe JD, Cohen AS (2000). Review: history of the amyloid fibril. J Struct Biol 130(2-3):88-98.

Sipe JD, Benson MD, Buxbaum JN, Ikeda SI, Merlini G, Saraiva MJ, Westermark P (2016). Amyloid fibril proteins and amyloidosis: chemical identification and clinical classification International Society of Amyloidosis 2016 Nomenclature Guidelines. Amyloid 23(4):209-213.

Sletten K, Westermark P, Natvig JB (1980). Senile cardiac amyloid is related to prealbumin. Scand J Immunol 12(6):503-506.

So M, Hata Y, Naiki H, Goto Y (2017). Heparin-induced amyloid fibrillation of β_2-microglobulin explained by solubility and a supersaturation-dependent conformational phase diagram. Protein Sci 26(5):1024-1036.

Stevens FJ, Kisilevsky R (2000). Immunoglobulin light chains, glycosaminoglycans, and amyloid. Cell Mol Life Sci 57(3):441-449.

Stoppini M, Bellotti V (2015). Systemic amyloidosis: lessons from β2-microglobulin. J Biol Chem 290(16):9951-8.

Sun X, Dyson HJ, Wright PE (2018). Kinetic analysis of the multistep aggregation pathway of human transthyretin. Proc Natl Acad Sci U S A115(27):E6201-E6208.

Sunde M, Blake C (1997). The structure of amyloid fibrils by electron microscopy and X-ray diffraction. Adv. Protein. Chem.; 50:123-59.

Tartaglia GG, Pawar AP, Campioni S, Dobson CM, Chiti F, Vendruscolo M (2008). Prediction of aggregation-prone regions in structured proteins. J Mol Biol 380(2):425-36.

Tawara S, Nakazato M, Kangawa K, Matsuo H, Araki S (1983). Identification of amyloid prealbumin variant in familial amyloidotic polyneuropathy (Japanese type). Biochem Biophys Res Commun 116(3):880-888.

Tennent GA, Lovat LB, Pepys MB (1995). Serum Amyloid P component prevents proteolysis of the amyloid fibrils of Alzheimer's disease and systemic amyloidosis. Proc Nat Acad Sci USA 92(10):4299-4303 .

Thylén C, Wahlqvist J, Haettner E, Sandgren O, Holmgren G, Lundgren E (1993). Modifications of transthyretin in amyloid fibrils: analysis of amyloid from homozygous and heterozygous individuals with the Met30 mutation. EMBO J 12(2):743-748.

Tomar D, Khan T, Singh RR, Mishra S, Gupta S, Surolia A, Salunke DM (2012). Crystallographic study of novel transthyretin ligands exhibiting

negative-cooperativity between two thyroxine binding sites. PLoS One 7(9):e43522.

Tucker HM, Kihiko M, Caldwell JN, Wright S, Kawarabayashi T, Price D, Walker D, Scheff S, McGillis JP, Rydel RE, Estus S (2000). The plasmin system is induced by and degrades amyloid-beta aggregates. J. Neurosci 20:3937-3946.

Valleix S, Gillmore JD, Bridoux F, Mangione PP, Dogan A, Nedelec B, Boimard M, Touchard G, Goujon JM, Lacombe C, Lozeron P, Adams D, Lacroix C, Maisonobe T, Planté-Bordeneuve V, Vrana JA, Theis JD, Giorgetti S, Porcari R, Ricagno S, Bolognesi M, Stoppini M, Delpech M, Pepys MB, Hawkins PN, Bellotti V (2012). Hereditary systemic amyloidosis due to Asp76Asn variant β2-microglobulin. N Engl J Med. 366(24):2276-83.

Valleix S, Verona G, Jourde-Chiche N, Nedelec B, Mangione PP, Bridoux F, Mange A, Dogan A, Goujon JM, Lhomme M, Dauteuille C, Chabert M, Porcari R, Waudby CA, Relini A, Talmud PJ, Kovrov O, Olivecrona G, Stoppini M, Christodoulou J, Hawkins PN, Grateau G, Delpech M, Kontush A, Gillmore JD, Kalopissis AD, Bellotti V (2016). D25V apolipoprotein C-III variant causes dominant hereditary systemic amyloidosis and confers cardiovascular protective lipoprotein profile. Nat Commun 7:10353.

Vendruscolo M, Paci E, Karplus M, Dobson CM (2003). Structures and relative free energies of partially folded states of proteins. Proc Natl Acad Sci USA 100(25):14817-14821.

Venters RA, Thompson R, Cavanagh J (2002). Current approaches for the study of large proteins by NMR. Journ Mol Struc 602-603:275-292.

Vrana JA, Gamez JD, Madden BJ, Theis JD, Bergen HR 3rd, Dogan A (2009). Classification of amyloidosis by laser microdissection and mass

spectrometry-based proteomic analysis in clinical biopsy specimens. Blood 114(24):4957-9.

Wallace MR, Dwulet FE, Conneally PM, Benson MD (1986). Biochemical and molecular genetic characterization of a new variant prealbumin associated with hereditary amyloidosis. J Clin Invest 78(1):6-12.

Watters AL, Deka P, Corrent C, Callender D, Varani G, Sosnick T, Baker D (2007). The highly cooperative folding of small naturally occurring proteins is likely the result of natural selection. Cell 128(3):613-624.

Weiss C, Seitel G, Bartsch P (1998). Coagulation and fibrinolysis after moderate and very heavy exercise in healthy male subjects. Med Sci Sports Exerc 30:246-251.

Westermark P, Sletten K, Johansson B, Cornwell GG (1990). Fibril in senile systemic amyloidosis is derived from normal transthyretin. Proc Natl Acad Sci USA 87(7):2843-2845.

Westermark P, Sletten K, Johnson KH (1996). Ageing and amyloid fibrillogenesis: Lessons from apolipoprotein AI, transthyretin and islet amyloid polypeptide. Ciba Found Symp 199:205-218, discussion 218-222.

Wojtczak A, Cody V, Luft JR, Pangborn W (1996). Structures of human transthyretin complexed with thyroxine at 2.0 Å resolution and 3′,5′-dinitro-N-acetyl-L-thyronine at 2.2 Å resolution. Acta Crystallogr D Biol Crystallogr 52(Pt 4):758-765.

Xu S, Laccotripe M, Huang X, Rigotti A, Zannis VI, Krieger M (1997). Apolipoproteins of HDL can directly mediate binding to the scavenger receptor SR-BI, an HDL receptor that mediates selective lipid uptake. J Lipid Res 38:1289 –1298.

Xue WF, Hellewell AL, Gosal WS, Homans SW, Hewitt EW, Radford SE (2009). Fibril fragmentation enhances amyloid cytotoxicity. J Biol Chem 284(49):34272-82.

Yan SD, Zhu H, Zhu A, Golabek A, Du H, Roher A, Yu J, Soto C, Schmidt AM, Stern D, Kindy M (2000). Receptor-dependent cell stress and amyloid accumulation in systemic amyloidosis. Nat Med 6(6):643-651.

Yazaki M, Liepnieks JJ, Kincaid JC, Benson MD (2003). Contribution of wild-type transthyretin to hereditary peripheral nerve amyloid. Muscle Nerve. 28(4):438-42.

Yazaki M, Tokuda T, Nakamura A, Higashikata T, Koyama J, Higuchi K, Harihara Y, Baba S, Kametani F, Ikeda S (2000). Cardiac amyloid in patients with familial amyloidmpolyneuropathy consists of abundant wild-type transthyretin. Biochem Biophys Res Commun 274(3):702-706.

Yee AW, Moulin M, Breteau N, Haertlein M, Mitchell EP, Cooper JB, Boeri Erba E, Forsyth VT (2016). Impact of deuteration on the assembly kinetics of transthyretin monitored by native mass spectrometry and implications for amyloidoses. Angew Chem Int Ed Engl 55(32):9292-6.

Zanotti G, Vallese F, Ferrari A, Menozzi I, Saldano TE, Berto P, Fernandez-Alberti S, Berni R (2017). Structural and dynamics evidence for scaffold asymmetric flexibility of the human transthyretin tetramer. *PLoS One* 12(12):e0187716.